The intraseasonal equatorial oceanic Kelvin wave and the central Pacific El Nino phenomenon

Kobi A. Mosquera Vasquez

Université de Toulouse

THÈSE

En vue de l'obtention du

DOCTORAT DE L'UNIVERSITÉ DE TOULOUSE

Délivré par :

Université Toulouse III Paul Sabatier (UT3 Paul Sabatier)

Discipline ou spécialité :

Dynamique océanique équatoriale

Présentée et soutenue par :

Kobi A. Mosquera Vásquez

le : 03/07/2015

Titre :

L'onde de Kelvin équatoriale océanique intrasaisonnière et les événements El Niño du Pacifique Central

---

Ecole doctorale :

Sciences de l'Univers, de l'Environnement et de l'Espace (SDU2E)

Unité de recherche :

Laboratoire d'Etudes en Géophysique et Océanographie Spatiale (LEGOS)

Membre(s) du jury :

Serge Chauzy, Université Toulouse III - LA, Président
Antonietta Capotondi, NOAA/ESRL/PSD, Rapporteur
Oscar Pizarro, UDEC, Rapporteur
Ken Takahashi, IGP, Examinateur
Christophe Menkes, IRD-LOCEAN, Examinateur
Boris Dewitte , IRD-LEGOS, Directeur
Serena Illig, IRD-LEGOS, Co-directrice

This thesis is dedicated to my daughter, Micaela.

Acknowledgments

To my advisors, Drs. Boris Dewitte and Serena Illig, for the full academic support and patience in the development of this thesis; without that I would have not reached this goal.

To IRD, for the three-year fellowship to develop my thesis which also include three research stays in the *Laboratoire d'Etudes en Géophysique et Océanographie Spatiales* (LEGOS).

To Drs. Pablo Lagos and Ronald Woodman, Drs. Yves Du Penhoat and Yves Morel for allowing me to develop my research at the *Instituto Geofísico del Perú* (IGP) and the *Laboratoire d'Etudes Spatiales in Géophysique et Oceanographic* (LEGOS), respectively.

To my coauthors of my first paper, Drs. Ken Takahashi and Gilles Garric, for their collaboration and support in each stage of it.

To Susana (my wife), Elba (my mother), Alberto (my father), and Clarita (my sister), for their unconditional support (in different ways) during the long way to finish this goal.

RÉSUMÉ

Le phénomène El Niño est le mode dominant de la variabilité du climat aux échelles de temps interannuelles dans le Pacifique tropical. Il modifie considérablement le climat régional dans les pays voisins, dont le Pérou pour lequel les impacts socio-économiques peuvent être dramatiques. Comprendre et prévoir El Niño reste un enjeu prioritaire pour la communauté climatique. Des progrès significatifs dans notre compréhension du phénomène El Niño et dans notre capacité à le prédire ont été réalisés dans les années 80, en particulier grâce à la mise en place du système d'observation dans le Pacifique tropical (programme de TOGA, en particulier, ainsi que l'émergence de l'ère des satellites). À la fin du XXe siècle, alors que de nouvelles théories scientifiques ont été proposées et testées, les progrès réalisés dans le domaine de la modélisation numérique et de l'assimilation de données ont conduit à l'idée que le phénomène El Niño pourrait être prévu avec au moins deux ou trois saisons à l'avance. Or, depuis le début du 21ième siècle, les manifestations du phénomène El Niño ont réduit cette expectative: un nouveau type d'El Niño est a été découvert - identifié par des anomalies de température moins intenses et localisées dans le centre du Pacifique équatorial. Ce phénomène, connu sous le nom CP El Niño pour El Niño Pacifique Central ou El Niño Modoki a placé la communauté scientifique devant un nouveau défi. Cette thèse est une contribution à l'effort international actuel pour comprendre la dynamique de ce nouveau type d'El Niño, dans le but de proposer des mécanismes expliquant sa présence accrue au cours des dernières décennies.

Plus précisément, l'objectif de cette thèse est d'étudier le rôle des ondes longues équatoriales dans le Pacifique tropical sur la dynamique océanique et la thermodynamique associées au phénomène El Niño de type Pacifique Central. Cette thèse s'intéresse tout d'abord au premier CP El Niño du 21ième siècle, le phénomène El Niño 2002/03, à partir des sorties d'un modèle de circulation océanique général. Ensuite, nous documentons les caractéristiques des ondes équatoriales de Kelvin aux fréquences Intra Saisonnières (ISKw) sur la période 1990-2011, fournissant une statistique de l'activité des ondes ISKw durant l'évolution des événements El Niño de type Central Pacifique. Nos résultats montrent que l'onde ISKw subit une forte dissipation dans le Pacifique Est, qui est interprétée comme provenant de la dispersion des ondes lorsqu'elles rencontrent le front zonal de la stratification dans l'Est du

Pacifique (i.e. la pente de la thermocline d'Ouest en Est). Une réflexion partielle de l'onde ISKw en onde de Rossby équatoriale de près de 120°W est également identifiée, ce qui peut expliquer le confinement dans le Pacifique central des anomalies de température de surface associées aux événements El Niño de type Central Pacifique. Nous suggérons que la fréquence accrue au cours des dernières années des événements CP El Niño peut être associée à l'état froid - de type La Niña - observé dans le Pacifique Equatorial depuis les années 90 et les changements dans la variabilité saisonnière de la profondeur de la thermocline depuis les années 2000.

ABSTRACT

The El Niño phenomenon is the dominant mode of climate variability at interannual timescales in the tropical Pacific. It modifies drastically the regional climate in surrounding countries, including Peru for which the socio-economical impacts can be dramatic. Understanding and predicting El Niño remains a top-priority issue for the climatic community. Large progress in our understanding of El Niño and in our ability to predict it has been made since the 80s thanks to the improvement of the observing system of the tropical Pacific (TOGA program and emergence of the satellite era). At the end of the Twentieth century, whereas new theories were proposed and tested, progress in numerical modeling and data assimilation led to the idea that El Niño could be predicted with at least 2 or 3 seasons in advance. The observations since the beginning of the 21st century have wiped out such expectation: A new type of El Niño, known as the Central Pacific El Niño (CP El Niño) or Modoki El Niño has put the community in front of a new challenge. This thesis is a contribution to the current international effort to understand the dynamics of this new type of El Niño in order to propose mechanisms explaining its increased occurrence in recent decades.

More specifically, the objective of the thesis is to study the role of the oceanic equatorial waves in the dynamic and thermodynamic along the equatorial Pacific Ocean, focusing on the CP El Niño. This thesis first takes a close look at the first CP El Niño of the 21st century of this type, i.e. the 2002/03 El Niño, based on an Oceanic General Circulation Model. Then it documents the characteristics of the IntraSeasonal Kelvin waves (ISKws) over the period 1990-2011, providing a statistics on the ISKws activity during the evolution of CP El Niño events. We find that the ISKw experiences a sharp dissipation in the eastern Pacific that is interpreted as resulting from the scattering of energy associated to the zonal contrast in stratification (i.e. sloping thermocline from west to east). Partial reflection of the ISKw as Rossby waves near 120°W is also identified, which may explain the confinement of CP El Niño warming in the central Pacific. We suggest that the increased occurrence of CP El Niño in recent years may be associated to the La Niña-like state since the 90s and changes in the seasonality of the thermocline since the 2000s.

Keywords: El Niño, equatorial Kelvin waves, Rossby waves, wave dispersion, intraseasonal variability

Content

Acknowledgments 4

Résumé 5

Abstract 7

Chapter 1: Overview

1.1 Introduction (*Version française*) 11

1.1.1 Bref historique du phénomène El Niño 11

1.1.2 Emergence des théories et prévisions du phénomène El Niño 13

1.1.3 Un nouveau type d'événement El Niño 14

1.1.4 Motivations et objectifs de cette thèse 15

1.2 Introduction (*English version*) 19

1.2.1 A brief history of El Niño phenomenon 19

1.2.2 El Niño theories and forecasts 20

1.2.3 A new type of El Niño 22

1.2.4 Motivations and objectives of the thesis 23

1.3 ENSO theories 27

1.3.1 Bjerknes theory 27

1.3.2 The delayed oscillator 27

1.3.3 Discharge and recharge oscillator theory 30

1.4 The Central Pacific El Niño (CP El Niño) 31

1.5 ENSO and the Kelvin wave 33

1.6 Processes impacting the Kelvin wave in the equatorial Pacific 38

Chapter 2: The 2002/03 El Niño: Equatorial waves sequence and their impact on Sea Surface Temperature

2.1 Overview 40

2.2 Article published in Journal Geophysical Research- Oceans 41

2.3 Thermodynamics associated to the El Niño phenomenon over 1990 – 2011 54

2.3.1 Introduction 54

2.3.2 Data and methodologies 54

2.2.3 Results 57

Chapter 3: The Central Pacific El Niño Intraseasonal Kelvin wave

3.1 Overview 66

3.2 Article published in Journal of Geophysical Research – Oceans 67

Chapter 4: **On the change in thermocline seasonal variability along the equatorial Pacific from before and after 2000**

4.1 Overview 85

4.2 Draft Article to be submitted to Journal of Geophysical Research – Oceans 86

Chapter 5: Conclusions and Perspectives

English version 118

Version française 122

Appendix A: Supplementary material for Chapter 4 126

Appendix B: Numerical simulations with the Regional Ocean Model System (ROMS) over the period 2000-2010.

B.1 Overview 137

B.2 Data 137

B.3 The Regional Oceanic Model System (ROMS) and the tropical Pacific configurations 138

B.3.1 Group 1 139

B.3.2 Group 2 145

Reference 147

Chapter 1: Overview

1.1 Introduction (*Version française*)

1.1.1 Bref historique du phénomène El Niño

À la fin du 19ème siècle, Carranza (1891) reporte pour la première fois les caractéristiques d'un événement climatique fort qui a lieu le long de la côte péruvienne en 1891. Il décrit un courant inhabituel dirigé vers le Sud, provenant apparemment du Golfe de Guayaquil, s'écoulant dans le sens contraire du courant côtier observé normalement. Ce courant anormal a perturbé les conditions océaniques et atmosphériques, occasionnant des températures de la surface de l'océan plus chaudes qu'à l'habitude, ainsi que de fortes précipitations le long de la côte péruvienne à l'origine d'inondations dans le Nord du Pérou en avril et mai 1891. Cet événement fut si fort que des anomalies de précipitation touche des villes comme Lima [77ºW; 12ºS] et Ica [75,7ºW; 14ºS] (Rodriguez, 2001) - villes qui ne reçoivent normalement aucune précipitation durant toute l'année. L'extension vers le Sud de cet événement inhabituel peut être observée sur la Figure 1.1 qui présente les anomalies interannuelles de la température de la surface de la mer (SST) en mars (Figure 1.1a) et avril (Figure 1.1b) en 1891 dans la région du Pacifique Sud-Est. Les anomalies de SST excèdent 2°C de mars à avril en moyenne le long de la côte du Pérou. Cet événement a surtout été décrit sur la base de son expression côtière et à cette époque la connexion avec la variabilité équatoriale n'était pas comprise. Le premier article scientifique qui mentionne pour la première fois "El Niño" le long de la côte du Pérou a été publié deux ans plus tard dans le bulletin de la Sociedad Geográfica de Lima, écrit par Carrillo (1892). Dans ce document, de nombreuses preuves d'un courant "étrange" observé dans l'océan au large du Pérou ont été rapportées. Ce courant, dirigé vers le Sud, a été observé juste après Noël et fut baptisé pour l'occasion: La corriente del Niño (le courant d'El Niño).

Ce fut l'événement El Niño qui s'est produit en 1925, le plus grand événement enregistré à l'époque et documenté par un ornithologue (Murphy, 1926) qui éveilla l'intérêt de la communauté scientifique internationale autour du phénomène El Niño. Tandis que le météorologue H. P. Berlage fut le premier à suggérer qu'El Niño pourrait

être lié à la circulation grande échelle dans le Pacifique tropical (Cushman, 2004), la première théorie a été proposée par Sir Bjerknes, suite aux travaux antérieurs de Sir Walker, expatrié en Inde afin de prévoir la mousson pour augmenter la production de coton - matière première importante en Europe à cette époque. Sir Walker a observé que les fluctuations de pression entre Tahiti et Darwin étaient en opposition de phase et qu'elles variaient beaucoup d'une année à l'autre. Il a utilisé ces données (la différence entre les deux) afin de prévoir la mousson indienne, qui est maintenant connue pour être associé à l'oscillation australe El Niño (ENSO). Sir Bjerknes fut le premier à laisser entendre que l'étrange phénomène qui était observé le long de la côte du Pérou (c.à.d. le réchauffement épisodique de la température de la surface de la mer au moment de Noël) pourrait être lié aux fluctuations grande échelle identifiées par Sir Walker. Il a poussé le concept en suggérant que le contraste zonal en SST le long du Pacifique équatorial était étroitement lié à la circulation de Walker, forcée par la différence de pression de surface entre Tahiti et Darwin.

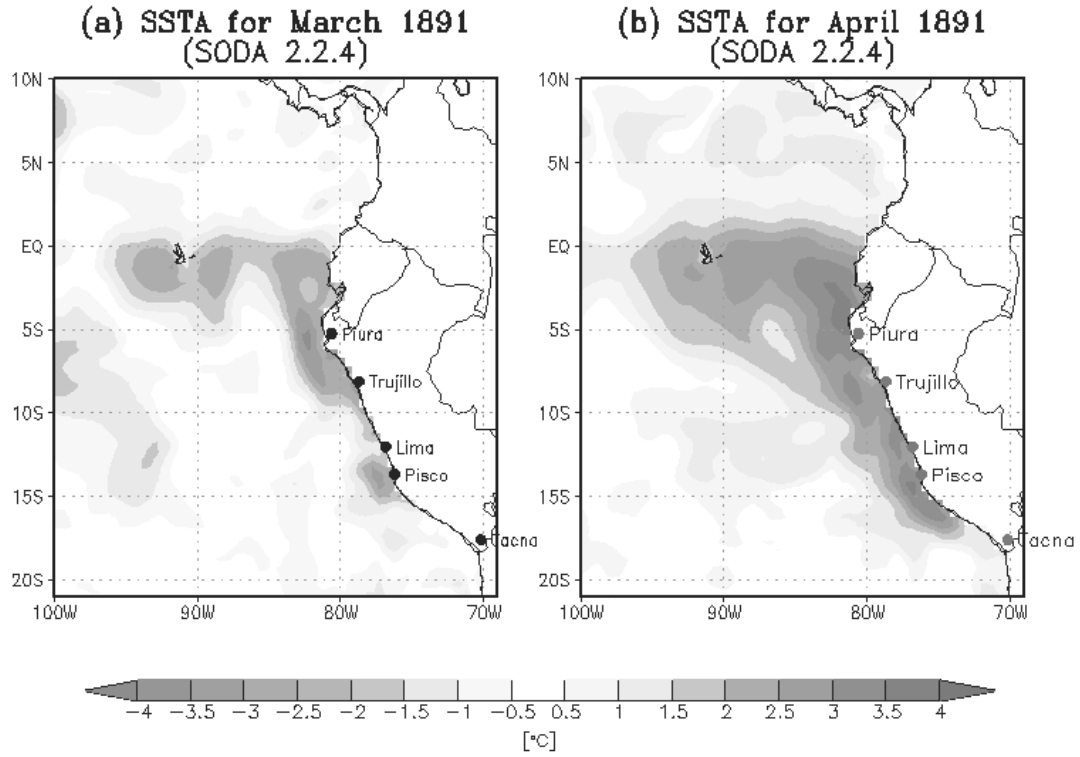

Figure 1.1 Anomalies interannuelles de la température de la surface de la mer dans le Pacifique Sud-Est pour les mois de Mars (a) et Avril (b) 1891, à partir des sorties de la réanalyse SODA (Simple Ocean Data Assimilation, version 2.2.4), calculées à partir de la climatologie estimée sur la période 1876 à 1906. L'unité est ºC.

1.1.2 Emergence des théories et prévisions du phénomène El Niño

Cette théorie n'expliquait cependant pas la nature oscillatoire d'ENSO: les événements El Niño chauds peuvent être suivis par une phase froide (c.a.d. La Niña) et reviennent après un certain temps, ce dernier définissant la « périodicité» de l'oscillation. Les années 80 et 90 sont une periode prospère pour l'émergence des théories d'ENSO, ce qui a été permis en partie grâce aux développements du système d'observation dans le Pacifique tropical: in situ (cf. programme TOGA-TAO lancé en 1985) et satellite (le premier altimètre (GEOSAT) a été lancé en 1985). En particulier, l'altimétrie a permis l'observation quasi-synoptique des ondes équatoriales planétaires, ce qui a permis de tester les différentes théories basées sur les réflexions des ondes équatoriales aux frontières méridionales du bassin Pacifique. Dans ces théories (par exemple, celle de l'oscillateur retardé, voir #1.3.2 pour plus de détails), l'effet retardé de l'onde réfléchie est le processus par lequel un événement El Niño est contraint à s'amortiret ce processus permet d'introduire le concept nécessaire à la nature oscillante d'ENSO.

Néanmoins, les dimensions zonales du bassin Pacifique Tropical associées à la propagation d'ondes libres ne pouvaient pas fournir une vue cohérente des échelles de temps de l'évolution d'ENSO et de sa périodicité. La théorie de recharge-décharge a émergé à la fin des années 90, en partie afin de résoudre cette question. Cette théorie considère un ajustement rapide qui a lieu à l'échelle du bassin Pacifique tropical. Le long de l'équateur, les alizés induisent un transport zonal, mais aussi un transport méridional associé à l'effet de la force de Coriolis (transport de Sverdrup). Ce dernier « recharge » la bande équatoriale en eaux chaudes lorsque la thermocline est remontée (processus de recharge) ou évacue les eaux chaudes de la bande équatoriale (décharge), ce qui constitue la rétroaction négative lente et permet au système d'osciller (voir schémas de la **Figure 1.2**). Cette théorie est basée sur l'observation qu'il a un ajustement différé entre la SST et le contenu thermique dans le Pacifique équatorial (i.e. Warm Water Volume). Cette théorie a fourni le cadre général pour l'étude d'ENSO durant les deux dernières décennies. Au moment où j'ai démarré cette thèse, la théorie de la recharge-décharge était encore le principal paradigme pour interpréter la variabilité interannuelle dans le Pacifique équatorial. Elle fournit des bases théoriques solides pour étudier divers aspects de l'ENSO, en particulier le changement de ses propriétés

(fréquence, amplitude, prévisibilité) sur de longues périodes de temps. Par exemple, à partir des années 80, ENSO a connu une augmentation de son amplitude, qui a été attribuée à l'état moyen plus chaud, après le « shift » climatique de la fin des années 70 (Yeh et al., 2001). Une augmentation de l'activité ENSO peut être liée à une diminution de la stabilité de l'oscillateur, qui peut être diagnostiquée à partir d'observations ou de produits de réanalyses et en utilisant ce formalisme (An et Jin, 2001). Ainsi les progrès de la modélisation numérique et de l'assimilation de données de la fin du XXe nous ont conduits à l'idée que le phénomène El Niño pourrait être prévu avec au moins deux ou trois saisons à l'avance.

1.1.3 Un nouveau type d'événement El Niño

Or, depuis le début du 21ième siècle, les manifestations du phénomène El Niño ont réduit ces expectatives. En particulier, depuis les années 2000, le score de prédictibilité de la théorie de recharge-décharge s'est significativement réduit, car la phase entre la SST dans la région NINO3 [150°W-90°W; 5°S-5°N] et l'indice de contenu thermique du bassin (WWV) a significativement diminué (McPhaden, 2012). Tout d'abord, il a été suggéré que cela était dû à la modification de la position de la région où les anomalies de tension de vent associées à ENSO sont observées. En particulier, il a été montré que plus l'anomalie de vent est à l'Ouest, plus le décalage entre l'indice NINO3 SST et le mode WWV est marqué (Clarke, 2010; Fedorov, 2010). En outre, les processus de dissipation pourraient jouer un rôle important dans la diminution du décalage entre NINO3 SST et l'index WWV (Thual et al., 2013). Toutefois, il n'est pas certain qu'un tel changement dans les caractéristiques d'ENSO observés après 2000 pourrait être interprété à la lumière de la théorie de recharge-décharge. En fait, un nouveau type d'El Niño, connu sous le nom de El Niño Pacifique Central (CP El Niño, Kug et al., 2009) ou El Niño Modoki (Ashock et al., 2007), caractérisé par des anomalies de température moins intenses et localisées dans le centre du Pacifique équatorial a placé la communauté scientifique devant un nouveau défi.

Cette thèse est une contribution aux efforts de la communauté pour comprendre ce changement. Elle se concentre sur l'étude de la variabilité équatoriale dans le bassin Pacifique au cours du siècle dernier, lorsqu'un seul type d'événement El Niño était observé. Ces nouveaux événements El Niño ont un centre d'action localisé dans le

Pacifique central, comparé aux événements El Niño Pacifique Est ou Cold Tongue El Niño qui ont des impacts plus graves pour le Pérou.

Pour résumer le positionnement de cette thèse dans l'histoire de la recherche consacrée au phénomène El Niño, la **Figure 1.2** présente un schéma de la chronologie de la recherche de la communauté ENSO au cours du XX^{e} siècle.

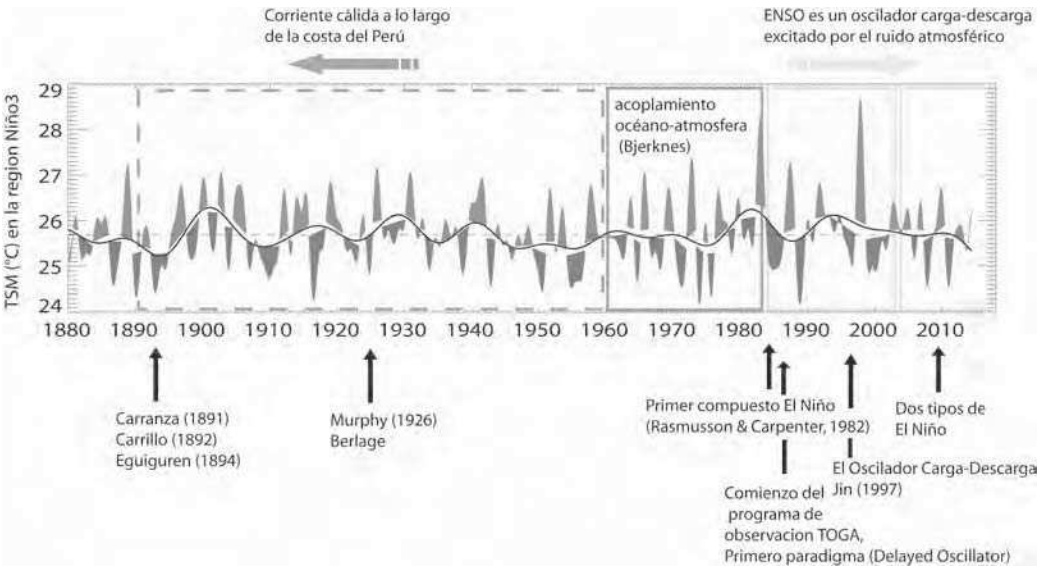

Figure 1.2 Chronologie de la recherche sur ENSO depuis le début du XXe siècle, illustrée à partir d'une série temporelle de la SST moyennée dans la région NINO3 (150°W-90°W; 5°S-5°N) à partir des données ERSST (Extended Reconstructed Sea Surface Temperature, Smith et al., 2008) v3b. L'unité est ° C. D'aprés Dewitte et al. (2014).

1.1.4 Motivations et objectifs de cette thèse

Il est maintenant reconnu qu'ENSO implique divers type de variabilité à des échelles de temps distinctes: de l'intrasaisonnier à l'interannuel. Un intérêt particulier a été porté à la variabilité atmosphérique intrasaisonnière dans le Pacifique tropical car elle a été observée avant le développement des événements El Niño récents et elle peut être impliquée dans la rectification d'ENSO (Kessler et Kleeman, 2000). Cette variabilité intra-saisonnière est en particulier composée de l'Oscillation Madden Julian (MJO, Madden and Julian, 1994) et les coups de vent d'ouest (Westerly Wind Bursts) dont les échelles de temps de variabilité s'étendent de 10 à 60 jours. Étonnamment,

l'onde de Kelvin IntraSaisonnière (ISKw) a un spectre de variabilité beaucoup plus large allant de (50 jours)-1 jusqu'à la fréquence semi-annuelle, avec un pic d'énergie marqué dans la bande de fréquence (90-120 jours)-1 (Cravatte et al., 2003, Dewitte et al., 2008a). Une étude récente (Guschina and Dewitte, 2012) suggère par ailleurs que la relation entre ENSO et la variabilité intrasaisonnière atmosphérique dans le Pacifique pourrait être distincte suivant le type d'El Nio. Il semble donc important d'étudier les caractéristiques de l'onde ISKw et sont rôle sur le développement et la décroissance des événements CP El Niño, considérant de plus que l'onde ISKw a un impact sur la dispersion des prévisions d'ENSO (Wang et al., 2011) et que les systèmes de prédiction présentent une capacité de prévision réduite sur la période récente (Hu et al., 2012; Xue et al., 2013).

D'autre part, il est également connu qu'une partie de l'énergie de l'onde de Kelvin équatoriale qui se propage le long de l'équateur à travers tout le Pacifique se propage vers les pôles le long de la côte du continent Sud-Américain, lorsque l'onde de Kelvin atteint la frontière Est du Pacifique. Le long de la côte péruvienne, l'onde de Kelvin de downwelling advecte des eaux chaudes équatoriales vers le Sud (surtout pendant les événements El Niño intenses) et approfondit également la thermocline, ce qui peut entraîner une augmentation de la SST associée à une diminution de l'advection ou du mélange vertical. La **Figure 1.3** illustre le phénomène de propagation depuis l'Ouest du Pacifique vers l'Est pour l'événement de 2002. En ce qui concerne la relation avec l'écosystème marin, l'onde de Kelvin de downwelling diminue l'efficacité de l'upwelling côtier, en termes d'enrichissement en nutriments (maintenant à la surface des eaux chaudes, faibles en nutriments; cf. Barber and Chavez, 1983). Les événements chauds associés à l'onde de Kelvin de downwelling incitent les anchois à se concentrer près de la côte et à se réfugier plus en sub-surface, et semblent influencer la stratégie d'exploitation des navires de pêche (Bertrand et al., 2008). L'augmentation de la SST dans le Nord du Pérou en l'été austral, en raison de l'impact de l'onde de Kelvin, peut également créer une instabilité atmosphérique qui engendre des précipitations le long des côtes péruviennes et des inondations dans la région de Piura [80,6°W; 5,3°S] (Takahashi, 2004). Les implications sociétales de la dynamique de l'onde de Kelvin le long de la côte du Pérou sont donc aussi une motivation à ce travail.

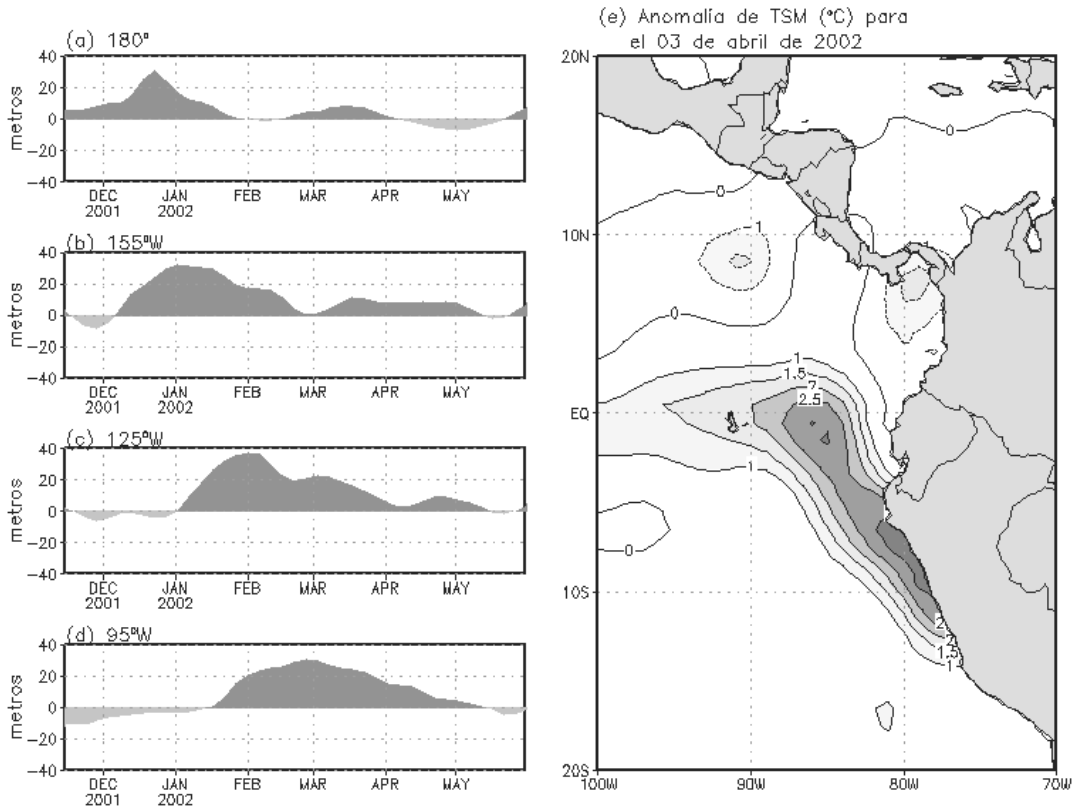

Figure 1.3 Sur la gauche, les séries temporelle des anomalies de profondeur de la thermocline (en mètres) le long du Pacifique équatorial estimées à partir des profils de température TAO situés à 180°E (a) , 155°W (b) , 125°W (c) et 95°W (d). Sur la droite (e), anomalies interannuelles de la SST (en °C, par rapport à la climatologie 2000-2013) pour le 3 Avril 2002. D'aprés Mosquera (2014).

L'objectif général de cette thèse est de mieux comprendre la variabilité interannuelle dans le Pacifique équatorial depuis 2000, compte tenu de l'évolution observée des caractéristiques de la dynamique associée à ENSO à depuis cette date. (McPhaden et al., 2011). En particulier depuis 2000, le Pacifique équatorial n'a connu que des événements El Niño de type Pacifique Central. Les raisons en reste inconnues. Cette thèse s'inscrit dans l'effort de la communauté internationale d'en comprendre les raisons. Elle s'intéresse en particulier à la dynamique ondulatoire et aux échelles de temps intrasaisonnières. Le chapitre 1 rappelle les théories actuelles d'ENSO, et synthétise l'état des connaissances sur la dynamique des événements CP El Niño. Il aborde aussi l'état des connaissances sur les processus agissant sur les caractéristiques de propagation des ondes de Kelvin équatoriales. Il est suivi par un examen détaillé d'un événement El Niño Pacifique Central, l'événement El Niño 2002/03, le premier CP El

Niño du 21^{e} siècle (chapitre 2). Dans cette étude, nous étudions les processus dans la couche de mélange associés aux ondes longues équatoriales et nous examinons si un tel événement satisfait la théorie de recharge-décharge. Puis, dans le chapitre 3, cette thèse aborde les échelles de temps intrasaisonnières, en documentant l'activité de l'onde ISKw au cours des événements CP El Niño des deux dernières décennies, et en étudiant les processus associés à la dissipation de l'onde ISKw. Enfin, considérant qu'El Niño est étroitement liée au cycle saisonnier, nous documentons les changements dans les caractéristiques du cycle saisonnier long de l'équateur avant et après 2000 (chapitre 4). Pour tous les chapitres, la méthodologie adoptée est basée sur l'analyse combinée de données (*in situ* et satellite) et de sorties de modèles, du modèle linéaire (Mosquera, 2009; Mosquera et al., 2010) aux modèles océaniques de circulation générale (OGCM).

1.2 Introduction (*English version*)

1.2.1 A brief history of El Niño phenomenon

At the end of 19th century, Carranza (1891) described for the first time the characteristics of a strong climatic event that took place along the Peruvian coast in 1891. He depicted an abnormal southward current apparently originating from the Guayaquil Gulf, and that was opposite to the southerly current. This abnormal current disrupted the oceanic and atmospheric climatological conditions, resulting in warmer than usual ocean conditions and heavy precipitations along the Peruvian coast and, as a consequence, flooding in the Northern edge of Peru in April and May of 1891. This event was so strong that precipitation anomalies reached cities such as Lima [77ºW, 12ºS] and Ica [75.7ºW, 14ºS] (Rodriguez, 2001) - cities that usually have no precipitation all year around. The southward extension of this unusual event can be appreciated from **Figure 1.1bis** that displays the Sea Surface Temperature (SST) interannual anomaly in March (**Figure 1.1bis-a**) and April (**Figure 1.1bis-b**) of 1891 over the South Eastern Pacific region and highlights that the SST anomaly increased by ~2°C from March to April on average along the coast of Peru. This event was mostly described based on its coastal expression and it was not clear at that time, how such event was connected to the equatorial variability. The first document that ever mentions "El Niño" along the coast of Peru was published two years later in the bulletin of the Sociedad Geográfica de Lima, written by Carrillo (1892), in which he reported the various evidences of a "strange" southward current observed in the ocean off Peru just after Christmas: La corriente del Niño (El Niño current).

It was the El Niño that occurred in 1925, the largest one registered at the time and documented by an ornithologist (Murphy, 1926) that first enticed the concern of the international scientific community on the El Niño phenomenon. Whereas the meteorologist H. P. Berlage was the first to suggest that El Niño could be linked to the large scale circulation in the tropical Pacific (Cushman, 2004), the first theory was proposed by Sir Bjerknes, following earlier works by Sir Walker who was sent to India to forecast the monsoon in order to improve the cotton production- an important raw material for Europe at that time. Sir Walker observed that the fluctuations of pressure at Tahiti and Darwin were opposite and they were varying a lot from one year to the other.

He used these data (the difference between both) to forecast the Indian monsoon that is now known to be associated with the El Niño Southern Oscillation (ENSO). Sir Bjerknes was the first to suggest that, the unusual phenomenon which was occurring along the coast of Peru (the episodic warming of sea water at Christmas time) could be related to the large scale fluctuations identified by Sir Walker. He spurred the concept that the zonal contrast in SST across the equatorial Pacific is tightly linked to the so-called Walker circulation driven by the difference in sea level pressure between Tahiti and Darwin.

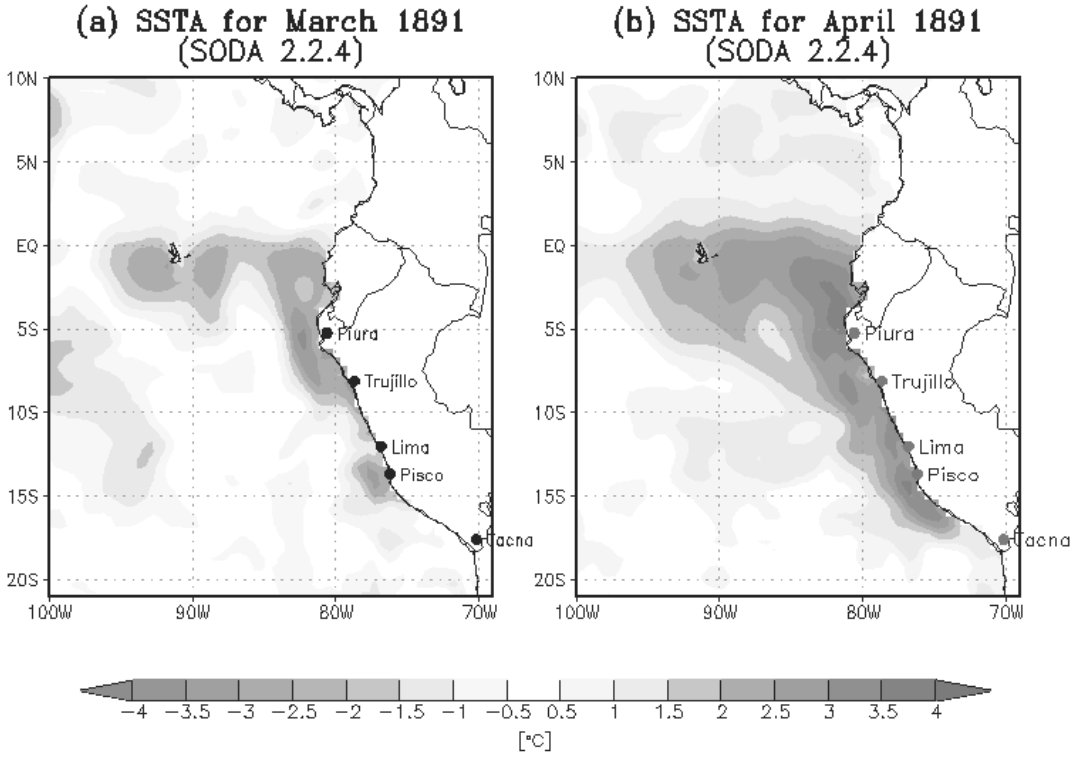

Figure 1.1bis SST interannual anomalies in the South Eastern Pacific for March (a) and April (b) 1891 from the outputs of the SODA (Simple Ocean Data Assimilation) reanalysis (version 2.2.4) calculated using a climatology estimated over the period expending from 1876 to 1906. Unit is ºC.

1.2.2 El Niño theories and forecasts

What was not explained by this theory is the oscillatory nature of ENSO: warm El Niño events can be followed by a cold phase (i.e. La Niña) and comes back after

some time, the later defining its "periodicity". The 80s and 90s were the decades of intense development in the theory of ENSO, which was allowed in part thanks to the development of the observing system in the tropical Pacific, both in situ (TOGA-TAO program launched in 1985) and from space (the first altimeter (GEOSAT) was launched in 1985). In particular, altimetry allowed for the quasi-synoptic observation of planetary equatorial waves, which permitted testing theories based on the reflections of equatorial waves onto the Pacific meridional boundaries. In these theories (for instance, the so-called delayed action oscillator, see #1.3.2 for more details), the delayed effect of the reflected wave is the process by which an El Niño event is suppressed, providing a concept for its oscillating nature.

Even if, at the time, the observation of long equatorial waves permitted to understand its role on the oscillatory process of El Niño, the basin scale adjustment associated with the free propagating waves could not provide a consistent view of the timescales of ENSO evolution and periodicity. The recharge-discharge theory emerged in the late 90s in part in order to resolve such issue. The recharge-discharge oscillator considers a fast adjustment that takes place at the scale of the tropical Pacific basin. Along the equator, the trade winds induced a zonal transport but also a meridional transport due to the effect of the Coriolis force (the so-called Sverdrup transport). The latter replenishes the equatorial band in warm waters when the thermocline has risen (recharge process) or evacuates the warm waters from the equatorial band (discharge), which provides the slow negative feedback for the system to oscillate (see details in Section 1.3). The theory is based on the observation that there is a delayed adjustment between the SST and the heat content over the equatorial Pacific (the so-called warm water volume). This theory has provided the most general framework for studying ENSO for the last two decades. At the time when I started this thesis, the recharge-discharge oscillator was still the main paradigm for interpreting the interannual variability in the equatorial Pacific. The recharge-discharge oscillator provides a solid theoretical basement for studying various aspects of ENSO, in particular its changes in properties (frequency, amplitude, predictability) over long-timescales. For instance, from the 80s, ENSO experienced an increase in its amplitude, which has been attributed to the warmer mean state after the climate shift of the late 70s. An increase in ENSO activity may be related to a decrease in the stability of the oscillator, which can be diagnosed from observations or Reanalysis products based on this formalism (An and

Jin, 2001). Hence, along with improvements in numerical modeling and data assimilation, at the end of the XXe, we came to the idea that El Niño could be predicted with at least 2 or 3 seasons in advance.

1.2.3 A new type of El Niño

However, the observations since the beginning of the 21st century have wiped out this expectation. In particular, it has been observed that since the 2000s, the predictive value of the recharge-discharge oscillator has been limited since the lag between the NINO3 SST [150°W-90°W; 5°S-5°N] and the WWV index has decreased significantly (McPhaden, 2012). First, this has been suggested to be due to changes in the location of the center of ENSO wind stress anomalies. In particular, it can be shown that the further to the west the wind stress forcing, the smaller the lag between NINO3 SST and the WWV mode (Clarke, 2010; Fedorov, 2010). Also, dissipation processes could play a significant part in explaining the lag between the NINO3 SST and WWV mode (Thual et al., 2013). However, it was not clear if such change in ENSO characteristics observed after 2000 could be fully interpreted in the light of the recharge-discharge theory. In fact, a new type of El Niño, known as the Central Pacific El Niño (CP El Niño, Kug et al., 2009) or Modoki El Niño (Ashock et al., 2007), characterized by weaker SST anomalies located in the central Pacific was described, which, since then, has put the community in front of a new challenge (Capotondi et al., 2015).

This thesis is a contribution to the efforts of the ENSO community for understanding such change. It focuses on the investigation of the equatorial variability in the Pacific over the last century, when only El Niño of one type has taken place. Those new El Niño events have a center of action in the central Pacific conversely to the Eastern Pacific or Cold Tongue El Niño that has the most severe impacts for Peru.

As a summary of where the thesis stands within the history of El Niño research, the **Figure 1.2bis** provides a schematic of the chronology of ENSO research over the Twentieth century.

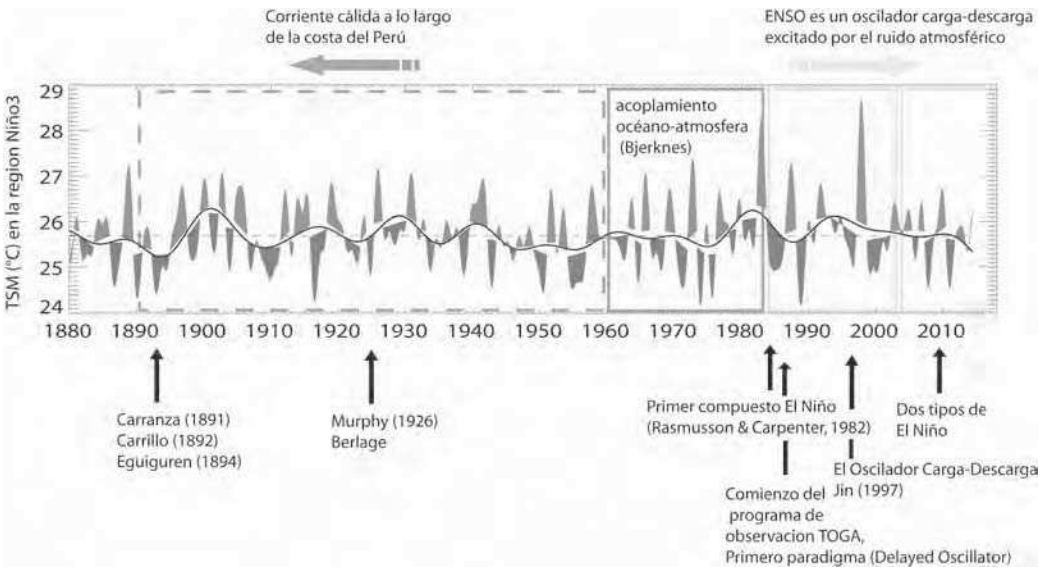

Figure 1.2bis Chronology of ENSO research since the beginning of the XX^{e} century, illustrated from a timeseries of the SST averaged in the NINO3 box (150°W-90°W; 5°S-5°N) from Extended Reconstructed Sea Surface Temperature (ERSST) v3b (Smith et al., 2008). Unit is °C. (After Dewitte et al. (2014))

1.2.4 Motivations and objectives of the thesis

It is now well known that ENSO involves a variety of variability timescales: from intraseasonal to interannual. The intraseasonal atmospheric variability in the tropical Pacific has a particular interest because it has been observed prior to the development of recent El Niño events and possibly involved in the rectification of the ENSO (Kessler and Kleeman, 2000). This intraseasonal atmospheric variability is in particular composed by the Madden and Julian oscillation (Madden and Julian, 1994) and the Westerly Wind Bursts (stochastic in nature) that are associated to periods of variability ranging from 10 to 60 days. Surprisingly, the IntraSeasonal Kelvin wave (ISKw) has a much wider spectrum of variability ranging from (50 days)-1 to the semi-annual frequency with a particular energy peak in the (90 -120 days)-1 frequency band (Dewitte et al., 2008a). A recent study (Gushchina and Dewitte, 2012) also indicates

that the relationship between ENSO and the intraseaonal atmospheric variability could be distinct among the two types of El Niño. It appears important to document the characteristics of the IEKws and its relationship with the CP El Niño development and decay, considering that the ISKw is influential on the spread of ENSO forecasts (Wang et al., 2011) and that prediction systems exhibit a distinct forecast skill depending on the El Niño type (Hu et al., 2012; Xue et al., 2013).

On the other hand, it is also known that the Kelvin wave, when reaching the eastern edge of the Pacific Ocean, keeps moving poleward along the coast of the South-American continent. Along the Peruvian coast, the downwelling Kelvin wave can advect southward warm waters from Ecuador (mostly during strong El Niño events) and also deepens the thermocline, which may result in increasing the SST through vertical advection and/or mixing. Figure 1.3bis illustrates the eastward propagation of thermocline disturbances along the equator during the 2002 El Niño and the resulting SST anomaly along the coast of Peru. Regarding the relationship with the marine ecosystem, the downwelling Kelvin wave induces a reduced coastal upwelling and so a decreased nutrient enrichment (bringing to the surface oceanic warm and low nutrient waters; see Barber and Chavez, 1983). In particular, a warming event due to a downwelling Kelvin wave causes generally the anchovies to concentrate close to the coast and to migrate to deeper depths, which has been also suggested to influence the fishing vessels exploration's strategy (Bertrand et al., 2008). The increase of SST along the northern region of Peru in Austral summer, due to the impact of a Kelvin wave, also create an atmospheric instability that produces rains along the coasts of Peru and floods in the Piura region (Takahashi, 2004). The societal implications of the Kelvin wave dynamics along the coast of Peru are thus also motivating this work.

The general objective of this thesis is to better understand the interannual variability in the equatorial Pacific since 2000 considering the likely shift in ENSO dynamics at that period (McPhaden et al., 2011; McPhaden, 2012). In particular since 2000, the equatorial Pacific has experienced only Central Pacific El Niño events. The reason for this remains unclear. More specifically the thesis focuses on the equatorial dynamics with a particular interest on the intraseasonal timescales. In the rest of this chapter, more details about the state of art of ENSO theories, the CP El Niño characteristics and the Kelvin wave dynamics are provided. It is followed by a close

look at a peculiar Central Pacific El Niño event, the 2002/03 El Niño phenomenon - the first CP El Niño of the 21st century (Chapter 2). In this study, we investigate the mixed-layer processes associated with the long equatorial waves and we question whether such an event fits with the Recharge-Discharge theory. Then, in Chapter 3, this thesis addresses the intraseasonal timescales documenting the ISKw activity during CP El Niño events and investigating the processes associated with the dissipation of the ISKw. Finally, considering that El Niño is tightly linked to the seasonal cycle, we document the changes in characteristics of the seasonal cycle along the equator from before and after 2000 (Chapter 4). The approach for all chapters is based on the combined analysis of data (in situ and satellite) and model outputs, from a linear model (Mosquera, 2009; Mosquera et al., 2010) to Oceanic General Circulation Models (OGCM).

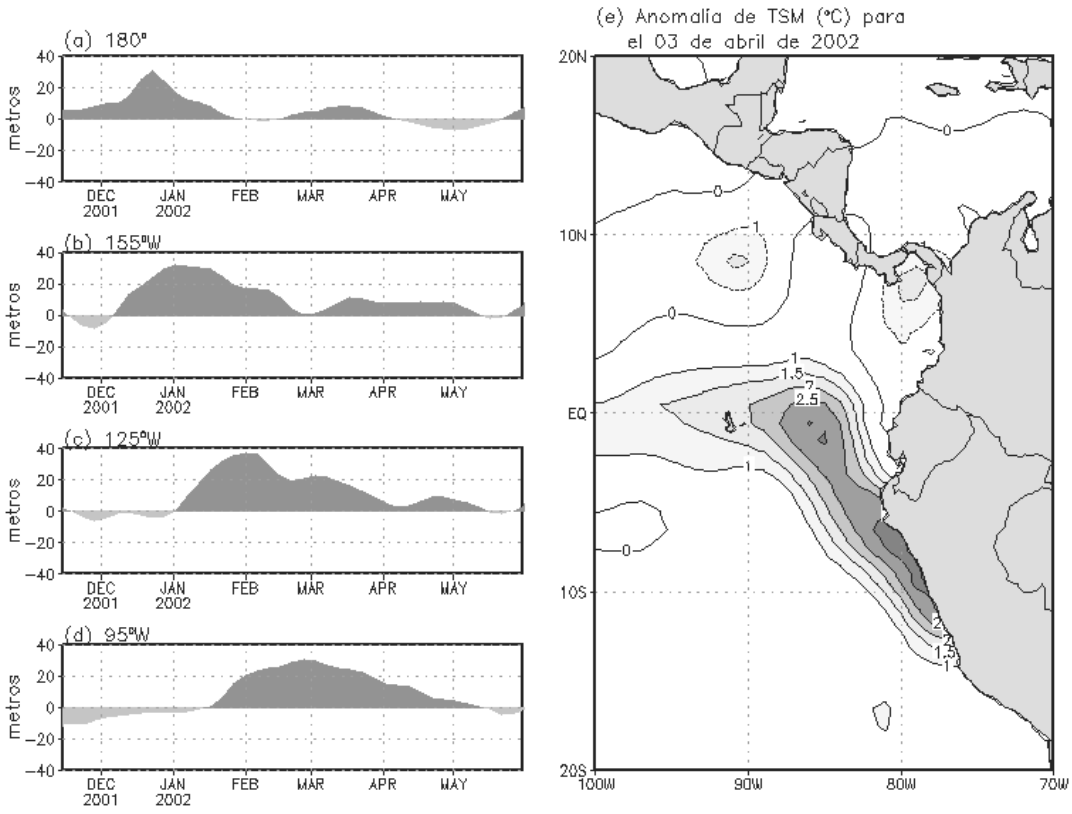

Figure 1.3bis On the left, time series of the thermocline depth (meters) anomaly along the equatorial Pacific estimated from TAO temperature profiles located in 180°E (a), 155°W (b), 125°W (c) and 95°W (d). On the right (e), the SST interannual anomaly (°C, relative to the 2000-2013 climatology) from Reynolds et al. (2002) is displayed for the 3rd of April 2002. Source: Mosquera (2014).

1.3 ENSO theories

1.3.1 Bjerknes theory

Whereas the meteorologist H. P. Berlage was the first to propose that El Niño could be linked to the large scale circulation in the tropical Pacific (Cushman, 2004), the first theory was proposed by Sir Bjerknes, following earlier works by Sir Walker that was sent to India to forecast the monsoon in order to improve the cotton production, an important raw material for Europe at that time. Sir Walker had observed that the fluctuations of pressure at Tahiti and Darwin were opposite and they were varying a lot from one year to the other. He used these data (the difference between both) to forecast the Indian monsoon that is now known to be related to ENSO. Sir Bjerknes (1969) was the first to propose that the east-west contrast in the equatorial ocean temperature during El Niño, in a warmer and colder eastern and western Pacific, respectively, could in turn generate a reduced atmospheric pressure in the east and an increased one in the west. This zonal contrast in pressure would result in winds from west to east, against normal atmospheric circulation (east to west) that Bjerknes baptized with the name of Walker circulation. These westerly winds favor further warming of the eastern Pacific, increasing the initial heating. This amplification process is now known as "Bjerknes feedback process" and is the basic theory that explains how an ENSO event grows in magnitude (see **Figure 1.4**).

1.3.2 The delayed oscillator

Even thought Bjerknes provided the first theory of El Niño, his theory could not explain the oscillatory nature of El Niño, which results from the fact that an El Niño event reverse to La Niña conditions and vice-versa. The delayed oscillator theory (Suarez and Schopf 1988; Battisti and Hirst, 1989) was an interesting concept that includes in its dynamic the long equatorial waves, Kelvin and Rossby, as the ingredients that allows the oscillatory property of El Niño. It is important to mention that the role of the long equatorial waves in the dynamics of the equatorial Pacific had been introduced in the 70's by Wyrtki (1975), McCreary (1976), Moore and Philander (1977) and Moore (1968).

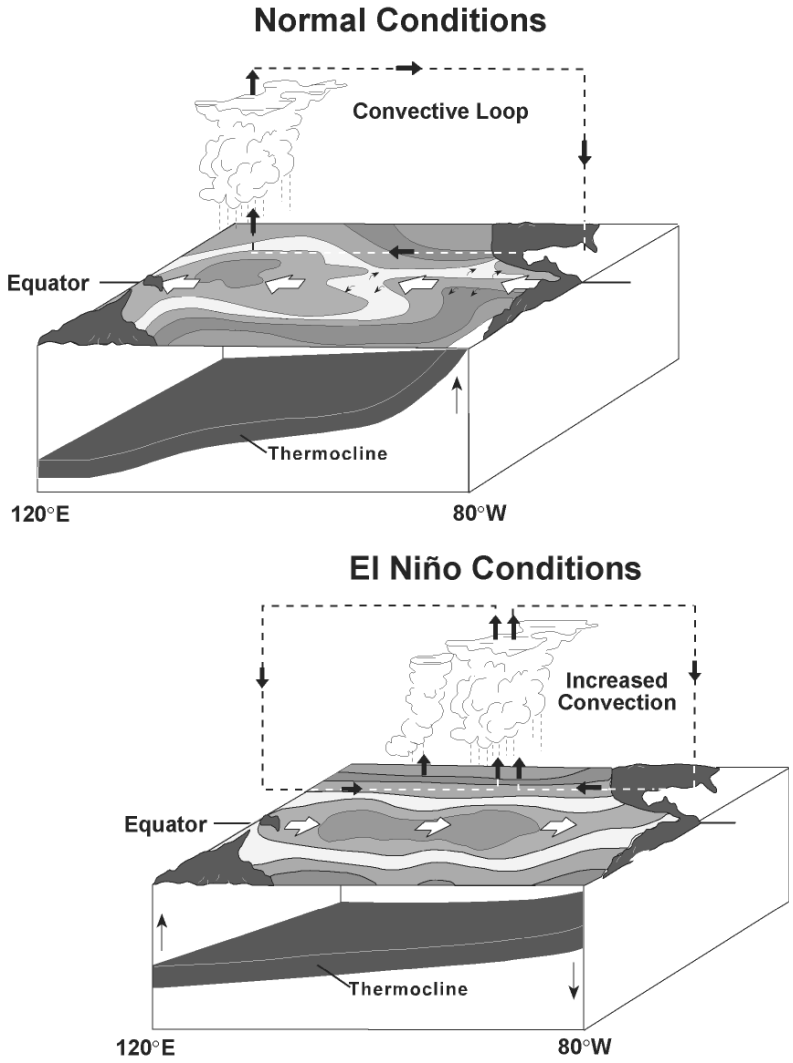

Figure 1.4 Schematic of normal and El Niño conditions in the equatorial Pacific (Figure 1 of McPhaden et al., 1998).

In general, the Delayed Oscillator Theory indicates that ENSO is an oscillatory system with an interaction between the atmosphere and ocean through the projection of eastward wind stress anomaly onto long equatorial oceanic waves. An eastward wind anomaly (westerly), generated by SST anomalies east of the dateline, drives a downwelling Kelvin wave that contributes to increase the SST anomalies in the eastern Pacific. The original eastward wind anomaly also forces a Rossby wave that propagates westward and is then reflected as an upwelling Kelvin wave at the western boundary. This Kelvin wave moves to the east and contributes with a negative feedback to the

coupled system. This process generates the alternation between El Niño and La Niña. **Figure 1.5** shows a schematic of this theory.

With the beginning of the satellite era dedicated to observing the earth surface, strong progresses were made in tropical dynamics. In particular, altimeters likes GEOdetic SATellite (GEOSAT) or more recent ones like TOPEX/POSEIDON and JASON series allowed for the investigation of long equatorial waves. Pioneered works in that field (Menkes et al., 1995ab; Boulanger and Menkes, 1995; Perigaud and Dewitte, 1996) led to a quantitative step in our understanding of the ENSO dynamics and testing paradigms (e.g. the delayed action oscillator). It takes about 12 months for a wave to go back and forth as Rossby wave from east to west, and as a reflected Kelvin wave from west to east. Meanwhile the period between El Niño and La Niña is 24 months. This was an inconsistency of the Delayed Oscillator Theory that encouraged developing other concepts.

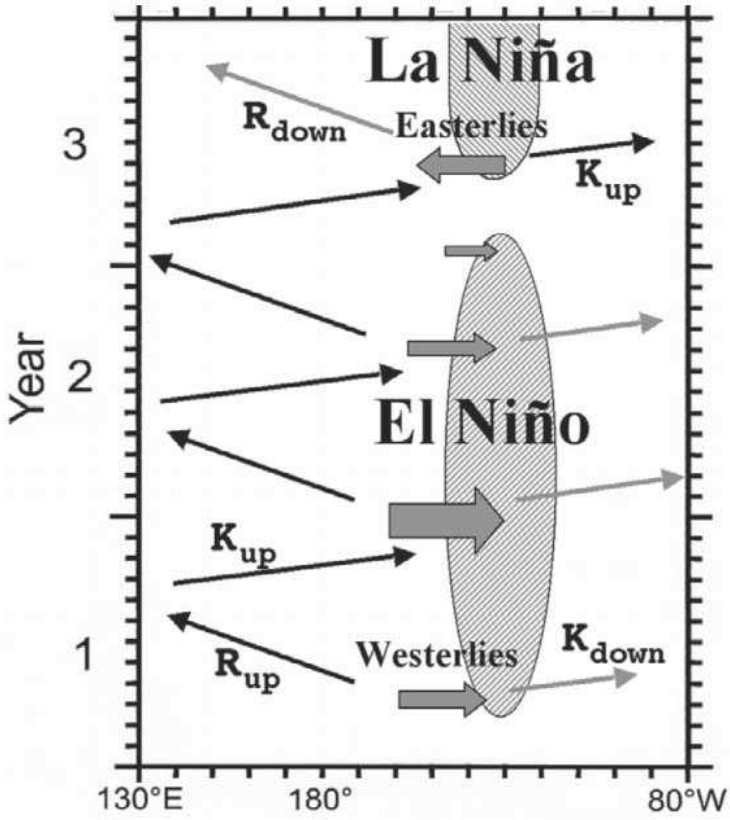

Figure 1.5 Schematic diagram of the delayed oscillator for ENSO. (After Wang and Picaut (2004))

1.3.3 Discharge and recharge oscillator theory

In front of the deficiency of the Delayed Oscillator, a new concept, named the Discharge and Recharge oscillator, was introduced (Jin, 1996; 1997). This model considers the importance of the heat content inside the Equatorial Pacific in the oscillatory process of ENSO. Clarke (2008) provided a comprehensive description of this theory and establishes an El Niño condition with a positive SST anomaly plus a depressed thermocline in the eastern Pacific (see **Figure 1.6 I**). The deep convection associated with the SST anomaly pattern induces eastward winds, which results in two consequences on the ocean: 1) eastward winds tilt the thermocline to the east increasing the heat content in the Eastern Pacific; and 2) they produce a Sverdrup poleward transport, allowing the evacuation of stored heat from the equatorial band. The latter is considered as the Discharged phase of the model that reduces the thermocline depth to values under the mean state (negative anomaly, **Figure 1.6 II**). This new thermocline depth influences the decreasing of the SST anomaly. The negative values of SST anomaly intensify with the presence of westward zonal currents anomalies that push the equatorial system to a Cool Phase (**Figure 1.6 III**). Finally, this new state induces westward zonal wind anomalies that transport warm water to the equatorial region. As a consequence, the system evolves to a Recharge phase (**Figure 1.6 IV**).

The fundamental mechanism for the oscillation is the delay between the adjustment of SST anomalies and the heat content of the entire basin (named WWV for Warm Water Volume). Note that the adjustment of the ocean in this model can be characterized through the temporal evolution of two zonal thermocline modes: a) “tilt” mode corresponding to the tipping (or tilting) of the thermocline around a pivot (located around 160°), and b) a WWV mode that corresponds to the heat accumulated in the equatorial band and that corresponds to a mode having its maximum (minimum) amplitude in the central Pacific. Clarke (2010) shows, in particular, that at interannual timescales, these modes incorporate the propagation of long equatorial Kelvin and Rossby waves. Thus, it may also explain the mechanism of recharge/discharge through the slow evolution of the residue (the WWV) from the propagation of the long equatorial waves, similar to the Delayed Oscillator Theory.

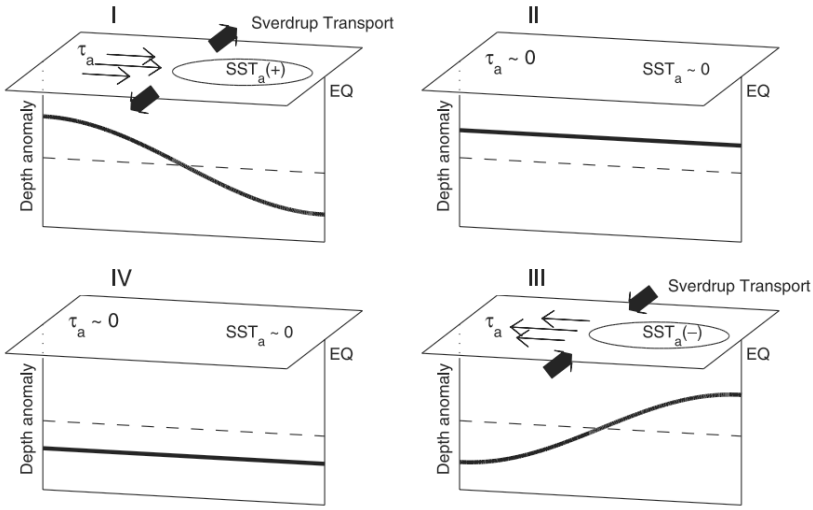

Figure 1.6 Schematic diagram of the four phases of the Recharge and Discharge Oscillator: (I) the warm phase, (II) the warm to cold transition, (III) The cold phase, and (IV) the cold to warm transition phase (from: Meinen and McPhaden, 2000).

1.4 The Central Pacific El Niño (CP El Niño)

The first El Niño of the 21th century took place in 2002/03 and has been categorized by the scientific community as a Central Pacific El Niño (CP El Niño) or Modoki El Niño. CP El Niño consists in a warming of the Sea Surface Temperature in the Central Pacific that is larger than the one occurring in the eastern Pacific at the peak phase of the event (see **Figure 1.7**), namely in December-January-February (DJF) (Ashok et al., 2007; Kug et al., 2009; Yeh et al., 2009). The occurrence of CP El Niño has increased in the recent decades (Lee and McPhaden, 2010; Yeh et al., 2009) and the last ten years has witnessed only El Niño events of this type, which has drawn the interest of the community in its dynamics and predictability (Ashok et al., 2007; Capotondi et al., 2015). Various hypotheses have been proposed to explain the emergence of such type of El Niño events since the 90s: First, changes in background state have been invoked which can result either from natural variability or anthropogenic activity. For instance, IPCC-class models predict an increased in stratification (i.e. shoaling thermocline depth in the central and western Pacific), which could modified the way the wind stress forcing projects onto to the ocean dynamics (Yeh et al., 2009). However the observations suggest that the thermocline in the western-central Pacific has deepened, which could be due to the residual effect of the

increased occurrence of CP El Niño (McPhaden et al., 2011). Other studies have suggested that non-linear processes could be involved due to La-Niña like conditions after 1990 (Xiang et al., 2013). The debate so far has been mostly on whether or not CP El Niño dynamics fits with the recharge-discharge theory (Jin, 1997). Kug et al. (2009) based on the NCEP Reanalysis product conclude that the discharge process of the equatorial heat content associated with the CP El Niño is not efficient due to the spatial structure of SST anomaly. They also show from composite analysis that the zonal advective feedback (i.e. zonal advection of mean SST by anomalous zonal currents) plays a crucial role in the development of a decaying SST anomaly associated with the CP El Niño, while the thermocline feedback is a key process during the EP El Niño. The decay phase of the CP El Niño is in their view controlled by thermal damping. Despite this contrasted feature in the dynamics of the CP and EP events, the classification of the El Niño into two types may still be oversimplified. In fact Kug et al. (2009) introduced three types of El Niño, i.e., CP, EP, and a mixed type, which corresponds to SST anomalies peaking in the NINO34 region [5°S-5°N; 170-120°W]. For instance, the last El Niño to date that took place in 2009-2010 can be categorized as a CP El Niño (Kim et al. 2011) but its ocean dynamical behavior resembles the EP El Niño. Yu et al. (2011) also propose to define CP El Niño and mixed-type El Niño based on subsurface indices that are more appropriate to capture the specificities of the events and account for the larger diversity of the El Niño types in nature than what is generally simulated by models (Yu and Kim, 2010; Kug et al., 2010; Dewitte et al., 2012). Takahashi et al. (2011) somehow reconciles these studies proposing to classify the El Niño event according to their privileged regimes defined in their study from the first two PC (Principal Component) time series of the SST anomalies in the tropical Pacific. In particular, the mixed-type El Niño of Kug et al. (2009) fits perfectly with the C regime of Takahashi et al. (2011) in terms of its spatial pattern, which suggests that within a regime, El Niño event can have in fact a different dynamics. A dynamically-based classification of the El Niño event is probably required, which implies documenting the balance between processes controlling the rate of SST changes in the equatorial Pacific during the evolution of these types of El Niño events.

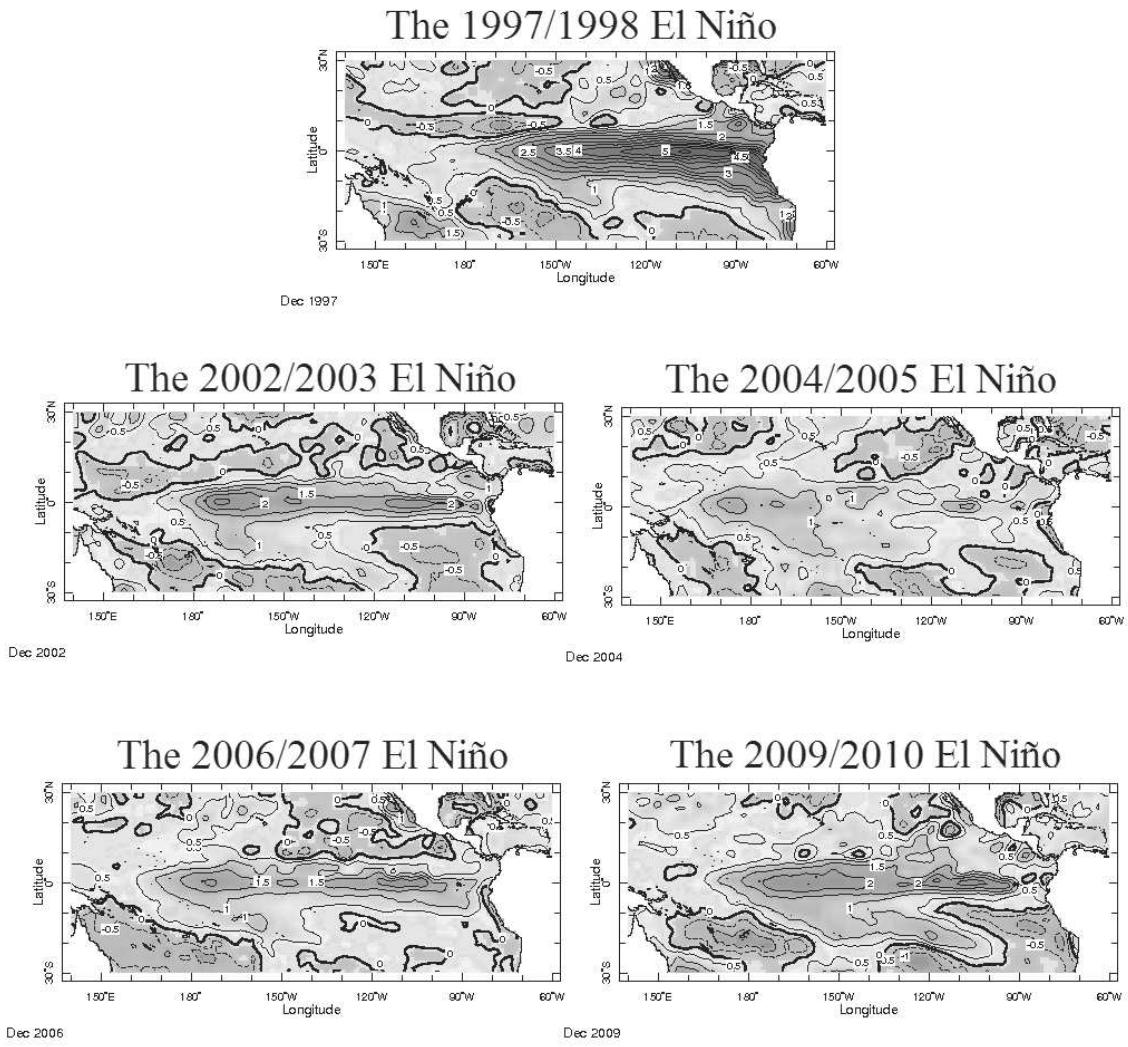

Figure 1.7 SST anomalies (Reynolds et al., 2002) for the month of December for five El Niño events since 1997. Pictures were created using the IRI Data Library (http://iridl.ldeo.columbia.edu/)

1.5 ENSO and the Kelvin wave

As it was mentioned in the previous section, the oceanic Kelvin has an important role in the development of El Niño. This disturbance can be forced by the zonal winds anomalies in the Equatorial Pacific, or by the reflection of Rossby waves on the western edge of the Pacific. Kelvin wave has the property of moving eastward with a typical theoretical speed of 2-3 meters per second (equivalent speed of the first baroclinic mode). This means, for example, that if a Kelvin wave is formed in the central

equatorial Pacific (around dateline), this will take between 1.5 month and two months to reach the South American coast (see **Figure 1.8**).

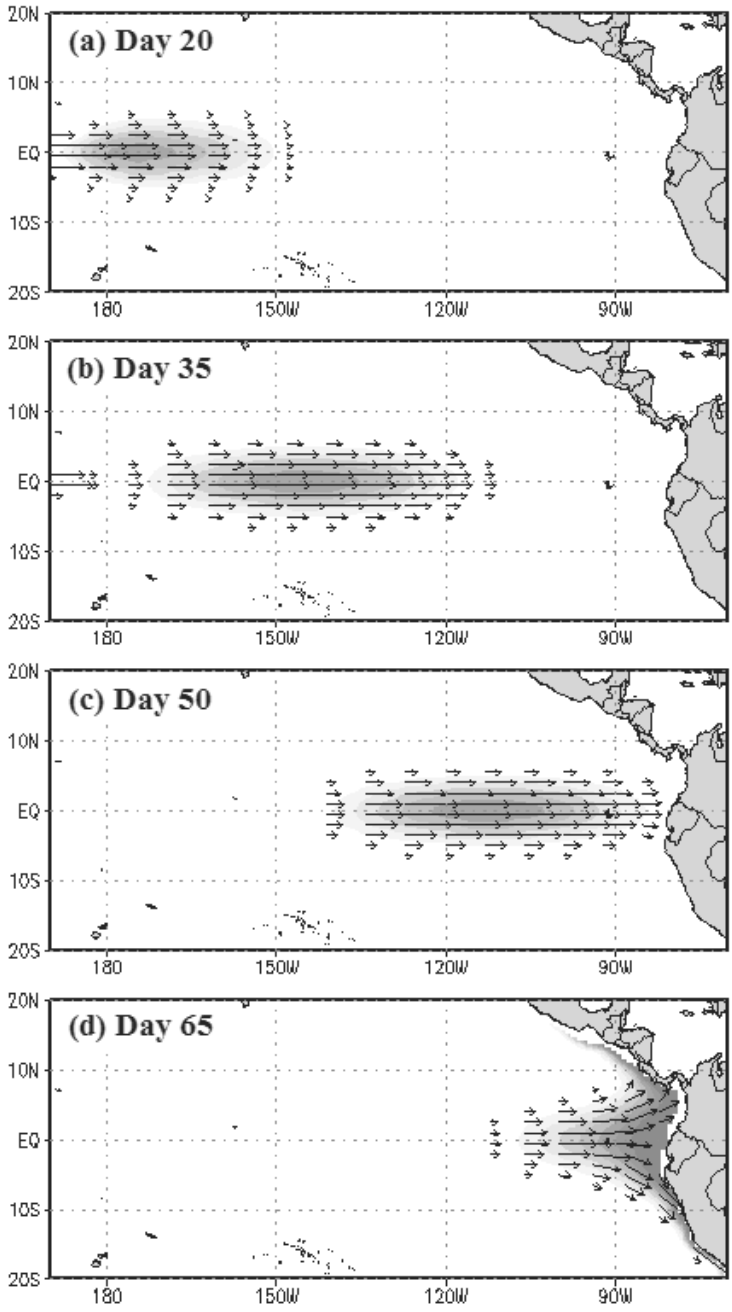

Figure 1.8 Evolution of an equatorial Kelvin wave simulated with a linear oceanic model (Mosquera, 2009) through the Equatorial Pacific. The model was forced during 30 days with a positive zonal wind anomaly (with a magnitude of 9 ms^{-1} as its maximal intensity in day 15). Sea level anomaly is displayed in colors and surface current anomalies are overplotted with black arrows. Source: Mosquera (2014).

Concerning its impact on state of the equatorial Pacific, Kelvin waves could be divided in two types: 1) Downwelling Kelvin wave, which is characterized by positive subsurface temperature anomaly, a deeper thermocline, sea level rise, and anomalies of currents from west to east, and 2) Upwelling Kelvin wave, with opposite characteristics.

As it was mentioned, Kelvin waves influence the Sea Surface Temperature through various processes. Anomalous currents associated with the wave may cause displacement of the cold or warm surface waters. While this effect can take place along the whole equatorial Pacific, it is prominent in the western region, where a downwelling or upwelling wave can advect the edge of the "warm pool" eastward or westward, respectively (see **Figure 1.9b** and **1.9d**). Also, the Kelvin wave can deepen or rise the thermocline (see **Figure 1.9c**), affecting the process of upwelling of cold water, producing an increase or decrease of the SST, respectively (**Figure 1.9d**), mostly in regions where the thermocline is shallow and/or the vertical stratification is marked.

Kelvin wave activity can also take place at a wide range of frequencies, from intraseasonal to interannual timescales. Most studies have focused on the interannual Kelvin wave because it is clearly observed from altimetry (Boulanger and Menkes, 1995; Perigaud and Dewitte, 1996; Boulanger and Fu, 1996) and is involved in strong El Niño events like the 1997/98 El Niño (Boulanger and Fu, 1996; Dewitte et al., 2002). The intraseasonal Kelvin wave has been observed as resulting from westerly wind events (WWBs) prior to the development of El Niño, in particular during strong events (Lengaigne et al., 2002). The intraseasonal Kelvin wave is in fact associated with the intraseasonal atmospheric variability that spans a wide range of frequencies and phenomenon. The later is composed of the Madden-Julian Oscillation (MJO), the Convectively Coupled Equatorial Waves (CCEW), Westerly Wind Burst (WWB) and Easterly Wind Surges (EWS). MJO is a source of variability with periods between 30 and 90 days in the tropical atmosphere. This oscillation is considered as a large-scale coupled process between atmospheric circulation and deep convection. All the disrupted variables in this process propagate to the east with a speed around 5 m s^{-1} (Zhang, 2005). MJO has been considered as a key factor to the onset of the 1997-1998 El Niño through episodes of westerlies that triggered downwelling Intraseasonal Kelvin waves (ISKw).

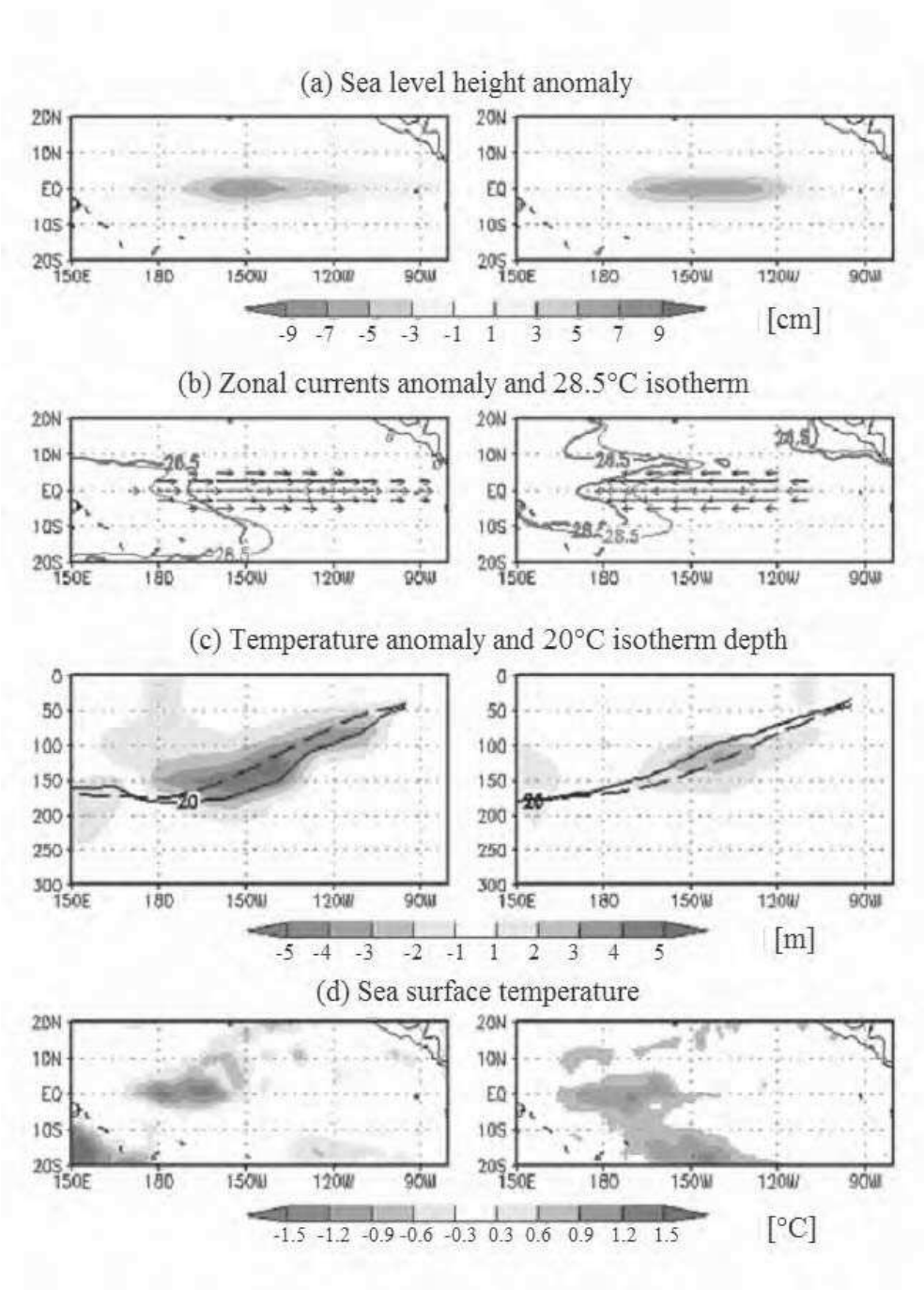

Figure 1.9 Impact of downwelling (left) and upwelling (right) Kelvin wave on January 2002 and September 2008, respectively, over: (a) Sea level, (b) zonal currents and 28.5°C isotherm from Reynolds OISST with thick (thin) blue line representing the total (climatology) SST, (c) temperature and 20°C isotherm depth with solid (dashed) black line representing the total (climatology) values, and (d) SST from Reynolds OISST. Source: Mosquera (2014)

The CCEW may be considered as having a ‘‘stochastic’’ character relative to the slow oceanic processes. This kind of atmospheric waves results from the interaction between convection and the atmospheric dynamics in the tropical Pacific. Theoretically, CCEW, which can be observed from Ongoing Long wave Radiation, are associated to atmospheric Kelvin and Rossby waves with an equivalent depth around 12-50 meters (see Wheeler and Kiladis (1999) for details). Like the MJO, their activity has a marked seasonal cycle, and through their imprint on wind stress can act on the ocean dynamics.

WWB can form under favorable conditions (i.e. When MJO activity is enhanced (Puy et al., 2015)) and consists in a westerly gust in the equatorial Pacific that has a period around 5-20 days and an intensity of at least 7 $m.s^{-1}$ (Harrison and Vecchi, 1997). In addition, WWB activity is associated with the onset of El Niño through the formation of downwelling Kelvin waves (Latif et al., 1988; Lengaigne et al., 2004, Luther et al., 1983; Perigaud and Cassou, 2000).

Recently EWS have been identified and documented (Chiodi and Harrison, 2015). It is a wind stress event with amplitude between 6 and 7 m s^{-1} and with a temporal scale of 6 and 7 days. EWS has an important impact in the dynamic and thermodynamic of the Tropical Pacific and is related with the onset of cold tongue cooling in La Niña event (Chiodi and Harrison, 2015).

Intraseasonal atmospheric variability is tightly linked to ENSO. There is in particular a seasonal relationship associated to strong Eastern Pacific El Niño, with WWBs forcing ISKw prior to the development of the event (Bergman et al., 2001; McPhaden et al., 2006). In particular the 1997/98 El Niño was associated with three pulses of ISKw prior to its development (Dewitte et al., 2003) which may have triggered the initial warming in the central Pacific leading to the growth of the SST anomalies (Lengaigne et al., 2004). The 1997/98 El Niño is rather peculiar because the peak activity of the ISKw took place ~6 months prior the El Niño peak (Ramos et al., 2008), which reflects the strong seasonal dependence of the MJO/ENSO relationship (i.e. MJO peak variance being in May-June prior to the ENSO peak in Nov.-Dec.) described in former studies (Hendon et al., 2007; McPhaden et al., 2006). Recent studies (Gushchina and Dewitte, 2012) have suggested that this seasonal dependence of

the MJO/ENSO relationship could be changed over the last decades due to the predominance of Central Pacific El Niño events.

1.6 Processes impacting the Kelvin wave in the equatorial Pacific.

As we will see in Chapter 3, CP El Niño events are tightly linked to the ISKw activity, which may explain its persistence and its seasonal evolution. The fact that CP El Niño events are not associated with a large SST anomaly in the eastern Pacific also suggests that the ISKw does not impact efficiently the SST through the thermocline feedback despite a shallow mean thermocline. The ISKw actually experience dissipation as it propagates eastwards. There is a variety of processes of dissipation through which the characteristics of ISKw (flux, phase speed, amplitude and vertical structure) can be altered in its displacement to the Eastern Pacific.

The tilt of the thermocline around 120ºW can changes the ISKw's amplitude, phase speed, vertical and meridional structure as it reaches the eastern Pacific due the difference of the vertical structure of ISKw from West to East (Dewitte et al., 1999). Also, the thermocline tilt, from the theoretical point of view, can produce a significant dispersion through its impact on stratification resulting in scattering of energy (Busalacchi and Cane, 1988; Giese and Harrison, 1990). The mixing produced by the Tropical Instability Waves (TIW; Luther and Johnson, 1990) in the eastern Pacific (where the thermocline is shallow and close to the mixed layer) affects the characteristics of ISKw through changes in the vertical stratification.

The physical mechanism responsible for changing the Kelvin wave characteristic that will be discussed in this thesis is the so-called modal dispersion mechanism (Busalacchi and Cane, 1988; Giese, 1989; Giese and Harrison, 1990; Dewitte et al., 1999). Modal dispersion occurs when the equatorial Kelvin wave experience a change in vertical structure (due to a change in vertical stratification). In this case, there is a leak of energy from the gravest baroclinic modes to the higher-order modes, and *vice versa*. Due to the fact that the mean thermocline varies at seasonal to interannual timescales, there is the possibility that the ISKw interacts with the mean thermocline through modal dispersion leading to an energy cascade. The modal dispersion can also act on the amplitude of the high-order baroclinic modes Kelvin wave, which can

influence the coastal circulation in Ecuador and Peru. In particular depending on the energy distribution on each baroclinic mode, the equatorial Kelvin wave can either be coastally trapped or can radiate off-shore as Rossby wave north of the critical latitude (Clarke and Shi, 1991; Dewitte et al., 2008b).

Chapter 2: The 2002/03 El Niño: Equatorial waves sequence and their impact on Sea Surface Temperature

2.1 Overview

In 2002, a strong equatorial Kelvin wave was triggered in Austral Summer producing an alert in the international agencies responsible for monitoring the global climate. The scenario was indeed very similar to 1997, when an extraordinary El Niño developed. However, according to current definitions, this event is now considered as a Central Pacific El Niño (CP El Niño) (Yeh et al., 2009; Takahashi et al., 2011) and did not develop as a strong Eastern Pacific El Niño. Along the equator, the 2002/03 El Niño is characterized by a comparable warming of the NINO3 (150°W-90°W; 5°S-5°N) and NINO4 (150°E-150°W; 5°S-5°N) regions of the order of 1°C. However, while during the developing phase, the NINO3 index is above the NINO4 index, at the peak phase (December-January-February season) the warming in the western Pacific is slightly larger, which implies its Central Pacific-type following Yeh et al. (2009). This event has been well observed and documented (McPhaden, 2004). There has been however very few studies that took a close look at its dynamics and thermodynamics. In this chapter, an OGCM (Ocean General Circulation Model) simulation is used to carry out a heat budget of the evolution of this particular El Niño event, highlighting the contribution of locally and remotely forced variability to the advection terms. The proposed analysis is aimed at providing material for the interpretation of the evolution of this event in the light of current ENSO theories, and in particular the recharge-discharge mechanism (Jin, 1997).

This chapter contains a paper published in Journal of Geophysical Research-Ocean that focuses on the 2002/03 El Niño event (Mosquera-Vásquez et al., 2013) and investigates the sequence of equatorial waves and their impact on zonal and vertical advection processes. In order to test the robustness of our results, the investigation of the first CP El Niño of the XXIst century is followed by complementary analyses (Section 2.3), which can be considered as an extension of Mosquera-Vásquez et al. (2013) and that investigate the dynamics and thermodynamics of other El Niño events over the period 1989-2011.

2.2 Article published in Journal Geophysical Research- Oceans

The 2002/2003 E Niño: Equatorial wave sequence and their impact on sea surface temperature

Kobi A. Mosquera-Vásquez, Boris Dewitte and Serena Illig

Abstract

The recent decades have experienced changes in the characteristics of the El Niño phenomenon, with in particular an increased occurrence of so-called Modoki or Central Pacific El Niños. Here the 2002/2003 El Niño, characterized as a Central Pacific El Niño, is studied from an Ocean General Circulation Model simulation. The focus is on the sequence of equatorial waves and their impact on zonal and vertical advection. The wave amplitude according to the most energetic baroclinic modes are first estimated, which allows inferring the sequence of the intraseasonal equatorial Kelvin (IKW) and Rossby (IRW) waves. It is shown that energetic downwelling IKWs, forced in the western-central Pacific, crossed the equatorial Pacific. Reflections of IKWs into IRWs onto the zonally varying thermocline and eastern boundary are also observed. A simplified heat budget of the surface layer is then carried out to infer the dominant processes at work during the evolution of this event focusing on the wave-induced advection terms. The results indicate that the warming phase (April–November 2002) is mainly controlled by zonal advection of mean temperature (accounted for by IKWs and locally wind-driven current) and by vertical advection in the eastern Pacific. The cooling phase (December 2002 to April 2003) is dominated by a reduction in solar radiation and the IRW-induced zonal advection of mean temperature respectively in the central and eastern equatorial Pacific. The recharge-discharge process is also showed to be at work with the recharge (discharge) process operating mainly through the second (first) baroclinic mode.

The 2002/2003 El Niño: Equatorial waves sequence and their impact on sea surface temperature

K. Mosquera-Vásquez,[1,2] B. Dewitte,[1,2] S. Illig,[1,2] K. Takahashi,[1] and G. Garric[3]

Received 25 September 2012; revised 30 November 2012; accepted 3 December 2012; published 30 January 2013.

[1] The recent decades have experienced changes in the characteristics of the El Niño phenomenon, with in particular an increased occurrence of so-called Modoki or Central Pacific El Niños. Here the 2002/2003 El Niño, characterized as a Central Pacific El Niño, is studied from an Ocean General Circulation Model simulation. The focus is on the sequence of equatorial waves and their impact on zonal and vertical advection. The wave amplitude according to the most energetic baroclinic modes are first estimated, which allows inferring the sequence of the intraseasonal equatorial Kelvin (IKW) and Rossby (IRW) waves. It is shown that energetic downwelling IKWs, forced in the western-central Pacific, crossed the equatorial Pacific. Reflections of IKWs into IRWs onto the zonally varying thermocline and eastern boundary are also observed. A simplified heat budget of the surface layer is then carried out to infer the dominant processes at work during the evolution of this event focusing on the wave-induced advection terms. The results indicate that the warming phase (April–November 2002) is mainly controlled by zonal advection of mean temperature (accounted for by IKWs and locally wind-driven current) and by vertical advection in the eastern Pacific. The cooling phase (December 2002 to April 2003) is dominated by a reduction in solar radiation and the IRW-induced zonal advection of mean temperature respectively in the central and eastern equatorial Pacific. The recharge-discharge process is also showed to be at work with the recharge (discharge) process operating mainly through the second (first) baroclinic mode.

Citation: Mosquera-Vásquez, K., B. Dewitte, S. Illig, K. Takahashi, and G. Garric (2013), The 2002/2003 El Niño: Equatorial waves sequence and their impact on sea surface temperature, *J. Geophys. Res. Oceans*, *118*, 346–357, doi:10.1029/2012JC008551.

1. Introduction

[2] The first El Niño of the 21st century took place in 2002/2003 and has been categorized for the scientific community as a Central Pacific El Niño (hereafter CP El Niño) or Modoki El Niño. CP El Niño consists in a warming of the sea surface temperature (SST) in the central Pacific that is larger than the one occurring in the eastern Pacific at the peak phase of the event, namely in December-January-February (DJF) [*Ashok et al.*, 2007; *Kug et al.*, 2009; *Yeh et al.*, 2009]. The occurrence of CP El Niño has increased in the recent decades [*Lee and McPhaden*, 2010; *Yeh et al.*, 2009] and the last 10 years has witnessed only El Niño events of this type, which has drawn the interest of the community in its dynamics and predictability [*Ashok et al.*, 2007]. *Kug et al.* [2009] tested the recharge-discharge process [*Jin*, 1997] that applies for the so-called eastern Pacific (hereafter EP El Niño) to this type of event based on a reanalysis product. They conclude that the discharge process of the equatorial heat content associated with the CP El Niño is not efficient owing to the spatial structure of SST anomaly. They also show from composite analysis that the zonal advective feedback (i.e., zonal advection of mean SST by anomalous zonal currents) plays a crucial role in the development of a decaying SST anomaly associated with the CP El Niño, while the thermocline feedback is a key process during the EP El Niño. Despite this contrasted feature in the dynamics of the CP and EP events, the classification of the El Niño into two types may still be oversimplified. In fact *Kug et al.* [2009] introduced three types of El Niño, i.e., CP, EP, and a mixed type, which corresponds to SST anomalies peaking in the NINO34 region (5°S–5°N; 170°W–120°W). For instance, the last El Niño to date that took place in 2009–2010 can be categorized as a CP El Niño [*Kim et al.*, 2011] but its ocean dynamical behavior resembles the EP El Niño. *Yu et al.* [2011] also propose to define CP El Niño and mixed-type El Niño based on subsurface indices that are more appropriate to capture the specificities of the events and account for the larger diversity of the El Niño types in nature than what is generally simulated in models [*Yu and Kim*, 2010; *Kug et al.*, 2010; *Dewitte et al.*, 2012]. *Takahashi et al.* [2011] somehow reconciles these studies proposing to classify the El Niño event according to their

[1]Instituto Geofisico del Perú (IGP), Calle Badajoz N° 169-171, Urbanización Mayorazgo, IV Etapa, Lima 3, Perú.
[2]LEGOS, 18, av. Edouard Belin, 31401, Toulouse cedex 9, France.
[3]MERCATOR, 8-10 rue Hermès, 31520, Ramonville St-Agne, France.

Corresponding author: K. Mosquera-Vásquez, Instituto Geofisico del Perú (IGP), Calle Badajoz N° 169–171, Urbanización Mayorazgo, IV Etapa, Lima 3, Perú. (kobi.mosquera@igp.gob.pe)

2169-9275/13/2012JC008551

privileged regimes defined in their study from the first two principal component time series of the SST anomalies in the tropical Pacific. In particular, the mixed-type El Niño of *Kug et al.* [2009] fits perfectly with the so-called C regime of *Takahashi et al.* [2011] in terms of its spatial pattern, which suggests that within a regime, El Niño event can have in fact a different dynamics. A dynamically based classification of the El Niño event is probably required, which implies documenting the balance between processes controlling the rate of SST changes in the equatorial Pacific during the evolution of these types of El Niño events. This study lies into this line of research focusing on the 2002/2003 El Niño, a CP El Niño according to current definitions [*Yeh et al.*, 2009; *Takahashi et al.*, 2011]. As an illustration, Figure 1 presents the evolution of the observed SST, sea surface height (SSH), 20°C isotherm depth anomalies over two different regions along the equator and along the coast of Peru. Along the equator, the 2002/2003 El Niño is characterized by a comparable warming of the NINO3 (150°W–90°W; 5°S–5°N) and NINO4 (150°E–150°W; 5°S–5°N) regions of the order of 1°C. However, whereas during the developing phase, the NINO3 index is above the NINO4 index, at the peak phase (December–January-February season) the warming in the western Pacific is slightly larger, which implies its central Pacific-type following *Yeh et al.* [2009]. As a consistency check of the nature of this El Niño event, we verify that it belongs to the C regime defined by *Takahashi et al.* [2011]: Figure 1d presents the evolution of these indices over the period of interest (based on HadISST data [*Rayner et al.*, 2003]). It shows that the *C* index is positive with values above its standard deviation where the *E* index is mostly negative except around November 2002 when it peaks to ~0.8°C. Clearly, the 2002/2003 El Niño belongs to the *C* regime but it also evidences some contribution from the *E* regime, which reflects its mixed nature. Interestingly, this CP El Niño is also associated to pulses of warm SST anomalies

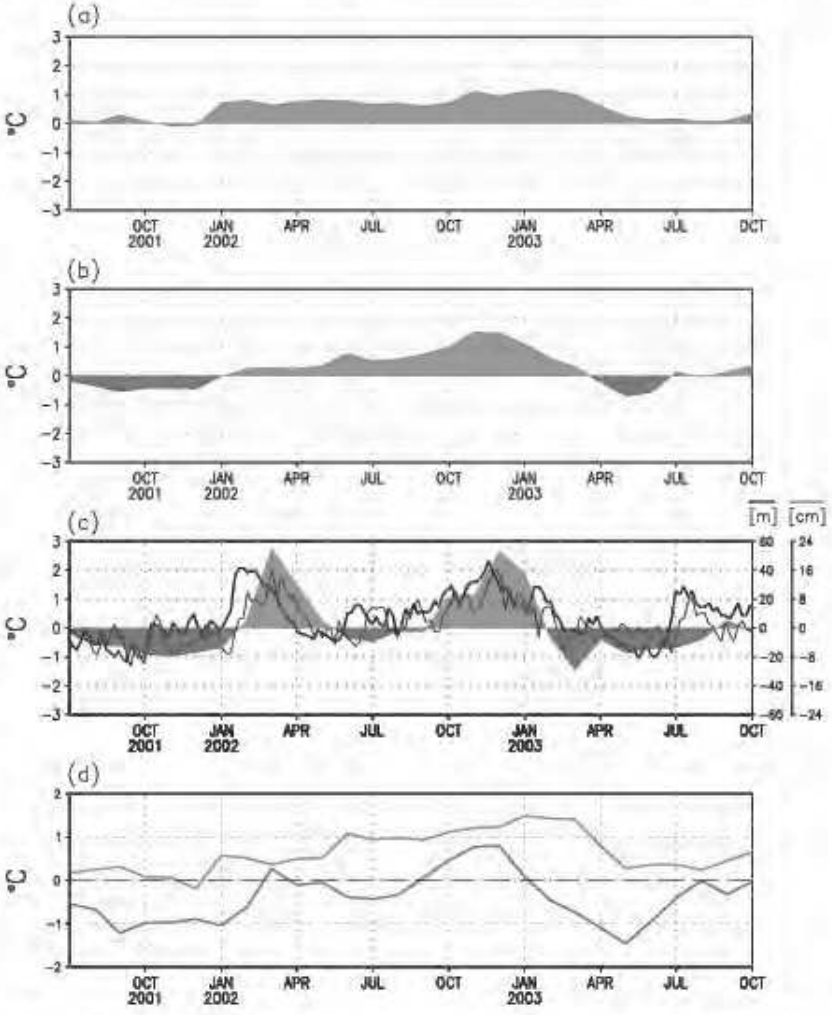

Figure 1. Time series for the period July 2001 to October 2003. Bicolor (red/blue) filled plot represents the TMI's SST anomaly for (a) NINO4 (150°E–150°W; 5°S–5°N), (b) NINO3 (150°W–90°W; 5°S–5°N), and (c) *Puerto Chicama* coastal station (Courtesy of IMARPE). In Figure 1c, thick (thin) black line indicates the 20 °C isotherm depth (sea level height) anomaly, in meters (centimeters), from TAO Project (Lobos de Afuera coastal station located at the Peruvian coast) at the equator (6°56′S) and 110°W (80°43′W). (d) The *C* (red) and *E* (blue) indices as defined in *Takahashi et al.* [2011]. Anomalies are relative to the climatology over 2000–2008 for Figures 1a, 1b, and 1c and over 1958–2008 for Figure 1d.

near the coast of Peru (Figure 1c) that may correspond to the arrivals of downwelling Kelvin waves at the Ecuadorian coast (Figure 1c), as suggested by the good correspondence of the SST anomalies at Chicama (8°S) and either the 20°C isotherm depth anomaly at 110°W or the sea level anomalies at Lobos de Afuera coastal station (Figure 1d). These perturbations observed at the coast suggest their intraseasonal nature because there is no corresponding anomalies of the NINO3 index and intraseasonal equatorial Kelvin wave are theoretically trapped at these frequencies [*Clarke and Shi*, 1991]. It indicates that the 2002/2003 El Niño was associated to energetic equatorial wave forcing. Still, the 2002/2003 El Niño, the first El Niño of this century, was very different from its predecessor in terms of magnitude, evolution and teleconnection [*McPhaden*, 2004]. *McPhaden* [2004] provided a comprehensive description of the evolution of this unusual event from the TAO array data and satellite observations. Whereas this event gathered some ingredients of the canonical El Niño-Southern Oscillation (ENSO), namely a build-up in heat content along the equator two to three seasons prior to its onset as well as strong Madden-Julian Oscillation related westerly winds prior to the peak phase, it was surprisingly weaker than the 1997/1998 El Niño. This was argued to be the results of processes (not identified) counteracting the tendency for remote forcing to deepen the thermocline in the eastern basin, leading to weaker SST anomalies that would have been expected there. The resulting anomalous zonal SST contrast suggests that the large-scale ocean-atmosphere feedbacks may not have fully engaged to amplify and sustain the El Niño warming. On the other hand, episodic westerlies, particularly that are related to the Madden-Julian Oscillation, may have participated to the persistence of warm anomalies in the central Pacific through the forcing of downwelling Kelvin waves. As pointed out by *McPhaden* [2004], a better understanding of the factors giving rise to the unusual SST pattern of the 2002/2003 El Niño requires a quantitative evaluation of the processes from a coupled ocean-atmosphere perspective. This is the objective of this paper that focuses on the analysis of the equatorial Kelvin waves and their contribution to the main ENSO feedback processes, namely the zonal advective feedback and the thermocline feedback. In particular, we use an OGCM (Ocean General Circulation Model) simulation to carry out a heat budget of the evolution of the 2002/2003 El Niño, highlighting the contribution of locally and remotely forced variability to the advection terms. The proposed analysis is aimed at providing material for the interpretation of evolution of this event in the light of current ENSO theories, and in particular the recharge-discharge mechanism [*Jin*, 1997].

[3] The paper is organized as follows: Section 2 describes the data sets, the model, and the methods. Section 3 provides a description of the wave sequence during the 2002/2003 El Niño and then analyzes the results of a simplified heat budget model during the different phases of the event. Section 4 is a discussion followed by concluding remarks.

2. Data and Methods Description

[4] The study is based on the analysis of an OGCM simulation over the period 2000–2008 that was previously validated from in situ and satellite observations (see section 2.4). The mean circulation and intraseasonal to interannual variability (anomalies) of the model are considered. Anomalies are calculated as the deviation from the mean seasonal cycle over the period 2000–2007. The seasonal cycle is derived from the monthly mean of the data, which is then interpolated on a 3 day mean temporal grid using spline functions. The seasonal cycle was smoothed with a 1-2-1 filter before calculating anomalies. The same postprocessing is performed for all data sets used in this study.

2.1. Temperature and Zonal Currents From TAO

[5] In situ temperature and current data from the Tropical Atmosphere Ocean (TAO) project array [*Hayes et al.*, 1991; *McPhaden et al.*, 1998] were used in this study for validating the model skills along the equator (see section 2.4). Vertical profiles of zonal current data from equatorial TAO moorings are considered at four sites: 147°E, 165°E, 140°W, and 110°W, whereas temperature data are taken at the 10 TAO mooring sites (147°E, 156°E, 165°E, 180°, 170°W, 155°W, 140°W, 125°W, 110°W and 95°W). The last group is used to derive the depth of the 20°C isotherm that is taken as a proxy for the thermocline depth. Daily current and temperature data were averaged into 3 day mean to compare with model outputs.

2.2. Sea Surface Temperature From Tropical Rainfall Measuring Mission Microwave Imager

[6] The 3 day mean SST data as derived from the Tropical Rainfall Measuring Mission Microwave Imager (TMI) (*Wentz et al.* [2000], http://www.remss.com/) is compared to the output model temperature at 0.49 m (the first vertical level) along the equatorial line. The estimated SST is based mainly on emissions at 10.7 GHz, and is also largely uninfluenced by cloud cover, rain, aerosols and atmospheric water vapor [*Wentz et al.*, 2000]. However, the microwave retrievals are sensitive to (wind-induced) sea-surface roughness. TMI comparisons with buoys give an RMS error of about 0.6 K [*Wentz et al.*, 2000] due to a combination of instrumental (buoy) collocation error [*Gentemann et al.*, 2003]. Comparisons of the TMI SST product with buoy-measured near-surface ocean temperature show that, on greater than weekly time scales, TMI SST reproduces the characteristics of the 1 m buoy-observed temperatures in the tropical Pacific [*Chelton et al.*, 2001].

2.3. Sea Level Height From Merged Product TOPEX-POSEIDON/JASON

[7] The gridded sea level anomaly data were supplied by AVISO/altimetry [*Ducet et al.*, 2000]. They were built by optimal interpolation of *T*/*P* and ERS data on a 1/4° × 1/4° grid every 10 days. If a precision of individual instantaneous measurements is of order of 6 cm RMS [*Fu et al.*, 1994], errors on such gridded data is estimated to 2–3 cm RMS for 10 day map and spatial scales of order of 200 km and more [*Le Traon and Ogor*, 1998].

2.4. OGCM Simulation

[8] The outputs of the MERCATOR global OGCM (http://www.mercator-ocean.fr/html/produits/index_en.html) are used. MERCATOR is an eddy-permitting ¼° model, based on the primitive-equation global ocean general circulation model Océan PArallélisé [*Madec et al.*, 1998] and developed

at the Laboratoire d'Océanographie et du Climat: Expérimentations et Approches Numériques. The model was forced with daily surface atmospheric conditions from the European Center for Medium Range Weather Forecast Integrated Forecast System analysis. The simulation is hereafter referred to as MERCATOR (see *Garric et al.* [2008] for more details). Here the experiment was initialized on 4 April 1998 with an ocean at rest and climatologic temperature and salinity from *Levitus et al.* [1998] data set. Three key fields were analyzed for the model validation: (1) the mean SST and its variability, (3) the mean thermocline depth and its variability, and (3) the sea level variability. Figure 2 presents the results of the comparison between observations and the simulation for these different fields along the equatorial line. It indicates that the model is skillful in capturing most aspects of the observed variability. In particular, the thermocline variability along the equator is rather realistic with correlation between model and observations reaching 0.76 on average along the equator. Such skill is comparable to other Reanalysis products like Simple Ocean Data Assimilation or Global Ocean Data Assimilation System for the monthly average outputs (not shown). Model biases include a tendency to simulate a slightly weaker SST anomaly variability than the observations and a cooler mean SST in the model (by ~1°C). The comparison between model and observation for SST, thermocline and sea level is summarized in Table 1. Comparison of model vertical zonal current (anomalies) and Acoustic Doppler Current Profiler measurements from TAO indicates that the model also realistically simulates the zonal circulation (see Table 2). This simulation was used in a recent study to derive an estimate of the intraseasonal equatorial Kelvin wave over 2000–2008 [*Dewitte et al.*, 2011].

Table 1. Validation of MERCATOR Along the Equator Over 2000–2008: Zonally Averaged (Between 140°E and 80°W) Correlation and RMS Error Between Model Outputs and Observations for SST Anomalies (TMI), the 20°C Isotherm Depth Anomalies (TAO Data) and Sea Level High Anomaly (TPJ Data)

	TMI -MERC (SSTA)	TAO-MERC (D20A)	TPJ-MERC (SLHA)
Mean correlation	0.7	0.76	0.81
Mean RMS error	0.75°C	10.2 m	3.53 cm

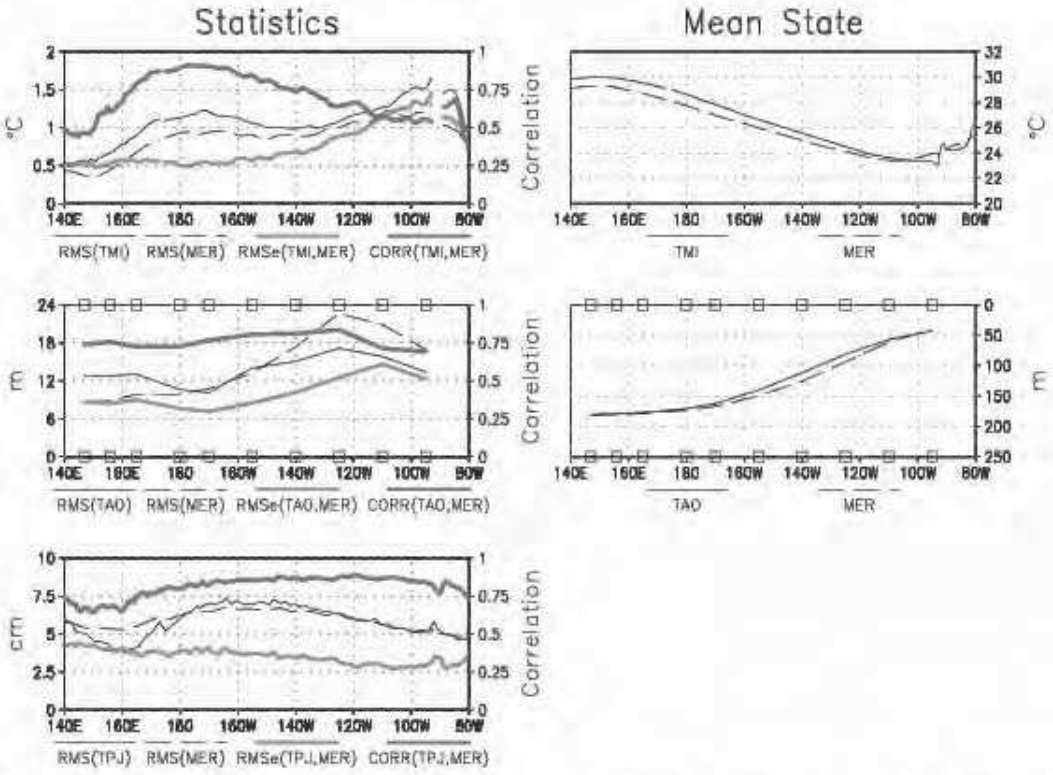

Figure 2. Comparison between model and observations. Left panels show the statistics for the anomaly of SST (upper), 20°C isotherm depth (center) and sea level high (SLH, bottom). In this side, each panel indicates the RMS of observed data, RMS of model results, RMS error (RMSe), and correlation (both between observed data and model results) using black solid line, black dashed line, red thick solid line, and blue thick solid line, respectively. The scale of RMS and RMSe is located on the left and correlation scale is on the right of each graphics. On the right-hand side, the mean SST (upper panel) and 20°C isotherm depth (lower panel) along the equator in 2000–2008 for model (dashed line) and observation (plain line). Open squares in the upper and lower borders of the panels indicate the position of the TAO mooring buoys in the equatorial line.

Table 2. Validation of MERCATOR Along the Equator Over 2000–2008 for Zonal Current Anomalies: Vertically Averaged (Between 0 and 55 m) Correlation and RMS Error Between Model Outputs and Observations. Observations Are From the TAO Array

Mooring Longitude	165°E	170°W	140°W	110°W
Mean correlation	0.61	0.67	0.59	0.54
Mean RMS error (cm/s)	17.0	16.6	20.9	20.1

2.5. Estimation of Wave Amplitude

[9] To derive the Kelvin wave amplitude for the most energetic baroclinic modes ($m = 1$, 2 and 3), a similar methodology to that described in *Dewitte et al.* [2003] is used. It consists in projecting the variability on the vertical (baroclinic) and horizontal (Kelvin and Rossby) modes as obtained from the vertical mode decomposition of the mean stratification over the period 2000–2008. Usually wave amplitude is considered as its contribution to sea level or zonal current anomalies. Here, to compare with observed thermocline fluctuations as derived from the TAO data, we consider the Kelvin and Rossby wave contributions to thermocline anomalies following *Dewitte et al.* [2012], namely considering the vertical isotherm displacements at the depth of the mean thermocline under the hydrostatic approximation. The details of the method can be found in *Dewitte et al.* [2012].

3. Results

3.1. Equatorial Wave Sequence in July 2001 to October 2003

[10] As a first step, the contribution of the n^{th} baroclinic mode Kelvin (AK_n), first-meridional Rossby wave ($R1_n$) and third meridional Rossby wave ($R3_n$) to thermocline depth anomalies are estimated (see section 2.5). Figure 3b presents the evolution of the summed-up contribution of the Kelvin and first-meridional Rossby waves to thermocline fluctuations. The contribution of the first three baroclinic modes is considered here. Figure 3c is equivalent to Figure 3b except that only the contribution of the Kelvin wave is considered. They can be compared to Figure 3a, which displays the TAO observations. It first indicates that the thermocline variability along the equator can be accounted for to a large extent by the summed-up contribution of the Kelvin waves of the first three baroclinic modes (Figure 3c) since the level of agreement between observations and Kelvin wave estimate in terms of

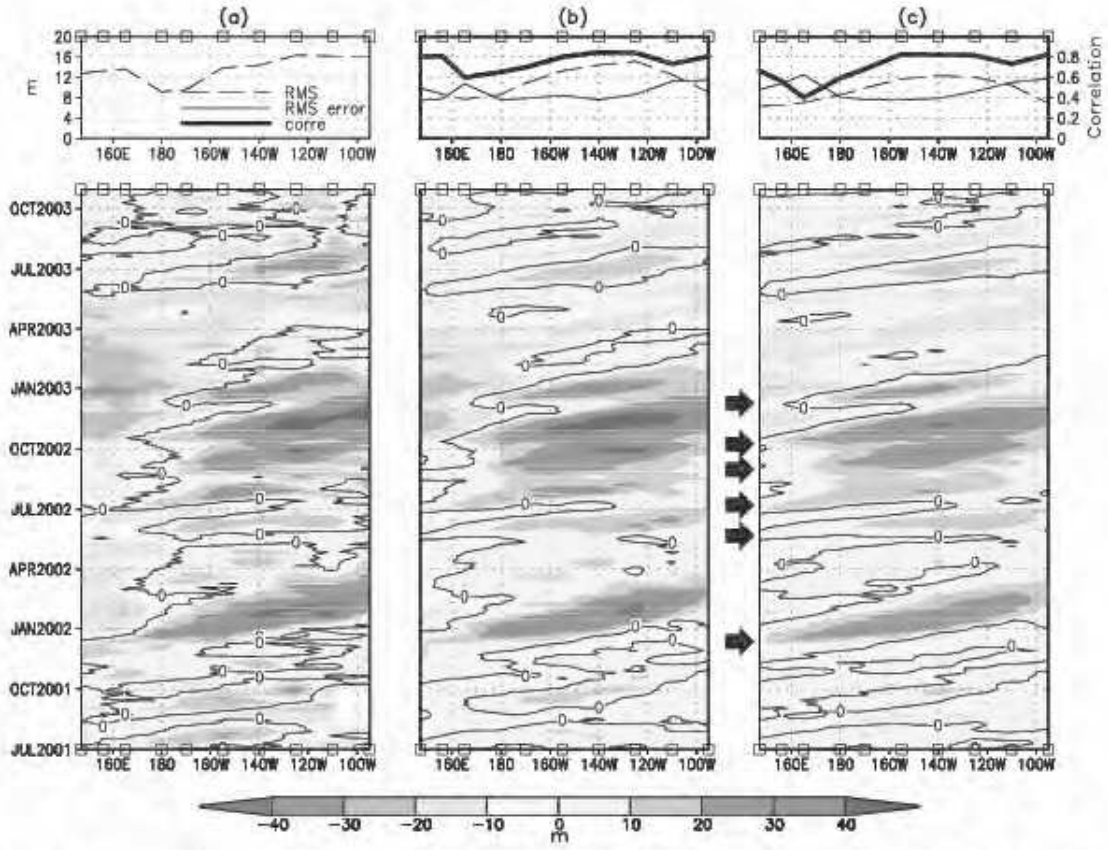

Figure 3. Evolution of thermocline depth anomalies along the equator between July 2001 and October 2003 (a) for the TAO data, (b) the contribution of the Kelvin and Rossby waves of the first three baroclinic modes, and (c) for the Kelvin wave contribution. Upper panels indicate the RMS (dashed line), RMS error (solid line), and correlation (thick solid line) between model and observation. Open squares in the superior axis of each graphic indicate the position of the TAO mooring buoys along the equator line. In Figure 3c, black arrows have been drawn to show the time of initiation of the downwelling Kelvin waves.

correlation and RMS error is comparable than for the total model thermocline anomalies (compare top Figure 3 with the left-center panel of Figure 2). Rossby waves contribute to the thermocline fluctuations mostly in the far western Pacific, but their contribution is more clearly seen around 4°N and 4°S. The simulated Kelvin wave can be clearly identified: It propagates as far as to the eastern boundary with a slight decrease in amplitude as it approaches the eastern boundary. During the developing phase of the 2002/2003 El Niño, two main episodes of downwelling Kelvin wave activity can be observed: An energetic downwelling Kelvin wave in January 2002 and a packet of five downwelling Kelvin wave (DKW) between April 2002 and January 2003 (see Figure 3c). Each DKW is associated to a westerly wind burst that took place in the western Pacific (Figure 4a).

[11] To visualize and infer the advection processes associated to the waves, the SST anomalies have been overlaid in Figures 4b, 4c, and 4d and only the amplitude of the Kelvin wave larger than 10 m is contoured. At the end of 2001, a westerly wind burst triggered a DKW that projected onto the first two baroclinic modes (Figure 4a, 4b, and 4c). This wave crossed the equatorial Pacific deepening the thermocline depth and slightly dissipating as it reaches the eastern Pacific in the austral summer of 2002. This wave slightly increased the SST over the eastern equatorial Pacific (Figure 1c) and may have been trapped along the Ecuadorian and Peruvian coasts producing coastal positive SST anomalies (Figure 1d). Also, this Kelvin wave, along its trajectory, encounters a steeper thermocline (i.e., increased zonal stratification) which may result in reflections into intraseasonal Rossby waves [*Busalacchi and Cane*, 1988] as suggested by the evidenced by the westward propagating current anomalies associated to the first-meridional Rossby wave (Figure 4e). After that, between mid and end of 2002, five DKWs of the first two baroclinic modes, produced by westerly wind bursts, appear in the equatorial Pacific and depressed the thermocline depth. This wave packet participated to the development of the 2002/2003 El Niño. In the eastern Pacific, around 120°W–110°W in November–December 2002, a Kelvin wave of the third baroclinic mode appeared as a consequence of the sloping thermocline that may have induced modal dispersion. Additionally, these waves transferred

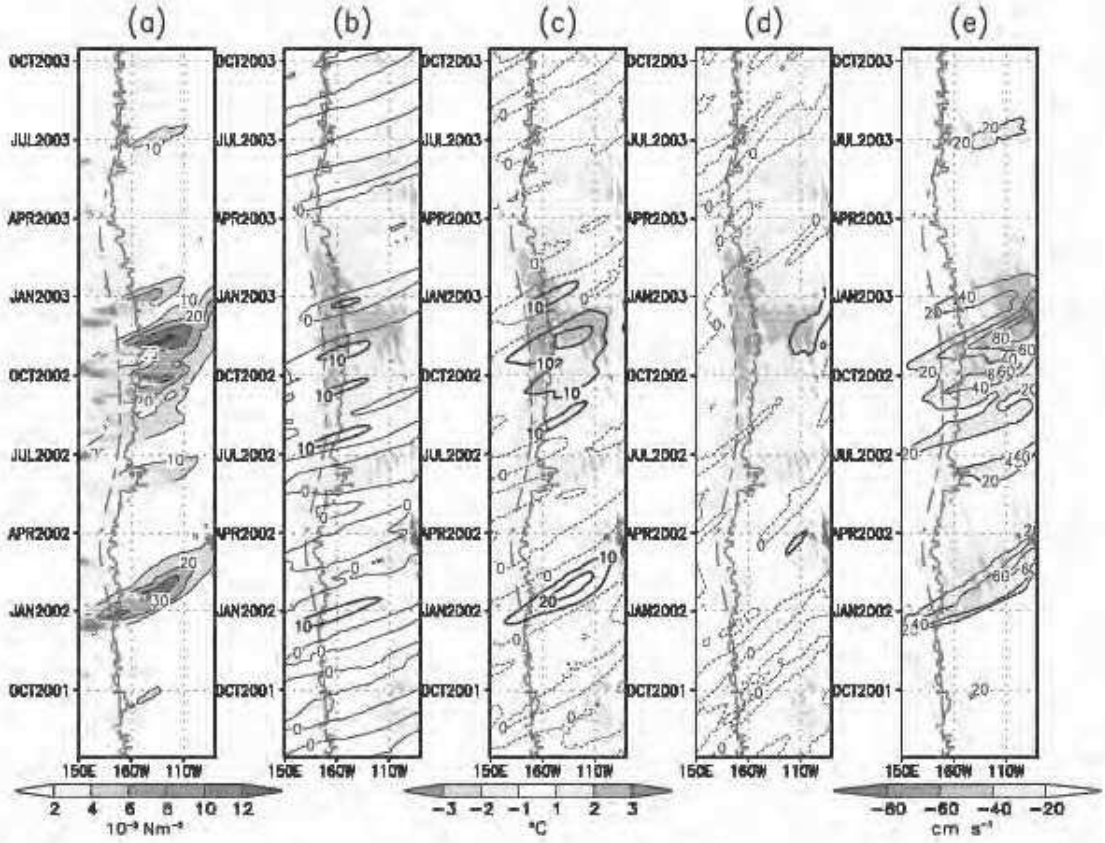

Figure 4. Evolution of equatorial zonal wind stress anomaly (ZWSA); the contribution of the Kelvin and Rossby waves to thermocline depth anomaly and zonal current anomaly, respectively; and SSTA along the equator line between July 2001 and October 2003. (a) Colors indicate the positive ZWSA (10^{-2} N m^{-2}) and gray scale, the contribution of DKW (sum of baroclinic modes 1, 2, and 3) (in meter). Shown in black lines are the contribution of the DKW from (b) mode 1, (c) mode 2, and (d) mode 3. In these three panels the SSTA from TMI is overlad in colors (scale is located at the bottom of Figure 4c). (e) The contribution of Kelvin and Rossby wave to the zonal current anomaly is drawn in black contours and in blue tones, respectively. The scale of the Rossby contribution is located at the bottom of Figure 4e. Also, the 28°C isotherm is overplotted in blue line for the climatological SST (dashed line) and the total SST (solid line) in all panels.

energy to the Rossby waves along their ways, eventually reflecting at the American boundary (Figure 4e). Note the slight eastward displacement of the warm pool associated to this wave packet (see the eastern movement of the 28°C isotherm—blue dashed line—in Figure 4), which indicates that the large-scale ocean-atmosphere feedbacks have fully engaged to amplify and sustain the CP El Niño warming. From January 2003, the Kelvin wave activity subsides and SST anomalies started to decrease and the 28°C isotherm reached its normal position around April of 2003.

3.2. Warming and Cooling Processes

[12] To document the processes at work during this CP El Niño event, a simplified heat budget model of a fixed depth layer ($h = 50$ m) is carried out from the MERCATOR data. The use of a constant depth is appropriate for estimating processes associated to wave dynamics in the equatorial Pacific and has been used in many ENSO studies (see *Zebiak and Cane* [1987] or *Belmadani et al.* [2010] among others). It is based on the following temperature anomaly equation:

$$\left\langle \frac{\partial T_A}{\partial t} \right\rangle_h = -\langle \mathbf{V}_A \cdot \nabla T_C \rangle_h - \langle \mathbf{V}_C \cdot \nabla T_A \rangle_h - \langle \mathbf{V}_A \cdot \nabla T_A \rangle_h + F_A + R \quad (1)$$

where $\langle X \rangle_h$ indicates the vertical average of the quantity X from the surface to the depth h, taken constant equal to 50 m. Subscript C and A, in some variables, represent climatology and anomaly, respectively. T, $\mathbf{V} = (u,v,w)$ and F are the temperature, velocity, and surface energy fluxes, respectively. The left-hand side term of equation (1) represents the tendency of T_A. On the right, the three advection terms, correspond to the combination of climatological and anomalous currents and gradients. The surface fluxes anomaly is estimated following *Wang and McPhaden* [1999], namely $F_A = (Q_0 + Q_P)/(\rho_0 C_p |h|)$, where Q_0 is the sum of anomalies of shortwave radiation (Q_{SW}), longwave radiation (Q_{LW}), latent heat (Q_L), and sensible heat (Q_S) (i.e., $Q_0 = Q_{SW} + Q_{LW} + Q_L + Q_S$), while Q_P is the outgoing shortwave fluxes that escape from the bottom of the layer: $Q_P = -0.45 \cdot Q_{SW} \cdot e^{-\gamma |h|}$. C_p, is the heat capacity (=3940 J kg^{-1} °C^{-1}), ρ_0 is the density of the seawater (=1022.4 kg m^{-3}) and $\gamma^{-1} = 25$ m is the attenuation length scale. Finally, R is the residual of the budget that includes physical processes such as vertical diffusion or entrainment.

[13] To estimate the role of the equatorial Kelvin waves on the rate of SST change during the evolution of the 2002/2003 El Niño, the contribution to zonal current anomalies is separated into its baroclinic component and a residual component calculated by the difference between total zonal current anomalies and the summed-up contribution of the baroclinic modes 1 to 3. This residual component therefore stands for the share of the variability that tends to be trapped into the fixed-depth mixed layer and accounts for the so-called locally wind-driven current anomalies along the equator. Such contribution could be also estimated considering a simple frictional layer of depth h forced by $\tau_f = \tau([1/h] - \sum_{i=1}^{3} P_i)$ [cf. *Blumenthal and Cane*, 1989] (P_i being the wind projection coefficient for the baroclinic mode i). As a consistency check, we have fitted such a frictional layer model so that residual component of the current, which leads to an estimation of the damping rate coefficient of ~(6 days)$^{-1}$. Although such estimated decay time is somewhat larger than what is usually used in intermediate complexity models [*Zebiak and Cane*, 1987], it is consistent with the interpretation of the residual component of the current anomalies as the locally wind-driven contribution.

[14] Equation (1) then writes as follows:

$$\begin{aligned} \frac{\partial T_A}{\partial t} = & -u_K \frac{\partial T_C}{\partial x} - u_R \frac{\partial T_C}{\partial x} - u_r \frac{\partial T_C}{\partial x} - v_A \frac{\partial T_C}{\partial y} - w_A \frac{\partial T_C}{\partial z} \\ & - u_C \frac{\partial T_A}{\partial x} - v_C \frac{\partial T_A}{\partial y} - w_C \frac{\partial T_A}{\partial z} \\ & - u_K \frac{\partial T_A}{\partial x} - u_R \frac{\partial T_A}{\partial x} - u_r \frac{\partial T_A}{\partial x} - v_A \frac{\partial T_A}{\partial y} - w_A \frac{\partial T_A}{\partial z} \\ & + \frac{Q_{SW}}{\rho_0 C_p h} + \frac{Q_{LW}}{\rho_0 C_p h} + \frac{Q_L}{\rho_0 C_p h} + \frac{Q_S}{\rho_0 C_p h} + \frac{Q_P}{\rho_0 C_p h} \\ & + R \end{aligned} \quad (2)$$

where u_K (u_R) is the contribution of the Kelvin (first and third meridional Rossby) wave, from the first three gravest baroclinic modes, to the zonal currents anomaly. Term u_r is the difference between u_A (total zonal current anomaly) and ($u_K + u_R$). Angle brackets ($< >_h$) has been omitted for clarity. Hereafter, each term are considered as its average within the layer h.

[15] Figure 5 displays the tendency terms of equation (1), as Hovmöller diagrams, over the period from July 2001 to October 2003 along the equator. The rate of SST changes (Figure 5a) clearly shows a warming and a cooling phase between April 2002 and November 2002, and December 2002 and April 2003, respectively. Advection (Figure 5b) is the most important process contributing to the warming of the 2002/2003 El Niño. It is partly compensated by surface flux anomalies (Figure 5c) that act as a thermal damping especially during the decaying phase of the event. The residual term (Figure 5d) does not exhibit a clear pattern. Its variability is the largest in the eastern Pacific where vertical diffusion and entrainment are likely to play a role due to the shallow fixed-depth mixed layer. Note however that the offline computation (based on 3 day mean averages of model variables) is not adequate for clearly separating entrainment and vertical mixing processes. What should appear as diurnal entrainment, for instance, appears in the offline computation as daily-mean vertical mixing. Anyway by construction our budget is closed. Only the interpretation of the physical process is limited in the eastern Pacific. With this limitation in mind, the following provides a description of the warming and cooling phases of the 2002/2003 El Niño in three equatorial regions having the zonal extent of the historical El Niño indices, namely N4Eq (160°E–150°W; 0°), N34Eq (170°W–120°W; 0°) and N3Eq (150°W–90°W; 0°). The periods of the warming and cooling phases are inferred from Figure 5a, i.e., April–November 2002 and December 2002 to April 2003, respectively.

3.2.1. Warming Phase

[16] Figure 6 displays the values of the tendency terms in the three regions along the equator during the warming phase. A contrasted situation between N3Eq and N4Eq is observed. In the central Pacific (N4Eq), the warming during the 2002/2003 El Niño is produced mainly by the zonal advection of the climatological temperature due to the Kelvin

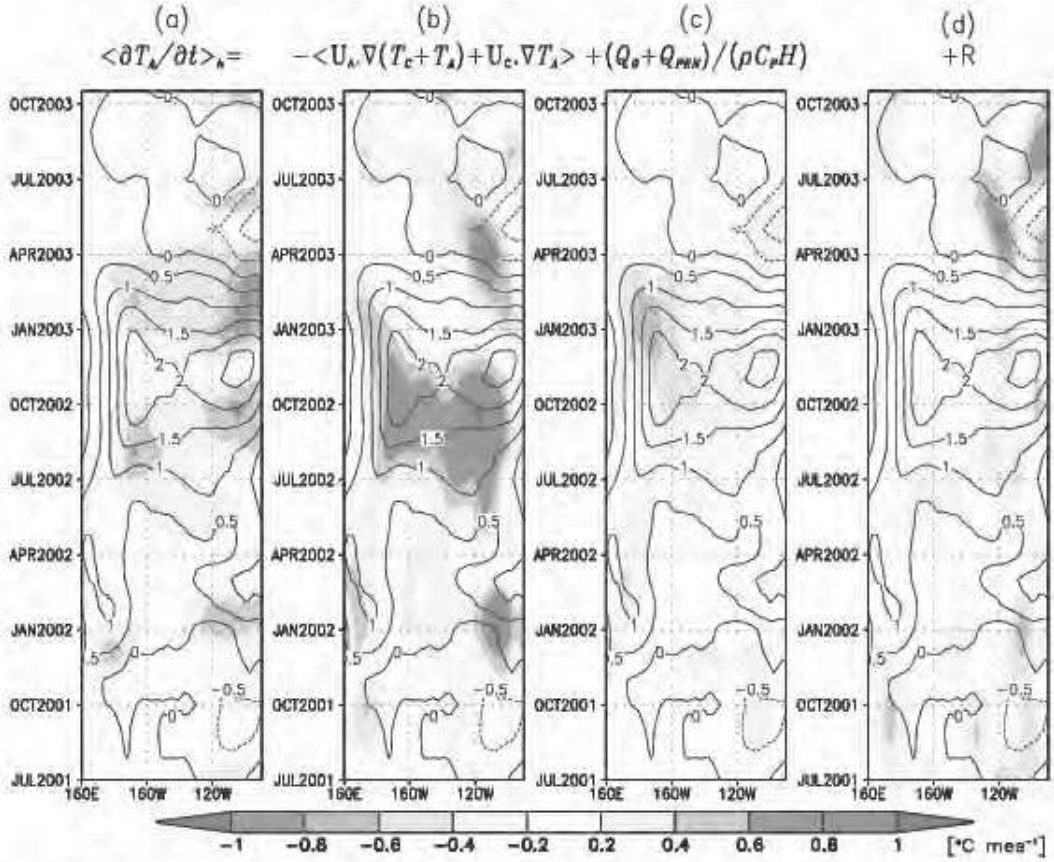

Figure 5. Evolution of the tendency terms (in colors) along the equator as defined in equation (1). (a) The rate of SST changes ($<\partial T_A/\partial t>_h$). (b) The advection terms, which means the sum of the first three terms on the right-hand side of equation (1). (c) The surface fluxes [fourth term of equation (1)]. (d) The residual term (R') that accounts for vertical mixing or entrainment. In each panel the SSTA is overlaid in black contours.

waves ($-u_K(\partial T_c/\partial x)$) and due to the locally wind-driven currents ($-u_t(\partial T_c/\partial x)$) whereas in the eastern Pacific (N3Eq), it is associated to the zonal advection of the climatological temperature due to the Kelvin waves ($-u_K(\partial T_c/\partial x)$) and the vertical advection of the temperature anomaly by climatology vertical velocity $-w_C(\partial T_A/\partial z)$. Consistently with Figure 4, the peak contribution of the zonal advection due to the Kelvin wave is found in the N34Eq region. Cooling processes during this warming phase are attributed to the Rossby wave component of the zonal advection term all along the equator (peaking in the N34Eq region) and to short wave radiation and latent heat in the N4Eq and N3Eq regions respectively. This is consistent with the increased convection in the N4 and the expected increased convergence east of it (N34Eq and N3Eq regions) during the warming of the warm pool. The residual term consists in a cooling tendency in the eastern Pacific which may be due to either the increase in vertical mixing at the crossing of the downwelling Kelvin wave or the unusual zonal extent of anomalous easterly stresses during this event [cf. *McPhaden*, 2004, Figure 5b].

3.2.2. Cooling Phase

[17] The cooling phase is associated to a different balance between terms (Figure 7) with in particular an enhanced contribution of the heat-flux damping through solar radiation reduction in the central Pacific (N4Eq) and increased evaporation along the equator (peaking in the N34Eq region). The zonal advection remains a major contributor to the rate of SST change, but mainly through its baroclinic component. The latter corresponds to the effect of the reflected downwelling Rossby waves that produces a cooling tendency in the N34Eq and N3Eq regions and the small warming tendency in the N4Eq region as a consequence of upwelling Rossby waves that, due to its zonal current structure at the equator, advect warm water from the western Pacific.

4. Discussion and Conclusions

[18] The 2002/2003 El Niño is characterized by SST anomalies developing and peaking in the central Pacific and a slight warming of the eastern Pacific. It is shown here that this event was associated to intraseasonal downwelling Kelvin wave activity of the first two baroclinic modes: a first downwelling Kelvin wave initiated ~8–9 month prior to the development of the CP El Niño that slightly warmed the equatorial Pacific and may have contributed to set up favorable conditions for its development; a second episode of downwelling Kelvin waves is diagnosed that occurred during the development phase from October 2002. These waves exhibit

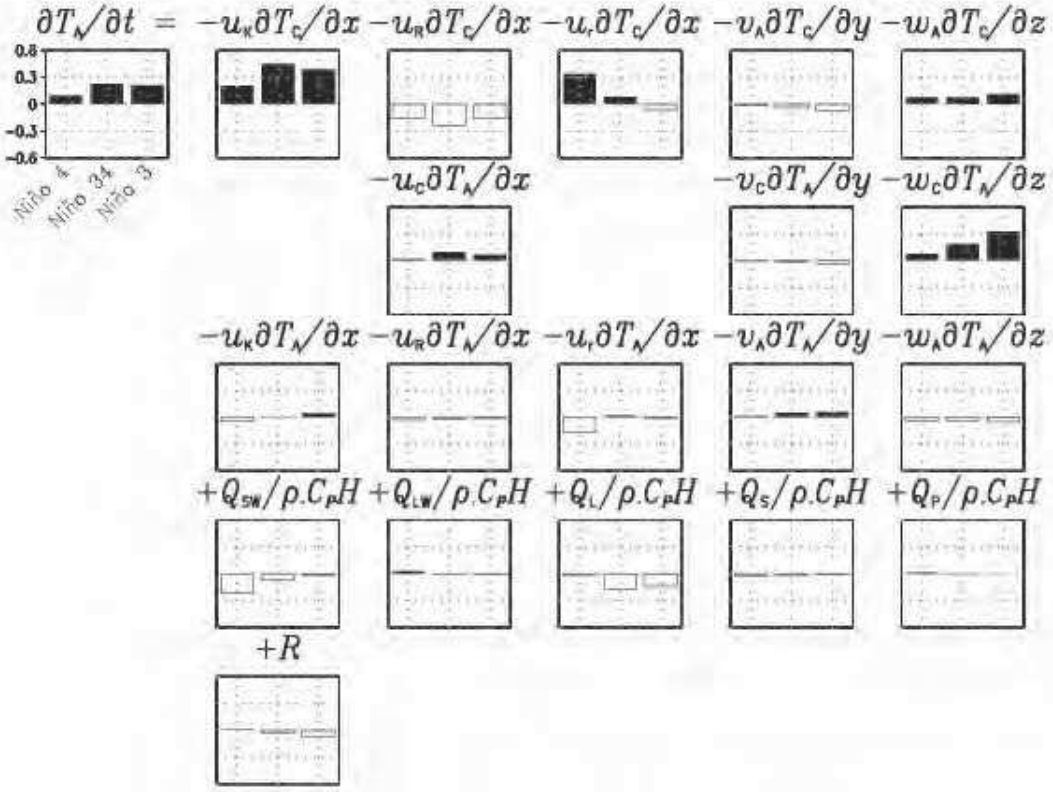

Figure 6. Three-bar plots for each term of equation (2) in the warming phase (April–November 2002) of 2002/2003 El Niño. The three bars indicate the mean value in regions El Niño 4 (left), El Niño 3.4 (center) and El Niño 3 (right); see text for the definition of regions. Filled (no filled) bar represents warming (cooling) contribution (°C month^{-1}).

a peak variability in the central Pacific, most prominent in the second baroclinic mode, and dissipate as they propagate eastward suggesting either vertical propagation, modal dispersion associated to the sloping thermocline from west to east, or mixing.

[19] A simplified heat budget analysis inside a fixed depth layer reveals that anomalous zonal advection of mean temperature and mean vertical advection of temperature anomaly are the major contributors to SST changes during the warming phase (April–November 2002), whereas the reversal toward cooler conditions (December 2002 to April 2003) is associated to zonal advection and net heat flux reduction. The zonal advection is further decomposed into a baroclinic component and a locally forced component trapped into the fixed-depth mixed layer. The latter reveals that the warming process in the central and eastern Pacific can be attributed to a large extent to the Kelvin waves. In the N4Eq region, it contributes as much as the direct wind forcing component to the zonal advection. Its effect in the eastern Pacific is enhanced by the contribution of the vertical advection. However there is a compensation by the latent heat and the vertical mixing, which may explain why SST anomalies in the N3Eq region do not exceed those in the N4Eq region. Noteworthy, there is a contribution of the Rossby waves to the zonal advection along the equator, which is apparently due to reflection of the Kelvin wave on the sloping thermocline. As a summary of the waves' sequence and their impact on advection, we provide a schematic of the evolution of the 2002/2003 El Niño (Figure 8).

[20] We now discuss our results in the light of previous works. Our analysis is overall consistent with the study by *Kug et al.* [2010] who analyzed a composite CP El Niño event as simulated by a Coupled General Circulation Model, in the sense that the zonal advection process is a dominant process to explain the development of the 2002/2003 El Niño whereas thermal damping is a major contributor to the "discharge process." Our results, however, suggest that there is a clear dynamical response in terms of equatorial wave, which does not rule out that processes relevant for the EP El Niño take place, which includes the recharge-discharge process [*Jin*, 1997]. In particular, *Dewitte et al.* [2012] showed that in the same OGCM simulation studied by *Kug et al.* [2010] that the recharge-discharge process could take place through the second baroclinic mode. Here we also find that different waves can have a different contribution to the evolution of heat content along the equator. However, conversely to the composite CP El Niño described in *Dewitte et al.* [2012], for the 2002/2003 El Niño, both baroclinic modes appear to contribute distinctively to the recharge and discharge processes. As an illustration, Figure 9 shows the evolution of the Warm Water Volume (WWV) anomaly for the contribution of the first and second baroclinic modes, for their summed-up contributions and the total field. The WWV is calculated following *Meinen and McPhaden* [2000]. Besides confirming the good agreement between the model used in this study and observations in terms of heat content anomalies, Figure 9 indicates that the

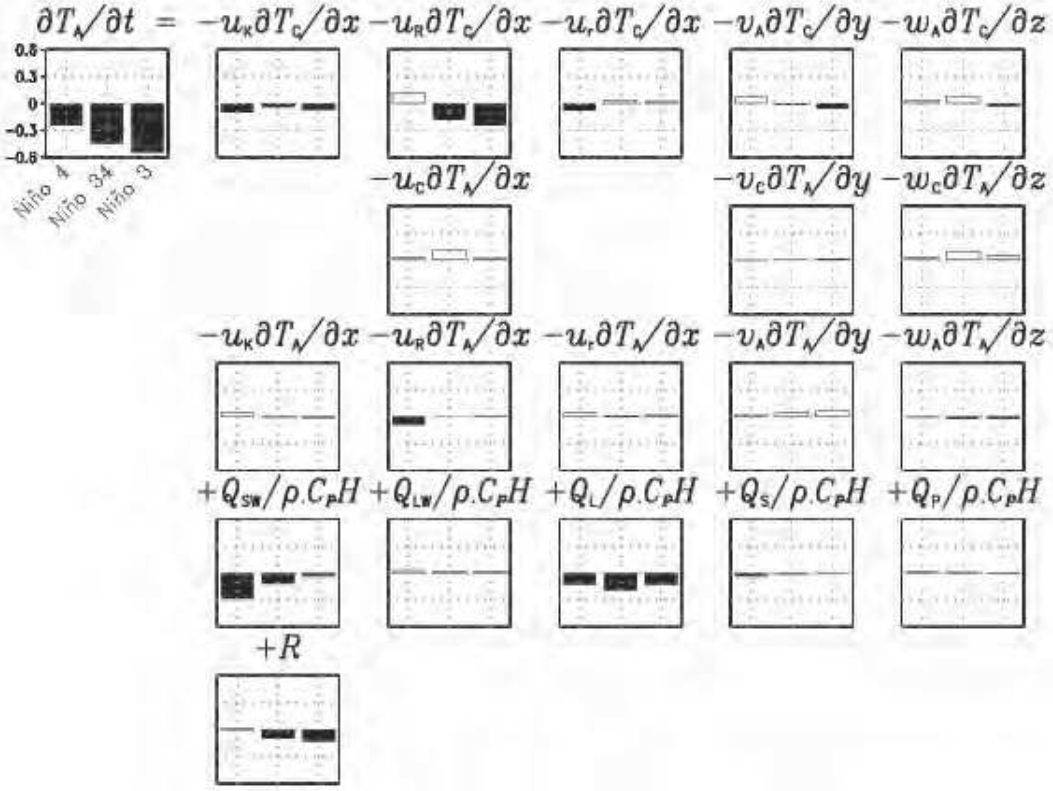

Figure 7. Similar to Figure 6 but for cooling phase (December 2002 to April 2003) of 2002/2003 El Niño. In contrast, filled (no filled) bar represents cooling (warming) contribution (°C month^{-1}).

second mode contributes to the recharge process whereas the first mode remains weak during this phase. After the peak phase (vertical dashed line) right after the peak SST anomaly, both modes experience a sharp decrease initiating the discharge process. The temporal integral of the first baroclinic mode contribution to the WWV anomaly over the cooling phase leads a negative value conversely to the second baroclinic mode, indicating that the first mode is dominating the discharge process. This suggests that there is a dynamical asymmetry between the recharge and discharge processes during the 2002/2003 El Niño with the second baroclinic mode contributing mostly to the recharge process and

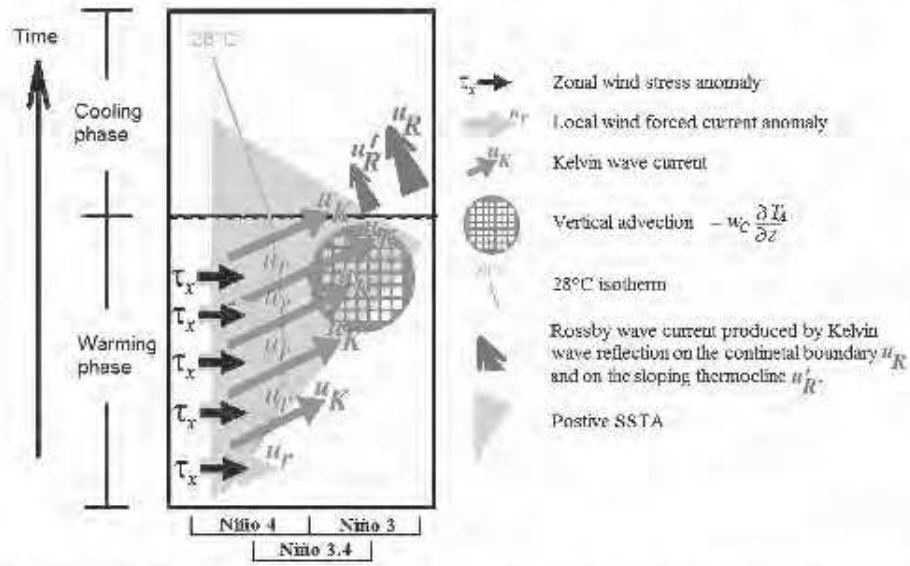

Figure 8. Schematic from derived results of the wave sequence and their impact on advection during the warming and cooling phases of the 2002/2003 El Niño along the equator.

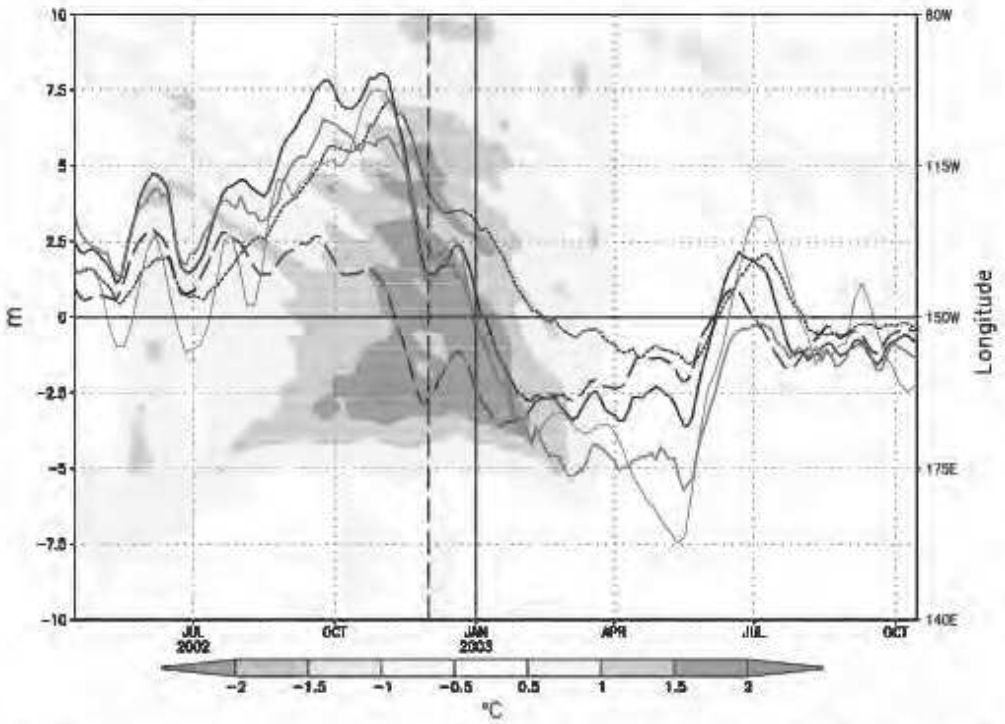

Figure 9. Evolution of the Warm Water Volume (WWV) as derived from TAO (thin blue line) and MERCATOR (thick blue line) between April 2002 and October 2003. The WWV is calculated from the spatial average of the 20°C isotherm depth anomaly over (145°E–95°E; 5°S–5°N) for TAO and (135°E–80°W; 5°S–5°N) for MERCATOR. The lines, in black, represent the contribution to the WWV of the sum of Kelvin and first meridional Rossby modes of the first two baroclinic modes. Dashed (dotted) line represents the first (second) baroclinic mode's contribution. The sum of vertical mode 1 and 2 is represented by a solid black line. As a background, the SSTA along the equatorial Pacific (mean over 5°S–5°N) is displayed (zonal axis is put on the right). Vertical dashed line indicates 1 December 2002, which is the limit between warming and cooling phase based in the tendency of SSTA (Figure 5).

the first baroclinic mode mostly amplifying the decay of the event. Because ENSO is sensitive to the thermocline depth and stratification [*Fedorov and Philander*, 2001], we may argue that such feature results from changes in stratification considering that the latter has been reduced during the last decade [*McPhaden et al.*, 2011]. Further investigation is required in order to document if such dynamical asymmetry pattern in the evolution of the WWV is a fundamental characteristic of the CP El Niño and may explain recent changes in the relationship between WWV anomalies and SST anomalies at the peak phase of ENSO [*McPhaden*, 2012].

[21] Our study also indicates that vertical mixing, taken into account here as a residual term (R'), also participates in the compensation of the effect of the Kelvin wave onto the vertical advection, which may explain the evolution of this event toward a CP type. Further investigation is required in order to separate the contribution of the different terms participating to vertical mixing, that is vertical diffusivity and entrainment. This can be achieved through an online computation of the heat budget, which we plan to do from another OGCM. In particular, *Lengaigne et al.* [2012] indicates that vertical mixing can significantly contribute to the WWV tendency during the 2002/2003 El Niño [see *Lengaigne et al.*, 2012, Figure 8]. This contribution as well as the one from the penetration solar forcing at the 20°C isotherm depth may explain the differences that we find between the total WWV and the estimate from the Kelvin and first meridional Rossby waves (summed-up of baroclinic modes 1 and 2) at the peak phases of the recharge and discharge (Figure 9). Our results indicate however that the main contribution to the WWV tendency originates from the wave dynamics, which is consistent with the results by *Bosc and Delcroix* [2008]. This suggests that, despite its weak amplitude, the CP El Niño may be as predictable as the EP El Niño, even though a modulation of the predictability may originate from change in mean state [*McPhaden et al.*, 2011]. Further study is certainly required to document the wave dynamics of such type of event to determine if the dynamical vertical structure of the WWV could explain the reduced seasonal time scale predictability during periods dominated by CP El Niños.

[22] **Acknowledgments.** K. Mosquera-Vásquez benefited from a Ph. D. scholarship received from Institut de Recherche pour le Développement (IRD). The authors also thank the two anonymous reviewers for their constructive comments. This work is part of the projects of the special agreement between IRD and IGP (2011–2013).

References

Ashok, K., S. K. Behera, S. A. Rao, H. Weng, and T. Yamagata (2007), El Niño Modoki and its possible teleconnection, *J. Geophys. Res.*, *112*, C11007, doi:10.1029/2006JC003798.

Belmadani A., B. Dewitte, and S.-I. An (2010), ENSO feedbacks and associated variability timescales in a multi-model ensemble, *J. Climate*, *23*, 3181–3204.

Bosc, C., and T. Delcroix (2008), Observed equatorial Rossby waves and ENSO-related warm water volume changes in the equatorial Pacific Ocean, *J. Geophys. Res.*, *113*, C06003, doi:10.1029/2007JC004613.

Blumenthal, M. B., and M. A. Cane (1989), Accounting for parameter uncertainties in model verification: An illustration with tropical sea surface temperature, *J. Phys. Oceanogr.*, *19*, 815–830.

Busalacchi, A. J., and M. A. Cane (1988), The effect of varying stratification on low-frequency equatorial motions, *J. Phys. Oceanogr.*, *18*, 801–812.

Chelton, D. B., S. K. Esbensen, M. G. Schlax, N. Thum, M. H. Freilich, F. J. Wentz, C. L. Gentemann, M. J. McPhaden, and P. S. Schopf (2001), Observations of coupling between surface wind stress and sea surface temperature in the eastern tropical Pacific, *J. Clim.*, *14*, 1479–1498.

Clarke, A. J., and C. Shi (1991), Critical frequencies at ocean boundaries, *J. Geophys. Res.*, *96*, 10,731–10,738.

Dewitte B., S. Illig, L. Parent, Y. duPenhoat, L. Gourdeau, and J. Verron (2003), Tropical Pacific baroclinic mode contribution and associated long waves for the 1994–1999 period from an assimilation experiment with altimetric data, *J. Geophys. Res.*, *108* (C4), 3121–3138.

Dewitte B., S. Illig, L. Renault, K. Goubanova, K. Takahashi, D. Gushchina, K. Mosquera, and S. Purca (2011), Modes of covariability between sea surface temperature and wind stress intraseasonal anomalies along the coast of Peru from satellite observations (2000–2008), *J. Geophys. Res.*, *116*, C04028, doi:10.1029/2010JC006495.

Dewitte B., J. Choi, S.-I. An, and S. Thual (2012), Vertical structure variability and equatorial waves during central Pacific and eastern Pacific El Niños in a coupled general circulation model, *Clim. Dyn.*, *38*, 2275–2289.

Ducet, N., P. Y. Le Traon, and G. Reverdin (2000), Global high resolution mapping of ocean circulation from TOPEX/POSEIDON and ERS-1/2, *J. Geophys. Res.*, *105*, 19,477–19,498.

Fedorov, A. V., and S. G. Philander (2001), A Stability Analysis of Tropical Ocean–Atmosphere Interactions: Bridging Measurements and Theory for El Niño, *J. Clim.*, *14*, 3086–3101.

Fu, L.-L., E. J. Christensen, C. A. Yamarone Jr., M. Lefebvre, Y. Menard, M. Dorrer, and P. Escudier (1994), Topex/Poseidon mission overview, *J. Geophys. Res.*, *99*, 24,369–24,381.

Garric G., R. Bourdalle-Badie, O. Le Galloudec, C. Bricaud, C. Derval, E. Durand, and Y. Drillet (2008), Description of the interannual experiment ORCA025-T09, 1998–2006, Mercator Ocean Report n°235, September 2008.

Gentemann, C. L., C. J. Donlon, A. Stuart-Menteth, and F. J. Wentz (2003), Diurnal signals in satellite sea surface temperature measurements, *Geophys. Res. Lett.*, *30*(3), 1140, doi:10.1029/2002GL016291.

Hayes, S. P., P. Chang, and M. J. McPhaden (1991), Variability of the sea surface temperature in the eastern equatorial Pacific during 1986–88, *J. Geophys. Res.*, *96*, 10,553–10,566.

Jin, F.-F. (1997), An equatorial ocean recharge paradigm for ENSO. Part I: conceptual model, *J. Atmos. Sci.*, *54*, 811–829.

Kim, W., S.-W. Yeh, J.-H. Kim, J.-S. Kug, and M. Kwon (2011), The unique 2009–2010 El Niño event: A fast phase transition of warm pool El Niño to La Niña, *Geophys. Res. Lett.*, *38*, L15809, doi:10.1029/2011GL048521.

Kug, J.-S., F.-F. Jin, and S.-I. An (2009), Two types of El Niño events: cold tongue El Niño and warm pool El Niño, *J. Clim.*, *22*, 1499–1515.

Kug, J.-S., J. Choi, S.-I. An, F.-F. Jin, and A. T. Wittenberg (2010), Warm Pool and Cold Tongue El Niño events as simulated by the GFDL 2.1 coupled GCM, *J. Clim.*, *23*, 1226–1239.

Le Traon, P. Y., and F. Ogor (1998), ERS-1/2 orbit improvement using T/P: the 2 cm challenge, *J. Geophys. Res.*, *103*, 8045–8057.

Lee, T., and M. J. McPhaden (2010), Increasing intensity of El Niño in the central-equatorial Pacific, *Geophys. Res. Lett.*, *37*, L14603, doi:10.1029/2010GL044007.

Lengaigne, M., U. Hausmann, G. Madec, C. Menkes, J. Vialard, and J. M. Molines (2012), Mechanisms controlling warm water volume interannual variations in the equatorial Pacific: diabatic versus adiabatic processes, *Clim. Dyn.*, *38*, 1031–1046.

Levitus, S., T. P. Boyer, M. E. Conkright, T. OBrian, J. I. Antonov, C. Stephens, L. Stathopolos, D. Johnson, and R. Gelfeld (1998), World Ocean Database 1998 - NOAA Atlas NESDID18, National Oceanographic Data Center, Silver Spring, MD.

Madec, G., P. Delecluse, M. Imbard, and C. Levy (1998), OPA 8.1 Ocean General Circulation Model reference manual, Nodes du pole de modélisation, Institut Pierre Simon Laplace (IPSL), France, 11, 91 pp.

McPhaden, M. J., et al. (1998), The Tropical Ocean-Global Atmosphere (TOGA) observing system: A decade of progress, *J. Geophys. Res.*, *103*, 14,169–14,240.

McPhaden, M. J. (2004), Evolution of the 2002/03 El Niño, *Bull. Am. Meteorol. Soc.*, *85*, 677–695.

McPhaden, M. J., T. Lee, and D. McClurg (2011), El Niño and its relationship to changing background conditions in the tropical Pacific, *Geophys. Res. Lett.*, *38*, L15709, doi:10.1029/2011GL048275.

McPhaden, M. J. (2012), A 21st Century Shift in the Relationship between ENSO SST and Warm Water Volume Anomalies, *Geophys. Res. Lett.*, *39*, L09706, doi:10.1029/2012GL051826.

Meinen, C. S., and M. J. McPhaden (2000), Observations of warm water volume changes in the equatorial Pacific and their relationship to El Niño and La Niña, *J. Clim.*, *13*, 3551–3559, doi:10.1175/1520-0442(2000)013 < 3551:OOWWVC > 2.0.CO;2.

Rayner, N. A., D. E. Parker, E. B. Horton, C. K. Folland, L. V. Alexander, D. P. Rowell, E. C. Kent, and A. Kaplan (2003), Global analyses of sea surface temperature, sea ice, and night marine air temperature since the late nineteenth century, *J. Geophys. Res.*, *108*(D14), 4407, doi:10.1029/2002JD002670.

Takahashi, K., A. Montecinos, K. Goubanova, and B. Dewitte (2011), ENSO regimes: Reinterpreting the canonical and Modoki El Niño, *Geophys. Res. Lett.*, *38*, L10704, doi:10.1029/2011GL047364.

Wang, W., and M. J. McPhaden (1999), The surface layer heat balance in the equatorial Pacific ocean. Part I: Mean seasonal cycle, *J. Phys. Oceanogr.*, *29*, 1812–1831.

Wentz, F. J., C. Gentemann, D. Smith, and D. Chelton (2000), Satellites measurements of sea surface temperature through clouds, *Science*, *288*, 847–850.

Yeh S.-W., S.-J. Kug, B. Dewitte, M.-H. Kwon, B. P. Kirtman, and F.-F. Jin (2009), El Niño in a changing climate, *Nature*, *461*, 511–514.

Yu, J.-Y., and S. T. Kim (2010), Three evolution patterns of Central Pacific El Niño, *Geophys. Res. Lett.*, *37*, L08706, doi:10.1029/2010GL042810.

Yu, J.-Y., H.-Y. Kao, T. Lee, and S. T. Kim (2011), Subsurface ocean temperature indices for Central-Pacific and Eastern-Pacific types of El Niño and La Niña events, Theoretical Appl. *Climatol.*, *103*, 337–344.

Zebiak, S. E., and M. A. Cane (1987), A model El Niño-Southern Oscillation, *Monthly Weather Review*, *115*, 2262–2278.

2.3 Thermodynamics associated to the El Niño phenomenon over 1990 - 2011

2.3.1 Introduction

This complementary analysis is an extension of the results published in Mosquera-Vásquez et al. (2013). The heat balance advection terms within the fixed depth layer (h=50m) are estimated during six El Niño events that occurred between 1989 and 2011: 1991/1992, 1994/1995, 1997/1998, 2004/2005 and 2009/2010. Note that the 2002/2003 El Niño is also considered in this analysis. This analysis focuses on the interannual timescales and can be viewed as a consistency check with previous studies (Kug et al., 2009; Xiang et al., 2013). In particular an estimate of the thermodynamical processes within the mixed-layer is provided for the seven CP El Niños that were present since 1989. An oceanic analysis carried out by MERCATOR (T323 configuration), with 50 vertical levels (~50% of them are located in the first 100 m) and forced by ERA Interim surface fluxes is used. The results indicate that the intensity of the InterAnnual Kelvin wave (IAKw) has decreased since 1997/1998 El Niño phenomenon and, as a consequence, its impact on the Sea Surface Temperature (SST) was reduced with slighter zonal advection feedback and thermocline feedback processes in the central and eastern Pacific, respectively. The interannual zonal wind in the western Pacific has been weak since the last 2002/2003 El Niño which is probably related to the permanent "La Niña state" that maintains a cooling (warming) tendency in the upper 100 (between 100 and 300) meters in the central eastern Pacific (western Pacific) as illustrated in **Figure 2.1**. Finally, the results indicate that in the central and eastern Pacific other physical processes (mixing and entrainment), not resolved by our simple heat budget model, become important in the warming phase of El Niño for the last three events.

2.3.2 Data and methodologies

Daily SST and 20°C isotherm depth (hereafter thermocline) anomalies from the Tropical Atmosphere Ocean (TAO) project moorings at 10 positions [147°E, 156°E, 165°E, 180, 170°W, 155°W, 140°W, 125°W, 110°W and 95°W] along the equatorial wave guide, are used to validate the interannual variability of the T323 reanalysis over the period 2000-2011. The data were downloaded from TAO's home page

(http://www.pmel.noaa.gov/tao/). More details about this *in situ* data can be found in McPhaden et al. (2001).

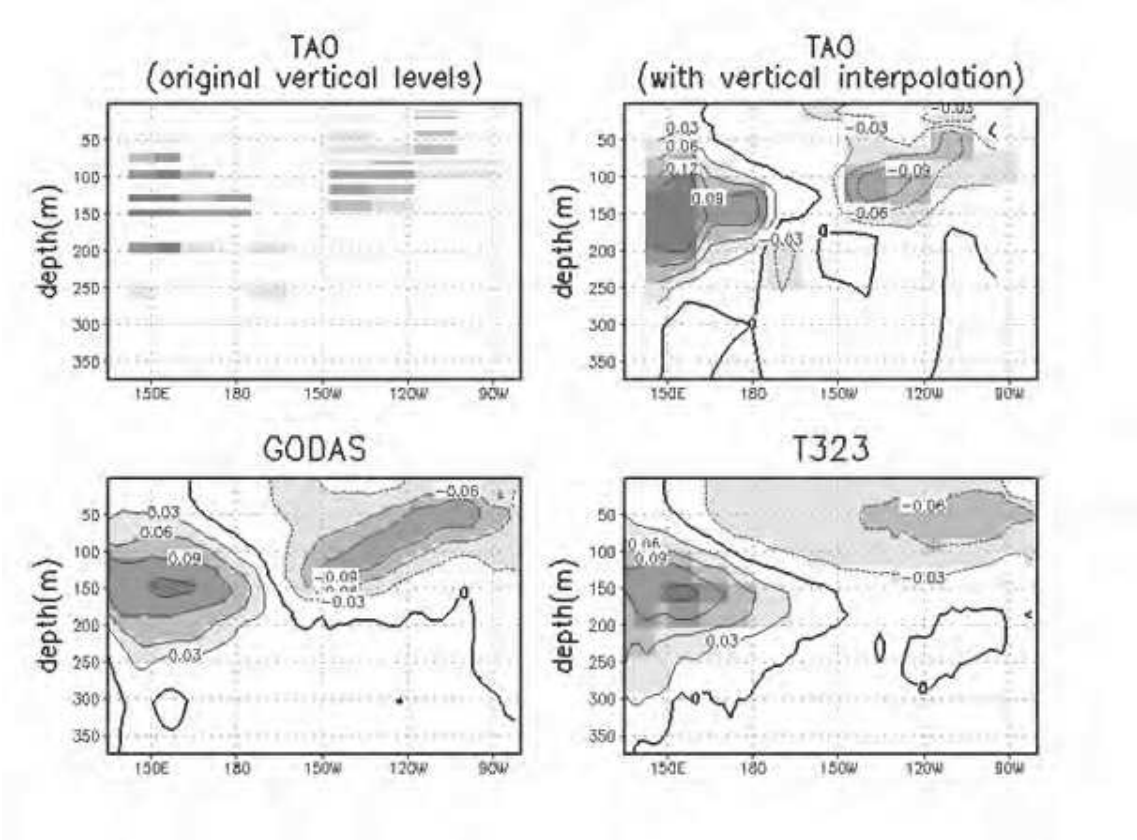

Figure 2.1 Linear trend in temperature in the first 360 meters (period 1989-2011) along the equator. Units are °C year^{-1}. Upper plots were estimated based on TAO data: on the left (right) using the raw data (interpolated version). Linear trend in the bottom left (right) panel is calculated from GODAS (T323) product.

The oceanic model outputs used in this complementary work are from a global Ocean General Circulation Model (OGCM) (http://www.mercator-ocean.fr/) and were provided by MERCATOR. This configuration, labeled as T323, is an eddy-permitting ¼ ° resolution model, that solves the primitive equations using the Océan PArallélisé (OPA) model [Madec et al., 1998] that has been developed at the Laboratoire d'Océanographie et du Climat: Expérimentations et Approches Numériques (LOCEAN, Paris, France). The model was forced with 3-hour and daily forcing (corrected precipitation and radiative fluxes only) from ERA-Interim. The experiment was initialized on January 1989 and ran until December 2011.

In order to calculate the Kelvin wave amplitude for the most energetic baroclinic modes (m= 1, 2 and 3), a similar methodology to that described in Dewitte et al. [2003] was used. It consists in projecting the variability on the vertical (baroclinic) and horizontal (Kelvin and Rossby) modes as obtained from the vertical mode decomposition of the mean stratification over the period 1989–2011. Usually wave amplitude is considered as its contribution to sea level or zonal current anomalies. Here, to compare with observed thermocline fluctuations as derived from the TAO data, we consider the Kelvin and Rossby wave contributions to thermocline anomalies following Dewitte [2000], namely considering the vertical isotherm displacements at the depth of the mean thermocline under the hydrostatic approximation. The details of the method can be found in Dewitte [2000].

Following Mosquera-Vásquez et al. (2013) we use a simplified mixed-layer model that considers the mixing and entrainment processes as a residual. The model further separates wave-induced horizontal advection terms from those associated with a wind-driven friction layer. The temperature equation writes as follows:

$$\begin{aligned}\frac{\partial T_A}{\partial t} = & -u_K \frac{\partial T_C}{\partial x} - u_R \frac{\partial T_C}{\partial x} - u_r \frac{\partial T_C}{\partial x} - v_A \frac{\partial T_C}{\partial y} - w_A \frac{\partial T_C}{\partial z} \\ & - u_C \frac{\partial T_A}{\partial x} \qquad - v_C \frac{\partial T_A}{\partial y} - w_C \frac{\partial T_A}{\partial z} \\ & - u_K \frac{\partial T_A}{\partial x} - u_R \frac{\partial T_A}{\partial x} - u_r \frac{\partial T_A}{\partial x} - v_A \frac{\partial T_A}{\partial y} - w_A \frac{\partial T_A}{\partial z} \\ & + \frac{Q_{SW}}{\rho_0 C_p h} + \frac{Q_{LW}}{\rho_0 C_p h} + \frac{Q_L}{\rho_0 C_p h} + \frac{Q_S}{\rho_0 C_p h} + \frac{Q_P}{\rho_0 C_p h} \\ & + R\end{aligned} \tag{2.1}$$

where all the terms included in Equation (2.1) have been averaged from the surface to the depth h (h = 50 m). Subscript C and A in some variables represent climatology and anomaly, respectively. The variables T, (u, v, w) and F are the temperature, velocity (zonal, meridional and vertical) and surface energy fluxes, respectively. Subscript K, R and r in zonal currents indicates the contribution of Kelvin, Rossby and the residual consisting in the difference between the total anomalous currents and the sum of Kelvin and Rossby current contribution (*i.e.* u_r=u_A-(u_K+u_R)). The surface heat fluxes anomaly is

estimated following Wang and McPhaden (1999), namely $F_A = \frac{Q_0 + Q_P}{\rho_0 C_p |h|}$, where Q_0 is the sum of anomalies of shortwave radiation (Q_{SW}), longwave radiation (Q_{LW}), latent heat (Q_L) and sensible heat (Q_S) (i.e. $Q_0 = Q_{SW} + Q_{LW} + Q_L + Q_S$), while Q_P is the outgoing shortwave fluxes that escapes from the bottom of the mixed layer: $Q_P = -0.45 \cdot Q_{SW} \cdot e^{-\gamma |h|}$. C_p and ρ_0 are the heat capacity (C_p =3940 J kg^{-1} °C^{-1}) and the density (ρ_0=1022.4 kg m^{-3}) of the seawater. γ^{-1} = 25 m is the attenuation length scale. Finally, R is the residual of the budget that includes unresolved physical processes in the model, such as vertical diffusion or entrainment.

2.2.3 Results

First, the model outputs (especially temperature and 20°C isotherm depth) are validated against *in situ* data (TAO) and an ocean reanalysis product (GODAS). The analysis of the long term trend in the model over the period 1989-2011 portrays a dipole pattern in the zonal and vertical axes, similarly to TAO and GODAS products (see **Figure 2.1**). On one hand, there is a negative tendency in the central and eastern Pacific in the upper 100 meters (T323 is weaker than TAO and GODAS), most likely associated with La Niña state observed in the last decade. On the other hand, a positive trend in the western Pacific (between 100 and 300 meters) is also represented correctly by T323 according with the GODAS product. Concerning the interannual variability, the model is compared to the SST and thermocline depth anomaly from TAO over the period 2000-2011 (interval of time that does not consider the very strong 1997/1998 El Niño in order to emphasize the intraseasonal timescales in the statistics). Results are displayed in **Figure 2.2**. The thermocline depth interannual variability is in agreement with the observation, with a correlation between model and TAO data that remains larger than 0.8, while the Root Mean Square error (RMSe) is lower than around 9 m. For SST interannual anomalies, the correlation between model and observations shows a maximum (~0.8) close to the dateline and then decrease towards the East where is reaches a value of 0.5. The peak in RMSe between model and observed SST interannual anomalies is located in the eastern Pacific and reaches 1.2 °C. Despite such bias, the model skill is consistent with other models that do have any data assimilation. The use of a free run is here motivated by the conservation of energy, which ensures that the

residual does not results from compensating errors associated with the assimilation process.

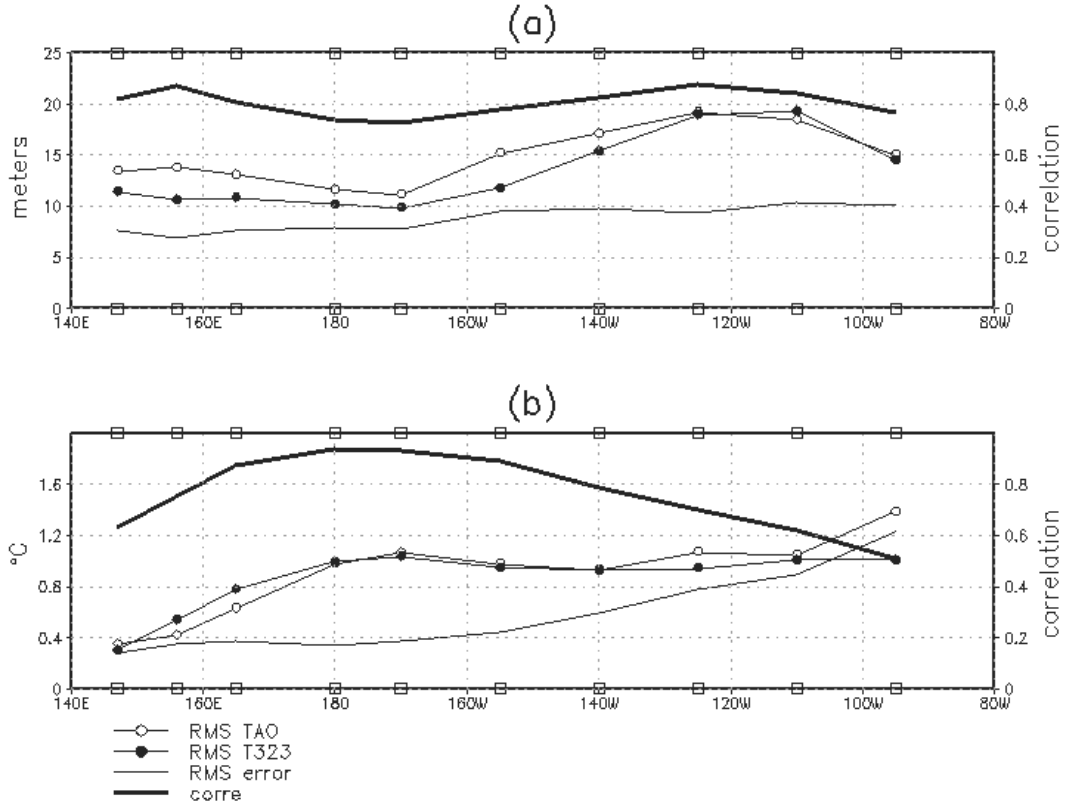

Figure 2.2 Validation of the T323 for the period 2000-2011 (interannual scale) for the thermocline (a) and SST (b). RMS for TAO (T323) is represented by opened (closed) circles and RMS-error (correlation) is displayed with thin (thick) line. Correlation scale is located on the right of each panel. Open squares, in the upper and lower edge of each panel, indicate the place of the equatorial mooring buoys of TAO project.

The heat budget analysis is performed for the following seven El Niño events: 1991/1992 (91EN92), 1994/1995 (94EN95), 1997/1998 (97EN98), 2002/2003 (02EN03), 2006/2007 (06EN07) and 2009/2010 (09EN10). This selection was performed based on the results of a wavelets analysis (using Paul wavelet function) of the zonal averaged [180-80°W] rate of temperature term at interannual timescales averaged within the mixed layer ($\partial T_A/\partial t$) and along the equator band. The analysis is displayed in **Figure 2.3**. The selected El Niño events exhibit a significant energy peak of the wavelet power in the frequency band between 0.5 and 2 year-1 (see **Figure2.3d**). Note that, this analysis indicate, except for the 97EN98 and 09EN10, the wavelet power

tends to peak around the period of ~ 1 year (see **Figure2.3c**), suggesting that these El Niño events could be interpreted as a modulation of the seasonal cycle.

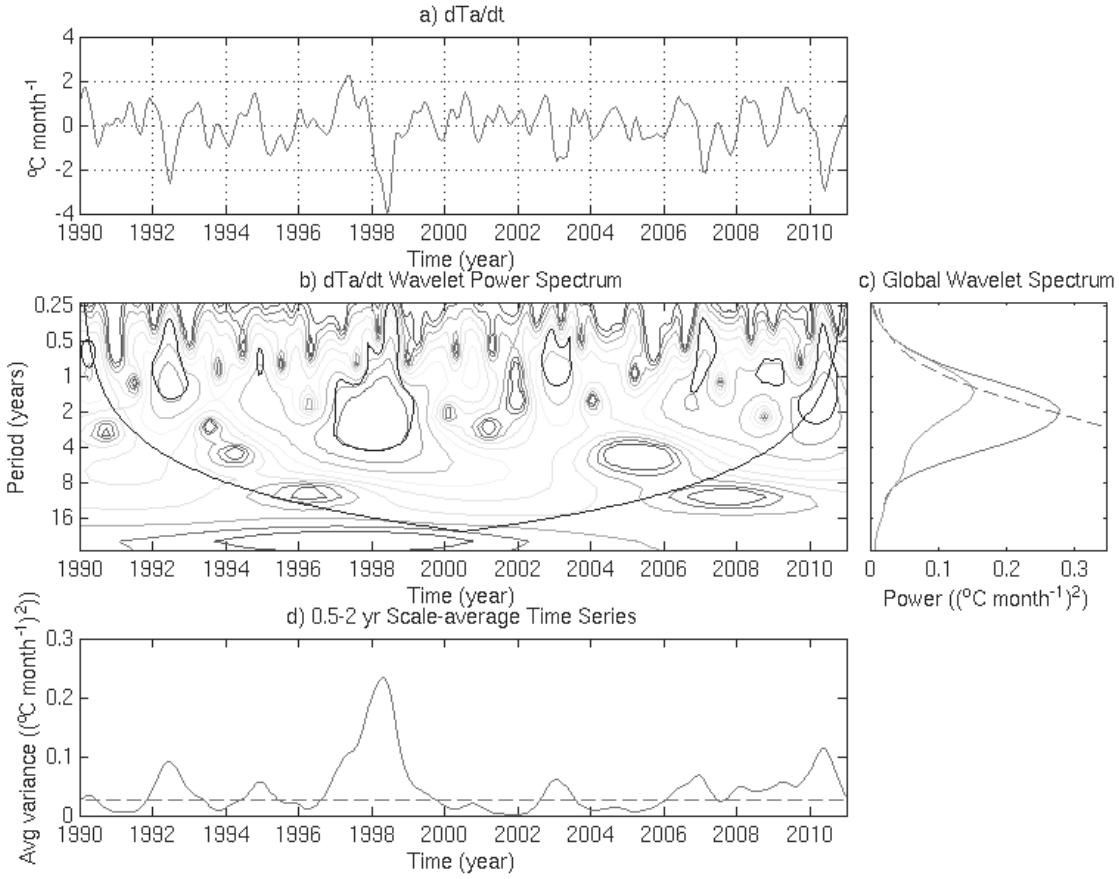

Figure 2.3 Wavelets power spectrum (using Paul wavelet function) applied to the spatial mean (180°E-80°W) of $\partial T_A / \partial t$. Panel (a) is the time series of $\partial T_A / \partial t$ (in °C.month^{-1}), (b) is the power spectrum, (c) is the mean of the power wavelet spectrum for the entire period (blue line) and for the period that does not include the 1996-2000 chunck (red line); (d) Scaled-average spectrum within the periods 0.5 years and 2 years .

Figure 2.4 shows the Hovmöller diagram of the SST anomaly (black contours with solid (dashed) line representing positive (negative) values), and Interannual Kelvin wave (IAKw) activity over the thermocline (colors) for the selected seven El Niño events. The figure shows that the intensity and frequency of the IAKw before 2000 are stronger than after 2000. Also, **Figure 2.4**, emphasizes that the maximum value of the SST anomaly is not located at the same period of the year: for instance the 91EN92 has its maximum SST anomaly value between January – February, whereas 97EN98 peaks in November-December.

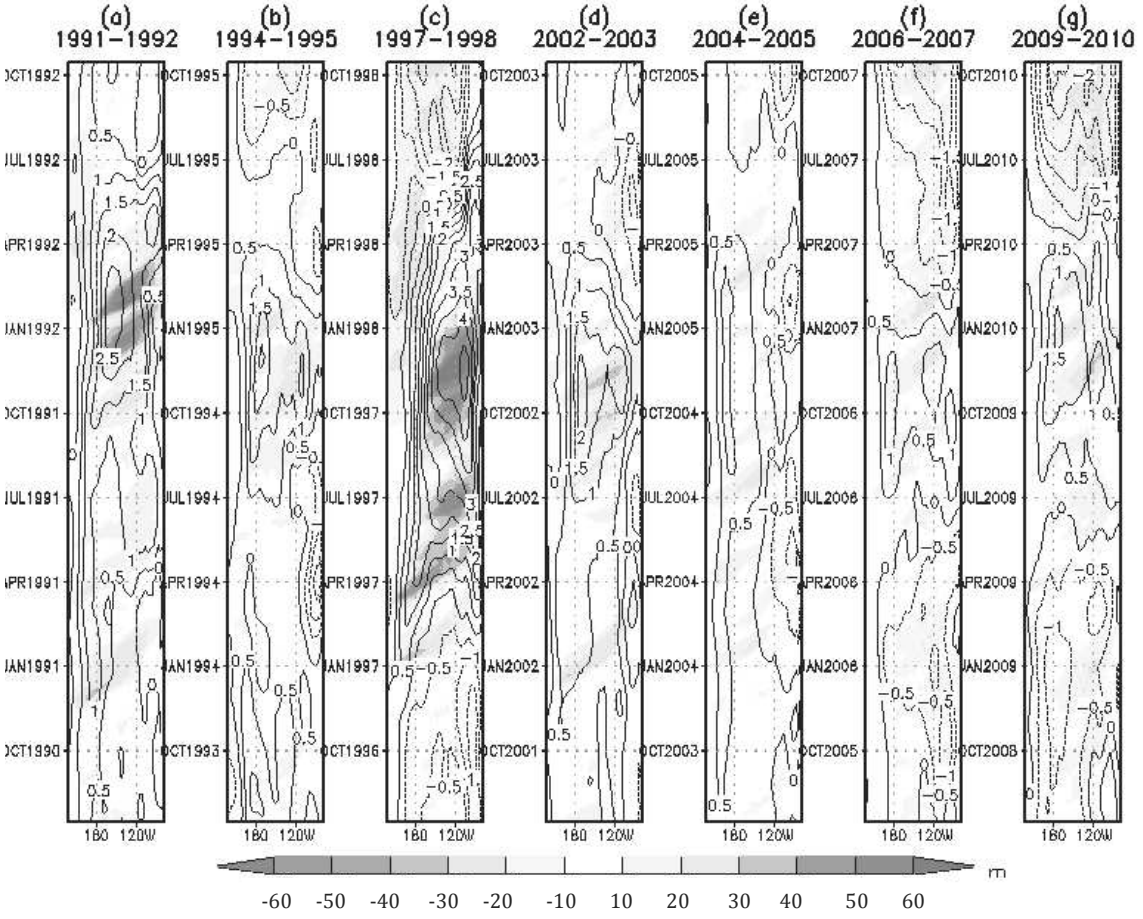

Figure 2.4 Hovmöller diagrams of the SST anomaly (contours) and the activity of the Interannual Kelvin waves (IAKw) over the thermocline (colors) along the equatorial Pacific for seven El Niño events.

In order to evaluate the dispersion of the physical processes involved in the seven selected El Niño events, we first identified the warming and cooling phases in each El Niño using the tendency term of the monthly SST interannual anomaly $\partial TA/\partial t$ in N3eq (150°-90°W, equatorial line) (region where this term has its maximum variability). The warming and cooling phases are used to adjust the Hovmöller diagrams of Figure 2.5. The motivation in this section is to provide an objective way to compare the characteristics of the time evolution of the El Niño events (e.g. duration of the warming and cooling phases), considering that they do not have the same climatological evolution. In the Figure 2.5, the SST anomaly is displayed using black lines and $<\partial TA/\partial t$ is shaded with colors. Then, the different fields were averaged in 3 boxes:

N4eq (160°E-150°W, equatorial line), N34eq (170°-120°W, equatorial line) and N3eq for the onset of the warming phase and for each event.

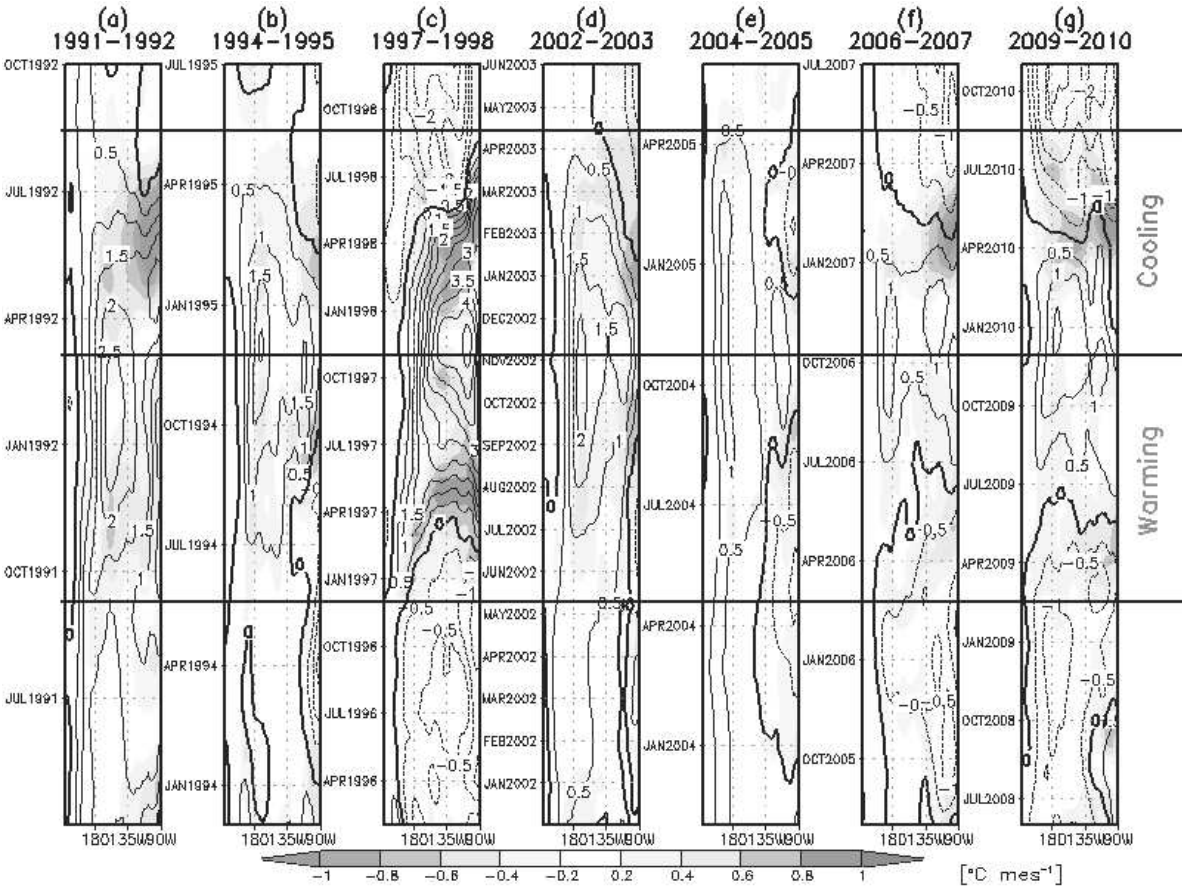

Figure 2.5 Hovmöller diagrams of the tendency of the SST anomaly ($\partial T_A/\partial t$, in colors) and SST anomaly (black contour) for seven El Niño events along the equatorial Pacific. To compare the warming and cooling phase of each event, the temporal scale of each diagram has been adjusted in base of the information indicated in Table 1. The scale of the tendency is located on the bottom. Horizontal dark lines indicate and separate the warming and cooling phase.

In the warming phase (see **Figure 2.6, 2.7** and **2.8**), the most important terms which play a significant part in changing the SST anomaly in the three equatorial regions (N3eq, N34eq and N4eq) are: the zonal (vertical) advection of the climatological SST by the anomalous zonal (vertical) currents, the vertical advection of the SST anomaly by climatological vertical current, the short wave radiation, the latent flux and the residual term.

In general, the rate of change in the SST anomaly (°C.month^{-1}) in N3eq is larger than in N34eq, and both rates are larger than in N4eq. The extraordinary 97EN98 El Niño event shows the largest tendency in N3eq and N34eq regions (~0.5 and 0.4 °C.months^{-1}, respectively), but in N4eq it shows comparable rate of change than 94EN95, 06EN07 and 09EN10 El Niño events. The 04EN05 has the most modest tendency in all the equatorial regions (around 0.1 °C.months^{-1}). The 91EN92, 94EN95, 02EN03, 06EN07 and 09EN10, in N3eq and N34eq, have similar rate of change ~0.25 °C.months^{-1} (see **Figure 2.6, 2.7** and **2.8**).

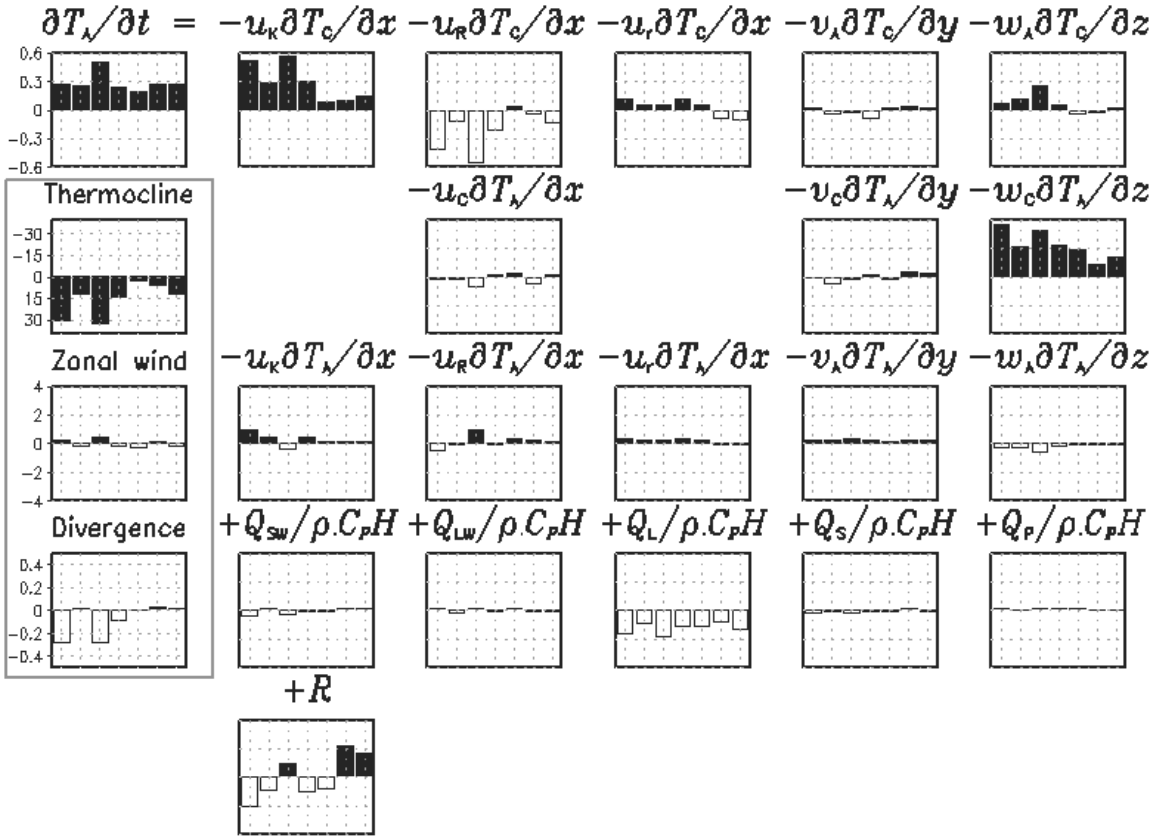

Figure 2.6 Seven-bar plots for each term of Equation (2.1) and, in the red square, thermocline (meters), zonal wind (m/s) and divergence (m/s/degree) anomaly. Each bar indicates each individual selected El Niño event in N3eq in the warming phase. From left to right, a bar indicates El Niño events: 1991/1992, 1994/1995, 1997/1998, 2002/2003, 2004/2005, 2006/2007 and 2009/2010. Filled (no filled) bar means warming (cooling) contribution (°C month^{-1}) in the terms of equation (1), while for the variables inside the red square the bars symbolizes positive (negative) anomaly.

The zonal advection of the climatological SST due to the zonal current anomaly (zonal advective feedback), in the three El Niño regions, is an important physical process in the first four El Niño phenomena analyzed in this work (91EN92, 94EN95, 97EN98 and 02EN03). The influence of the interannual long equatorial waves is important in the three El Niño regions, but with more intensity in N3eq and N34eq, where Kelvin ($u_K \partial T_C/\partial x$) and Rossby ($u_R \partial T_C/\partial x$) waves contributions to the zonal advection terms leads to a warming and cooling respectively. The wind tress anomalies in the N3eq and N34eq regions associated to these waves can be observed in in **Figure2.7** and **Figure 2.8,** respectively. On the other hand, ur∂TC/∂x, the zonal advection associated to the residual currents (i.e. associated with the wind energy that is not projected onto the wave dynamics) is more important in the central and western Pacific. Finally, the last three El Niño events appears to be less influenced (compared with the first four El Niño) by the interannual long equatorial waves and the residual zonal current anomaly.

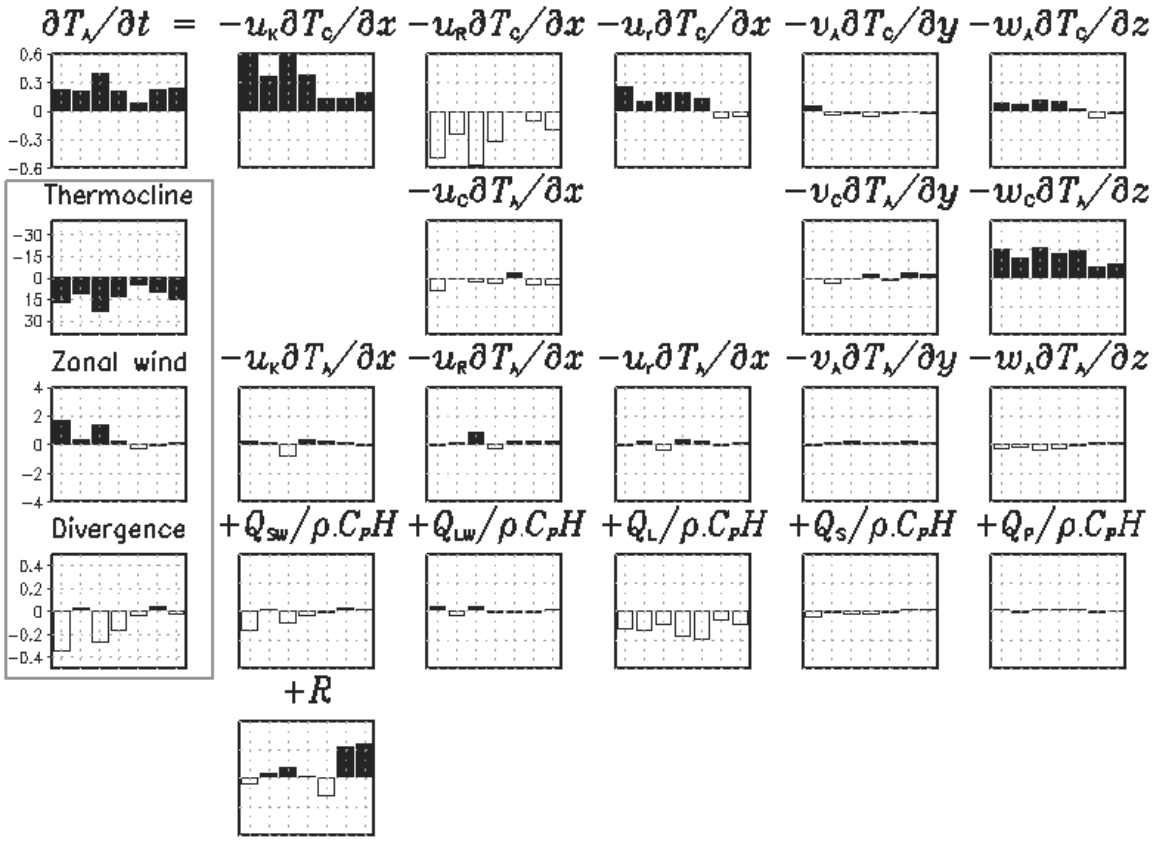

Figure 2.7 Similar to Figure 2.6, but for N34eq region.

Again, in the first four El Niño events the $w_A \partial T_C/\partial z$ term has a significant role in the warming phase, with a maximum value in N3eq in 97EN98. $w_A \partial T_C/\partial z$ does not have a signitificant contribution to the SST anomalies during the others three El Niño.

The so-called "thermocline feedback" ($w_C \partial T_A/\partial z$) term (related with IAKw), as it is expected, is more important in the central and eastern Pacific. The results show that thermocline feedback has an important impact over N3eq in 91EN92 associated with the downwelling IAKw driven by the strong zonal wind anomaly (compared with the 97EN98) in the western Pacific (see **Figure 2.8**). It is possible to speculate that there is a negative tendency of this term in N3eq from 91EN92 to 06EN07 in N3eq, probably related with the decreased activity in IAKw in the last decade (see **Figure 2.4** to see activity of the IAKw over the thermocline). Also, over N4eq (Figure 2.8) the zonal wind anomaly is strong only in the first four El Niño.

As it is expected, the impact of the short wave radiation ($-Q_{SW}/(\rho C_p H)$) is reduced due the increase of the convection in N4eq that is associated with the increase in the SST anomaly. Six of the seven El Niño have this characteristic, except the 06EN07 that has a positive value. Moreover, the latent heat fluxes ($-Q_L/(\rho C_p H)$) in N34eq and N3eq, also has negative values that is a consequence of increased low level wind convergence in that regions. In N3.4eq (N3eq) the maximum values is observed in 02EN03 (91EN92 and 97EN98).

The residual term (R), which contains unresolved terms by our mixed-layer model (entrainment and vertical diffusion), does not exhibit a disctintive pattern . In N4eq (N3.4eq - N3eq), the positive value is a characteristic of 91EN92, 94EN95, 02EN03 and 09EN10 (94EN95, 97EN98, 06EN07 and 09EN10 – 97EN98, 06EN07 and 09EN10). The other El Niños have negative tendency.

Concerning the non-linear terms, the $u_r \partial T_A/\partial x$ has a cooling effect in the warming phase, mainly, for the first four El Niño phenomena over N4eq. The term $u_K \partial T_A/\partial x$ in N3.4eq and N3eq has a positive effect almost in all El Niño events, except in 97EN98.

This analysis also highlights the changes in the intensity of IAKw after 02EN03, which are driven by zonal wind anomaly in the western Pacific. The latter has showed also an abrupt change in intensity after 02EN03 (see Zonal Wind in **Figure 2.8**).

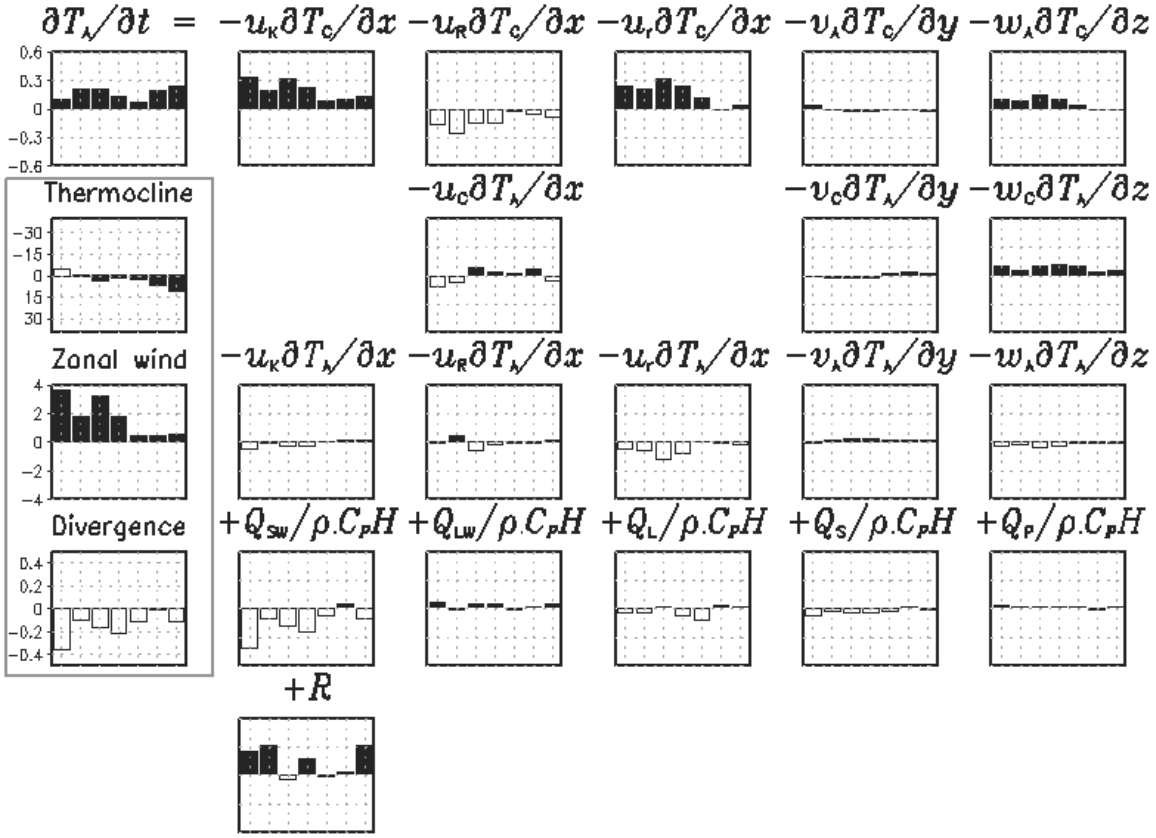

Figure 2.8 Similar to Figure 2.6, but for N4eq region.

As a summary, these results indicate that the intensity of the IAKw has decreased since the 1997/1998 El Niño event and, as a consequence, its impact on the SST was reduced with slighter zonal advection feedback and thermocline feedback processes in the central and eastern Pacific, respectively. The interannual zonal wind in the western Pacific has been weak after the 2002/2003 El Niño which is probably related to the permanent "La Niña state" that maintain a cooling (warming) state tendency in the upper 100 (between 100 and 300) meters in the central eastern Pacific (western Pacific). Finally, the results indicate that in the central and eastern Pacific other physical processes (mixing and entrainment), not resolved by our simple heat budget model, become important in the warming phase of El Niño for the last three events.

Chapter 3: The Central Pacific El Niño Intraseasonal Kelvin wave

3.1 Overview

This chapter focuses on the study of the IntraSeasonal Kelvin wave (ISKw) in the equatorial Pacific. The characteristics of the ISKw is documented and interpreted over the 1989-2011 period, based on observations, simulation with a linear model (Mosquera, 2009) and the outputs of an Ocean General Circulation Model (OGCM). The wave activity during the Central Pacific (CP) El Niño events is contrasted with the extraordinary El Niño of 1997/1998. One of the most important results is that ISKw activity is enhanced in Austral Summer (Spring) in the central Pacific (west of ~120°W) during CP El Niño events. Experimentation with the linear model indicates that the Austral Summer peak is wind-forced, while the Austral Spring peak is not and consequently results from non-linear processes. In addition, a strong dissipation of the ISKws is observed east of 120°W which cannot be accounted for by a linear model using a Rayleigh friction. A vertical and horizontal mode decomposition of the OGCM simulation further confirms the sharp changes in characteristics of the ISKws as well as the reflection of the latter into first-meridional Rossby wave at the longitude where the maximum zonal gradient of the thermocline is found (~120°W). The analysis suggests that the confinement of CP El Niño warming in the central Pacific may result from the reinforcement of the zonal gradient in stratification associated with the cold La Niña-like conditions since the 90s, favoring the scattering of energy of the ISKws in the eastern Pacific.

This chapter contains the paper by Mosquera-Vásquez et al. published in Journal of Geophysical Research in 2014.

3.2 Article published in Journal of Geophysical Research - Oceans

The Central Pacific El Niño Intraseasonal Kelvin Waves

Kobi A. Mosquera-Vásquez, Boris Dewitte and Serena Illig

Abstract

In this study, we document and interpret the characteristics of the IntraSeasonal Kelvin wave (ISKw) in the Pacific over the 1989–2011 period, based on observations, a linear model, and the outputs of an Ocean General Circulation Model (OGCM). We focus on the wave activity during the Central Pacific (CP) El Niño events contrasting with the extraordinary El Niño of 1997/1998. We find that the ISKw activity is enhanced in Austral summer (spring) in the central Pacific (west of ~120ºW) during CP El Niño events. The linear model experiment indicates that the Austral summer peak is wind-forced, while the Austral spring peak is not and consequently results from nonlinear processes. In addition, a strong dissipation of the ISKws is observed east of 120ºW which cannot be accounted for by a linear model using a Rayleigh friction. A vertical and horizontal mode decomposition of the OGCM simulation further confirms the sharp changes in characteristics of the ISKws as well as the reflection of the latter into first-meridional Rossby wave at the longitude where the maximum zonal gradient of the thermocline is found (~120ºW). Our analysis suggests that the confinement of CP El Niño warming in the central Pacific may result from the reinforcement of the zonal gradient in stratification associated with the La Niña-like conditions since the late of the 1990s, leading to scattering of the energy of the ISKws in the eastern Pacific.

AGU PUBLICATIONS

JGR

Journal of Geophysical Research: Oceans

RESEARCH ARTICLE
10.1002/2014JC010044

The Central Pacific El Niño intraseasonal Kelvin wave

K. Mosquera-Vásquez[1], B. Dewitte[2], and Serena Illig[2]

[1]Instituto Geofísico del Perú, Lima, Perú, [2]Laboratoire d'Etudes en Géophysique et Océanographie Spatiales, Toulouse, France

Key Points:
- Intraseasonal temperature variability is dominant in the vicinity of the thermocline
- CP El Niño is associated with an increase in intraseasonal equatorial Kelvin activity
- Intraseasonal Kelvin wave starts strongly dissipating around 120°W

Correspondence to:
K. Mosquera-Vásquez,
kobi.mosquera@igp.gob.pe

Citation:
Mosquera-Vásquez, K., B. Dewitte, and S. Illig (2014), The Central Pacific El Niño intraseasonal Kelvin wave, *J. Geophys. Res. Oceans*, *119*, 6605–6621, doi:10.1002/2014JC010044.

Received 10 APR 2014
Accepted 27 AUG 2014
Accepted article online 2 SEP 2014
Published online 6 OCT 2014

Abstract In this study, we document and interpret the characteristics of the IntraSeasonal Kelvin wave (ISKw) in the Pacific over the 1989–2011 period, based on observations, a linear model, and the outputs of an Ocean General Circulation Model (OGCM). We focus on the wave activity during the Central Pacific (CP) El Niño events contrasting with the extraordinary El Niño of 1997/1998. We find that the ISKw activity is enhanced in Austral summer (spring) in the central Pacific (west of ~120°W) during CP El Niño events. The linear model experiment indicates that the Austral summer peak is wind-forced, while the Austral spring peak is not and consequently results from nonlinear processes. In addition, a strong dissipation of the ISKws is observed east of 120°W which cannot be accounted for by a linear model using a Rayleigh friction. A vertical and horizontal mode decomposition of the OGCM simulation further confirms the sharp changes in characteristics of the ISKws as well as the reflection of the latter into first-meridional Rossby wave at the longitude where the maximum zonal gradient of the thermocline is found (~120°W). Our analysis suggests that the confinement of CP El Niño warming in the central Pacific may result from the reinforcement of the zonal gradient in stratification associated with the La Niña-like conditions since the late of the 1990s, leading to scattering of the energy of the ISKws in the eastern Pacific.

1. Introduction

Recent studies have reported the existence of at least two types of El Niño events [*Ashok et al.*, 2007; *Kao and Yu*, 2009; *Kug et al.*, 2009]: one with anomalies peaking in the eastern Pacific (i.e., Eastern Pacific (EP) El Niño or cold tongue El Niño) like in 1997/1998, and one having its center of action in the central Pacific referred to as Modoki El Niño or Central Pacific (CP) El Niño (as referred hereafter) or warm pool El Niño. The exact nature and mechanism of the latter have been the subject of debate in the community [*Capotondi et al.*, 2014] due in part to its apparent increase in occurrence in recent decades [*Yeh et al.*, 2009; *Lee and McPhaden*, 2010] and the difficulty to interpret these two types of events as the expression of either two distinct regimes [*Takahashi et al.*, 2011] or a continuum in the ENSO variability [*Giese and Ray*, 2011; *Johnson*, 2013]. There have been also some difficulties in interpreting the recent El Niño events from current ENSO theories [*Xiang et al.*, 2013]. For instance, although *Ren and Jin* [2013] suggest that CP El Niño can be understood to a large extent by the recharge oscillator mechanism, *Kug et al.* [2009] indicate that CP El Niño are characterized by a weak recharge-discharge process and the phase relationship between the two dominant modes of the thermocline variability (i.e., the so-called tilt and warm water volume modes) has changed at the beginning of the 21st century [*McPhaden*, 2012]. In term of thermodynamical processes within the mixed-layer, CP El Niño events tend to be dominated by the zonal advective feedback in the central Pacific with a weak contribution from thermocline feedback in the eastern equatorial Pacific [*Kug et al.*, 2009; *Ren and Jin*, 2013]. On the other hand, CP El Niño events are also associated with equatorial Kelvin wave dynamics [*Dewitte et al.*, 2012a] that have the potential to produce anomalous vertical advection in the eastern Pacific [*Mosquera-Vásquez et al.*, 2013]. The former studies, however, do not explain why the SST warming remains confined in the central Pacific, calling for the investigation of other processes including nonlinear ones [*Xiang et al.*, 2013; *Dommenget et al.*, 2012]. The fact that the recharge-discharge process is weak during CP El Niño, implying that the ocean state prior to its development is weakly influential, suggests that CP El Niño evolution are more likely to be influenced by random atmospheric forcing during its development phase. Random atmospheric noise usually refers to the components of the Intraseasonal atmospheric Tropical Variability (ITV) [*Wheeler and Kiladis*, 1999] including the Madden Julian Oscillation (MJO) [*Madden and*

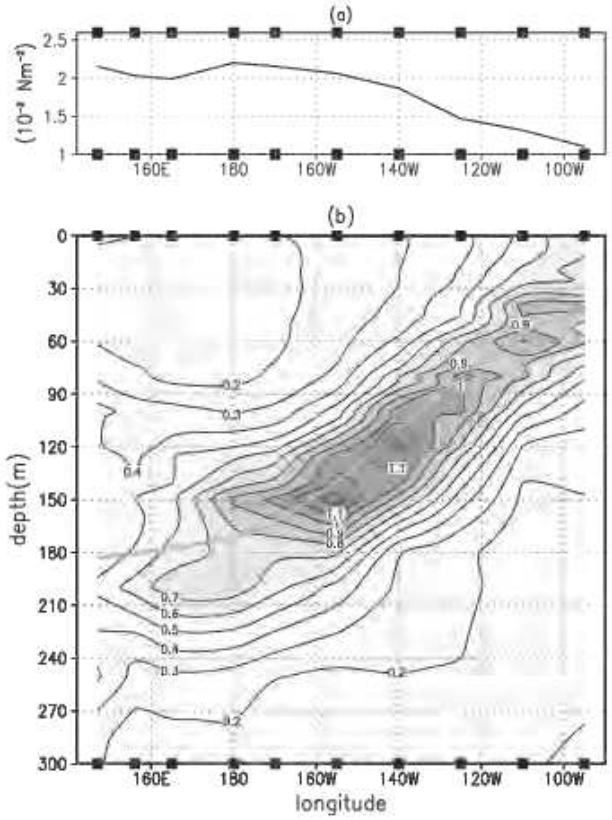

Figure 1. Root mean square (RMS) along the equatorial band (2°S–2°N) of the (a) intraseasonal zonal wind stress as a function of longitude (in 10^{-2} N m^{-2}) and (b) intraseasonal temperature as a function of longitude and depth (in °C) from TAO data for the period 2000–2011. The green thick line in Figure 1b indicates the mean thermocline depth (20°C isotherm depth). The squares on the longitude axis indicate the positions of the TAO mooring buoys.

Julian, 1972] and Westerly Wind Bursts (WWBs). The MJO and WWBs, however, may be influenced by the background oceanic state during ENSO [*Eisenman et al.*, 2005; *Roundy and Kravitz*, 2009; *Seiki and Takayabu*, 2007]. For instance, *Roundy and Kravitz* [2009] indicated that weather patterns, comprising those associated with MJO, tend to evolve differently in association with oceanic Kelvin waves during different phases of ENSO. These former studies are consistent with the notion that the ENSO-state dependence of the ITV serves as a source of stochastic forcing for ENSO [*Jin et al.*, 2007; *Kug et al.*, 2009]. The oceanic expression of the ITV is composed of the intraseasonal Kelvin wave (ISKw) that is forced by WWB and was shown to be influential for triggering strong EP El Niño events [*Bergman et al.*, 2001; *McPhaden et al.*, 2006]. In particular, the 1997/1998 El Niño was associated with two pulses of ISKw prior to its development [*Dewitte et al.*, 2003] which may have triggered the initial warming in the central Pacific leading to the growth of the SST anomalies [*Lengaigne et al.*, 2004]. The 1997/1998 El Niño is rather peculiar because the peak activity of the ISKw took place ~6 months prior the El Niño peak [*Ramos et al.*, 2008], which reflects the strong seasonal dependence of the MJO/ENSO relationship (i.e., MJO peak variance being in May to June prior to the ENSO peak in November to December) described in former studies [*Hendon et al.*, 2007; *McPhaden et al.*, 2006].

Here we investigate the ISKw activity during CP El Niño events over the last two decades based on observations and model outputs. Our motivation is first to better understand its relationship with the CP El Niño development and decay, considering that the ISKw is influential on the spread of ENSO forecasts [*Wang et al.*, 2011] and that prediction systems exhibit a distinct forecast skill depending on the El Niño type [*Hu et al.*, 2012; *Xue et al.*, 2013]. We also aim at documenting some characteristics of the ISKw activity that cannot be inferred directly from the available observation data sets and sheding light on processes that may explain why CP El Niño events do not expand to the eastern Pacific and remain confined in the central Pacific. Former studies have largely contributed to better understanding the forcing mechanisms of the ISKw in the Pacific in particular exploiting TAO (Tropical Atmosphere Ocean project) and altimetry observations. For instance, *Cravatte et al.* [2003] used TOPEX/POSEIDON and TAO data to study the ISKws over the 1992–1999 period. They found that the ISKw characteristics (frequency, amplitude) could not be explained in a straightforward manner from linear theory. For instance, energy at (120 day)$^{-1}$ was found in the eastern Pacific that could not be attributed to wind forcing. They also noted a complex vertical structure variability associated with at least the first two baroclinic modes. Interestingly, the intraseasonal variability of temperature along the equator has also a fine vertical scale (Figure 1), with a peak amplitude in the vicinity of the

thermocline and a weak amplitude at the surface. Although the pattern of Figure 1b cannot be solely interpreted as resulting from ISKw, it is expected that vertical isotherm displacements near the thermocline along the equator will be to a large extent explained as resulting from the forced equatorial Kelvin wave [e.g., *Kessler et al.*, 1995; see also *Dewitte et al.* [2009] for the theoretical background]. Note that the variability decreases to the east of ~120°W by a factor of 1.4 that is an indication of a marked dissipation. TAO data also revealed that intraseasonal variability in the range of frequencies $[60–90 \text{ days}]^{-1}$ was also prominent in subsurface zonal current at 140°W and 110°W [*McPhaden and Taft*, 1988]. Most studies of the oceanic ISKw have argued that it is tightly linked to the MJO-induced wind stress anomalies [e.g., *Kessler et al.*, 1995; *Hendon et al.*, 1998; *Zhang*, 2001; *Roundy and Kiladis*, 2006; *Shinoda et al.*, 2008] and that it can act as a trigger of El Niño events [*Kessler and McPhaden*, 1995a, 1995b; *McPhaden*, 1999, 2002; *Kessler and Kleeman*, 2000; *Seo and Xue*, 2005]. However, the latter studies have focused on a period encompassing the strong 1997/1998 El Niño, for which there is a well-known delayed ENSO-MJO seasonal relationship [*Hendon et al.*, 2007; *McPhaden et al.*, 2006]. Recently, *Gushchina and Dewitte* [2012] have shown that the seasonal dependence of the ENSO-MJO relationship was distinctive during CP and EP El Niño events and that such difference between the two types of El Niño could reflect into the ISKw activity. They proposed in particular, that MJO activity is enhanced during the mature phase of the CP El Niño events, extending their persistence compared to EP El Niño events. This issue is worth tackling because it suggests that ITV and its oceanic expression might be tightly linked to the CP El Niño dynamics, rather than just acting as a noise maker for ENSO triggering. It calls for better understanding the ISKw dynamics during such type of ENSO event, that is, its forcing mechanism and dissipation process. This is the topic of the present paper that can be viewed as an extension of *Gushchina and Dewitte* [2012] focusing on the oceanic ISKw characteristics and its forcing mechanism. Of particular interest is the dissipation process associated with the horizontal anisotropy of the mean density in the upper thermocline. In the recent decades, the mean thermocline has been steeper due to La Niña-like conditions since the late of the 1990s [*Xiang et al.*, 2013]. Our analysis suggests that this may have favored scattering of energy of the ISKw, leading to a "trapping" of its energy in the central equatorial Pacific.

The paper is organized as follows: section 2 introduces the observed data sets and the ocean model outputs used in this study, as well as the methodology. Section 3 documents the characteristics of the propagating variability in both the observations and two models having different physics. Section 4 provides evidences of modal dispersion of the intraseasonal equatorial Kelvin wave in the eastern Pacific. Section 5 is a discussion of the results followed by concluding remarks and perspectives to this work.

2. Data and Method

The intraseasonal (IS) anomalies are estimated as the difference between the original data (either daily mean, 3 day mean or 7 day mean, depending on its source) and the filtered (1–2–1) monthly mean data interpolated at the temporal resolution of the original data. This methodology was suggested by *Lin et al.* [2000] to study intraseasonal atmospheric variability in the tropics and is similar to a high-pass filter with a transfer function characterized by a −1, −3, and −10 dB attenuation (79%, 50%, and 10% of the input power survives) at $(117 \text{ day})^{-1}$, $(168 \text{ day})^{-1}$, and $(466 \text{ day})^{-1}$, respectively. It has been used recently to study the intraseasonal oceanic variability in the upwelling systems of north Benguela [*Goubanova et al.*, 2013] and Peru [*Illig et al.*, 2014].

Interannual (IA) anomalies correspond to monthly mean data, which is smoothed with a 1–2–1 filter, relative to the mean climatology calculated over the period 1990–2011.

CP El Niño years are selected following *Yu and Kim* [2013], which leads to 1992, 1994, 2002, 2004, 2006, and 2009 as CP El Niño years. Note that the 2006 year is classified as a mixed-type El Niño year by *Yu and Kim* [2013]. However, we consider this event as a CP El Niño event considering its closer similarity to the other El Niño events of the record used in this study compared to the 1997 El Niño event. We will therefore contrast the characteristics of the CP El Niño events with the ones of the 1997/1998 El Niño that is clearly the only extreme El Niño event over the period of interest in this paper.

2.1. Sea Level Height From Altimetry

The gridded sea level anomaly (hereafter referred to as TPJ) data over the period 1993–2011 were supplied by AVISO/altimetry [*Ducet et al.*, 2000]. They were built using optimal interpolation of T/P and ERS data on a

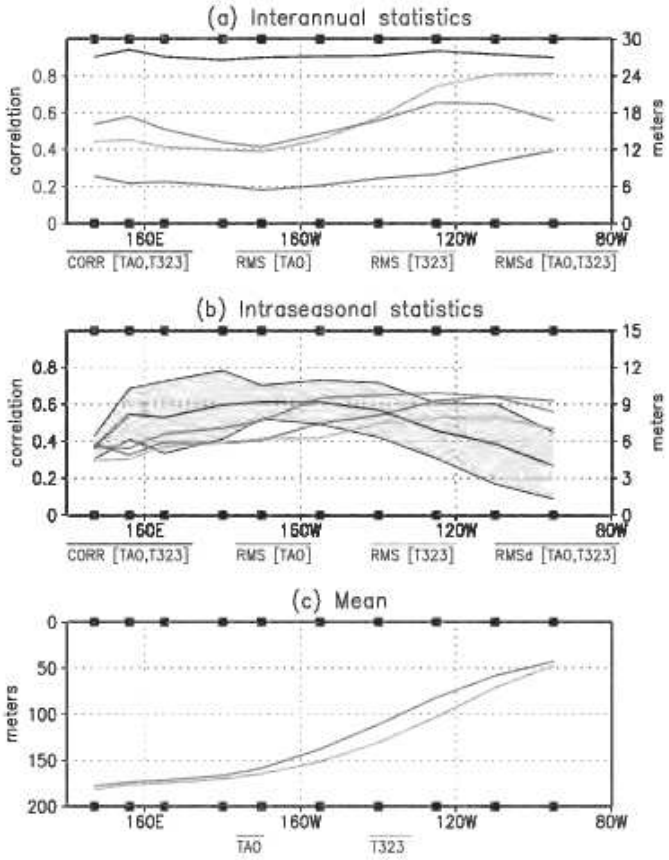

Figure 2. Validation of T323 from TAO data for the period 1990–2011: (left) correlation (black line) and (right) root mean square (RMS) difference (blue line) between observations and model for the thermocline depth (a) interannual and (b) intraseasonal anomalies. The RMS for observations and model is also displayed (red line for observations and green line for the model). The gray shading in Figure 2b provides the range of values of the correlation between model and observation over one calendar year taken within the period 1990–2011. (c) Mean thermocline depth for model (green) and observation (red). The squares on the longitude axis indicate the positions of the TAO mooring buoys. Units are in meters.

1/4°×1/4° grid every 7 days. If a precision of individual instantaneous measurements is of the order of 6 cm Root Mean Square (RMS) [*Fu et al.*, 1994], errors on such gridded product have been estimated to 2–3 cm RMS for 7 day-averaged maps and spatial scales larger than 200 km [*Le Traon and Ogor*, 1998].

2.2. SST and 20°C Isotherm Depth From TAO

In this study, we also take advantage of the TAO data [*Hayes et al.*, 1991; *McPhaden et al.*, 1998], where the SST and 20°C isotherm depth are obtained from 29 mooring buoys (2°N, 0°, and 2°S at 147°E, 156°E, 165°E, 180°, 170°W, 155°W, 140°W, 125°W, 110°W, and 95°W). In order to fill gaps in the data, a vertical linear interpolation is first applied to each time series (daily mean data) and then a linear interpolation in the zonal direction is applied in order to fill data gaps only if both neighboring data are available. Then, a meridional mean (2°S, 0°, and 2°N) provides an estimated equatorial section without missing data. Note that some linear temporal interpolations are necessary, especially at 95°W. Such interpolation procedure is acceptable until 2011 when the density of the TAO data remains reasonable (above 60% at 100 m in the eastern equatorial Pacific) but cannot be performed beyond that date due to the maintenance suspension of the TAO array (density of data falls below ~25% at 100 m from 2012, see *Takahashi et al.* [2014], Figure 5.2). The limitations associated with the interpolation of the TAO data have motivated the use of a model simulation for the interpretation of the observational results.

2.3. The OGCM Simulation (T323)

The model product used in this work belongs to the set of MERCATOR global OGCM simulations (http://www.mercator-ocean.fr/). The configuration, referred to as T323, is an eddy-permitting 1/4° model with 50 vertical levels (whom 23 belong to the upper 100 m). It is based on the primitive-equation global OGCM Océan PArallélisé (OPA) [*Madec et al.*, 1998] and is developed at the Laboratoire d'Océanographie et du Climat: Expérimentations et Approches Numériques (LOCEAN, Paris, France). T323 was forced with 3 h (surface winds) and daily forcing (corrected precipitation and radiative fluxes only) from ERA-Interim. Here the experiment was initialized on January 1989 from rest and with temperature and salinity from Levitus data [*Levitus and Boyer*, 1994]. Since no spin-up is used, only intraseasonal to interannual variability will be discussed in the paper and the year 1989 is disregarded in the estimation of the reference climatology.

Table 1. Validation of Thermocline Depth Interannual Variability: Zonal Mean for RMS, Correlation, and RMS Difference Between T323 and Observations (TAO) at 147°E, 156°E, 165°E, 180°, 170°W, 155°W, 140°W, 125°W, 110°W, and 95°W (Mooring Locations)

Mean Correlation [T323,TAO]	Mean RMS [T323] (m)	Mean RMS [TAO] (m)	Mean RMS Difference [T323,TAO] (m)
0.91	17.0	16.3	7.7

Despite the fact that there is no data assimilation in this experiment, the model is skillful in capturing most aspects of the equatorial variability in the Pacific Ocean. In particular, a comparable model configuration has been evaluated previously [*Dewitte et al.*, 2007; *Mosquera-Vásquez et al.*, 2013], which indicated that the model simulates realistically the fundamental features relevant to the equatorial wave dynamics at interannual timescales, including the mean temperature vertical structure. Despite the increased vertical resolution of the present version of the model compared to the version used in *Mosquera-Vásquez et al.* [2013], the realism of the mean thermocline (Figure 2c) is comparable, with a bias that consists in a weaker zonal and vertical gradient in the central equatorial Pacific than the observations. The interannual variability simulated by the model is rather realistic (Figure 2a, Tables 1 and 2). Regarding intraseasonal variability (Figure 2b), the realism of the model is reduced compared to interannual timescales, with still a fair agreement with observations. Since the ISKw activity is modulated at seasonal [*Illig et al.*, 2014] and interannual [*Dewitte et al.*, 2008] timescales, the validation of intraseasonal variability over the relative long record used here is a rather stringent test. The dispersion of the annual correlation is indicated in Figure 2b that shows that the correlation can reach up to 0.7 in the western Pacific for some specific periods. The most realistic period is 2004–2008, with 1996–1998 being the period with the lowest skill (not shown). Such limitation should be kept in mind for the interpretation of the results, considering that T323 is used as a diagnostic tool for the interpretation of the results derived from TAO.

The model outputs are further used to derive an estimate of the equatorial waves (sum of the first three baroclinic modes) based on a modal decomposition of the variability (pressure and zonal current), which is not possible to estimate from the available observations. The modal decomposition consists in deriving the vertical modes from the zonally slow-varying stratification over which pressure and zonal current anomalies are projected. This provides the baroclinic mode contribution to sea level and zonal current anomalies which are then projected onto the theoretical Kelvin and Rossby wave structures to derive the wave coefficients. The method is similar to *Dewitte et al.* [1999] and has been shown to extract the salient features of the equatorial waves [*Mosquera-Vásquez et al.*, 2013], including the effect of the zonally varying stratification, which is of major interest in this paper (see section 3.2).

2.4. Linear Ocean Model (LOM)

A simple Linear Ocean Model (hereafter referred to as LOM) for the tropical Pacific is used to interpret the characteristics of the ISKw in the equatorial Pacific as estimated in the OGCM T323 simulation. The linear model was used previously in *Mosquera* [2009]. It consists in one active layer with a linear friction of time decay τ. Note that the value of τ can varies from 6 to 30 months depending on the studies [*Picaut et al.*, 1993; *Dewitte et al.*, 1999] which reflects that dissipation processes may be frequency dependent and/or that a linear friction is not perfectly adequate to simulate wave dissipation. In this study, we will also use a linear friction to test to which extent it is adequate for simulating wave dissipation evidenced in the OGCM. Three experiments are carried out that differ either from the values used for friction or the structure of the thermocline: LOM-CR (control run) is the experiment that uses a constant friction of $(24\ \text{month})^{-1}$, while LOM-Rx uses a zonally varying time decay for friction, both experiments having a constant depth thermocline (H = 150 m). LOM-Hx is the experiment in which a zonally varying thermocline is used (derived from *Levitus and Boyer* [1994] data) along with a constant linear friction of $(24\ \text{month})^{-1}$.

Table 2. Correlation and RMS Difference of the Zonal Current Anomalies Averaged in the First 55 m Between T323 and TAO (1993–2010) at Five Mooring Locations

Mooring Longitude	147°E	165°E	170°W	140°W	110°W
Mean correlation	0.8	0.84	0.67	0.5	0.64
Mean RMS difference (cm s^{-1})	14.7	14.8	17.3	20.1	21.4

Consistently with the T323 simulation, LOM is forced with wind stress anomalies derived from ERA-Interim data. Note that we also used wind stress from the NCEP/NCAR reanalysis and the results presented here are similar for both surface forcings. For consistency with the T323 outputs, only the results of the linear model with forcing from ERA-Interim fluxes are presented here.

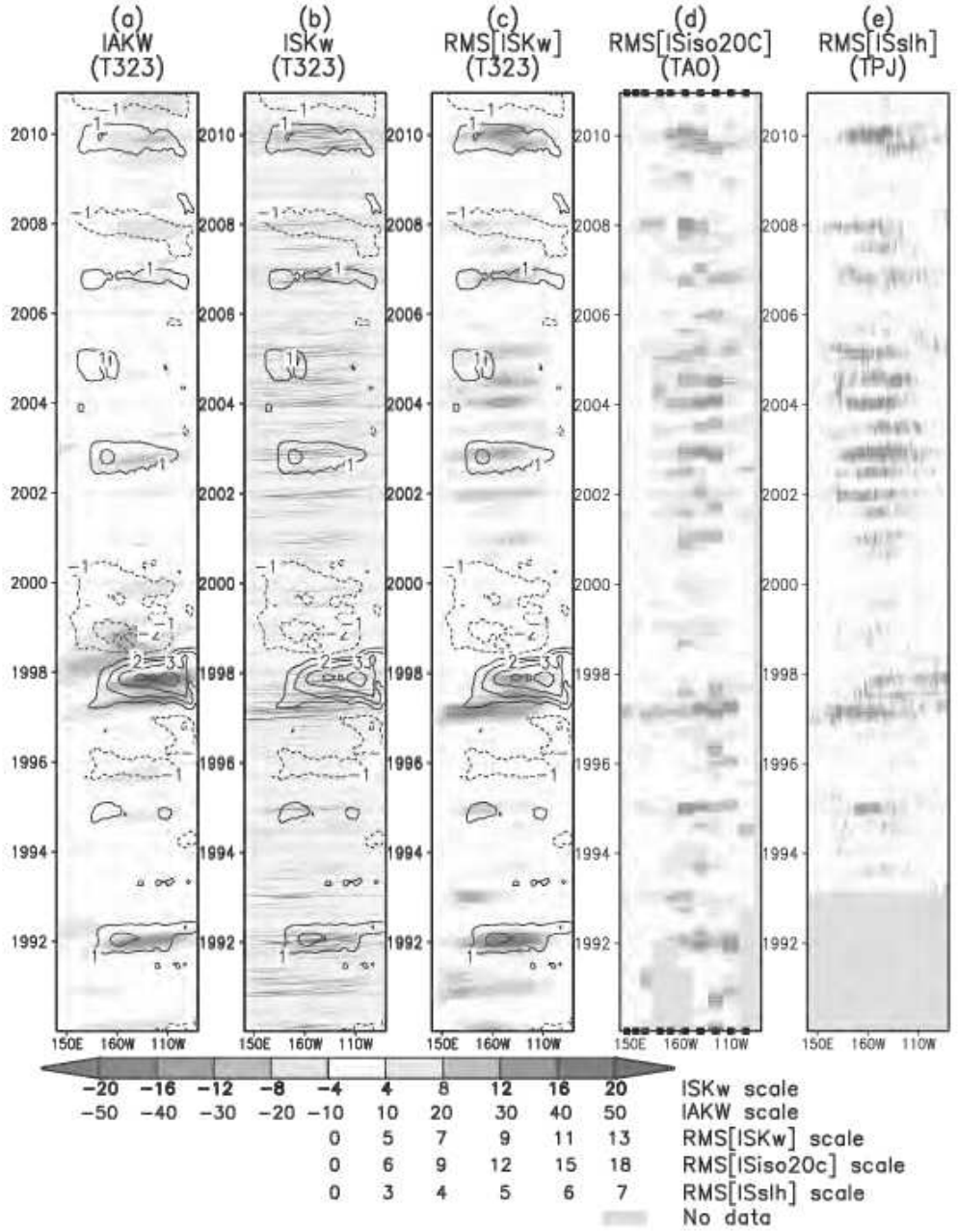

Figure 3. Time evolution of (a) interannual and (b) intraseasonal Kelvin wave contribution to thermocline depth (sum of the first three baroclinic modes) along the equator from T323. (c) Three month running RMS of the ISKw from T323, (d) TAO intraseasonal thermocline (20°C isotherm) depth anomalies, and (e) TPJ intraseasonnal sea level anomalies. Units are in meters, except in Figure 3e which is in centimeters. The contours in Figures 3a, 3b, and 3c indicate the interannual SST anomalies for T323 that is used to compare the maximum Kelvin wave activity with El Niño event along the Equatorial Pacific. Filled squares on the *x* axis in Figure 3d indicate the position of the TAO mooring buoys and the gray shading in Figures 3d and 3e corresponds to periods and locations when observations are not available.

3. Intraseasonal Kelvin Wave Activity

As a first step, we evaluate the contribution of the Interannual Kelvin wave (IAKw) and ISKw to the variability of thermocline depth along the equator, stressing on the distinct characteristics of the two types of El Niño events (Figure 3). The Kelvin wave anomalies consist here in the summed-up contribution of the first three baroclinic modes to the thermocline depth anomalies. The visual inspection of Figure 3a reveals clearly that

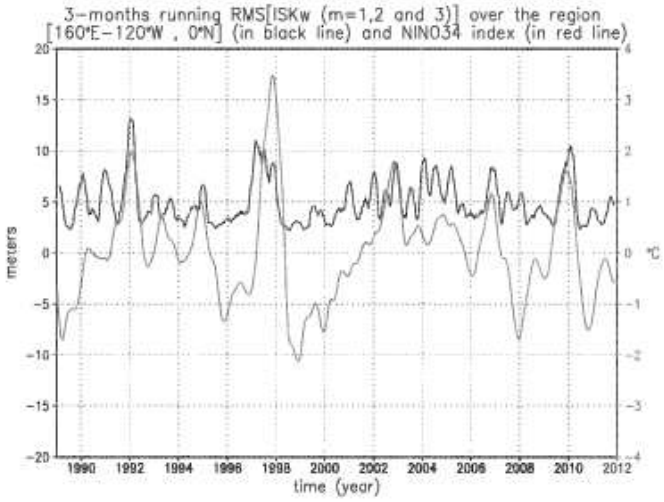

Figure 4. Time evolution of the 3 month running RMS of the (left scale) ISKw contribution to thermocline depth (sum of the first three baroclinic modes), averaged over the region [160°E–120°W; 0° N] (black line in meters), and (right scale) of the NINO343.4 index (red line in °C).

the CP El Niño events are associated with a relatively weak IAKw amplitude compared to the eastern Pacific 1997/1998 El Niño. The ratio of the peak amplitude of the IAKw between the 1997/1998 El Niño and the CP El Niño composite amplitude reaches 3. On the other hand, the inspection of the ISKw (Figure 3b) does not reveal any distinguishable differences in terms of amplitude between events. This is further illustrated in Figure 3c that shows the 3 month running RMS of the ISKw for T323. Peak in the ISKw activity is found for the periods 1991–1992, 1997–1999, 2002–2003, 2007–2008, and 2009–2010, which coincides with warming and cooling events at intraseasonal timescale (Figure 3b). Figure 3c thus indicates that the magnitude of the ISKw activity is comparable between events, which is also evidenced in the in situ (Figure 3d) and altimetric (Figure 3e) data.

The time series of the T323 ISKw activity (3 month running RMS) averaged over the region (160°E–120°W; 0°) are displayed in Figure 4 along with the Niño 3.4 SST index (NINO34 (150°E–150°W; 5°S–5°N)), which indicates that the ISKw activity does not present the large positive asymmetry of the NINO34 index. In order to delineate the relative role of CP and EP El Niño events, we use the C and E indices obtained from the EOF analysis of SST in the tropical Pacific (see *Takahashi et al.*, [2011], for details). The ISKw activity index of Figure 4 correlates (with the maximum value at lag = 0) more to the C index (c = 0.5) than to the E index (c = 0.2), suggesting that ISKw activity is tightly linked to CP El Niño events during their peak phase. This is further illustrated by the composite evolution of the ISKw activity during CP El Niño events comparing to the ISKw variance during the 1997/1998 El Niño (Figure 5). This figure indicates that the ISKw activity during CP El Niño peaks in D(0)JF(+1), similar to interannual SST anomalies, whereas for the 1997/1998 El Niño, the peak variance is found around March(0), which is consistent with former studies [*Hendon et al.*, 2007; *McPhaden et al.*, 2006]. During a strong eastern Pacific event, the western Pacific tends to cool at the mature phase suppressing convection over the Maritime Continent region, so that MJO convective events maintain less continuity from the Indian basin to the central Pacific [*Hendon et al.*, 2007], explaining the reduced ISKw activity. Figure 5 further reveals the apparent strong dissipation of the ISKw activity in the eastern Pacific (around 120°W). Such dissipation may result from the shallowing thermocline that induces a slower phase speed of the wave or from local wind forcing at intraseasonal timescales [*Shinoda et al.*, 2008]. As a consistency check, the lag correlation as a function of longitude for a reference point at 120°W for the model (ISKw) and at 125°W for the thermocline depth intraseasonal anomalies as derived from TAO data is estimated and the result is presented in Figure 6. The equivalent plot for the altimetric data is also provided. It indicates that there is a slight change in characteristics of the propagating variability (slower phase speed, lower coherency) around 120°W for thermocline anomalies of TAO and T323. An estimation based on the slope of the straight line fitted to the maximum correlation west and east of 120°W indicates that the phase speed changes from 2.2 (2.7) to 1.5 (1.2) m s^{-1} for TAO data (T323). Interestingly, the altimetric data do not evidence changes in phase propagation, which is related to the fact that there is a larger contribution of the gravest baroclinic modes to sea level anomalies than to thermocline fluctuations in the eastern equatorial Pacific. These changes in propagating characteristics east of 120°W are also distinguishable directly on the amplitude of the intraseasonal anomalies. This is illustrated in Figure 7 that displays the RMS of the ISKw at each longitude normalized by the RMS of the ISKw at 120°W. The significant decrease of the ISKw

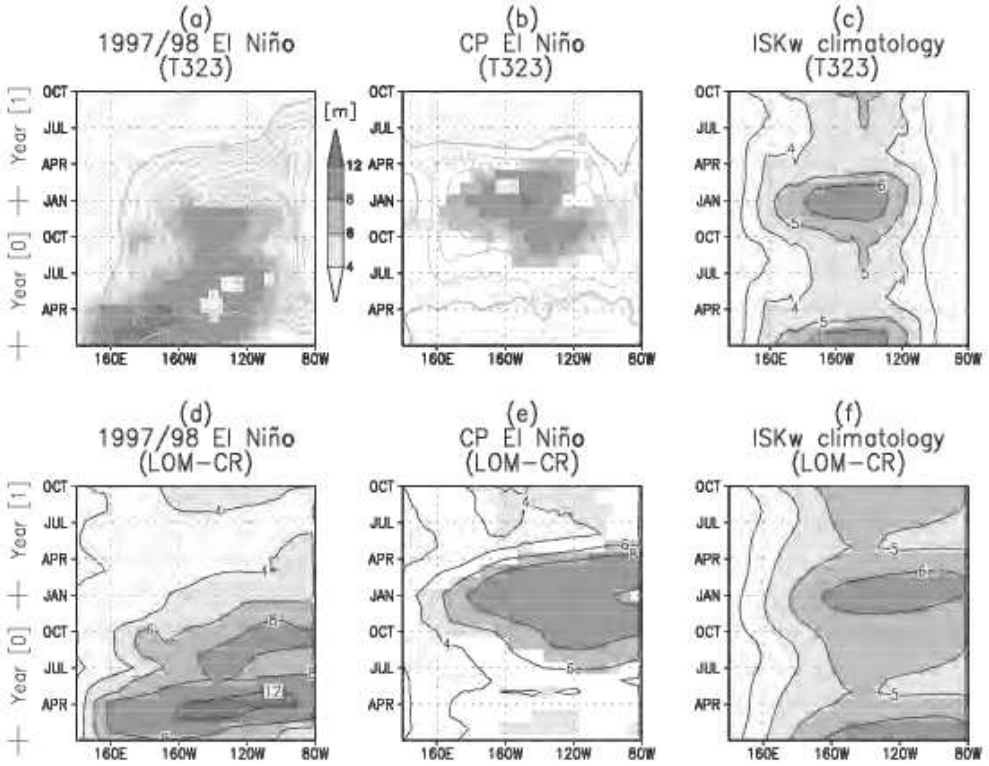

Figure 5. Longitude–time diagram along the equator of the ISKw activity (ISKw 3 month running RMS) for (top plots) T323 and (bottom plots) LOM-CR: for the 1997/1998 (left plots) El Niño event, (center plots) the composite of CP El Niño events, and (right plots) the averaged seasonal cycle. Units are in meters. The year [0] on the time axis of Figures 5a, 5b, 5d, and 5e refers to the El Niño years, that is El Niño peaking around December of year [0]. The interannual T323 SST anomalies corresponding to the 1997/1998 El Niño and the CP El Niño events composite are overlaid in Figures 5a and 5b in gray contour (°C). The shading in Figures 5a, 5b, 5d, and 5e indicates where values are significant at the 95% level, whereas in Figures 5c and 5f it only corresponds to values larger than 4 m. Significance levels were estimated using the bootstrap method [*Efron*, 1982].

variance east of 120°W indicates that a strong dissipation is taking place there. Similar dissipation characteristics cannot be accounted for by the linear model unless a very strong friction is applied east of 120°W. As a consistency check, an experiment is carried out with the linear model, in which the time decay for friction is reduced to 2 months east of 120° W. This location corresponds to the maximum in zonal gradient of the thermocline (blue line in Figure 7). West of 120°W, the time decay remains equal to 24 months as in the control experiment (LOM-CR). This experiment is called LOM-Rx and the results for the RMS of intraseasonal thermocline depth anomalies are displayed as a green curve in Figure 7. Even with such a strong friction, the decrease in RMS of the thermocline anomalies east of 120°W is not as strong as in T323, suggesting that other processes than just a linear dissipation is at work. This will be investigated further in section 4.

As a consistency check of the former statements inferred from the model outputs, TAO data are further analyzed using EOF decomposition. CP El Niño years are selected (from June (0) to May (+1)) and EOF analysis is carried out on the subsurface temperature intraseasonal anomalies of the first 300 m along the equator. The results are compared to the EOF analysis carried out for the EP El Niño event (June 1997 to May 1998). For both types of El Niño events, the result consists in two dominant modes exhibiting comparable explained variance, with associated time series phase-lagged by a quarter of period (not shown), indicating that the modes can be paired and corresponds to the eastward propagating variability associated with the ISKw along the thermocline (Figure 8). The second mode of the CP years is equivalent to a tilt mode of the thermocline, i.e., with a pattern consisting in a zonal seesaw with a node around 150°W. It has been verified that the associated time series are significantly correlated to the zonal wind stress anomalies at 165°E (maximum correlation of 0.43 for the wind stress ahead of the PC time series by 12 days) which indicates that this mode responds

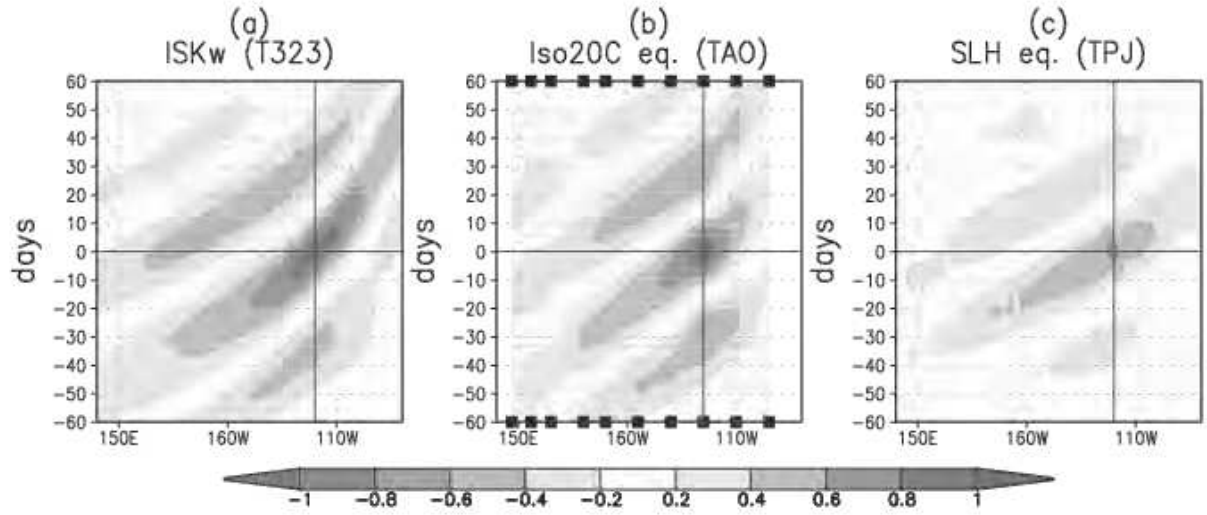

Figure 6. Lagged-correlation (from −60 to +60 days) along the equatorial line for a reference point equal or near to 120°W for (a) ISKw from T323, (b) intraseasonal thermocline depth anomalies from TAO, and (c) intraseasonal sea level anomalies from TPJ. The vertical thin line in Figures 6a and 6c indicates the longitude of 120°W (reference point) meanwhile in Figure 6b it is 125°W. The squares on the longitude axis (Figure 6b) indicate the positions of the TAO mooring buoys.

relatively rapidly to the wind stress forcing. On the other hand, the first mode has a pattern with an approximate zonal wave number of 2, which reflects the propagation nature of the paired EOF modes. Interestingly, the dominant EOF modes for CP El Niño years exhibit an overall much larger loading in the central Pacific than during the 1997 El Niño years. During the latter, the intraseasonal variability peaks in the eastern Pacific at a depth that corresponds to the mean thermocline depth over this period (see orange dashed line in Figures 8b and 8d) and the paired modes are indicative of eastward propagation as far as the eastern boundary. In contrast, during the CP El Niño years, the variability peaks along (or just below) the mean thermocline and east of ~120°W, it exhibits a very weak amplitude of the paired modes, evidencing the strong dissipation taking place east of 120°W.

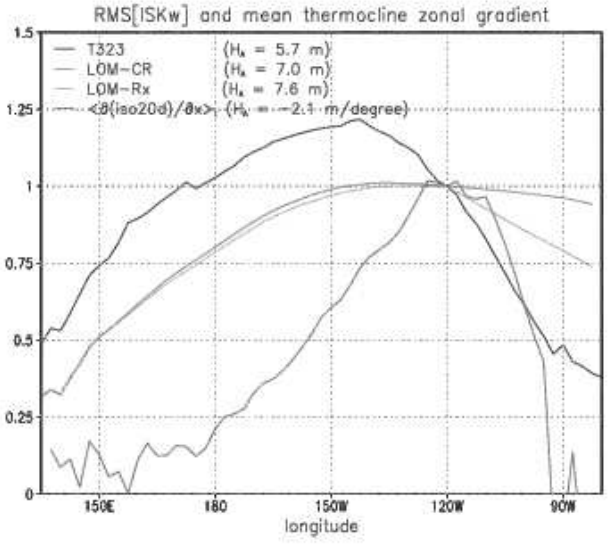

Figure 7. RMS of ISKw for T323 (black line), LOM-CR (red line), and LOM-Rx (green line). The blue line shows the temporal mean of the zonal gradient of the 20°C isotherm (thermocline) depth from T323. Values are adimensionalized by their respective values at 120°W (indicated in the upper left corner as H_x).

Further, the amplitude of the EOF time series is estimated as $\sqrt{PC_1(t)^2 + PC_2(t)^2}$ where $PC_n(t)_{n=[1,2]}$ are the normalized time series associated with the EOF modes, and monthly mean climatologies are derived, which indicates the privileged seasons for intraseasonal activity. The results are presented in Figure 8e. They indicate that the peak season for intraseasonal variability along the thermocline during CP El Niño years is December to February, which is consistent with the model results (Figure 5). The range of values associated with the dispersion of the six CP El Niño years (shading in Figure 8e) suggests that such feature is significantly different from the

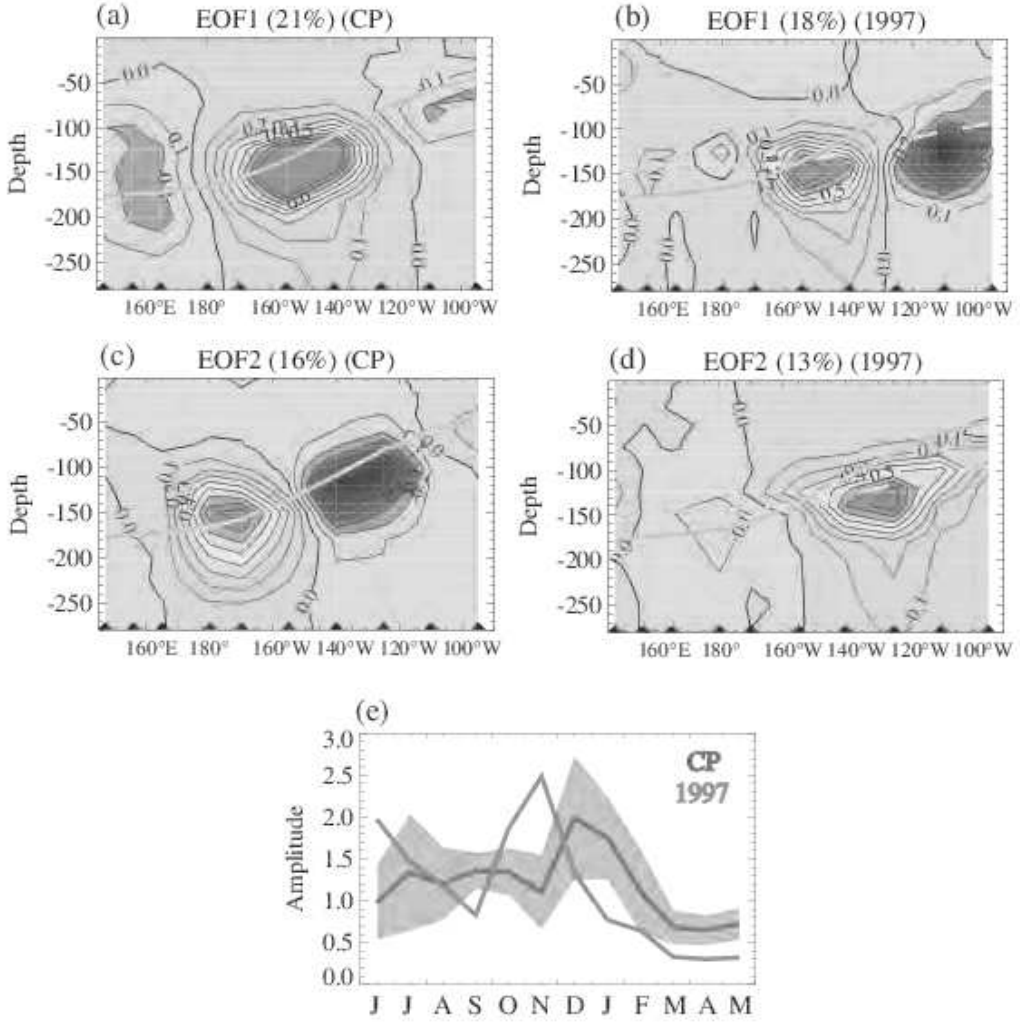

Figure 8. EOF decomposition of (a, c) observed (TAO) subsurface temperature intraseasonal anomalies along the equator over the years of CP El Niño events and (b, d) of the 1997/1998 El Niño event. First (second) EOF patterns in the first 300 m are displayed in the top (center) plots. Years are considered from June (0) to May (+1). The orange thick plain (dashed) line indicates the mean thermocline depth over the 2000–2011 period (June 1997 to May 1998). The black triangles on the longitude axis indicate the positions of the TAO mooring buoys. (e) Monthly mean climatology of the amplitude of the intraseasonal mode defined as $\sqrt{PC_1(t)^2 + PC_2(t)^2}$ where $PC_n(t)_{n=\{1,2\}}$ are the normalized time series associated with the EOF modes for (blue line) CP El Niño years. The shading indicates the dispersion over the six CP El Niño years (i.e., + and − the variance among the CP years). The red line corresponds to the monthly mean of the amplitude of the intraseasonal mode for the 1997/1998 El Niño event, i.e., during the period June 1997 to May 1998.

1997 El Niño year during which the intraseasonal variability peaks around November and then decreases sharply, maintaining a low amplitude until May 1998.

Both model results and observations suggest that dissipation processes take place around 120°W during CP El Niño years. The next section investigates to which extent such feature can be interpreted in terms of modal dispersion that is the process of the scattering of energy between baroclinic modes when the wave crosses a region with distinct density [*Busalacchi and Cane*, 1988; *Harrison and Giese*, 1991].

4. Wave Dispersion in the Eastern Pacific

4.1. Rossby Wave Activity and Role of Wind Forcing

To further get insights on the processes taking place in the eastern equatorial Pacific, we display the Intra-Seasonal Rossby wave (ISRw) variance (3 month running RMS) (Figure 9a) as derived from the modal

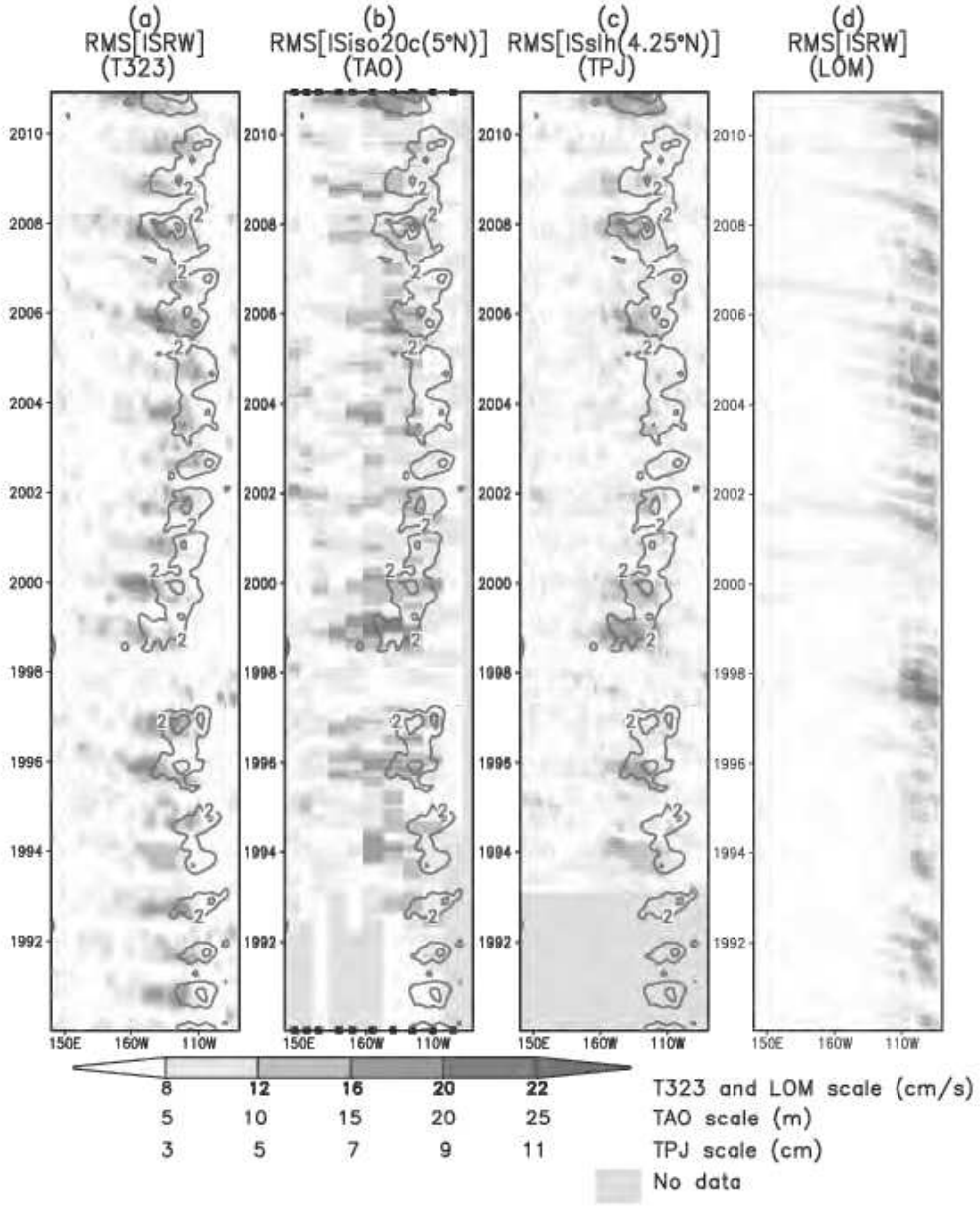

Figure 9. Time evolution of the 3 month running RMS of (a) the ISRw (equivalent zonal current, first-meridional mode, cm s^{-1}) from T323 along the equatorial line and (b) the intraseasonal thermocline (20°C isotherm) depth anomalies (in m) from TAO at 5°N. (c) Same as (b) but for TPJ sea level anomalies at 4.25°N (in cm). (d) Same as (a) but for LOM-Hx. Filled squares indicate the position of the TAO mooring buoys and the gray shading where data are not available. The blue contours indicate the zonal gradient of the thermocline from T323 in absolute value. Units are in $m/^{\circ}$. Only gradients larger than 2 $m/^{\circ}$ are shown.

decomposition of the T323 simulation. The Rossby wave consists here in the first three baroclinic mode summed-up contribution of the first-meridional Rossby modes in term of zonal current and can be compared to the variance of the observed sea level anomalies or thermocline anomalies at 5°S (i.e., where first-meridional Rossby wave structure of the first baroclinic mode is maximum) (Figures 9b and 9c). Figures 9a–9c evidence westward propagating variability for T323, TAO, and TPJ data. Strikingly the propagation is only clearly observable west of ~120°W from which the ISRw activity seems to originate. The region where the ISRw variance originates coincides with the location of the maximum zonal gradient of the thermocline depth (blue contour overplotted in Figures 9a–9c) suggesting that the ISRw results either from the

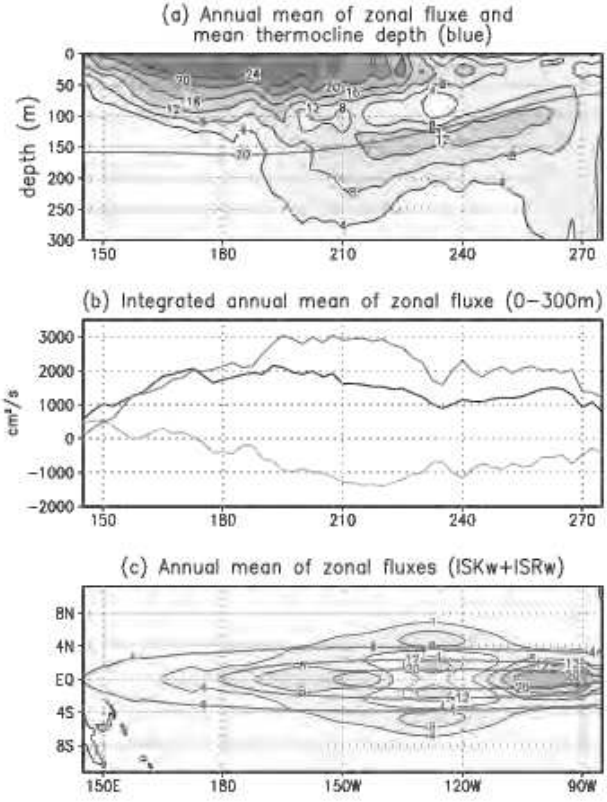

Figure 10. Annual mean of the zonal energy flux for (a) the depth-integrated (from bottom to surface) zonal flux for the ISKw and ISRw, (b) depth-integrated (0–300 m) zonal flux, and (c) the total flux as a function of longitude and latitude. In Figure 10b, the black line represents the total zonal flux, the solid red line is the sum of the first three baroclinic modes, and the green line is the residual (see text). In Figure 10c, the blue line indicates the mean thermocline depth. Units are in $m^2\ s^{-1}$ for Figures 10a and 10c, and $cm^2\ s^{-1}$ for Figure 10c.

reflection of the ISKw on the sharp zonal density front (see next section) or from wind forcing. As a consistency check, the ISRw is derived from the linear model control run (LOM-CR) and displayed in Figure 9d. It reveals that the ISRw cannot be accounted for by the wind stress forcing since the maximum of variability is confined to the far eastern Pacific in the linear model experiment indicating that the ISRw variability originates from the reflections of the ISKw at the eastern boundary. Noteworthy, the ISRw activity in 2001–2002 west of 120°W in T323 could be explained to some extent by the wind stress forcing consistently with the study by *Shinoda et al.* [2008]. The linear model is further used to test if ISRw can be modified by the zonally varying thermocline. The results indicate that, within a realistic range of values for the thermocline slope, the model does not simulate significant Kelvin wave reflection at the longitude where the thermocline gradient is maximum. A composite analysis of the ISKw and wind stress anomalies during CP El Niño years also revealed that an easterly wind stress event follows the peak phase of the main downwelling ISKw (not shown), which could have the potential to alter the downwelling ISKw in the eastern Pacific and contribute to the dissipation observed at 120°W. However, the easterly wind stress event is located slightly to the west of the previous westerly wind stress event and does not coincide with the crest of the downwelling ISKw, which rules out any role of the easterly wind stress event in dissipating the downwelling ISKw in the eastern Pacific. The linear model results confirm this interpretation (not shown). This indicates that the features observed in T323 cannot be accounted for by the linear model, and that the maximum variance in ISRw west of 120°W results from nonlinear processes.

4.2. Energy Scattering

The former analysis suggests that the energy of the ISKw is scattered near 120°W corresponding to the region where the largest zonal gradient in stratification (thermocline) is found. In order to evidence the dispersion, we estimate from T323 simulation, the zonal energy flux along the equator [*Eliassen and Palm*, 1960]. It consists in calculating the quantity $\langle u'(x, y=0, z, t).p'(x, y=0, z, t)\rangle$, where $'$ denotes intraseasonal anomalies and the brackets stand for the temporal average performed over the CP El Niño years. This horizontal energy flux is displayed along the equator within the first 300 m between 140°W and 90°W (Figure 10a). It indicates that the zonal energy flux experiences an eastward change in vertical structure, with the energy concentrated in the upper layer (first 100 m) in the central-western Pacific (accounting for mixing associated with the local wind power) and just below the thermocline in the eastern Pacific (which cannot be accounted for the local winds). It was checked that energy flux is enhanced during CP El Niño years

compared to the mean energy flux calculated over the whole record with a comparable pattern (not shown). The change in vertical structure of the zonal energy flux from west to east is indicative of modal dispersion associated with the zonal gradient in mean thermocline. In order to quantify this, we consider the depth-integrated zonal energy flux within the first 300 m (ZF300). Assuming that u' and p' can be decomposed into an infinite sum of baroclinic modes such as $u' = \sum_{n=1}^{\infty} u_n F_n(z)$ and $p' = \sum_{n=1}^{\infty} p_n F_n(z)$, the 300 m depth-integrated zonal flux can write as follows:

$$ZF300 = \int_{-300}^{0} \langle u'.p' \rangle dz = \sum_{n=1}^{3} \sum_{m=1}^{3} \langle u'_n.p'_m \rangle \int_{-300}^{0} F_n(z).F_m(z) dz + R$$

Here $F_n(z)$ are the baroclinic mode functions that also depend on longitude [*Dewitte et al.*, 1999], and R is a residual accounting for the contribution of the high-order baroclinic modes. R therefore writes as follows:

$$R = \sum_{n=1}^{3} \sum_{m=4}^{\infty} \langle u'_n.p'_m \rangle \int_{-300}^{0} F_n(z).F_m(z) dz + \sum_{n=4}^{\infty} \sum_{m=1}^{3} \langle u'_n.p'_m \rangle \int_{-300}^{0} F_n(z).F_m(z) dz + \sum_{n=4}^{\infty} \sum_{m=4}^{\infty} \langle u'_n.p'_m \rangle \int_{-300}^{0} F_n(z).F_m(z) dz$$

The term $\sum_{n=1}^{3} \sum_{m=1}^{3} \langle u'_n.p'_m \rangle \int_{-300}^{0} F_n(z).F_m(z) dz$ represents the zonal flux in the upper 300 m associated with the propagating waves, while R accounts for the energy flux associated with locally forced variability that can originate from either local wind forcing or mixing. Both terms implicitly include the effect of modal dispersion onto the zonal energy flux if any, and their zonal variability may be indicative of such a process. If there is no scattering of energy, change in energy flux is to be due to dissipation process if local wind forcing is weak, and therefore the flux should decrease eastward. Figure 10b shows the depth-integrated zonal flux along the equator for the aforementioned terms. Interestingly, the integrated zonal flux associated with the first three baroclinic mode (black curve) has a local minimum at ~120°W, from which it increases eastward. Such increase can be interpreted in term of the larger trapping of zonal flux along the equator by the Kelvin wave due to the finer meridional scales (smaller phase speed) in the eastern Pacific, which is also evidenced in Figure 10c that shows the zonal flux associated with the Kelvin and Rossby waves (first three baroclinic modes) integrated over the whole water column (i.e., $\sum_{n=1}^{3} \langle u'_n.p'_n \rangle$ where only the contributions of the Kelvin and first to third meridional Rossby waves to (u'_n, p'_n) are considered). Figure 10c shows that the zonal flux associated with the Kelvin wave is increased eastward due to the decrease in meridional scale of the Kelvin wave (resulting from the shallower thermocline). West of 120°W, the signature of the Rossby waves on the zonal flux is more prominent than east of 120°W, indicative of the partial reflection of the Kelvin waves into Rossby waves on the zonal front in stratification, consistently with results of Figure 9. The increase in the zonal flux east of 120°W also results from a redistribution of energy between baroclinic modes toward the higher-order modes as evidenced by the slight increase of the residual term (R) east of 120°W (green curve in Figure 10b).

Another indication of modal dispersion is provided by the spectral analysis of the thermocline depth fluctuations west and east of the density front at ~120°W, which can be estimated from the TAO data. The variations of thermocline depth are estimated from the EOF analysis of intraseasonal temperature anomalies in the vicinity of the mean thermocline in the central Pacific (i.e., at 180°, 170°W, 155°W between 120 and 215 m) and the eastern Pacific (i.e., at 110°W, 95°W between 30 and 80 m). Only the six CP El Niño years are considered. We retain the first two modes which summed-up contribution explains more than 79% of the explained variance. A wavelet decomposition of the EOF time series is then performed. Since there is a marked seasonal dependence of the intraseasonal variability, the climatological wavelet spectrum is estimated which consists in calculating the climatology of the wavelet power coefficient at each frequencies. Wavelet power was first normalized following equation (14) of *Torrence and Compo* [1998] in order to compare the magnitude of the wavelet power at different frequencies, following the method introduced in *Goubanova et al.* [2013]. The results are presented in Figure 11. Figure 11 shows that there is a significant change in the seasonality of the intraseasonal variability of the thermocline depth fluctuations: intraseasonal variability peak in Austral summer west of 120°W, whereas it tends to peak in Austral winter east of 120°W. In addition, there is a tendency for a broadening of the global wavelet spectrum from west to east, in particular toward lower frequencies. Since the wind forcing is weak in the eastern Pacific at intraseasonal

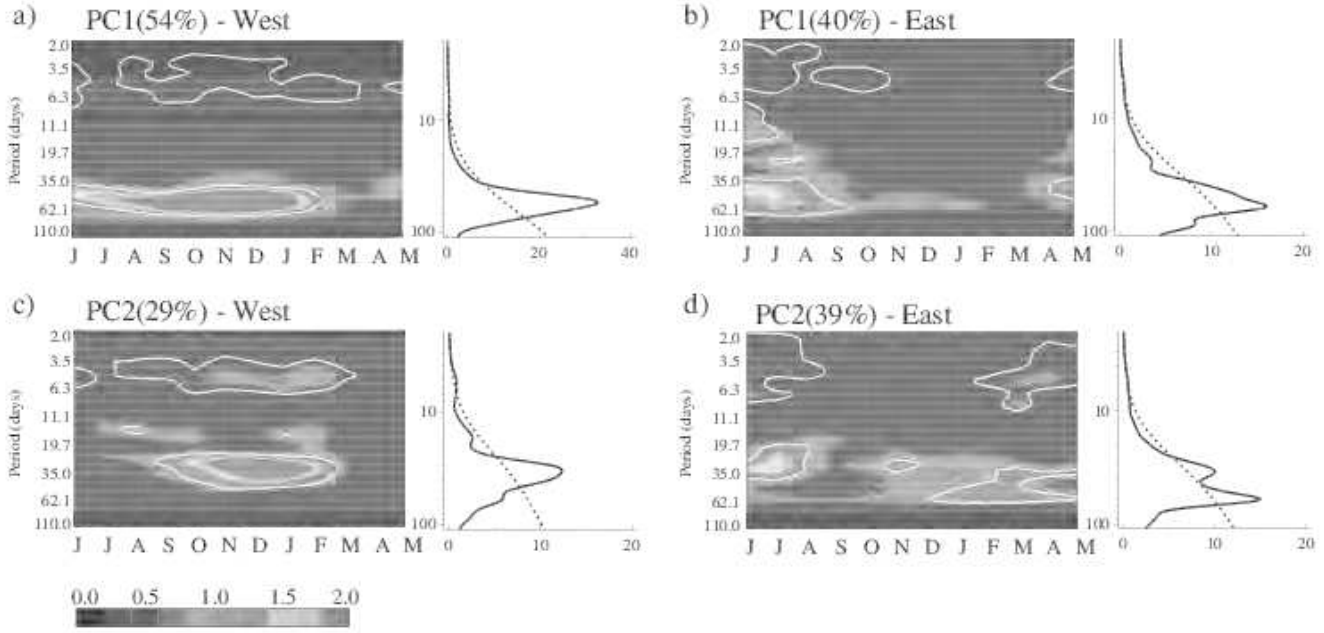

Figure 11. Spectral analysis of the intraseasonal thermocline depth anomalies from TAO in the (a, c) central Pacific (180°, 170°W, 155°W) and the (b, d) eastern Pacific (110°W, 95°W): climatological normalized power wavelet (Morlet) spectrum and global wavelet spectrum of the time series associated with the Figures 11a and 11b first and Figures 11c and 11d second EOF modes of intraseasonal temperature anomalies in the vicinity of the mean thermocline. The climatological normalized power wavelet spectrum consists in a wavelet decomposition of the time series followed by a calculation of the climatology of the Wavelet Power coefficient at each frequencies. Wavelet Power was first normalized following equation (14) of *Torrence and Compo* [1998] in order to compare the magnitude of the wavelet power at different frequencies. Scale is indicated on the bottom of Figure 11c. Unit is adimensionalized (but scaled by 10^{-1}) since EOF time series are normalized. The percentage of explained variance of the EOF modes is indicated on top of each plot. The dashed black line in the global wavelet spectrum and the white contour in the climatological wavelet spectrum indicate the 95% confidence level estimated from a red noise (Markov model).

timescales, the change in the spectral characteristics of the thermocline fluctuations from west to east is due to changes in the background state, inducing to modal dispersion.

5. Discussion and Conclusions

The characteristics of the intraseasonal Kelvin wave in the Pacific are examined based on observations (TAO data and altimetry) and an OGCM simulation covering the period 1989–2011. We show that the expression of the intraseasonal temperature variability is dominant in the vicinity of the thermocline (and not at the surface), which is associated with the contribution of the first three baroclinic mode Kelvin waves to the thermocline anomalies. It is then evidenced that the CP El Niño events are associated with an increase in intraseasonal equatorial Kelvin activity compared to neutral years. The peak variance takes place during the mature phase of the CP El Niño events which is in contrast with the extreme 1997/1998 El Niño event for which the peak variance takes place 5–6 months earlier. Whereas the peak variance of the intraseasonal Kelvin wave during CP El Niño event is wind-forced in the central Pacific as inferred from the linear model simulations performed in this study, the Kelvin wave in the eastern Pacific experiences a drastic change in its characteristics, which cannot be accounted for by just a linear dissipation in the linear model and wind stress forcing. It is shown that the region from which the Kelvin wave starts strongly dissipating coincides with the location of the maximum thermocline zonal gradient (~120°W). This region also corresponds to the location where intraseasonal Rossby waves originate, which cannot be accounted for by a linear model, suggesting scattering of energy of the Kelvin wave as it propagates eastward and partial reflections on the density front. An analysis of the zonal flux in the OGCM is consistent with this interpretation revealing in particular a sharp change in its vertical structure near 120°W and an increase in the zonal flux associated with the high-order baroclinic modes in the far eastern Pacific. The eastward change in spectral characteristics of the thermocline fluctuations from TAO data is also consistent with the process of modal dispersion.

Our results may have implications for the understanding of the modulation of ENSO; in particular, the increased occurrence of CP El Niño events over the recent decades [*Yeh et al.*, 2009; *Lee and McPhaden*, 2010]. In the light of our results, it may be hypothesized that an increase in the zonal contrast of the thermocline is favorable for modal dispersion of the intraseasonal Kelvin wave preventing its free propagation in the far eastern Pacific where it could trigger a local wind response (local Bjerknes feedback) through its impact on SST via the strong thermocline feedback there. Interestingly since the late of the 1990s, the tropical Pacific has entered a La Niña-like state [cf. *Xiang et al.*, 2013] that is associated with a slightly steeper thermocline. A Coupled General Circulation Model (CGCM) that simulates a decadal variability in the ratio of occurrence of CP El Niño and EP El Niño events indicates that the latter is associated with a decadal mode in the thermocline zonal gradient across the equatorial Pacific [*Choi et al.*, 2011] with the periods of increased occurrence of CP El Niño characterized by a steeper mean thermocline. Such feature has also been suggested from observations for the transition in mean state of the 2000s [*McPhaden et al.*, 2011]. The intraseasonal Kelvin wave could thus be "trapped" in the central Pacific during periods when the zonal contrast in stratification is increased [see *Dewitte et al.*, 2012b, Figure 8] for the estimate of the Kelvin wave in the GFDL_CM2.1 model for CP El Niño events). Note that this is consistent with the study by *Hu et al.* [2013] which suggests that the combination of a steeper thermocline slope with stronger surface trade winds has hampered the eastward migration of the warm waters along the equatorial Pacific since 2000, favoring the occurrence of CP El Niño events. The steeper thermocline leads to a strong zonal contrast in stratification which can alter the Intraseasonal Kelvin wave characteristics through modal dispersion. This is in contrast with recent studies [*Xiang et al.*, 2013; *Dommenget et al.*, 2012] that rather suggest a nonlinear atmospheric process for explaining the predominance of CP El Niño events under a La Niña-like mean state, which calls for further study. The latter could be based on the experimentation with a tropical Pacific OCGM allowing the analysis of an explicit heat budget to diagnose mixing and diffusive processes. In particular, it could be interesting to assess if there is a threshold associated with the amplitude of the equatorial Kelvin wave from which vertical diffusivity increases sharply, mixing baroclinic modes, and preventing the Kelvin wave to propagate freely. There is also the possibility that the intraseasonal Kelvin wave propagates vertically along steep WKB ray paths from its forcing region at the surface in the central Pacific and encounters the stratification front associated with the mean thermocline further east. There is indication of such a process in the OGCM used here (not shown) suggesting that scattering of energy in the east might be taking place both in the zonal and vertical directions. Further study will be dedicated to the investigation of such process.

Acknowledgments
CNES is thanked for his support through the Modokalt project. We are thankful to Gilles Garric and Clément Bricaut (Mercator-Ocean, Toulouse) for providing the T323 model outputs and for discussions regarding the model's skill. The two anonymous reviewers are also thanked for their constructive comments. This work is part of K. Mosquera-Vásquez's PhD who benefited from a scholarship from Institut de Recherche pour le Développement (IRD).

References

Ashok, K., S. K. Behera, S. A. Rao, H. Weng, and T. Yamagata (2007), El Niño Modoki and its possible teleconnection, *J. Geophys. Res.*, *112*, C11007, doi:10.1029/2006JC003798.

Bergman, J. W., H. H. Hendon, and K. M. Weickmann (2001), Intraseasonal air-sea interactions at the onset of El Niño, *J. Clim.*, *14*, 1702–1719.

Busalacchi, A. J., and M. A. Cane (1988), The effect of varying stratification on low-frequency equatorial motions, *J. Phys. Oceanogr.*, *18*(6), 801–812.

Capotondi, A., et al. (2014), Understanding ENSO diversity, *Bull. Amer. Met. Soc.*, in press.

Choi, J., S.-I. An, J.-S. Kug, and S.-W. Yeh (2011), The role of mean state on changes in El Niño's flavor, *Clim. Dyn.*, *37*, 1205–1215, doi:10.1007/s00382-010-0912-1.

Cravatte, S., J. Picaut, and G. Eldin (2003), First and second baroclinic Kelvin modes in the equatorial Pacific at intraseasonal timescales, *J. Geophys. Res.*, *108*(C8), 3266, doi:10.1029/2002JC001511.

Dewitte, B., G. Reverdin, and C. Maes (1999), Vertical structure of an OGCM simulation of the equatorial Pacific Ocean in 1985–1994, *J. Phys. Oceanogr.*, *29*, 1542–1570.

Dewitte, B., S. Illig, L. Parent, Y. duPenhoat, L. Gourdeau, and J. Verron (2003), Tropical Pacific baroclinic mode contribution and associated long waves for the 1994–1999 period from an assimilation experiment with altimetric data, *J. Geophys. Res.*, *108*(C4), 3121, doi:10.1029/2002JC001362.

Dewitte, B., S.-W. Yeh, B.-K. Moon, C. Cibot, and L. Terray (2007), Rectification of the ENSO variability by interdecadal changes in the equatorial background mean state in a CGCM simulation, *J. Clim.*, *20*, 2002–2021, doi:10.1175/JCLI4110.1.

Dewitte, B., S. Purca, S. Illig, L. Renault, and B. Giese (2008), Low frequency modulation of the intraseasonal equatorial Kelvin wave activity in the Pacific ocean from SODA: 1958–2001, *J. Clim.*, *21*, 6060–6069.

Dewitte, B., S. Thual, S.-W. Yeh, S.-I. An, B.-K. Moon and B. Giese (2009), Low frequency variability of temperature in the vicinity of the equatorial thermocline in SODA: Role of equatorial wave dynamics and ENSO asymmetry, *J. Climate*, *22*, 5783–5795.

Dewitte, B., S.-W. Yeh, and S. Thual (2012a), Reinterpreting the thermocline feedback in the central-western Pacific and its relationship with the ENSO modulation, *Clim. Dyn.*, *41*(3–4), 819–830, doi:10.1007/s00382-012-1504-z.

Dewitte, B., J. Choi, S.-I. An, and S. Thual (2012b), Vertical structure variability and equatorial waves during central Pacific and eastern Pacific El Niño in a coupled general circulation model, *Clim. Dyn.*, *38*(11–12), 2275–2289, doi:10.1007/s00382-011-1215-x.

Dommenget, D., T. Bayr, and C. Frauen (2012), Analysis of the non-linearity in the pattern and time evolution of El Niño Southern Oscillation, *Clim. Dyn.*, *40*, 2825–2847.

Ducet, N., P. Y. Le Traon, and G. Reverdin (2000), Global high resolution mapping of ocean circulation from TOPEX/POSEIDON and ERS-1/2, *J. Geophys. Res., 105*, 19,477–19,498.

Efron, B. (Ed.) (1982), *The Jackknife, the Bootstrap, and Other Resampling Plans, CBMSNSF Monogr. 38*, 92 pp., Soc. for Ind. and Appl. Math, doi:10.1137/1.9781611970319.

Eisenman, I., L. Yu, and E. Tziperman (2005), Westerly wind bursts: ENSO's tail rather than the dog?, *J. Clim., 18*(24), 5224–5238, doi:10.1175/JCLI3588.1.

Eliassen, A., and E. Palm (1960), On the transfer of energy in stationary mountain waves, *Geofys. Publ., 22*(3), 1–23.

Fu, L.-L., E. J. Christensen, C. A. Yamarone Jr., M. Lefebvre, Y. Menard, M. Dorrer, and P. Escudier (1994), Topex/Poseidon mission overview, *J. Geophys. Res., 99*, 24,369–24,381.

Giese, B. S., and D. E. Harrison (1991), Eastern equatorial Pacific response to three composite westerly wind types, *J. Geophys. Res., 96*, 3239–3248.

Giese, B. S., and S. Ray (2011), El Niño variability in simple ocean data assimilation (SODA), 1871–2008, *J. Geophys. Res., 116*, C02024, doi:10.1029/2010JC006695.

Goubanova, K., S. Illig, E. Machu, V. Garçon, and B. Dewitte (2013), SST subseasonal variability in the central Benguela upwelling system as inferred from satellite observations (1999–2009), *J. Geophys. Res. Oceans, 118*, 4092–4110, doi:10.1002/jgrc.20287.

Gushchina, D., and B. Dewitte (2012), Intraseasonal tropical atmospheric variability associated to the two flavors of El Niño, *Mon. Weather Rev., 140*(11), 3669–3681.

Hayes, S. P., P. Chang, and M. J. McPhaden (1991), Variability of the seasurface temperature in the eastern equatorial Pacific during 1986–88, *J. Geophys. Res., 96*, 10,553–10,566.

Hendon, H. H., B. Liebmann, and J. D. Glick (1998), Oceanic Kelvin waves and the Madden-Julian oscillation, *J. Atmos. Sci., 55*, 88–101.

Hendon, H. H., M. C. Wheeler, and C. Zhang (2007), Seasonal dependence of the MJO–ENSO relationship, *J. Clim., 20*, 531–543, doi:10.1175/JCLI4003.1.

Hu, Z.-Z., A. Kumar, B. Jha, W. Wang, B. Huang, and B. Huang (2012), An analysis of warm pool and cold tongue El Niños: Air-sea coupling processes, global influences, and recent trends, *Clim. Dyn., 38*(9–10), 2017–2035, doi:10.1007/s00382-011-1224-9.

Hu, Z.-Z., A. Kumar, H.-L. Ren, H. Wang, M. L'Heureux, and F.-F. Jin (2013), Weakened interannual variability in the tropical Pacific Ocean since 2000, *J. Clim., 26*(8), 2601–2613, doi:10.1175/JCLI-D-12-00265.1.

Illig, S., B. Dewitte, K. Goubanova, G. Cambon, J. Boucharel, F. Monetti, C. Romero, S. Purca, and R. Flores (2014), Forcing mechanisms of intraseasonal SST variability off Central Peru in 2000–2008, *J. Geophys. Res. Oceans, 119*, 3548–3573, doi:10.1002/2013JC009779.

Jin, F.-F., L. Lin, A. Timmermann, and J. Zhao (2007), Ensemble-mean dynamics of the ENSO recharge oscillator under state-dependent stochastic forcing, *Geophys. Res. Lett., 34*, L03807, doi:10.1029/2006GL027372.

Johnson, N. C. (2013), How many ENSO flavors can we distinguish?, *J. Clim., 26*, 4816–4827, doi:10.1175/JCLI-D-12-00649.1.

Kao, H.-Y., and J.-Y. Yu (2009), Contrasting eastern-Pacific and central-Pacific types of ENSO, *J Clim., 22*, 615–632.

Kessler, W. S., and R. Kleeman (2000), Rectification of the Madden-Julian Oscillation into the ENSO cycle, *J. Clim., 13*, 3560–3575.

Kessler, W. S., and M. J. McPhaden (1995a), The 1991–93 El Niño in the central Pacific, *Deep Sea Res., Part II, 42*, 295–333.

Kessler, W. S., and M. J. McPhaden (1995b), Oceanic equatorial waves and the 1991–93 El Niño, *J. Clim., 8*, 1757–1774.

Kessler, W. S., M. J. McPhaden, and K. M. Weickmann (1995), Forcing of intraseasonal Kelvin waves in the equatorial Pacific, *J. Geophys. Res., 100*, 10,613–10,631.

Kug, J.-S., F.-F. Jin, and S.-I. An (2009), Two types of El Niño events: Cold tongue El Niño and warm pool El Niño, *J. Clim., 22*, 1499–1515.

Lee, T., and M. J. McPhaden (2010), Increasing intensity of El Niño in the central-equatorial Pacific, *Geophys. Res. Lett., 37*, L14603, doi:10.1029/2010GL044007.

Lengaigne, M., E. Guilyardi, J. P. Boulanger, C. Menkes, P. Delecluse, P. Inness, J. Cole, and J. Slingo (2004), Triggering of El Niño by westerly wind events in a coupled general circulation model, *Clim. Dyn., 23*, 601–620.

Le Traon, P. Y., and F. Ogor (1998), ERS-1/2 orbit improvement using T/P: The 2 cm challenge, *J. Geophys. Res., 103*, 8045–8057.

Levitus, S., and T. P. Boyer (1994), World Ocean Atlas 1994 Volume 4: Temperature, in *NOAA Atlas NESDIS 4*, 117 pp., U.S. Dep. of Commer., Washington, D. C.

Lin, J. W. B., J. D. Neelin, and N. Zeng (2000), Maintenance of tropical intraseasonal variability: Impact of evaporation-wind feedback and midlatitude storms, *J. Atmos. Sci., 57*, 2793–2823.

Madden, R., and P. Julian (1972), Description of global-scale circulation cells in the tropics with a 40–50 day period, *J. Atmos. Sci., 29*, 1109–1123.

Madec, G., P. Delecluse, M. Imbard, and C. Levy (1998), *OPA 8.1 Ocean General Circulation Model Reference Manual, Nodes du pole de modélisation 11*, 91 pp., Inst. Pierre Simon Laplace, France.

McPhaden, M. J. (1999), Genesis and evolution of the 1997–98 El Niño, *Science, 283*, 950–954.

McPhaden, M. J. (2002), Mixed layer temperature balance on intraseasonal time scales in the equatorial Pacific Ocean, *J. Clim., 15*(18), 2632–2647.

McPhaden, M. J. (2012), A 21st century shift in the relationship between ENSO SST and warm water volume anomalies, *Geophys. Res. Lett., 39*, L09706, doi:10.1029/2012GL051826.

McPhaden, M. J., and B. A. Taft (1988), On the dynamics of seasonal and intraseasonal variability in the eastern equatorial Pacific, *J. Phys. Oceanogr., 18*, 1713–1732.

McPhaden, M. J., et al. (1998), The Tropical Ocean-Global Atmosphere (TOGA) observing system: A decade of progress, *J. Geophys. Res., 103*, 14,169–14,240.

McPhaden, M. J., X. Zhang, H. H. Hendon, and M. C. Wheeler (2006), Large scale dynamics and MJO forcing of ENSO variability, *Geophys. Res. Lett., 33*, L16702, doi:10.1029/2006GL026786.

McPhaden, M. J., T. Lee, and D. McClurg (2011), El Niño and its relationship to changing background conditions in the tropical Pacific, *Geophys. Res. Lett., 38*, L15709, doi:10.1029/2011GL048275.

Mosquera, K. (2009), Variabilidad intra-estacional de la Onda de Kelvin Ecuatorial en el Pacífico (2000–2007): Simulación numérica y datos observados, MS thesis, 76 pp., Univ. Nacl. Mayor de San Marcos, Lima, Perú.

Mosquera-Vásquez, K., B. Dewitte, S. Illig, K. Takahashi, and G. Garric (2013), The 2002/03 El Niño: Equatorial wave sequence and their impact on sea surface temperature, *J. Geophys. Res., 118*, doi:10.1029/2012JC008551.

Picaut, J., C. Menkes, J.-P. Boulanger, and Y. duPenhoat (1993), Dissipation in the Pacific Equatorial long wave model, *TOGA Notes, 10*, 11–15.

Ramos, M., B. Dewitte, O. Pizarro, and G. Garric (2008), Vertical propagation of the extra-tropical Rossby wave during the 1997/98 El Niño off the west coast of South-America in a medium-resolution OGCM simulation, *J. Geophys. Res.*, *113*, C08041, doi:10.1029/2007JC004681.

Ren, H.-L., and F.-F. Jin (2013), Recharge oscillator mechanisms in two types of ENSO, *J. Clim.*, *26*, 6506–6523, doi:10.1175/JCLI-D-12-00601.1.

Roundy, P. E., and G. N. Kiladis (2006), Observed relationships between oceanic Kelvin waves and atmospheric forcing, *J. Clim.*, *19*, 5253–5272.

Roundy, P. E., and J. R. Kravitz (2009), The association of the evolution of intraseasonal oscillations to ENSO phase, *J. Clim.*, *22*, 381–395.

Seiki, A., and Y. N. Takayabu (2007), Westerly wind bursts and their relationship with intraseasonal variations and ENSO. Part II: Energetics over the Western and central Pacific, *Mon. Weather Rev.*, *0072*, 3346–3361.

Seo, K., and Y. Xue (2005), MJO-related oceanic Kelvin waves and the ENSO cycle: A study with the NCEP Global Ocean Data Assimilation System, *Geophys. Res. Lett.*, *32*, L07712, doi:10.1029/2005GL022511.

Shinoda, T., P. E. Roundy, and G. N. Kiladis (2008), Variability of intraseasonal Kelvin waves in the equatorial Pacific Ocean, *J. Phys. Oceanogr.*, *38*, 921–944, doi:10.1175/2007JPO3815.1.

Takahashi, K., A. Montecinos, K. Goubanova, and B. Dewitte (2011), ENSO regimes: Reinterpreting the canonical and Modoki El Niño, *Geophys. Res. Lett.*, *38*, L10704, doi:10.1029/2011GL047364.

Takahashi, K., R. Martínez, A. Montecinos, B. Dewitte, D. Gutiérrez, and E. Rodriguez-Rubio (2014), TPOS White Paper #8a – Regional applications of observations in the eastern Pacific: Western South America. In Proceedings of the Tropical Pacific Observing System 2020 Workshop, A Future Sustained Tropical Pacific Ocean Observing System for Research and Forecasting, WMO and Intergovernmental Oceanographic Commission, La Jolla, Calif., 27–30 January. [Available at http://www.wmo.int/pages/prog/gcos/Publications/gcos-184_II.pdf.]

Torrence, C., and G. P. Compo (1998), A practical guide to wavelet analysis, *Bull. Am. Meteorol. Soc.*, *79*, 61–78.

Wang, W., M. Chen, A. Kumar, and Y. Xue (2011), How important is intraseasonal surface wind variability to real-time ENSO prediction?, *Geophys. Res. Lett.*, *38*, L13705, doi:10.1029/2011GL047684.

Wheeler, M. C., and G. N. Kiladis (1999), Convectively coupled equatorial waves: Analysis of clouds and temperature in the wavenumber-frequency domain, *J. Atmos. Sci.*, *56*, 374–399.

Xiang, B., B. Wang, and T. Li (2013), A new paradigm for the predominance of standing central Pacific warming after the late 1990s, *Clim. Dyn.*, *41*(2), 327–340, doi:10.1007/s00382-012-1427-8.

Xue, Y., M. Chen, A. Kumar, Z.-Z. Hu, and W. Wang (2013), Prediction skill and bias of tropical Pacific sea surface temperatures in the NCEP climate forecast system version 2, *J. Clim.*, *26*, 5358–5378.

Yeh, S.-W., S.-J. Kug, B. Dewitte, M.-H. Kwon, B. P. Kirtman, and F.-F. Jin (2009), El Niño in a changing climate, *Nature*, *461*, 511–514.

Yu, J. Y., and S.-T. Kim (2013), Identifying the types of major El Niño events since 1870, *Int. J. Climatol.*, *33*(8), 2105–2112.

Zhang, C. (2001), Intraseasonal perturbations in sea surface temperatures of the equatorial eastern Pacific and their association with the Madden-Julian Oscillation, *J. Clim.*, *14*, 1309–1322.

Chapter 4: On the change in thermocline seasonal variability along the equatorial Pacific from before and after 2000

4.1 Overview

The previous chapter has suggested that the strong dissipation of the ISKws in the eastern equatorial Pacific could explain the confinement of warm SST anomalies in the central Pacific during CP El Niño events. Because there is evidence of increased occurrence of CP El Niño events since the 90s (Lee and McPhaden, 2011), there has been a debate whether or not changes in mean state could be responsible for this. From the perspective of this thesis, such changes would have to favor the scattering of energy of the ISKws. A change in the mean slope of thermocline has been observed from before and after 2000 (McPhaden et al., 2011), which has the potential to impact the ISKws characteristics. However the change in the mean thermocline depth is weak (~5m). Here instead on investigating mean state variations, changes in the seasonality of the thermocline depth are investigated, considering there is a seasonal phase locking of the ISKws activity (cf. Chapter 3). Based on *in situ* observations (TAO array) and a Reanalysis product (GODAS), the seasonal variability of the thermocline depth is analyzed and interpreted over the period 2000-2011 (P2) and compared with the period 1988-1996 (P1). The results are interpreted in the light of linear model experiments that provide estimation of the contribution of Kelvin and Rossby wave to the observed changes in seasonality of the thermocline depth. The methodology is similar to Yu and McPhaden (1999) that focused on the 1988-1996 period. Significant changes in seasonality are found between the two periods, which consists in an enhanced Austral summer shallowing of the thermocline after 2000. The chapter is organized as a paper and consists in a draft document to be submitted to *Journal of Geophysical Research – Oceans*. Supplementary materials are organized as an Appendix A.

4.2 Draft article to be submitted to Journal of Geophysical Research - Oceans

On the change in seasonal cycle in the equatorial Pacific from before and after 2000

Abstract

The equatorial Pacific has experienced a shift in its mean state since 2000, which has been suggested to result from the residual effect of ENSO property changes. Here we show that the seasonal cycle of the thermocline has also changed (both in magnitude and phase) which is associated with the wind stress forcing. In particular the seasonal cycle of thermocline exhibits a westward propagation pattern after 2000, which was not observed before 2000. The differences between the periods before and after 2000 can be interpreted as an enhanced upwelling Kelvin wave response due to the absence of wind convergence (divergence) in the far western Pacific after 2000. The enhanced seasonal shallowing of the thermocline in the eastern Pacific during Austral summer intensifies the zonal thermocline contrast, which is suggested to either damp the intraseasonal Kelvin wave during El Niño developments or induce an anomalous cooling through mean vertical advection of anomalous temperature.

Changes in the seasonal cycle of thermocline depth in the equatorial Pacific from before and after 2000

Kobi Mosquera-Vásquez and Boris Dewitte

To be submitted to Journal of Geophysical Research-Ocean

23/03/2015

Abstract

The equatorial Pacific has experienced a shift in its mean state since 2000, which has been suggested to result from the residual effect of ENSO property changes. Here we show that the seasonal cycle of the thermocline has also changed (both in magnitude and phase) which is associated with the wind stress forcing. In particular the seasonal cycle of thermocline exhibits a westward propagation pattern after 2000, which was not observed before 2000. The differences between the periods before and after 2000 can be interpreted as an enhanced upwelling Kelvin wave response due to the absence of wind convergence (divergence) in the far western Pacific after 2000. The enhanced seasonal shallowing of the thermocline in the eastern Pacific during Austral summer intensifies the zonal thermocline contrast, which is suggested to either damp the intraseasonal Kelvin wave during El Niño developments or induce an anomalous cooling through mean vertical advection of anomalous temperature.

1 Introduction

It is now recognized that El Niño has changed properties over the last 5 decades. In particular, there has been an increased occurrence of Central Pacific El Niño events (Yeh et al., 2009; Lee and McPhaden, 2010): since the beginning of the 21st century only Central Pacific El Niño events (hereafter CP El Niño) have taken place. The reason for that remains unclear although some aspects of change in mean states could be involved. For instance Luo et al. (2012) showed that the Walker circulation increased from 2000, which is associated with the La-Niña mean state observed in recent decades (Xiang et al., 2013). The change towards a cooler mean state can be related to the enhancement of non-linear processes for the low-level circulation that could explain why CP El Niño events have been more frequent in recent decades (Xiang et al., 2013). Recently Mosquera-Vásquez et al. (2014) suggested that characteristics of the mean thermocline could be also a key player. In particular, the intraseasonal Kelvin wave activity during CP El Niño events is strongly dissipated East of 120°W and model results suggest that such dissipation is associated with scattering of energy onto the zonal density gradient in the eastern Pacific. Whereas most recent studies have focused on change in mean state after 2000 in order to explain changes in ENSO properties (Thual et al., 2013; Luebbecke et al., 2014; Wen et al., 2014), to the authors' knowledge, none have investigated changes in the seasonal cycle, although the latter interacts with ENSO and may explain its irregularity by producing deterministic chaos through a two-way interaction (Chang et al., 1994, 1995; ; Tziperman et al., 1994, 1995; Jin, 1997; Wang and Fang, 1996; Wang et al.,1999; Timmermann et al., 2003). Another view is that, because ENSO is seasonally-phase locked (Rasmusson and Carpenter, 1982; Galanti and Tziperman, 2000; An and Wang, 2001), the ENSO (amplitude and

asymmetry) modulation can rectify on the seasonal cycle and produce changes in it. An and Choi (2009) suggest in particular that the changes in the seasonality of the asymmetry of ENSO may modify the amplitude of the annual and semi-annual cycles of the tropical eastern Pacific SST via a nonlinear process. A change in the ENSO asymmetry took place from the 2000s (Boucharel et al., 2011), which has an imprint on the equatorial wave dynamics (Dewitte et al., 2012). It mostly consists in a sharp reduction of the ENSO positive asymmetry from before and after 2000 as illustrated by the **Figure 1**, which shows the climatological skewness of the NINO3 region for two periods. **Figure 1** indicates that the changes are more pronounced during Austral summer, i.e. when El Niño peaks.

As a first step towards a better understanding of the mechanisms that leads to ENSO properties changes after 2000, the thorough investigation of observed changes in the seasonal cycle of the equatorial circulation is required, which this paper contributes to. Our focus is on the seasonal changes in the thermocline and surface winds due to the availability of data over a sufficiently long record to assess changes in seasonality at decadal timescales. We also analyse oceanic and atmospheric Reanalysis products and carry out model experiments in order to provide a dynamical interpretation of the changes in seasonality.

The paper is organized as follows: data and methodology are described in Section 2. The results are presented in Section 3 and the section 4 is a discussion followed by concluding remarks.

2. Data and method

For each data set, two periods are considered to derive the seasonal cycle: 1988-1996 (P1) and 2000-2011 (P2). The 1997-1998 El Niño is not considered in the statistics due to exceptional amplitude. The monthly mean is calculated and a 1-2-1 filter is applied to filter out the remaining intra-seasonal variability. At last, the mean seasonal cycle is derived. P1 covers nine years, which has been shown appropriate for accounting for the seasonal variability. Yu and McPhaden (1999) in particular compared the climatologies estimated from different products over this period and found a good agreement between them. The period P2 covers twelve years due to the low density of in *in situ* data collection in the equatorial Pacific from 2012 (see Takahashi et al. (2014)), preventing in particular to estimate properly the 20°C isotherm depth in the eastern equatorial Pacific in 2013-2014. Despite such limitation, we showed that our estimate of the seasonal variability over P2 from observations is comparable to estimate from Reanalysis products over 2000-2014 (not shown). Similar analysis was applied to period of nine years and the results are similar (not shown).

2.1 Winds and 20°C isotherm depth from TAO

TAO (Tropical Atmosphere Ocean Project) is the cornerstone of the now defunct TOGA project. With around 70 mooring buoys, deployed in the tropical Pacific since the 80s, the ocean in this region has been monitored with high temporal resolution. The variables used in this work are: 20°C isotherm depth (hereafter thermocline depth) and zonal (u) and meridional (v) winds. Variables were downloaded from the TAO homepage and interpolated between 2ºS and 2ºN in order to fill gaps in the equatorial

wave guide. Zonal and meridional wind at a daily resolution are used to estimated the zonal pseudo stress (U) using the following formula: .

2.2 GODAS Reanalysis

The GODAS (Global Ocean Data Assimilation System) is a model developed to initialize a numerical coupled model at National Environmental Prediction Center (NCEP) used to operational ENSO prediction. The current version of GODAS has 40 vertical levels with a 10 m resolution in the upper twenty meters and extends meridionally from 75°S to 65°N. GODAS is forced by the momentum flux, heat flux and fresh water flux from the NCEP atmospheric Reanalysis 2 (R2). The oceanic model assimilates SST from Reynolds Optimal Interpolation product (OISST, Reynolds et al., 2002), temperature vertical profiles from TAO project (see Section 2.2.1) and expendable bathy thermographs (XBT) observations from NODC World Ocean Database 1998 (information before 1990) and Global Temperature-Salinity Profile Project (after 1990). The current version does not assimilate satellite sea level information but has a comparative sea level diagnostic. More information could be found in Behringer and Xue (2004).

Like for TAO data, GODAS temperature is used to derive the seasonal cycles of thermocline depth over P1 and P2. As mention above, we also use an extended P2 period (2000-2014) allowed by the availability of the data until November 2014 in order to test the sensitivity of the results to the period over which the climatology is calculated. It is expected that GODAS, due to the assimilation of TAO data, compare

wells with the TAO data, although differences can emerge due to the assimilation process.

GODAS is also used to derive information needed to tune a Multi-modal linear oceanic model (see below) that is used for interpreting the results. In particular a vertical mode decomposition of the GODAS mean stratification over both periods is performed in order to derive the wave parameters required for the linear model. The analysis also allows estimating the baroclinic mode contributions to thermocline variability and zonal current in GODAS (See Dewitte et al. (1999) for the details of the method).

Wind at 10 meters from NCEP-DOE Reanalysis 2 (R2; Kanamitsu et al., 2002), which is the surface momentum fluxes for GODAS model, is used to compare with the TAO data. Climatological wind stress is obtained from monthly mean data to be employed to force the linear model experiments (see Section 2.5).

2.3 Multi-modal linear ocean model (MMLOM) and derivation of long equatorial waves

For the interpretation of the results, following Yu and McPhaden (1999), a linear oceanic model is used. The model is described in Mosquera-Vásquez et al. (2014) where it is used in a single mode version. Here three baroclinic modes are used, which characteristics (c_n , H_n) are derived from a vertical mode decomposition of the mean stratification from GODAS. (c_n , H_n) are respectively the phase speed and the equivalent depth for the nth baroclinic modes. The model outputs are further decomposed in

157 Kelvin and first meridional Rossby waves for each mode, which can be compared to the
158 decomposition of GODAS. The friction r_n has the form $r_n = (c_1 / c_n)^2 (30 \text{ months})^{-1}$.
159 Two seasonal simulations are carried out that corresponds to the different
160 periods P1 and P2. The model is run for ten years to ensure that we are in steady state at
161 climatological time scale and only the last year is analyzed.
162
163 **3 Results**
164
165 *Thermocline depth*
166
167 The **Figure 2** (bottom panels) shows the seasonal variability (represented in two
168 consecutive years in order to emphasize the complete variation) of the thermocline
169 depth from TAO for P1 and P2. The fluctuations of the thermocline depth exhibits
170 contrasted difference between the two periods. For P1, the variations indicate that the
171 Upwelling Phase (UP) is concentrated mainly between March and September with a
172 maximum value in May-June, which corresponds to period when trade winds intensify
173 seasonally (see Figure 5a). The location of the upwelling centers (where the thermocline
174 becomes shallow) are at 155°W and 125°W. Between October and February, the
175 thermocline deepens with a maximum depth around November at the same location of
176 the UP. The central and eastern Pacific are in phase, evidencing no propagation of the
177 seasonal cycle. These results, in general, are consistent to those found by Yu and
178 McPhaden (1999) using the same information to characterize the seasonal variability in
179 the equatorial Pacific region. On the other hand, for P2, the variations in thermocline
180 depth are indicative of a westward propagation, with the UP starting in Austral summer
181 in the east and evolving to the west until winter. The eastern (western) Pacific in P2 has

182 a prominent semi-annual (annual) oscillation compared with P1. Interestingly the
183 difference between P2 and P1 (**Figure 2c**) evidences an eastward propagating seasonal
184 variability in the central Pacific with a peak variability in the eastern Pacific more
185 pronounced for the UP and DP. This results in particular in a shallower thermocline
186 (5m) in the eastern Pacific during P2 compared to P1 (**Figure 2c**). On the other hand,
187 the mean thermocline is deeper (10m) in the central Pacific during P2 (**Figure 2d**),
188 which has been suggested to result from the rectified effect of CP El Niño events
189 (McPhaden et al., 2011).
190
191 To further document the change in seasonality in thermocline depth, the
192 amplitude and phase of the annual and semiannual oscillations are derived from both
193 periods using a Harmonic Regression Model (for details of the methodology, refer to
194 Emery and Thomson, 2001) for each period. The **Figure 3** shows the results. They
195 indicate that, after 2000 the magnitude of the annual cycle has been reduced along the
196 equatorial Pacific to the east and to the west of 140°W. The maximum value of around
197 12 m during P1 is decreased to 7 m during P2. In the case of the semi-annual cycle, the
198 magnitude in P2 increases (decreases) at 125°W (central and western Pacific). The
199 phase has changed from before and after 2000: during P1, the phase is indicative of a
200 seasonal cycle propagating eastward, contrary to during P2 when the phase indicates a
201 slow westward propagation from the far eastern Pacific (see **Figure 3f**).
202
203 Due to uncertainty associated with variations in data density (in particular in the
204 eastern equatorial Pacific), GODAS is also analyzed, which somehow provides a
205 consistency check of the above results. The **Figure 4** indicates that annual and semi-
206 annual cycles of thermocline depth in GODAS is comparable to the one of TAO, with

207 in particular the annual cycle in P1 (P2) showing a fast eastward (slow westward)
208 propagation (**Figure 4a**, **c**), while the semi-annual cycle has an eastward propagating
209 pattern (**Figure 4b**, **d**). In **Figure 4e**, it is clear that the magnitude of the 1st harmonic
210 has been reduced in most of the equatorial Pacific region, except to the west of the
211 dateline, where the magnitude during P2 is greater than during P1. The phase of the 1st
212 harmonic also shows differences between P1 and P2, revealing opposite movements:
213 eastward and westward during P1 and P2, respectively (**Figure 4f**).
214
215 *Wind stress*
216
217 Thermocline variability in the equatorial at seasonal timescales is to a large
218 extent due to the adjustment to momentum flux in the equatorial Pacific (Xie and
219 Philander, 1994; Yu and McPhaden, 1999). To elucidate the causes of the observed
220 changes in the thermocline seasonal variability, the changes in the seasonal cycle of
221 zonal pseudo stress (UU) is thus documented. The **Figure 5** displays the results of the
222 harmonic regression model applied to UU estimated from TAO winds. The amplitude of
223 the annual cycle is larger during P2 than during P1 and evidences a clear westward
224 propagation that extends to the west more during P2 than during P1 (**Figure 5a** and
225 **Figure 5c**). This is clearly evidenced in the amplitude (**Figure 5e**) and phase (**Figure**
226 **5f**). On the other hand, the semi-annual cycle does not exhibit significant changes from
227 P1 to P2, except in the far western Pacific where the phase indicates a slower westward
228 propagation than in the central Pacific during P2 (**Figures 5bdef**).
229
230 The analysis of the NCEP-DOE wind stress reveals comparable features (**Figure**
231 **6**), that is, the amplitude (**Figure 6e**) and phase (**Figure 6f**) of the annual cycle has a

marked westward propagating signal during P2 that extends over the entire equatorial Pacific region, whereas during P1, the westward propagation is no longer taking place around the dateline.

Dynamical interpretation

In this section we investigate to which extent the changes in seasonally described above can be interpreted in terms of the dynamical response to wind stress forcing. The vertical mode decomposition of GODAS as well as results of linear model experiments are used. The linear model is tuned based on the parameters derived from the GODAS vertical mode decomposition. The latter is performed at each grid point along the equator, which provides wave parameters of the first three baroclinic modes (n=1, 2, and 3) as a function of longitude. They are then averaged between 170ºW-120ºW (see **Table 1** for values) and prescribed into the linear model. The linear model outputs that are analyzed here consist in the summed-up contribution of the Kelvin wave contribution to sea level anomalies for the three baroclinic modes (HK) and the summed-up contributions of the first and third meridional mode Rossby wave contribution to sea level anomalies for the three baroclinic modes (HR).

The **Figure 7** displays the results of the harmonic analysis applied to the linear model outputs. The focus is on the annual harmonic considering that the semi-annual cycle has a much lower amplitude. The results reveals that the changes in the seasonality of the thermocline can be interpreted to a large extent as a dynamical linear response to the changes in the seasonal wind stress. In particular the sea level anomalies simulated by the model after 2000 propagate westward, which is not observed before

2000. The prominent westward propagation during P2 is due to the change in the Kelvin wave response to the wind stress as indicated by the meridional decomposition. During P1, there is an annual upwelling Kelvin wave forced in the western Pacific during April-June that propagates freely eastward and reaches the eastern Pacific in August-October where it intensifies. This free annual Kelvin wave is no longer present during P2, which emphasizes the annual Rossby wave and so the westward propagation along the equator. The Kelvin wave response during P2 consists in a westward propagation indicating that it is mostly wind forced. Even though the magnitudes are similar in both periods (1st and 2nd harmonic, see **Figure 7g**), the phases of the annual cycle are not (see **Figure 7i**). Regarding the Rossby wave, the phase is identical in both periods (westward propagation, **Figure 7c** and **7f**). However the amplitude is significantly larger during P2 to the west of 150ºW (**Figure 7h**). Similar features are obtained from the vertical mode decomposition of GODAS (not shown). The difference in the annual Kelvin wave response between both periods explains to a large extent the difference in thermocline depth observed in TAO.

4. Summary and Discussion

Due to the tied relationship between the ENSO and seasonal cycle, the low frequency modulation of the later is worth investigating for understanding ENSO property changes. Here the focus is on changes in the seasonality of thermocline depth from before and after 2000 considering that a change in ENSO dynamics has been observed around 2000 (McPhaden et al., 2011). The analysis is based on *in situ* data (TAO), the NCEP reanalysis and a linear model simulation. It reveals significant changes in the characteristics of the seasonal variability of the thermocline depth. In

282 particular, whereas the seasonal cycle of thermocline depth is stationary before 2000, it
283 exhibits a westward propagation similar to SST after 2000. This is interpreted as a
284 changes in the forcing of seasonal Kelvin and Rossby waves: After 2000, the seasonal
285 Kelvin wave is locally forced by the westward propagating wind stress, whereas before
286 2000, the Kelvin was is forced in the far western Pacific and then propagates freely
287 towards the eastern Pacific where it is intensified. As a result, the change in seasonality
288 of the thermocline depth consists in an apparent Kelvin wave response leading to a
289 shallowing (deepening) of the thermocline in Austral Spring-Summer (Fall-Winter) in
290 the far eastern Pacific. Another striking difference between the two periods is the
291 amplification of the semi-annual cycle in the eastern Pacific after 2000. The latter
292 explains the change in asymmetry of the seasonal cycle in the eastern Pacific from
293 positive to negative.
294
295 Where changes in the seasonality of thermocline depth in the eastern Pacific
296 may not impact significantly the seasonal SST because the latter is mostly driven by the
297 meridional winds (Xie, 1994), it can alter the ENSO dynamics in two ways: 1) First,
298 since a shallowing of the thermocline is observed after 2000 during Autral Summer, it
299 may induce an anomalous cooling through vertical advection of mean temperature
300 during the development phase of ENSO, damping the Bjerknes feedback and so the
301 growth rate of the ENSO mode. 2) Second, the enhanced shallowing of the thermocline
302 in Austral winter is propitious for the scattering of energy of the Kelvin wave due to the
303 enhanced zonal contrast of the thermocline and the proximity of the thermocline to the
304 mixed-layer (inducing a more diffuse thermocline). Such process has been suggested to
305 be at work onto the intraseasonal equatorial Kelvin wave during CP El Niño events
306 (Mosquera-Vásquez et al., 2014). Whether or not such process would be at work and

307 enhanced after 2000 needs to be further investigated. At this stage it is interesting to
308 note that the seasonal changes in thermocline depth described in the paper have not been
309 observed over the last 5 decades. The **Figure 8** displays the cross-correlation between
310 the seasonal cycle of thermocline depth calculated over 10-year running windows from
311 1958 to 2008 (SODA) over different regions along the equator. It clearly shows that
312 changes in seasonality are the most prominent in the far eastern Pacific and for the
313 period after 2000. Further studies are necessary in order to better understand the
314 mechanisms associated with such seasonal changes and how they could affect ENSO
315 dynamics.
316
317

References:

An, S.-I, and B. Wang, 2001: Mechanisms of locking the El Nino and La Nina mature phases to boreal winter. J. Climate. 14, 2164-2176.

An, S.-I., and J. Choi, 2009: Seasonal locking of the ENSO asymmetry and its influence on the seasonal cycle of the tropical eastern Pacific sea surface temperature. Atmos. Res., 94, 3-9

Behringer, D. W., and Y. Xue, 2004: Evaluation of the global ocean data assimilation system at NCEP: The Pacific Ocean. Eighth Symposium on Integrated Observing and Assimilation Systems for Atmosphere, Oceans, and Land Surface, AMS 84th Annual Meeting, Washington State Convention and Trade Center, Seattle, Washington, 11-15.

Boucharel J., B. Dewitte, Y. duPenhoat, B. Garel, S.-W. Yeh & J.-S. Kug, 2011: El Niño nonlinearity in a warming climate. Climate Dynamics. DOI 10.1007/s00382-011-1119-9.

Chang, P., B. Wang, T. Li, and L. Ji., 1994: Interactions between the seasonal cycle and the Southern Oscillation—Frequency entrainment and chaos in a coupled ocean–atmosphere model. Geophys. Res. Lett., 21, 2817–2820.

Chang, P., L. Ji, B. Wang, and T. Li, 1995: Interactions between the seasonal cycle and El Niño–Southern Oscillation in an intermediate coupled ocean–atmosphere model. J. Atmos. Sci., 52, 2353– 2372.

343

344 Emery, W. and R. Thompson, 2001: Data analysis methods in physical oceanography,
345 Second edition, Elsevier, Amsterdam, The Netherlands, 638 pp.
346

347 Dewitte B., G. Reverdin and C. Maes, 1999: Vertical structure of an OGCM simulation
348 of the equatorial Pacific Ocean in 1985-1994, J. Phys. Oceanogr., 29, 1542-1570.
349

350 Dewitte B., J. Choi, S.-I. An, and S. Thual, 2012: Vertical structure variability and
351 equatorial waves during central Pacific and eastern Pacific El Niños in a coupled
352 general circulation model, Clim. Dyn., 38, 2275–2289.
353

354 Galanti E. and E. Tziperman, 2000: ENSO's Phase Locking to the Seasonal Cycle in the
355 Fast-SST, Fast-Wave, and Mixed-Mode Regimes, Journal of the Atmospheric Sciences,
356 57, No. 17, pp. 2936-2950.
357

358 Kanamitsu, M., W. Ebisuzaki, J. Woollen, S-K Yang, J.J. Hnilo, M. Fiorino, and G. L.
359 Potter, 2002: NCEP-DOE AMIP-II Reanalysis (R-2). Bull. Amer. Met. Soc., 83, 1631-
360 1643.
361

362 Jin, F.-F., 1997: An equatorial ocean recharge paradigm for ENSO. Part I: Conceptual
363 model. J. Atmos. Sci., 54, 811–829.
364

365 Lee T. and M. J. McPhaden, 2010: Increasing intensity of El Niño in the central-
366 equatorial Pacific, Geophys Res Lett 37:L14603. doi:10.1029/2010GL044007.
367

368 Luo, J.-J., W. Sasaki, and Y. Masumoto, 2012: Indian Ocean warming modulates
369 Pacific climate change, *Proceedings of the National Academy of Sciences of the United*
370 *States of America*, 109(46), pp.18701-18706, doi:10.1073/pnas.1210239109.
371
372 Luo J-J, W. Sasaki, Y. Masumoto, 2012: Indian Ocean warming modulates Pacific
373 climate change. Proceedings of the National Academy of Sciences 109 (46):18701-
374 18706. doi:10.1073/pnas.1210239109
375
376 Lübbecke, J. F. and M. J. McPhaden, 2014: Assessing the 21st century shift in ENSO
377 variability in terms of the Bjerknes stability index. J. Climate, 27, 2577-2587. doi:
378 http://dx.doi.org/10.1175/JCLI-D-13-00438.1.
379
380 McPhaden, M. J., T. Lee, and D. McClurg, 2011: El Niño and its relationship to
381 changing background conditions in the tropical Pacific, Geophys. Res. Lett., 38,
382 L15709, doi:10.1029/2011GL048275.
383
384 Mosquera-Vásquez, K., B. Dewitte, and S. Illig, 2014: The Central Pacific El Niño
385 intraseasonal Kelvin wave, J. Geophys. Res. Oceans, 119, 6605–6621,
386 doi:10.1002/2014JC010044.
387
388 Rasmusson E. M. and T. H. Carpenter, 1982: Variations in Tropical Sea Surface
389 Temperature and Surface Wind Fields Associated with the Southern Oscillation/El
390 Niño. Mon. Wea. Rev., 110, 354–384.
391
392

393 Takahashi, K., R. Martínez, A. Montecinos, B. Dewitte, D. Gutierrez, and E.
394 Rodriguez-Rubio, 2014: TPOS White Paper #8a – Regional applications of observations
395 in the eastern Pacific: Western South America. In Proceedings of the Tropical Pacific
396 Observing System 2020 Workshop, A Future Sustained Tropical Pacific Ocean
397 Observing System for Research and Forecasting, WMO and Intergovernmental
398 Oceanographic Commission, La Jolla, Calif., 27–30 January. [Available at
399 http://www.wmo.int/pages/prog/gcos/Publications/gcos-184_II.pdf.]
400
401 Timmermann, A., F-F Jin and J. Abshagen, 2003: A nonlinear theory for El Niño
402 bursting. J.Atmos.Sci.60: 152–165.
403
404 Tziperman, E., L. Stone, M. Cane, and H. Jarosh, 1994: El Nin˜o chaos: Overlapping of
405 resonances between the seasonal cycle and the Pacific Ocean–atmosphere oscillator.
406 Science, 264, 72– 74.
407
408 Tziperman, E., M. A. Cane, and S. Zebiak, 1995: Irregularity and locking to the
409 seasonal cycle in an ENSO prediction model as explained by the quasi-periodicity route
410 to chaos. J. Atmos. Sci., 52, 293– 306.
411
412 Thual, S., B. Dewitte, S.-I. An, S. Illig, and N. Ayoub, 2013: Influence of Recent
413 Stratification Changes on ENSO stability in a Conceptual Model of the Equatorial
414 Pacific, J. Climate, 26, 4790–4802.
415
416 Wang, B. and Z. Fang, 1996: Chaotic Oscillation of the tropical climate: A dynamic
417 system theory for ENSO. J. Atmos. Sci., 53, 2786-2802.

Wang, B., R. Wu, and R. Lukas, 1999: Roles of the western North Pacific wind variation in thermocline adjustment and ENSO phase transition. J. Meteor. Soc. Japan, 77, 1-16. Ab

Wen, C., A. Kumar, Y. Xue, and M. J. McPhaden, 2014: Changes in Tropical Pacific Thermocline Depth and Their Relationship to ENSO after 1999. *J. Climate*, vol. 27, 7230-7249.

Xiang, B., B. Wang, and T. Li, 2013: A new paradigm for the predominance of standing Central Pacific Warming after the late 1990s. Clim. Dyn., 41 (2), 327-340, doi:10.1007/s00382-012-1427-8.

Xie, S.-P., and S. G. H. Philander, 1994: A coupled ocean–atmosphere model of relevance to the ITCZ in the eastern Pacific. Tellus, 46A, 340–350.

Xie, S.-P., 1994: Oceanic response to the wind forcing associated with the intertropical convergence zone in the northern hemi- sphere. J. Geophys. Res., 99 (C10), 20 393–20 402.

Yeh S-W, S-J Kug, B. Dewitte, M-H Kwon, B. P. Kirtman, F-F Jin, 2009: El Niño in a changing climate, Nature 461:511–514.

Yu, X. and M. J. McPhaden, 1999: Seasonal Variability in the Equatorial Pacific, Journal of Physical Oceanography, 29, 925-947.

443

444

445

446

447 **Table Captions**

448

449 **Table 1.** Parameters used in the MMLOM for each baroclinic mode (columns) averaged

450 between 170º - 120ºW.

451

452

453

454

	Baroclinic modes		
	m=1	m=2	m=3
c_n (m s^{-1})	2.77	1.62	1.06
H_n (m)	313	257	864
$1/r_n$ (months)	30	23	18

455

456 **Table 1**. Parameters used in the MMLOM for each baroclinic mode (columns) averaged

457 between 170ºW- 120ºW.

458

459 **Figures Captions**

460

461 **Figure 1.** Climatology skewness of the El Niño 3 index for the periods 1981-1999
462 (black line) and 2000-2014 (red line) based in the version 3 of ERSST product
463 (http://www.cpc.ncep.noaa.gov/).

464

465 **Figure 2.** Seasonal variability of the observed (TAO) thermocline in the period P1 (a) y
466 P2 (b). Units are meter. The panel (c) shows the difference between the two periods (P2
467 minus P1). In the three upper panels the grey shading indicates negative values. The
468 panel (d) displays the mean thermocline depth over P1 (black solid line) and P2 (red
469 solid line) and the difference between P2 and P1 (black dashed line with an axis on the
470 right). Open squares located in the upper and lower axes of each panel indicate the
471 location of the mooring buoys.

472

473 **Figure 3.** Annual and semi-annual harmonics of the thermocline depth from TAO along
474 the equator during P1 (panels (a) and (b)) and during P2 (panels (c) and (d)). The
475 bottom panels display the magnitude (e) (scaled by the maximum value) and phase (f)
476 during P1 (black) and P2 (red). The 1st (2nd) harmonic is represented with a thick (thin)
477 line. Open squares located in the upper and lower axes of each panel indicate the
478 location of the mooring buoys.

479

480 **Figure 4.** Similar to Figure 3 but for GODAS. The period P2 is here 2000-2014

481

482 **Figure 5.** Similar to Figure 3 but for pseudo stress (m2s-2) estimated from TAO winds.

Figure 6. Similar than Figure 3 but for pseudo stress (m2s-2) estimated from NCEP-DOE winds.

Figure 7. The 1st harmonic seasonal SLH simulation results from MMLOM for period P1 (first row) and P2 (second row). The first (second, third) column of the first two rows displays the sum of HK and HR (HK, HR). The last four panels (j, h, i and j) display harmonic analysis results for HK and HR: panels (g) an (h) indicate the magnitude of HK and HR, respectively; panel (i) and (j) represent the phase. Thick (thin) line indicates 1st (2nd) harmonic and black (red) line represents P1 (P2).

Figure 8. Cross-correlation between the seasonal cycles of thermocline depth calculated over 10-year running windows between 1950 to 2008 along the equator. Data are from SODA: (a) Whole Pacific region, (b) Western Pacific, (d) Central Pacific and (d) Eastern Pacific.

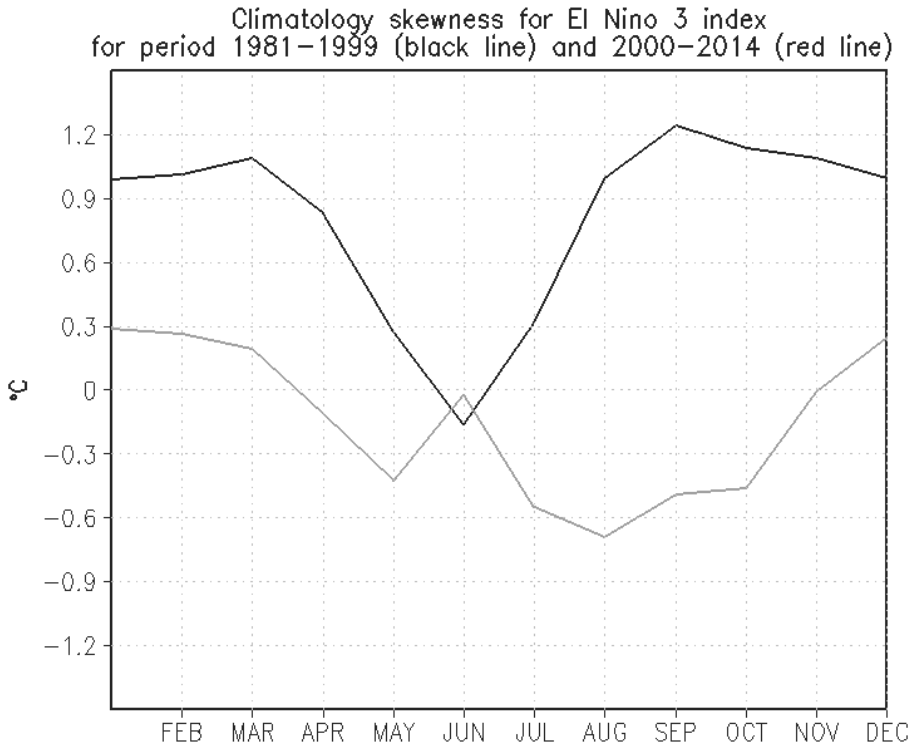

Figure 1. Climatological skewness of the El Niño 3 index for the periods 1981-1999 (black line) and 2000-2014 (red line) based in the version 3 of ERSST product (http://www.cpc.ncep.noaa.gov/).

507

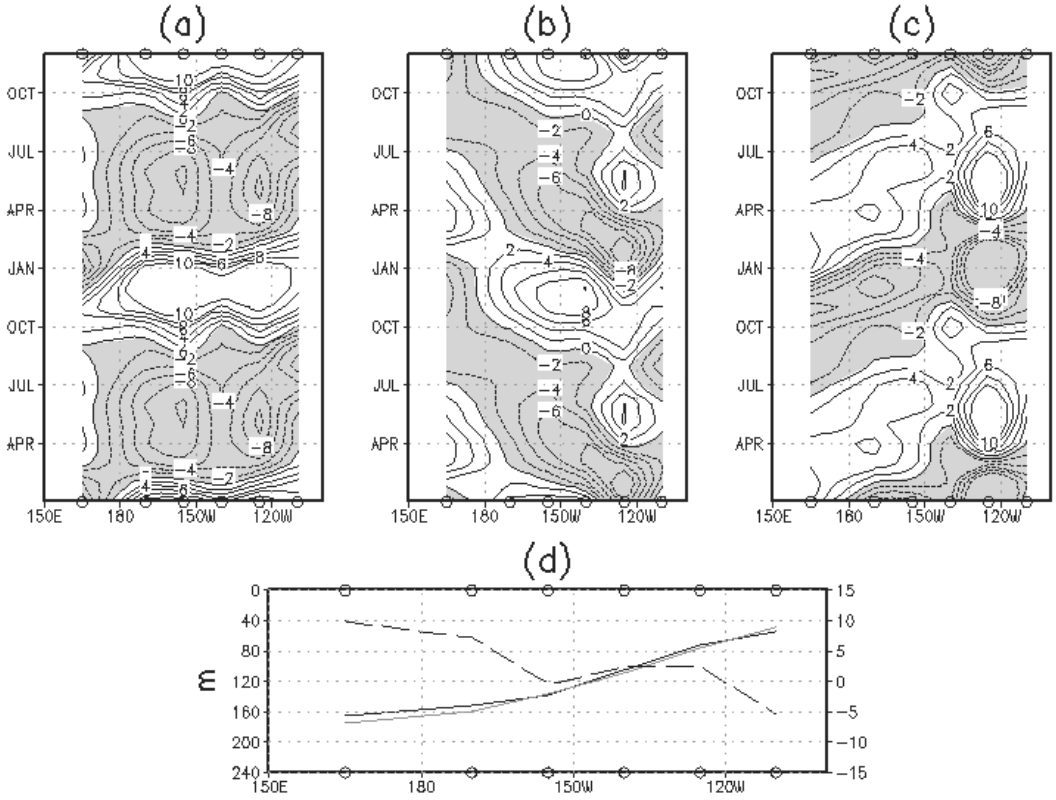

508

509 **Figure 2.** Seasonal variability of the observed (TAO) thermocline in the period P1 (a) y
510 P2 (b). Units are meter. The panel (c) shows the difference between the two periods (P2
511 minus P1). In the three upper panels the grey shading indicates negative values. The
512 panel (d) displays the mean thermocline depth over P1 (black solid line) and P2 (red
513 solid line) and the difference between P2 and P1 (black dashed line with an axis on the
514 right). Open squares located in the upper and lower axes of each panel indicate the
515 location of the mooring buoys.

516

517

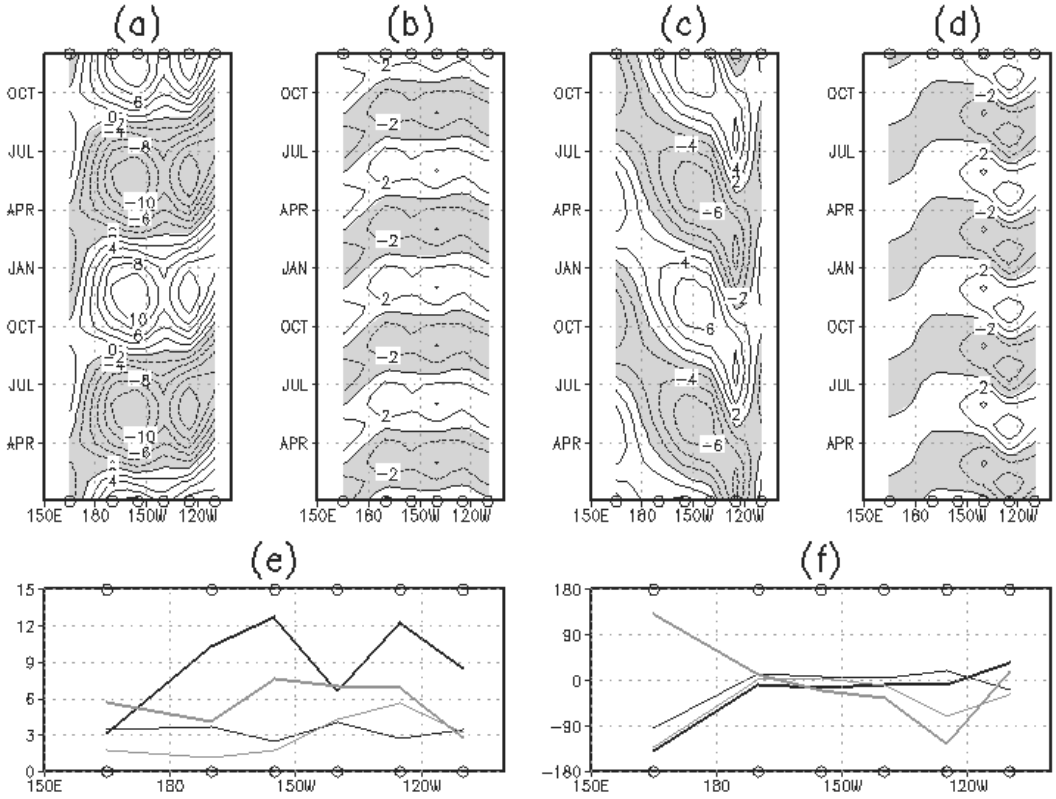

518

519 **Figure 3.** Annual and semi-annual harmonics of the thermocline depth from TAO along
520 the equator during P1 (panels (a) and (b)) and during P2 (panels (c) and (d)). The
521 bottom panels display the magnitude (e) (scaled by the maximum value) and phase (f)
522 during P1 (black) and P2 (red). The 1st (2nd) harmonic is represented with a thick (thin)
523 line. Open squares located in the upper and lower axes of each panel indicate the
524 location of the mooring buoys.

525

526

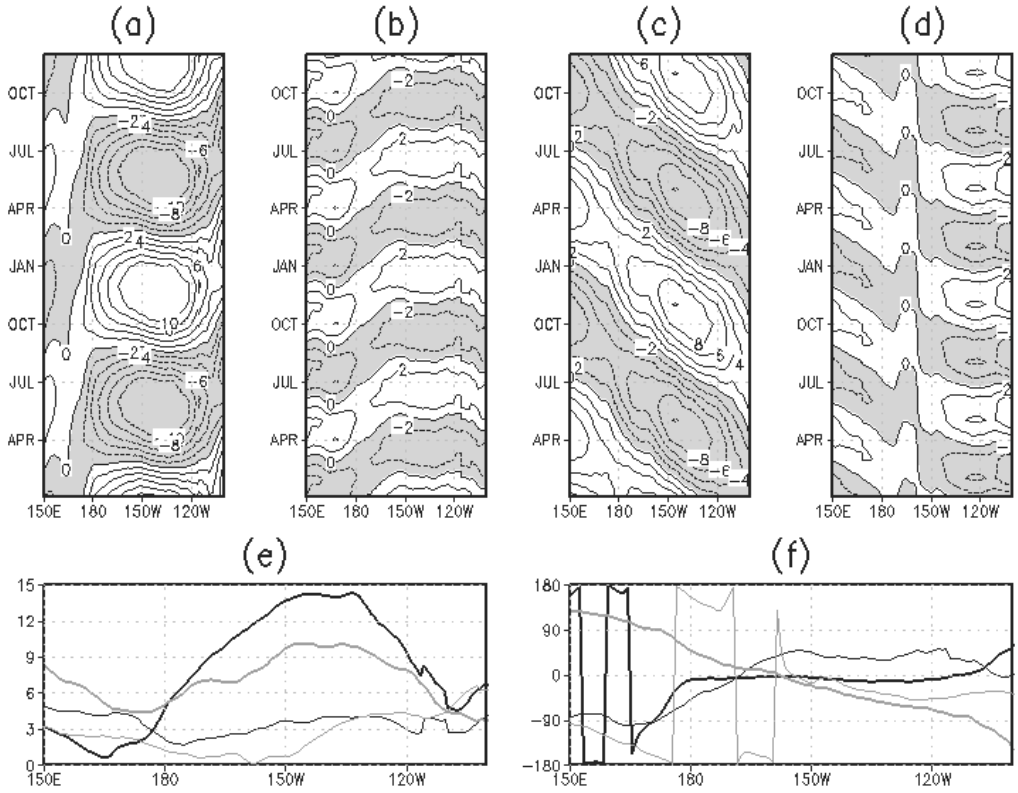

527

528 **Figure 4.** Similar to Figure 3 but for GODAS. The period P2 is here 2000-2014.

529

530

531

532

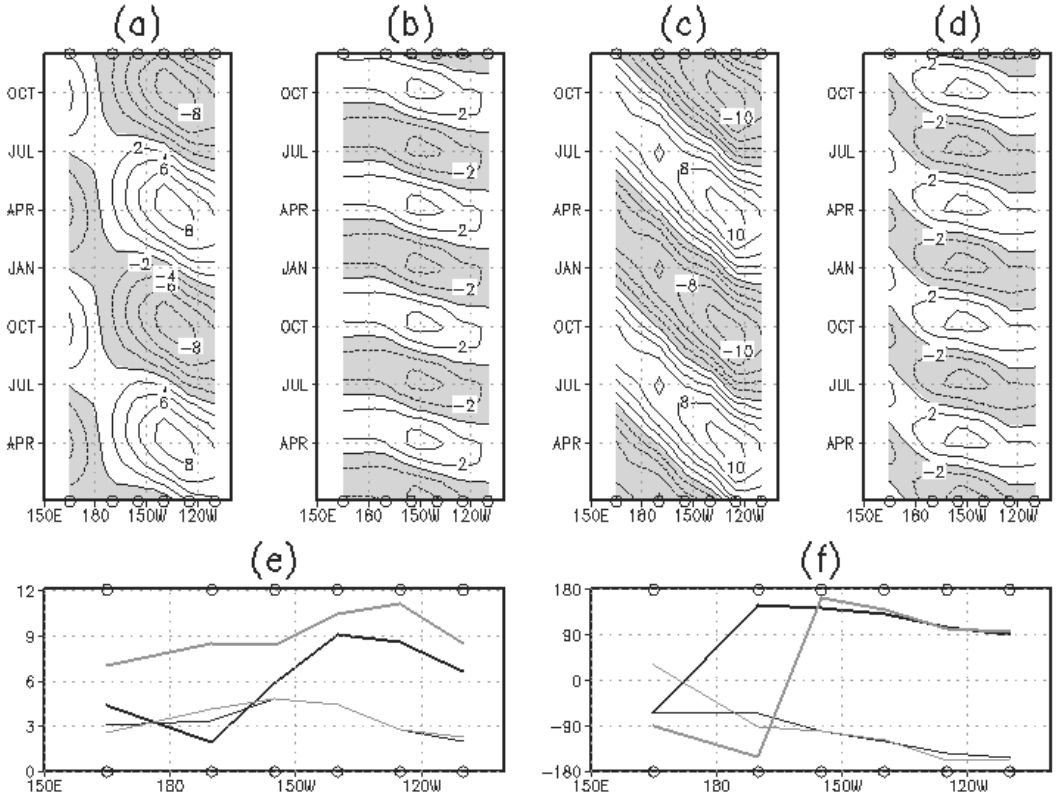

533

534 **Figure 5.** Similar to Figure 3 but for pseudo stress (m^2s^{-2}) estimated from TAO winds.

535

536

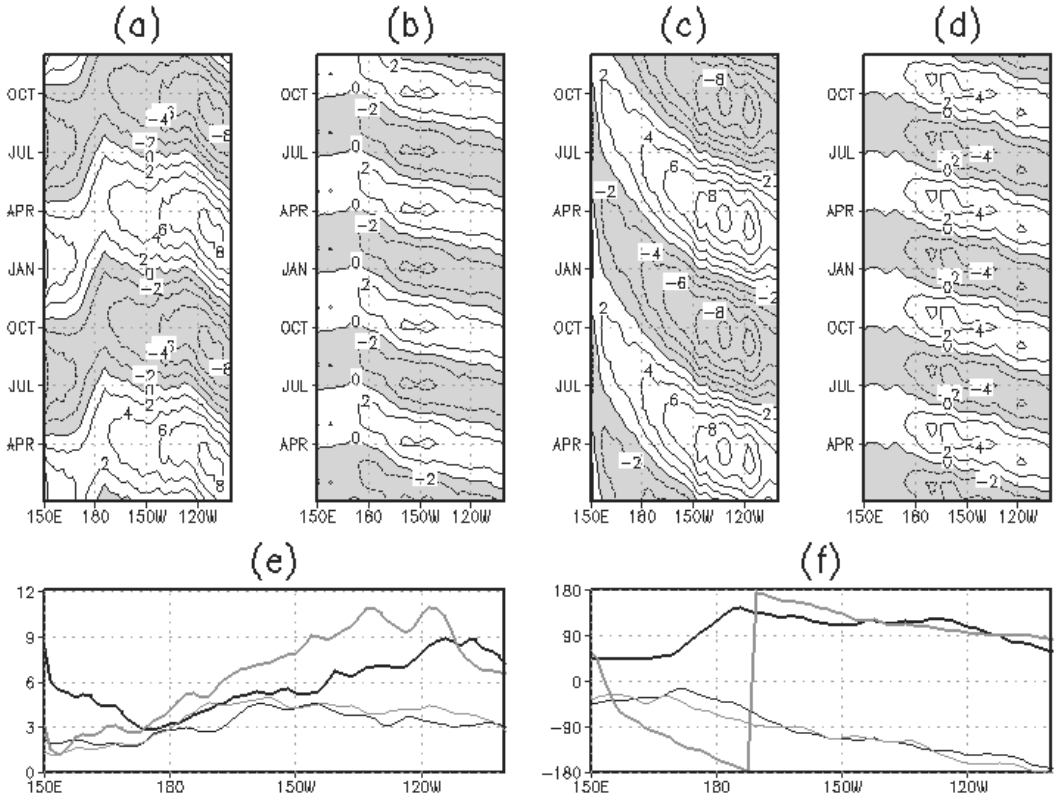

Figure 6. Similar than Figure 3 but for pseudo stress (m^2s^{-2}) estimated from NCEP-DOE winds.

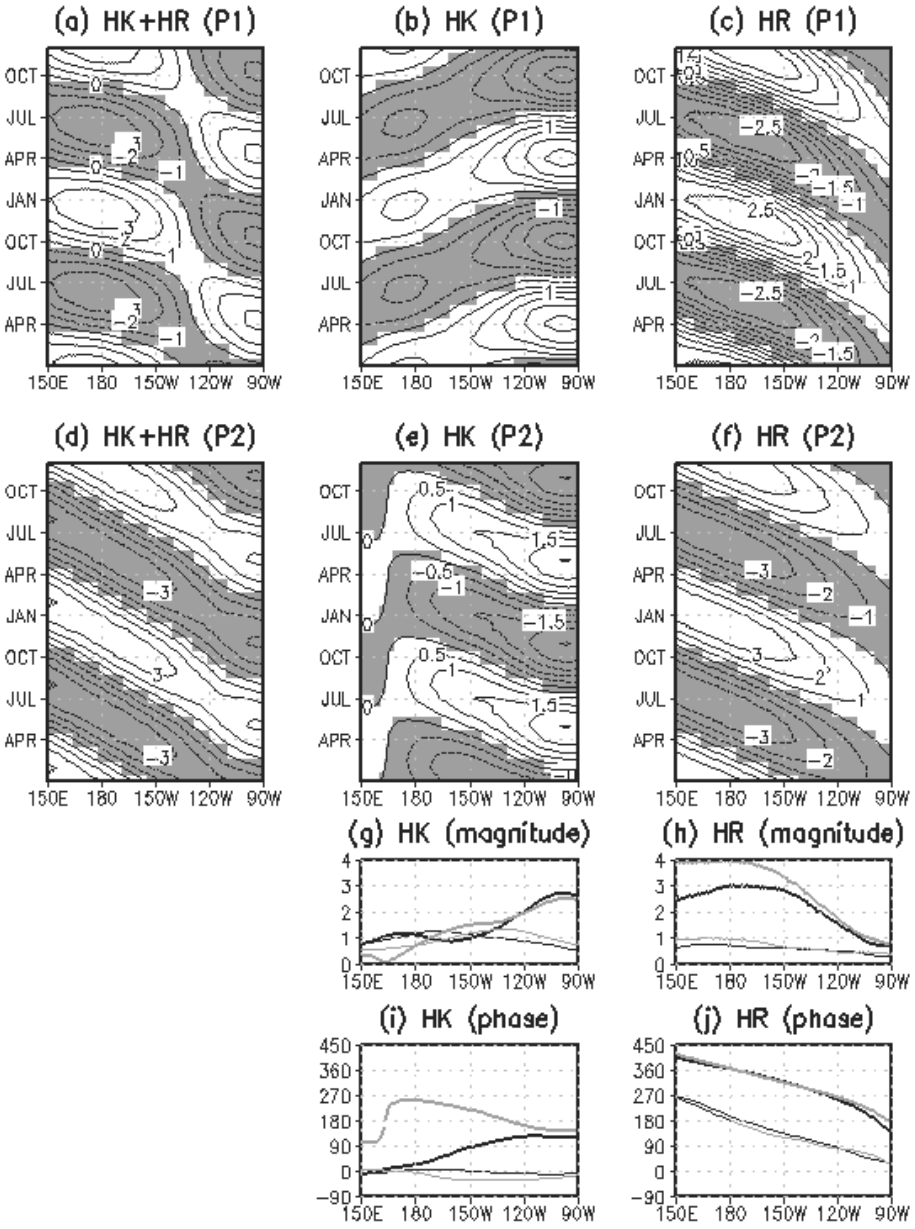

Figure 7. The 1st harmonic seasonal SLH simulation results from MMLOM for period P1 (first row) and P2 (second row). The first (second, third) column of the first two rows displays the sum of HK and HR (HK, HR). The last four panels (j, h, i and j) display harmonic analysis results for HK and HR: panels (g) an (h) indicate the magnitude of HK and HR, respectively; panel (i) and (j) represent the phase. Thick (thin) line indicates 1st (2nd) harmonic and black (red) line represents P1 (P2).

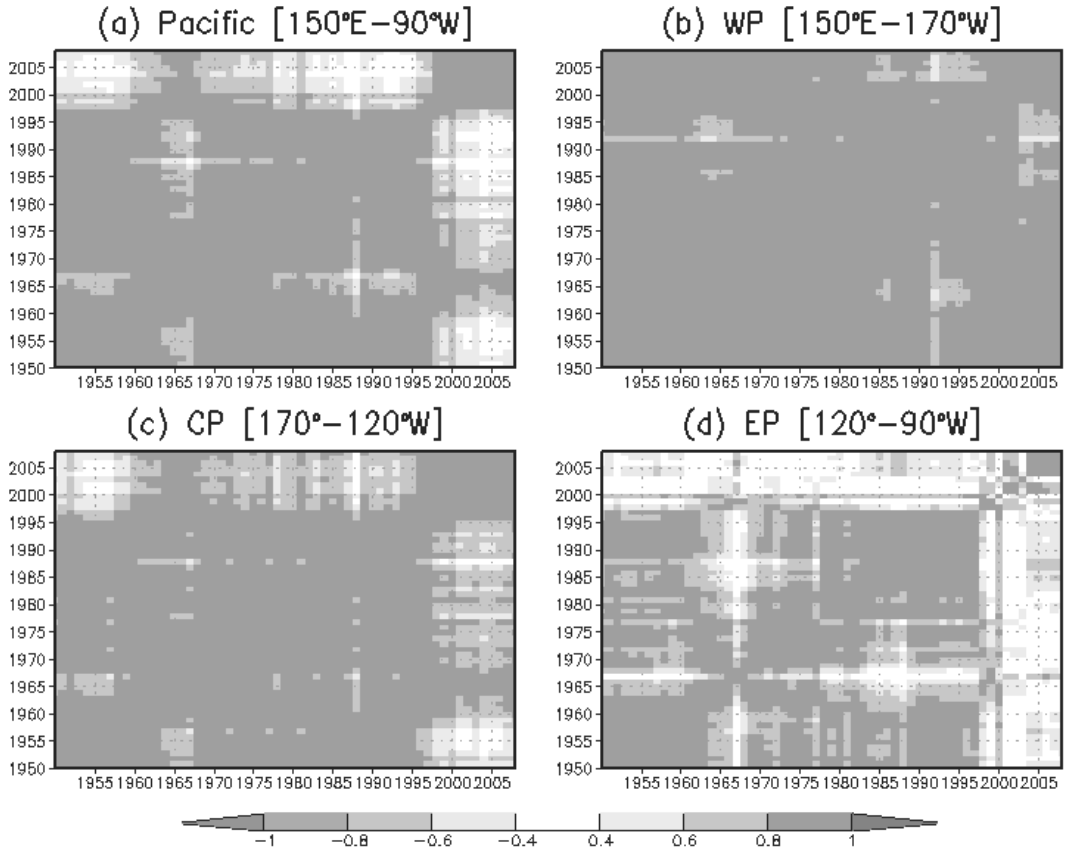

553

554

555 **Figure 8** Cross-correlation between the seasonal cycles of thermocline depth calculated
556 over 10-year running windows between 1950 to 2008 along the equator. Data are from
557 SODA: (a) Whole Pacific region, (b) Western Pacific, (d) Central Pacific and (d)
558 Eastern Pacific.

Chapter 5: Conclusions and perspectives

(English Version)

In this thesis, the oceanic intraseasonal variability during Central Pacific El Niño (CP El Niño) events is investigated with emphasis on the long equatorial wave dynamics. Whereas Mosquera-Vásquez et al. (2013) focuses on a single event (the 2002/03 El Niño), Mosquera-Vásquez et al. (2014) provides a more generalized view of the intraseasonal Kelvin wave (ISKw) activity during the development and evolution of CP El Niño events that took place from 1990. The most significant and new finding is that ISKws during CP El Niño events experiences a drastic dissipation in the Eastern Pacific that is interpreted as resulting from modal dispersion due to the zonally varying stratification (sloping thermocline). Since during CP El Niño events, there is a weak Sea Surface Temperature (SST) variability in the eastern equatorial Pacific, it suggests that this strong eastward dissipation of the ISKws could be responsible for the CP El Niño spatial structure, *i.e.* a zonal seesaw of SST anomaly, positive in the central Pacific and negative (near zero) in the eastern Pacific. If the ISKw did not dissipate, it would be effective in inducing SST anomaly in the eastern Pacific because the thermocline feedback is effective there (due to the shallow thermocline). It could therefore explain why CP El Niño does not develop as an Eastern Pacific El Niño once they are initiated: the dissipation of the ISKws does not allow the warming in the eastern Pacific through the thermocline feedback and as a consequence does not contribute to a local Bjerknes feedback there, prone to increase the growth rate of ENSO instability (Takahashi and Dewitte, 2015).

This thesis also suggests that there have been changes in the circulation in the equatorial Pacific that have enhanced the dissipation of long equatorial waves in recent years since CP El Niño have occurred more frequently since the 90s (Lee and McPhaden, 2011). The equatorial Pacific has a La Niña-like state since the 90s (Xiang et al., 2013), which has the potential to increase the zonal contrast in vertical stratification (Thual et al., 2013). So our findings are consistent with the idea that change in mean state could influence the dissipation process of the ISKws. A recent observational study has suggested that changes in mean state could be a response of the

increased occurrence in CP El Niño through a rectification process (McPhaden et al., 2011), whereas modeling studies suggest that a two-way feedback between change in mean state and CP El Niño could exist leading to a decadal variability of the ENSO properties (Choi et al., 2011; 2012). In line with these studies, this thesis has thus explored decadal changes in the seasonal cycle, considering that the ISKw activity has a marked seasonality during CP El Niño events. The focus is on the change in the seasonal cycle of the thermocline depth from before and after 2000s. The results, which are based on in situ data (TAO), the NCEP reanalysis and a linear model simulation, show that there exist significant changes in the seasonality of the thermocline depth from before and after 2000. This has been interpreted as partly resulting from changes in the forcing of the seasonal Kelvin and Rossby waves along the equatorial Pacific. Another striking difference between the two periods is the amplification of the semi-annual cycle in the eastern Pacific after 2000. The latter explains the change in asymmetry of the seasonal cycle in the eastern Pacific from positive to negative. These results are consistent with the hypothesis that ISKws would be more dissipated over the recent decade during Austral Summer, implying an inhibition of the thermocline feedback in the eastern Pacific. Although we show that these changes in thermocline slope can be explained to a large extent through equatorial wave dynamics, there is a local amplification of these changes in the eastern Pacific, which could be explained by other processes. These includes mixing associated with Tropical Instability Waves that could erode the stratification near the shallow thermocline in the east, or buoyancy fluxes associated with nonlocal mixing within the mixed-layer when non-solar heat fluxes are larger than the solar flux that penetrates the surface layer and would destabilized locally the fluid (Large et al., 1994). Model simulations can provide material for the understanding of such process. Along the evolution of this thesis, a ROMS (Regional Oceanic Model System) configuration of the equatorial Pacific (15ºS-15ºN) was implemented (see Appendix B) with the perspective to carry out a heat budget analysis of the surface layer. This is a direction for future work. The model could be further coupled to an atmospheric model to elucidate to which extent there can be an air-sea positive feedback associated with the mixing process. Note that there has been indication that the ISKws could be coupled to the low-level circulation during the Madden Julian Oscillation activity (Hendon et al., 1998; Roundy and Kravitz, 2009). This is a process that cannot be diagnosed from a forced model, so the coupled model would be ideal to tackle this issue. Such a model could also have a value for seasonal

prediction at basin scale and at regional scale (along the Peruvian coast) and serve as a seasonal prediction system for Peru.

This thesis also calls for a better understanding of the mechanisms associated with the propagation of the ISKws along the South America coast and for the investigation how the latter impacts the circulation and SST. A recent study has suggested that the ISKw was weakly influential on SST along the coast of Peru, although the ISKws was propagating efficiently along the thermocline (Illig et al., 2014). Although this study is peculiar to the 2000-2008 period, it highlights the likely role of local stratification in influencing the oceanic teleconnection off Peru. An observational platform off Peru could be set up to investigate this, which the author of this thesis is keen on contributing to within a national and international context (Takahashi et al., 2014).

At the time this thesis was written, a warm event developed along the Peruvian coast in 2014 (See **Figure 5.1**). This warm event has again challenged our understanding of El Niño since it did not develop as expected: It was anticipated to lead to an El Niño event as strong as the 1997/98 El Niño but it was not at basin scale (Menkes et al., 2014). This event was still significant for Peru, leading to warm anomalies along the coast. Such event remains unexplained[1] and it is likely to mobilize the ENSO community for a few years in order to propose a mechanism by which this event vanished at a moment when ENSO scientists thought it would lead to a strong eastern Pacific El Niño. Again, around 9th of March 2015, a huge MJO signal was followed by wind stress anomalies that are expected to force intense downwelling ISKws (see **Figure 5.1**). The ENSO community is again pending how this event will develop.

Based on the work presented in this thesis, its author is willing to participate to such effort in the coming years. Since the afore-mentioned proposed processes potentially leading to the amplification or erosion of the zonal contrast in stratification (and thus to the dissipation of the ISKws in the eastern Pacific) has not been

[2] Dr. Mike McPhaden is having a poster at the EGU 2015 entitled "Who Killed the Big 2014-15 El Niño?"

investigated yet, there is still plenty work to be done. This should guide the author's research in the next years at *Instituto Geofísico del Perú* (IGP) considering the socio-economical consequences associated with coastal warmings (not just El Niño events) along the coast of Peru.

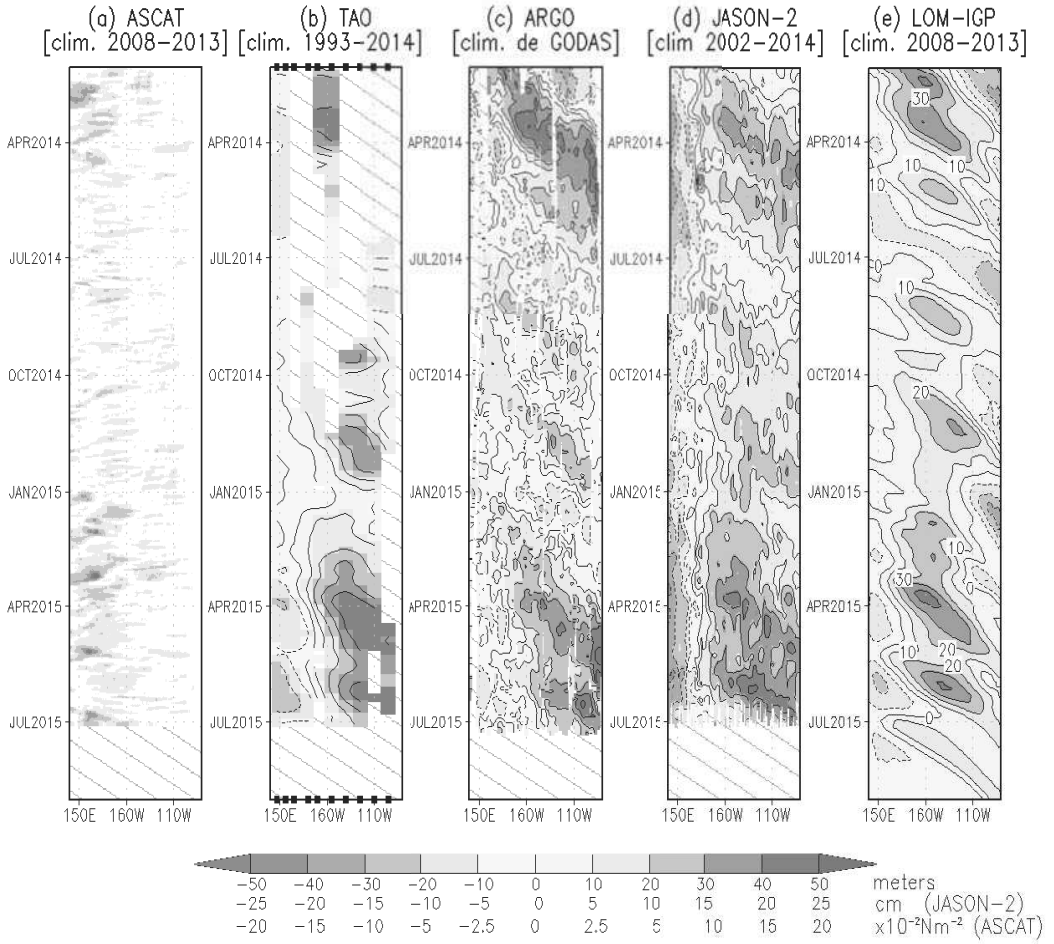

Figure 5.1 Höwmöller diagram along the equatorial region of the zonal wind stress anomaly from ASCAT (a); thermocline depth anomaly from TAO (b), and ARGO drifters (c); and sea level anomaly from JASON-2 (d), (e) the thermocline depth anomaly, calculated with a linear oceanic model that was forced by ASCAT winds, is displayed. For prediction purpose, the linear model is forced with (taux, tauy) = (0, 0) when ASCAT data are no longer available.

(Version française)

Dans cette thèse, la variabilité intra-saisonnière océanique durant les événements El Niño de type Pacifique Central (CP El Niño) est étudiée en mettant l'accent sur la dynamique des ondes longues équatoriales. Tandis que Mosquera-Vásquez et al. (2013) se concentre sur un événement particulier (El Niño 2002/03), Mosquera-Vásquez et al. (2014) présente une vue plus générale de l'activité IntraSaisonnière de l'onde de Kelvin (ISKw) pendant le développement et l'évolution des événements CP El Niño qui ont eu lieu à partir de 1990. Le résultat le plus important et original de cette thèse est que durant les événements CP El Niño, l'onde ISKw subit une forte dissipation dans le Pacifique Est. Celle ci est interprétée comme résultant de la dispersion modale en raison de la variation zonale de la stratification (i.e. la remontée de la thermocline d'Ouest en Est). Puisque lors des événements CP El Niño, la variabilité de la température de la surface de la mer (SST) est faible dans l'Est du Pacifique équatorial, cela suggère que cette forte dissipation des ISKws pourrait être responsable de la structure spatiale des événements CP El Niño, *i.e.* un dipole zonal de l'anomalie de SST, positive dans le Pacifique central et négative (proche de zéro) dans le Pacifique oriental. Si l'onde ISKw ne se dissipait pas, elle pourrait induire des anomalies de SST dans le Pacifique Est, car le processus de *thermocline feedback* est efficace dans cette région (en raison de la thermocline peu profonde). Cela pourrait donc expliquer pourquoi l'événement El Niño de type Central Pacifique ne se développe pas comme un événement El Niño Pacifique Est une fois l'événement initié: la dissipation des ISKws ne permet pas le réchauffement dans le Pacifique Est par le *thermocline feedback* et par conséquent ne permet pas de déclencher la retro-alimentation locale de Bjerknes (« Bjerknes feedback »), qui conduit à la croissance de l'instabilité ENSO pendant les événements forts (Takahashi et Dewitte, 2015, *soumis*).

Cette thèse suggère également qu'il ya eu des changements de la circulation dans le Pacifique équatorial qui ont intensifié la dissipation des ondes longues équatoriales au cours des dernières années, puisque les événements CP El Niño ont été plus fréquents depuis les années 90 (Lee et McPhaden, 2011). Le Pacifique équatorial est dans un état froid - de type La Niña - depuis les années 90 (Xiang et al., 2013), ce qui a le potentiel d'augmenter le contraste zonal de la stratification verticale (Thual et al., 2013). Ainsi, nos résultats sont cohérents avec l'idée qu'un changement d'état moyen pourrait

influencer le processus de dissipation des ISKws. Une étude observationnelle récente (McPhaden et al., 2011) a suggéré que le changement de l'état moyen du Pacifique équatorial pourrait expliquer la fréquence accrue des événements CP El Niño à travers un processus de rectification, alors que les études de modélisation suggèrent qu'une rétroaction entre le changement de l'état moyen et l'occurrence des CP El Niño pourrait exister, conduisant à une variabilité décennale des propriétés ENSO (Choi et al., 2011 ; 2012). Dans ce contexte, cette thèse a donc exploré les changements décennaux du cycle saisonnier, estimant que l'activité de l'onde ISKw a une saisonnalité marquée au cours des événements CP El Niño. L'accent a été mis sur le changement du cycle saisonnier de la profondeur de la thermocline avant et après 2000. Les résultats, qui sont basés sur des données in situ (TAO), la réanalyse NCEP et une simulation d'un modèle linéaire, montrent qu'il existe d'importants changements dans la saisonnalité de la profondeur de la thermocline avant et après 2000. Cela a été interprété comme résultant en partie de changements dans le forçage des ondes de Kelvin et de Rossby saisonnières, le long du Pacifique équatorial. Une autre différence frappante entre les deux périodes est l'amplification du cycle semi-annuel dans le Pacifique Est après 2000. Ce dernier explique le changement de l'asymétrie du cycle saisonnier dans le Pacifique Est, passant de positif à négatif. Ces résultats sont cohérents avec l'hypothèse que l'onde ISKw se dissiperait davantage au cours de la dernière décennie durant l'été austral, ce qui implique une inhibition du processus de *thermocline feedback* dans le Pacifique Est. Bien que nous montrions que ces changements de pente de la thermocline peuvent être expliqués dans une large mesure par la dynamique des ondes équatoriales, il y a une amplification locale de ces changements dans le Pacifique Est, qui pourrait être expliquée par d'autres processus. Par exemple, le mélange associé aux ondes d'instabilité tropicales pourrait éroder la stratification dans l'Est, où la thermocline est peu profonde. Aussi, les flux de flottabilité associés au mélange non local dans la couche de mélange qui est activé lorsque les flux non solaires sont plus important que le flux solaire qui pénètre dans la couche de surface et auraient ainsi tendance à déstabiliser localement le fluide (Large et al., 1994). Les simulations numériques sont utiles pour la compréhension de ces processus. Au cours de cette thèse, une configuration du Pacifique équatorial (15ºS-15ºN) à partir du modèle régional ROMS (Regional Oceanic Model System) a été mise en place (voir Annexe B), dans le but de réaliser une analyse du budget de chaleur de la couche de surface. C'est une perspective pour les travaux futurs. En outre, le modèle peut être couplé à un modèle atmosphérique

régional pour étudier dans quelle mesure il peut y avoir une rétroaction positive air-mer associée aux processus de mélange. Il est à noter que les ondes ISKws pourraient être couplées à la circulation atmosphérique de surface pendant les pic d'activité de la MJO (Madden-Julian Oscillation (Hendon et al., 1998; Roundy et Kravitz, 2009). C'est un processus qui ne peut pas être diagnostiqué à partir de simulations forcées, et par conséquent un modèle couplé océan-atmosphère serait un outil idéal pour aborder cette question. Un tel modèle pourrait également être très utile pour la prévision saisonnière à l'échelle du bassin et à l'échelle régionale (le long de la côte péruvienne) et servir comme système de prévision saisonnière pour le Pérou.

Cette thèse appelle également à une meilleure compréhension des mécanismes liés à la propagation des ondes ISKws le long de la côte Sud-Américaine et à étudier comment ces dernières modifient la circulation océanique régionale et de SST. Une étude récente a suggéré que l'impact de l'onde ISKw était faible sur la variabilité de la SST le long de la côte du Pérou, bien que l'onde ISKw se propage efficacement le long de la thermocline (Illig et al., 2014). Bien que cette étude soit propre à la période 2000-2008, elle met en évidence le rôle probable de la stratification locale sur les caractéristiques de la téléconnection océanique le long des côtes du Pérou. Une plate-forme d'observation au large du Pérou pourrait être mise en place pour étudier cela, et l'auteur de cette thèse est désireux de contribuer à cet effort dans un contexte national et international favorable (Takahashi et al., 2014).

Au moment où cette thèse a été écrite, un événement chaud s'est développé le long de la côte péruvienne en 2014 (Voir **Figure 5.1**). Cet événement chaud a de nouveau mis au défit notre savoir sur le phénomène El Niño, car il ne s'est pas développé comme prévu: On attendait un événement El Niño aussi fort que l'événement El Niño de 1997/98, mais il disparu à l'échelle du bassin (Menkes et al., 2014). Néanmoins, cet événement a été important pour le Pérou, avec des anomalies chaudes le long de la côte. Un tel événement demeure inexpliqué[2] et il est susceptible de mobiliser la communauté ENSO pour quelques années afin de proposer un mécanisme qui explique pourquoi cet événement s'est affaibli au moment où les scientifiques spécialistes d'ENSO pensaient que les conditions allaient conduire à un fort événement

[2] Dr. Mike McPhaden présente un poster à l'EGU 2015 intitulé "Who Killed the Big 2014-15 El Niño?"

de type Pacifique Est. A nouveau, vers le 9 Mars 2015, un énorme signal MJO a été suivi par des anomalies de tension du vent de surface qui théoriquement vont forcer d'intense ondes ISKws de downwelling (Voir **Figure 5.1**). La communauté ENSO est à nouveau dans l'attente de savoir comment cet événement va se développer.

A partir du travail présenté dans cette thèse, son auteur est disposé à participer à un tel effort dans les années à venir. Puisque les processus énoncés précédemment, qui peuvent conduire à l'amplification ou à l'érosion du contraste zonal de la stratification (et donc à la dissipation des ondes ISKws dans le Pacifique Est) n'ont pas encore été étudiés, il y a encore beaucoup de travail à faire. Cela devrait guider la recherche de l'auteur dans les prochaines années à l'*Instituto Geofísico del Perú* (IGP) dont une des missions est l'étude et la prévision du phénomène El Niño.

Appendix A: Supplementary material for Chapter 4

This appendix contains complementary material to verify that the changes in the seasonality of the wind stress forcing, sea level and zonal currents from before and after 2000 are consistent among products. Statistical tests are performed to estimate the significance of the changes (Figure A.2 – A.6). Different data sets are used: TAO, NCEP-DOE Reanalysis, ERA-Interim Reanalysis and GODAS Reanalysis. The oceanic products (GODAS Reanalysis) help in the interpretation of the observed changes along the equatorial Pacific.

To derive statistical significance of the difference between climatology in P1 and P2 the following methodology is followed:

To reach a formal Climatological Monthly Mean (CMM), each variable is processed to obtain confidence interval (90%) for each month. For this, an analysis of Student t-distribution is implemented assuming that each year is independent. As a consequence the following equation is used to estimate the interval of confidence of the real mean (μ):

$$\mu = \bar{x} \pm \zeta \tag{A.1}$$

where $\bar{x}$ is the mean of each month in each time series (P1 or P2) and ζ is expressed as:

$$\zeta = t_{0.05} \frac{s}{\sqrt{N-1}} \tag{A.2}$$

with s as a standard deviation, N the number of samples (number of years, with the exclusion of TAO data, where N means the available monthly information) and $t_{0.05}$ is the value of t statistic for which only 0.05 (5 %) of the values of t would be expected to be greater.

After that, a statistical test for Difference of Mean is used to get the significance difference between CMM 1988-1996 and CMM 2000-2009 from many datasets.

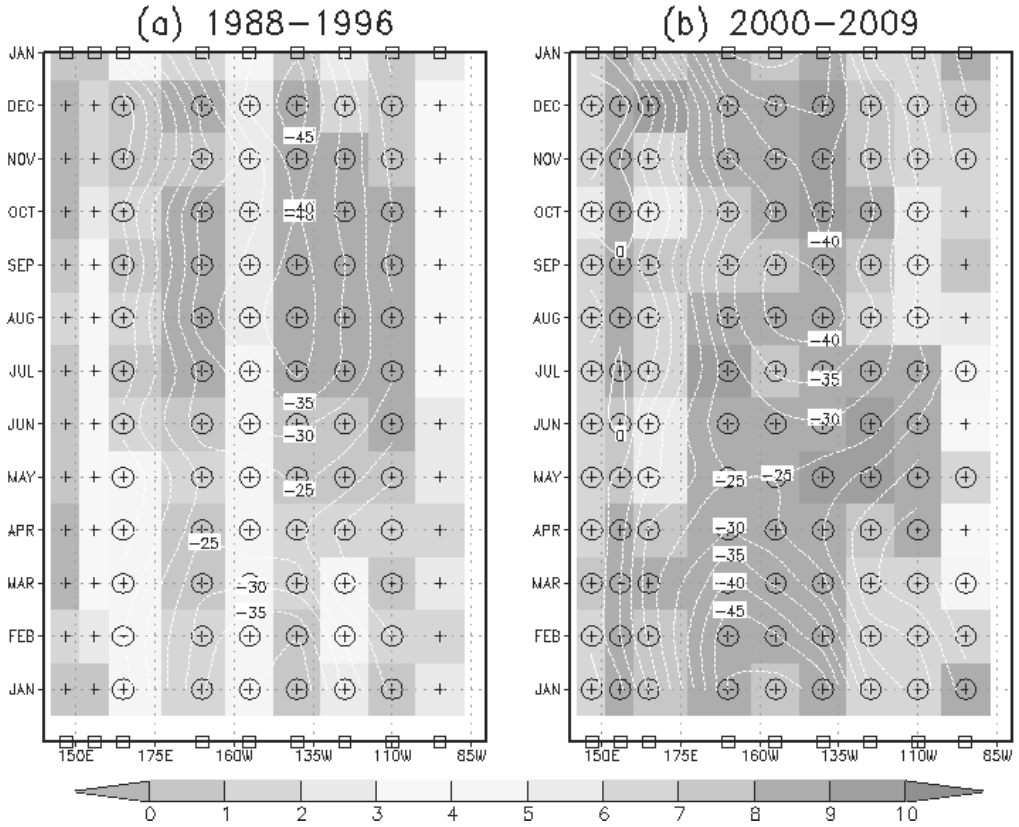

Figure A.1 Number of data (in colour) for each month to calculate the Climate Monthly Mean (CMM) from TAO's pseudostress (m^2 s^{-2}). (a) And (b) indicate the period 1988-1996 and 2000-2009, respectively. Crosses are the position for each mooring buoys and circles around them display that there is enough information to calculate the CMM. White contours display the CMM.

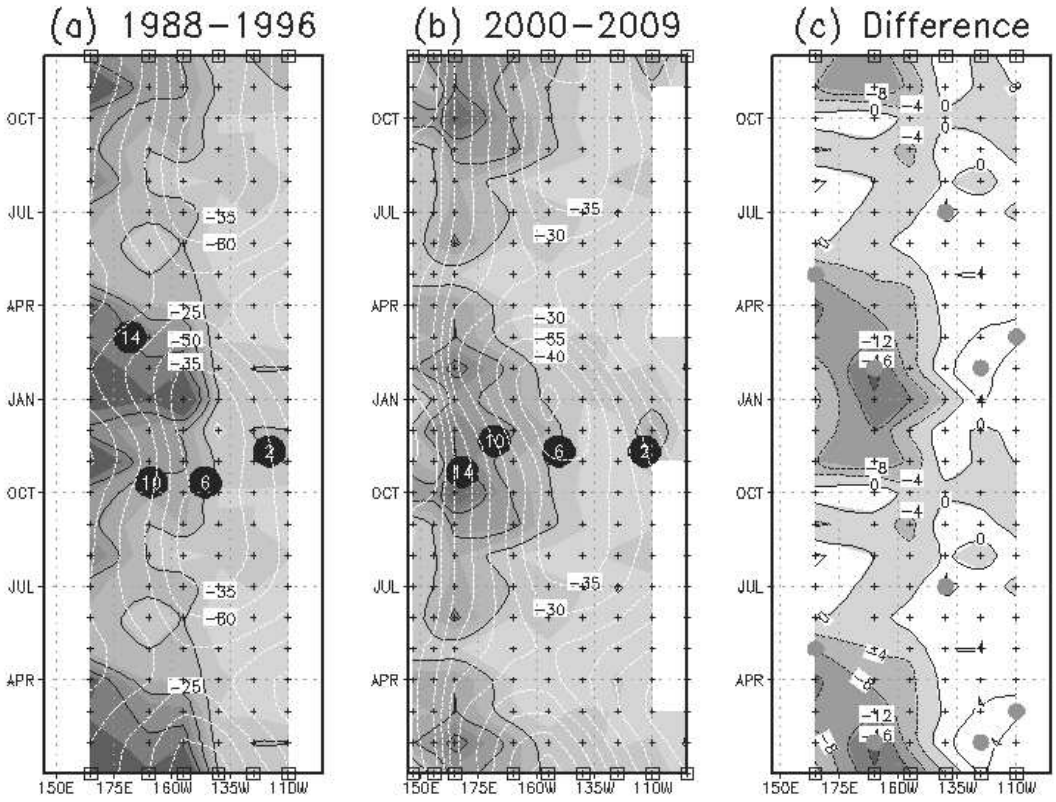

Figure A.2 Pseudo-stress (m^2 s^{-2}) analysis from TAO data along the equator where mooring buoys location are marked with open squares on the x-axis, and crosses along the figures. (a) and (b) show the climatologic pseudo-stress (m^2 s^{-2}) for the period 1988-1996 and 2000-2009, respectively. In both panels, white lines are the climatologic variability, expressed in two years, and black contours and gray scales are the ζ parameter of equation (A.2), that means the (+/-) 90% confidence limit. (c) Is the difference (in gray scale an black contours) between both climatologic wind stress, whereas red fill circles indicate the points where the significance difference are important in 90% after a Student's t-distribution test.

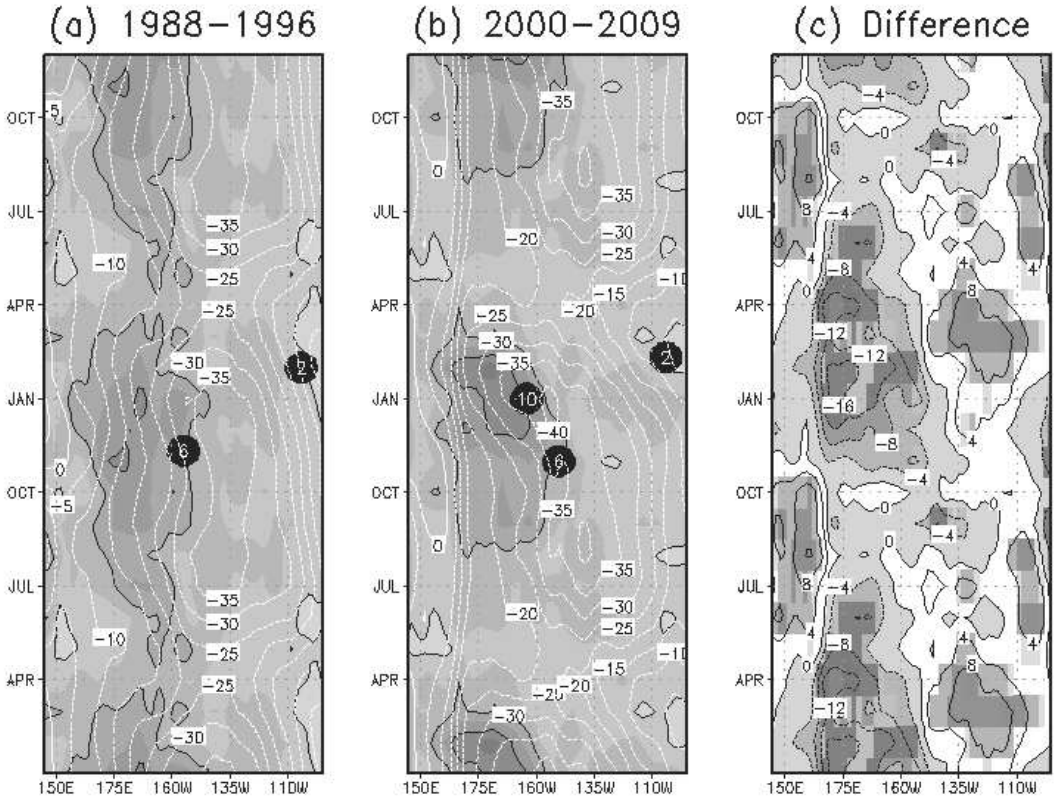

Figure A.3 As in Figure A.2 but for pseudo-stress from the NCEP-DOE reanalysis. Colors in (c) indicate where the differences are significant.

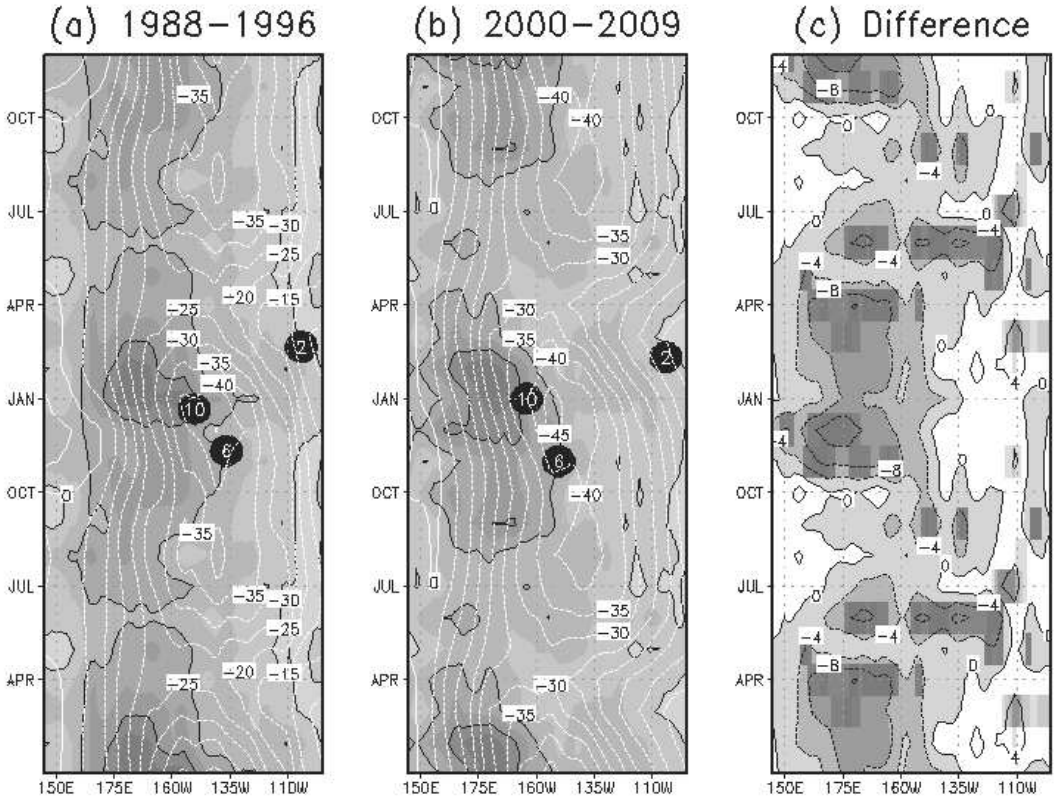

Figure A.4 As in Figure A.2 but for pseudostress from the ERA-Interim reanalysis. Colors in (c) indicate where the differences are significant.

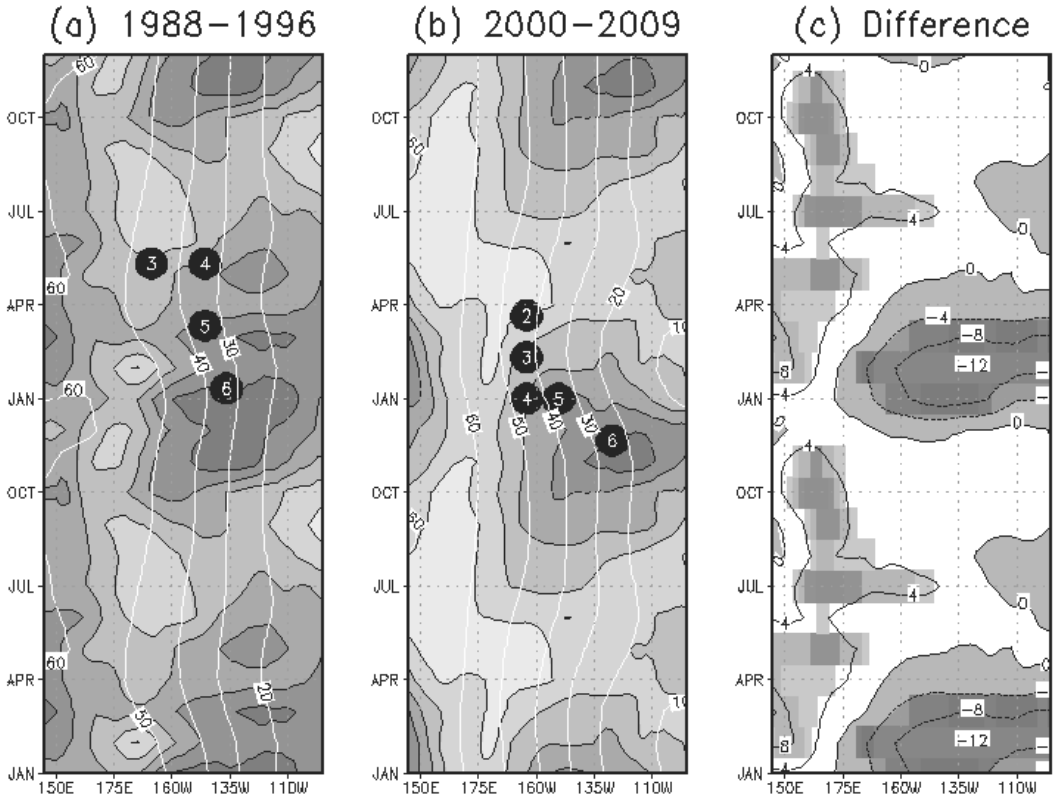

Figure A.5 As in Figure A.2 but for the sea level (cm) from GODAS. Colors in (c) indicate where the differences are significant.

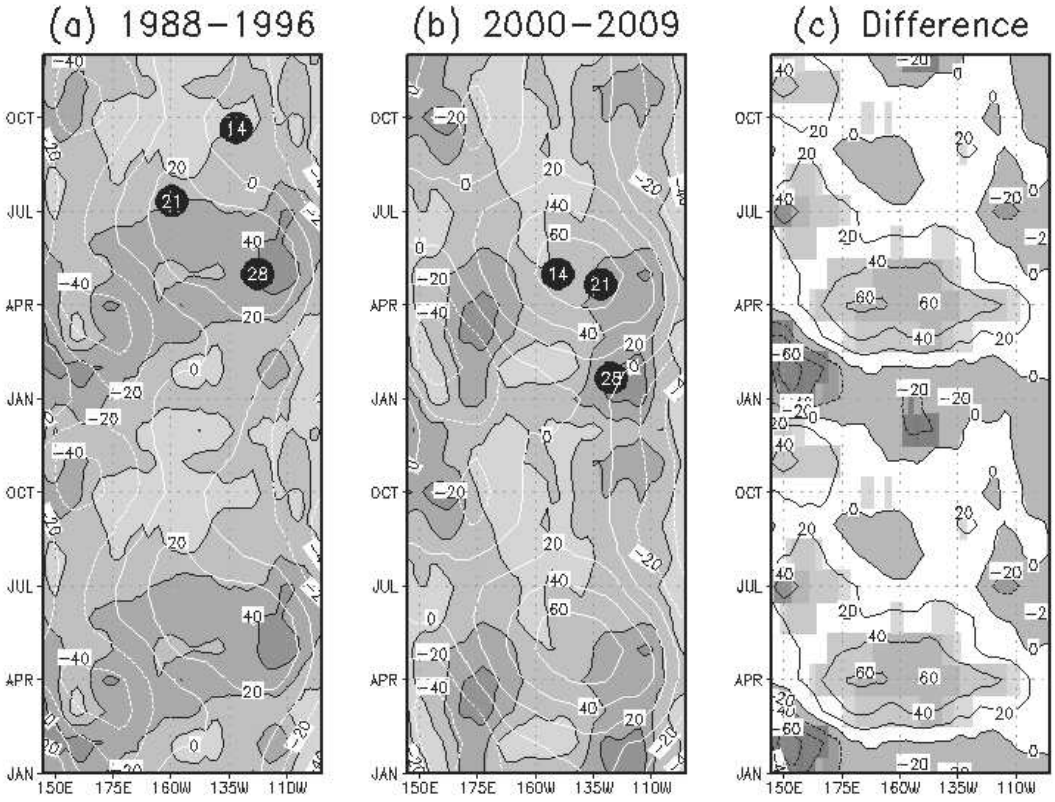

Figure A.6 As in Figure A.2 but for the zonal currents (cm s^{-1}) from GODAS. Colors in (c) indicate where the differences are significant.

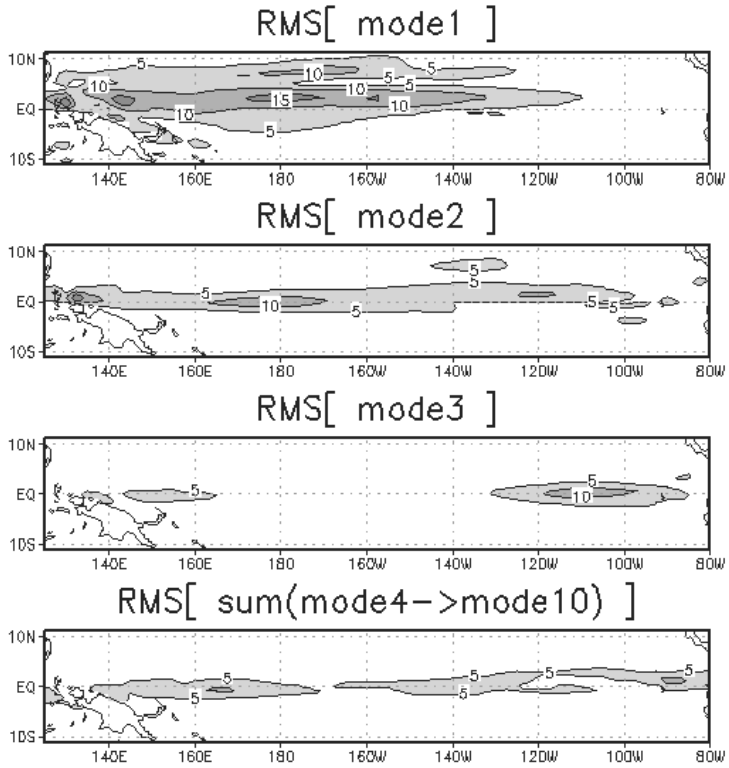

Figure A.7 RMS of the baroclinic mode contribution to the climatological zonal currents (ZC) from GODAS for P1: (a) mode 1, (b) mode 2, (c) mode 3 and (d) summed-up modes 4 to 10. The first three baroclinic modes accounts for the equatorial wave dynamics, while the sum of the higher-order modes accounts for the Ekman layer dynamics. In (a) the highest variability of the ZC is located in the central western Pacific with a maximum value of 15 m s^{-1} around the dateline and to the north of the equatorial line. The peak variability of the second mode (b) is found around the dateline with a value of 10 m s^{-1}. On the other hand, the third mode variability peaks in the eastern Pacific.

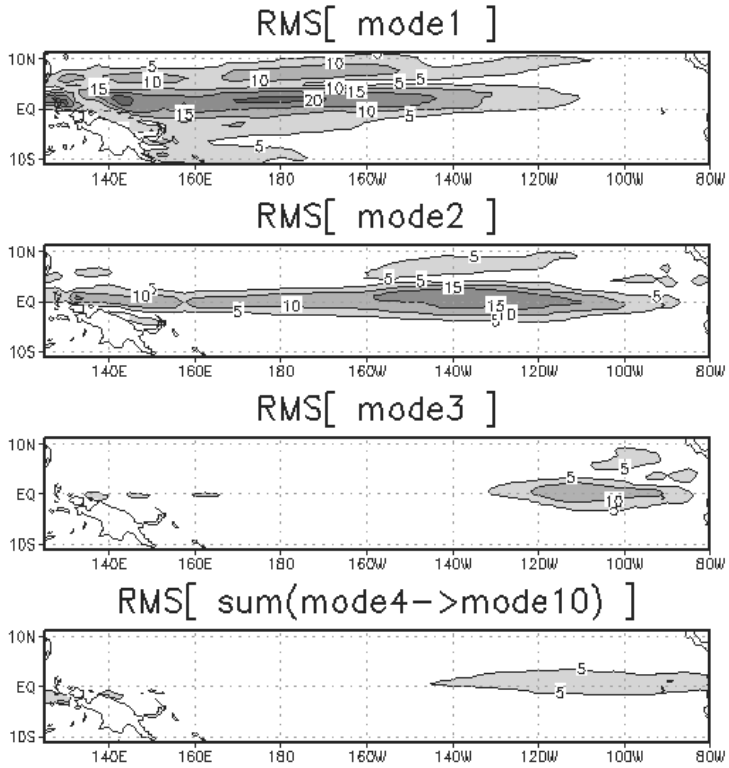

Figure A.8 This figure is similar to Figure A.7 but for P2. Compare to P2, we observe an eastward shift of the variability for the second baroclinic mode.

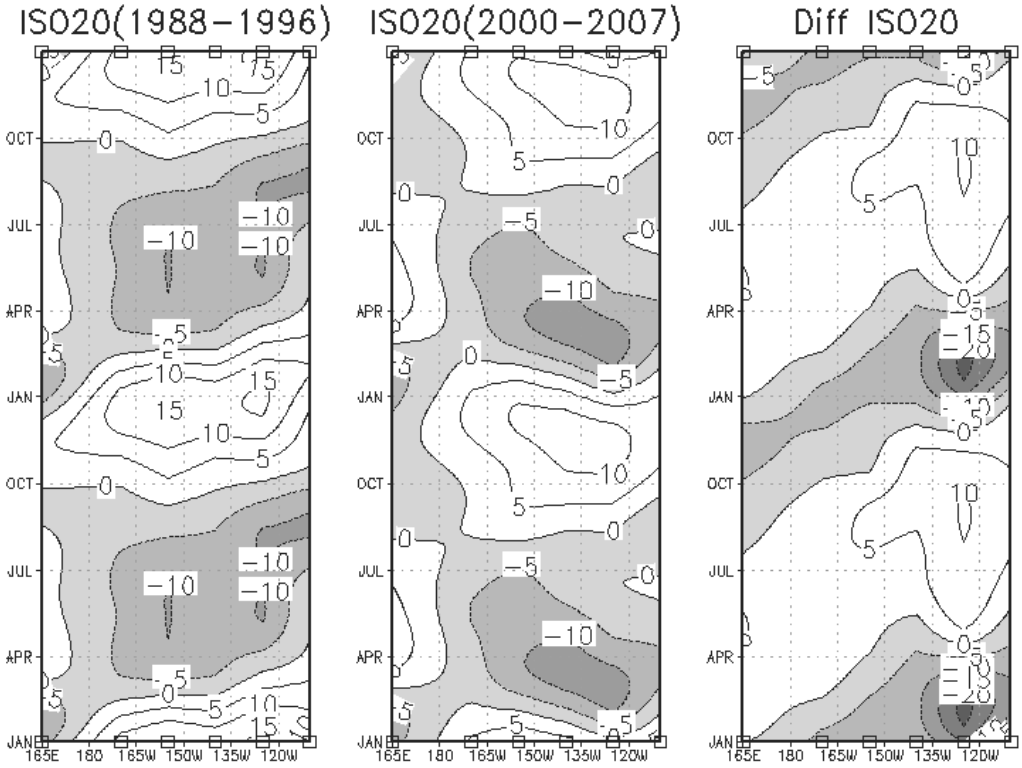

Figure A.9 Seasonal variability of the 20°C isotherm depth (meters) for P1 (a) and P2 (b), and for the difference between P2 and P1 (c). In this figure the position of each mooring buoys is represented by an open square located in the upper and lower axis of each graphics. Negative values (gray scale) indicate an elevation and positive values indicate a shallowing of the thermocline.

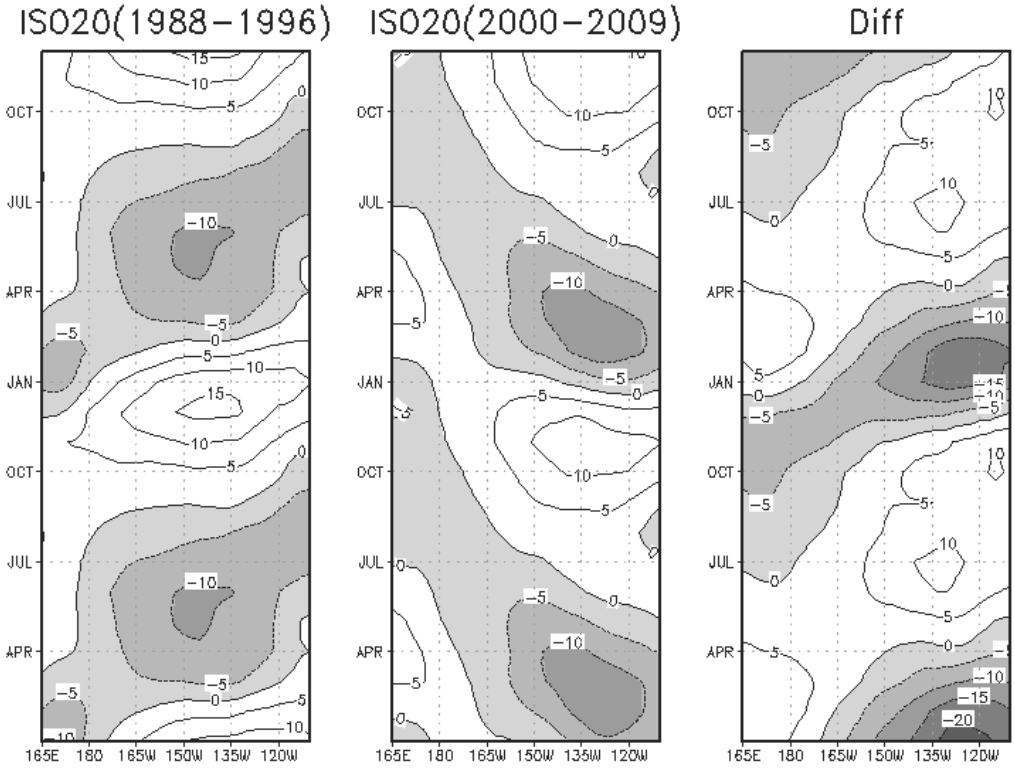

Figure A.10 Similar to Figure A.9, but for GODAS.

Appendix B: Numerical simulation with the Regional Ocean Model System (ROMS) over the period 2000-2010.

B.1 Overview

This Appendix describes the efforts done in the implementation of an OGCM (ROMS) over the equatorial Pacific (15°S and 15°N) and its validation. The model is aimed at providing a tool for sensitivity experiments to wind forcing and stratification characteristics. It could also be used for the operational forecast of the equatorial Kelvin wave, something that already exist based on a linear model at IGP. The model uses boundary and initial conditions from SODA and forcing from ERA-I. Twelve experiments were performed with the main objective to represent correctly the mean thermocline depth. Basically, the increase of vertical levels in the upper ocean, opened and closed boundaries in the western Pacific and increase of intensity of mean zonal winds were tested. As mentioned above this configuration will be useful for research, in particular for diagnostic the thermodynamic and dynamic of the equatorial Pacific during El Niño events, with emphasis on the far eastern Pacific. This tool shall also contribute to the monthly analysis of the ENFEN (*Estudio Nacional del Fenómeno El Niño*) Technical Committee in Perú (www.imarpe.gob.pe), governmental entity in charge of the diagnosis and prediction of El Niño in base of international and national information (data in situ and numerical models).

B.2 Data

The information used in this work covers the period 2000-2008 and each calculation is based 5-day averaged outputs (pentads). The mean state is determined by the mean of the original time series; the seasonal variability is defined as a multi-annual monthly mean obtained from the result of the original time series minus the mean state; and, finally, the interannual time series is calculated by subtracting the sum of the mean state and seasonal variability to the original time series.

In this appendix, daily *in situ* data (temperature and zonal currents) along the equatorial Pacific, obtained from the Tropical Atmospheric and Oceanic Project (TAO),

is used for validating the model configuration. For temperature, ten mooring buoys (147ºE, 156ºC,165ºC, 180º, 170ºW, 155ºW, 140ºW, 125ºW, 110ºW and 95ºW) are selected and for ADCP (Acoustic Doppler Current Profiler) only five are used (147ºE, 165ªE, 170ºW, 140ªW and 110ºW).

Daily sea surface temperature, estimated by the Tropical Rainfall Measuring Mission (TRMM) Microwave Imager (TMI, Wentz et al., 2000) was obtained from the Remote Sensing System's home page (http://www.ssmi.com/). The most important characteristic of this instrument is the ability to estimate the SST, even in the presence of clouds. Only the data along the equator are used for the validation.

The outputs from ORCA0.25_LIM that was provided by the MERCATOR project (a French consortium: IRD, CNES, CNRS, IFREMER, SHOM, the Meo-France weather service) is also used for compairson purpose. The ORCA0.25_LIM configuration uses the oceanic model named OPA 8.1 (*Océan PArallélisé*) developed by Madec et al (1998) at the *Laboratoire d'Océanographie DYnamique et de Climatologie* (LODYC). The horizontal resolution is 0.25° and there is 31 vertical levels. Details of this MERCATOR configuration is described in Garric et al. (2008). The simulation was also used in the paper presented in Chapter 2.

The version 2.1.6 of the Simple Ocean Data Assimilation (SODA) product is used in this work. This product used the ocean model POP 2.1 (Parallel Ocean Program, Smith et al., (1992)) that was forced by European Center for Medium Range Weather Forecasts ERA-40 reanalysis and QSCAT for the period 1958-2008 and assimilated information of temperature and salinity from the World Ocean Database 2009 (WOD09). Temperature and zonal currents, every five days, are used in ROMS as initial and boundary conditions for the experiments. The SODA data are also used for the comparison between the different products. Details of the characteristic of this model can be found in Carton et al. (2000) and Carton and Giese (2008).

B.3 The Regional Oceanic Model System (ROMS) and the tropical Pacific configurations

The Regional Ocean Modelling System (ROMS; Shchepetkin and McWilliams, 2005) solves the hydrostatic primitive equations with a free-surface explicit scheme, and stretched, terrain-following sigma coordinates. Subgrid-scale vertical mixing is parameterized using the KPP boundary layer scheme (Large et al., 1994). Bathymetry from ETOPO has been interpolated on to the model grid, smoothed as in Penven et al. (2005) in order to reduce pressure gradient errors and modified at the open boundaries to match with bottom topography from the boundary forcing of the SODA outputs. The horizontal resolution is 1/4 degree.

Two groups of experiments are considered: Group 1 which considers changes in the model domain, the number of vertical levels and the climatological wind speed to force the model; and Group 2 that gather sensitivity experiments to ocean boundary forcing (i.e. climatological boundary conditions or interannual boundary conditions) and the boundary conditions at the western boundary (i.e. with and without a closed western boundary). The experiments in each group are denominated TROP_PAC (TP) plus the number of the experiment (for example, experiment 7 is TP07). The Tables B.1 and B.2 summarizes the characteristics of each experiments.

B.3.1 Group 1

This set of experiments is aimed at assessing the sensitivity to the vertical resolution of the model. 32 to 54 sigma layers are consisdered. Two positions of the western boundary are also tested: 170° and 135°E; the existence or not of the Galápagos islands; and finally a change, by a factor 1.1, of the zonal wind speed are tested in order to improve the realism of the thermocline slope. In total eight experiments of 13 years (3 years of spin up repeating the year 2000 three times and 9 years corresponding to the 2000-2008 period) each were done (see **Table B.1**).

Mean State

The best experiment in Group 1 is TP07, which has 54 vertical levels, with a domain having the zonal (meridional) extension between 135°E to 70°W (15°S to 15°N). Additionally, the Galapagos Islands are included although there is not much influence of this topographical aspect. In TP08 (that is similar to TP07), the intensity of

the wind forcing is increased in 1.1, which was implemented after a comparative analysis of the 20°C isotherm depth between TP07 and TAO in order to improve the thermocline depth. The results indicate that the TP08 is the most skillful in simulating the caracteristics of the mean thermocline (depth and "strength") However, the 24°C isotherm depth in the Eastern Pacific is too close to the surface, inducing a cool bias in the model. Due to this cool bias, the TP07 configuration is favored for the addition tests.

Table B.1 Experiments from Group 1

Experiments	Zonal extension	Vertical levels	Zonal wind speed (ERAI)	Period
TROP_PAC01	135°E to 70°W	32	U,V	2000-2001
TROP_PAC02	135°E to 70°W	32	U,V	2000-2001
TROP_PAC03	135°E to 70°W	32	U,V	2000-2001
TROP_PAC04	170°E to 70°W	54	U,V	2000-2001
TROP_PAC07	135°E to 70°W	54	U,V	2000-2001
TROP_PAC08	135°E to 70°W	54	1.1*U,V	2000-2001

The mean thermocline depth of the different simulations of Group 1 is presented in **Figure B.1**, which indicates that the zonal structure of the thermocline (including its the vertical gradient with the thermocline, see 16, 20 and 24°C isotherms) simulated by TP07 is realistic (TAO data in black line). TP07 has a best representation of the 16°C isotherm depth compared to MERCATOR, which simulates a too warm state at such depth. The difference between products is further illustrated by the **Figure B.1b** that shows, for the four products, the difference between 20°C isotherm depth and 16°C isotherm depth (negative values) and between 20°C isotherm depth and 24°C isotherm depth (positive values). It is clear from Figure B.1b that MERCATOR has the largest bias with the products, whereas TP07 is comparable to SODA. **Figure B.1c**, that displays the difference between 16 and 24°C isotherm depth, diagnoses the realism of the vertical stratification along the equator that is a key parameter for the wave dynamics. The results indicates that TP07 has a slightly too diffuse thermocline in the

central and eastern Pacific. Despite such bias, it is rather realistic, close to what is obtained from SODA.

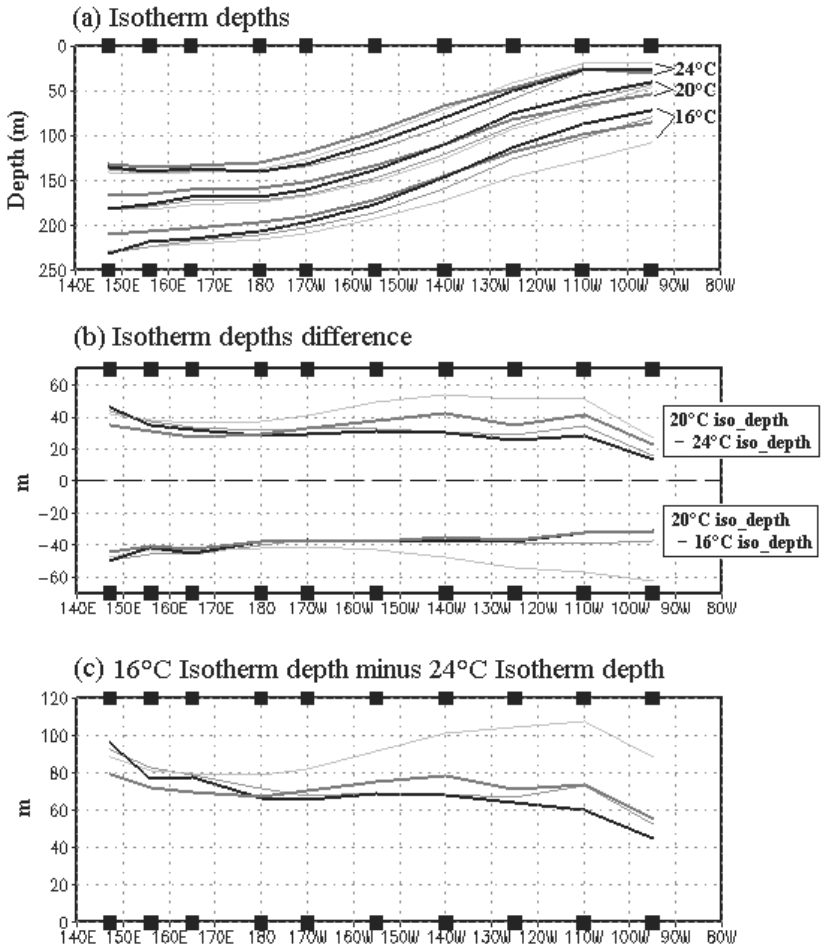

Figure B.1 Isotherms depths (ISOd) for TAO (black thick line), TP07 (blue thick line), SODA (red line) and MERCATOR (green line) products. (a) Mean state of ISOd for 16°C, 20°C and 24°C for each product. (b) Difference between ISOd: lines over zero level are the difference between 20°C ISOd and 24°C ISOd, on the other hand, lines under zero level are the difference between 20°C ISOd and 16°C ISOd for each product. Finally, (c) difference between 16°C ISOd and 24°C ISOd.

Regarding SST, (upper panel of **Figure B.2**), TP07 is, in general, around -0.7°C cooler than TMI with a reduce error in the far eastern pacific (blue dashed line). The agreement in terms of SST for TP07 is close to the MERCATOR product (green dashed line) but still not as good as SODA (red dashed line). It is important to mention that, in detail, the SODA product underestimates (overestimates) the mean SST in the western and eastern (central) Pacific by around -0.3 (0.3) °C.

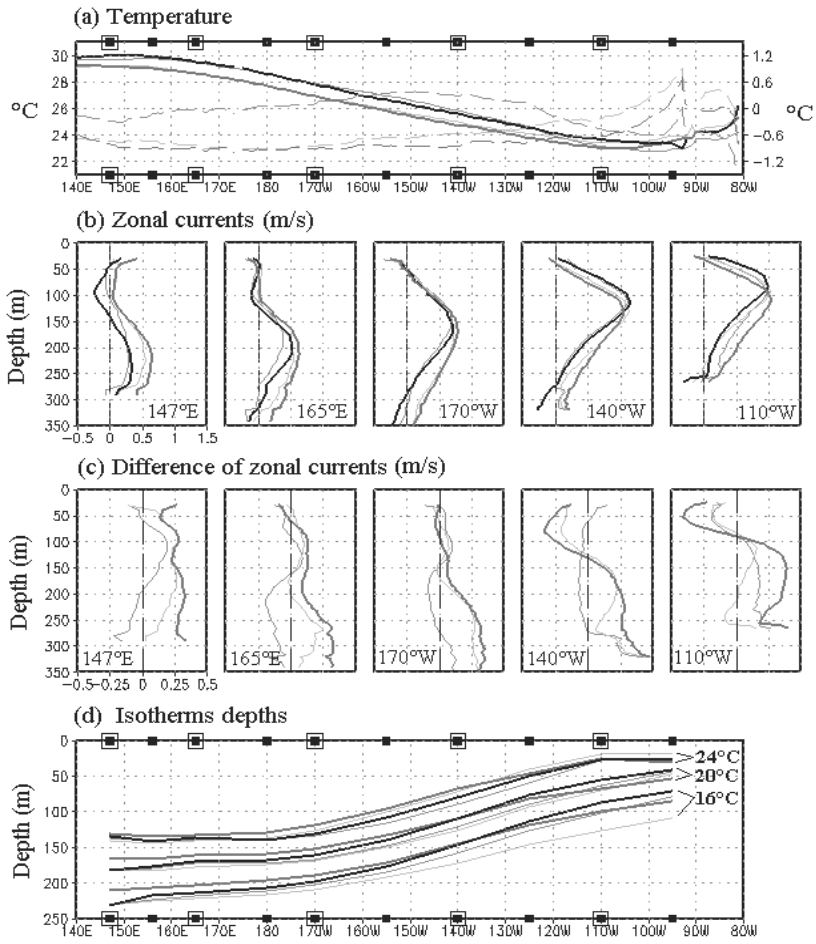

Figure B.2 Mean state of sea surface temperature (SST) and zonal currents (ZC) along the equatorial Pacific line. At the top (a) the SST is plotted for TMI (black line), TP07 (blue line), SODA (red line) and MERCATOR (green line). In the same panel, three difference of the SST: between TP07 and TMI (blue dashed line), SODA and TMI (red dashed line) and, finally, MERCATOR and TMI (green dashed line). The axis of this product is on the right. In the middle (b), five panels, that represent five position along the equatorial line, display the mean state of ZC for TAO (dark line), TP07 (blue line), SODA (red line) and MERCATOR (green line). The vertical dashed line represents the position for ZC equal zero. At the end of the figure, the five panels on the bottom show the difference of ZC: TP07-TAO (blue line), SODA-TAO (red line) and MERCATOR-TAO (red line).

Regarding zonal currents along the equator (see the five panels of the second and third rows in **Figure B.2**), TP07 is quite realistic, although the core of the Equatorial

Undercurrent (EUC) is deeper than in TAO (black line), MERCATOR (green line) and SODA (red line), especially at 140°W and 110°W and in the western Pacific edge (147ºE) the TP07 simulation has an eastward position. The five panels in the third row display the difference between TAO and each product. Despite the fact that TP07 has the poorest agreement with observation in the eastern Pacific, its skills in simulation the vertical structure of the zonal current along the equator is comparable to MERCATOR and SODA in the upper 150 m.

Interannual variability

The interannual SST anomaly from TP07 is compared to TMI . The results are provided in **Figure B.3** in which the upper panels indicate the statistical results of the validation and the two Hövmuller diagrams are for TMI (left) and TP07 (right). The correlation between TP07 and TMI (black thick line) is better than between MERCATOR and TMI (blue thick line) but still below the one between SODA and TMI (red thick line). As MERCATOR and SODA, the maximum correlation (around 0.83) is located between 170°E and 160°W and decreases eastward and westward with a minimum value of 0.5. TP07 exhibits a little less variability than TAO in the Eastern Pacific, which leads to a larger RMS difference than the other products there. These statistics are indicative that TP07 simulates realistically the sequence of warm and cool events over the period 2000-2008, as illustrated by the **Figure B.3**.

The Sea Level Height (SLH) was also analyzed: TP07 and TPJ has a correlation of around 0.8 along the equator (**Figure B.4**). The RMS in both products has similar distribution with a maximum in the Central Pacific. On the other hand, the RMS difference has a maximum in the Easter Pacific (~6 cm) and a minimum around 160°E (~0.4). This results are quite similar than other OGCMs.

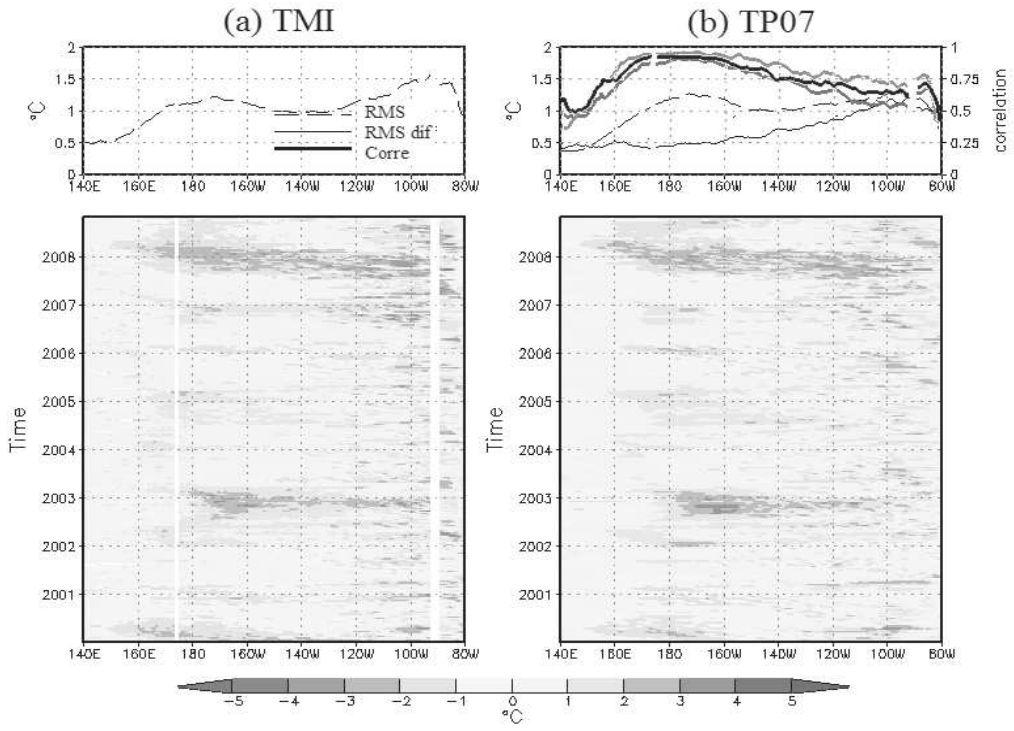

Figure B.3 Statistical results of the interannual SST (2000-2008) validation between TMI and TP07 are plotted in the upper panels. The Root Mean Square (RMS) is represented with a dashed line in both products (a) and (b), correlation is plotted in the upper top panel with thick black line and RMS difference is represented by a thin black line in the upper right panel. The thick blue (red) line represents the correlation between TMI product and MERCATOR (SODA). Longitude vs Time diagrams of the SST anomaly from TMI (left) and TP07 (right) is displayed in the bottom two panels, respectively.

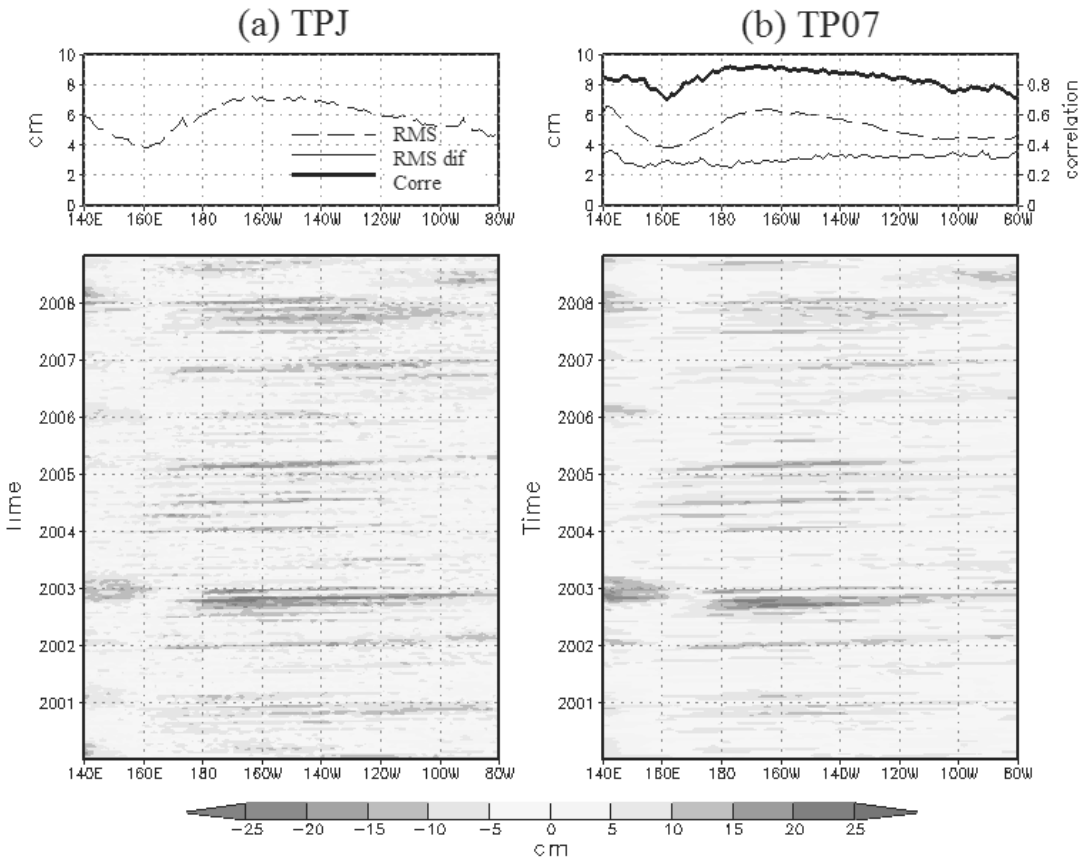

Figure B.4 Similar than Figure B.3, but for SSH

B.3.2 Group 2

The Group 2 builds upon the results obtained from Group 1 and is aimed at testing the sensitivity to the boundary conditions. Climatological conditions for temperature and currents from SODA are used in the Northern, Southern and Western boundary. Additionally, in some experiments a closed western boundary was used. This configuration would allow using the model in operational mode using only available atmospheric fluxes. However there would be limitations associated to the possible change of the oceanic circulation near the boundaries at low freqeuncy timescales. . A summary of the characteristics of these experiments is provided in **Table B.2**.

The results of these simulations indicate that, over the period of interest (2000-2008) there is hardly no difference between TP07 and the experiments of Group 2. This can be interpreted by the fact that the 2000-2008 period experiences only CP El Niño events for which the contribution of the reflected Rossby wave at the western boundary

is weak. The influence of the circulation at the meridional boundary is also weak in the equatorial band over such a short period of time, which is expected.

Table B.2 Experiments of Group 2

Experiment	**Period**	**Atmospheric forcing (ERAI)**	**Oceanic boundary conditions (SODA)**
TROP_PAC09	2000-2008	4-day fluxes	5-day SODA Clim. (N-S-W)
TROP_PAC10	2000-2008	4-day fluxes	5-day SODA Clim. (N-S)
TROP_PAC11	2000-2011	Daily fluxes	5-day SODA Clim. (N-S)

References

An, S.-I., and F.-F. Jin, 2001: Collective Role of Thermocline and Zonal Advective Feedbacks in the ENSO Mode, Journal of Climate, 14, 3421- 3432.

Ashok, K., S. K. Behera, S. A. Rao, H. Weng, and T. Yamagata, 2007: El Niño Modoki and its possible teleconnection, J. Geophys. Res., 112, C11007, doi: 10.1029/2006JC003798.

Bertrand S., B. Dewitte, J. Tam, A. Bertrand and E. Diaz, 2008: Impact of Kelvin wave forcing in the Peru Humboldt Current system: Scenarios of spatial reorganization from physics to fishers. Prog. Oceanogr., 79, 278-289.

Barber, R.T., Chavez, F.P., 1983. Biological consequences of El Niño. Science 222, 1203–1210.

Battisti, D.S. and A.C. Hirst, 1989: Interannual Variability in the Tropical Atmosphere-Ocean System: Influences of the Basic State, Ocean Geometry and Nonlinearity, Journal of Atmospheric Sciences, 46, 1687-1712.

Bergman, J. W., H. H. Hendon, and K. M. Weickmann, 2001: Intraseasonal Air-Sea Interactions at the onset of El Niño, J. Clim., 14, 1702–1719.

Bjerknes, J., 1969: Atmospheric teleconnections from the equatorial Pacific, Mon. Wea. Rev., 97 (3), 163-172.

Boulanger, J.-P. and C. Menkes, 1995: Propagation and reflection of long equatorial waves in the Pacific Ocean during the 1992– 1993 El Niño. J. Geophys. Res., 100, 25 041–25 059.

Boulanger, J.-P. and L.-L. Fu, 1996: Evidence of boundary reflection of Kelvin and first-mode Rossby waves from TOPEX/Poseidon sea level data. J. Geophys. Res., 101, 16 361–16 371.

Busalacchi, A. J., and M. A. Cane, 1988: The effect of varying stratification on low-frequency equatorial motions. J. Phys. Ocean- ogr., 18, 801–812.

Capotondi, A., et al., 2014: Understanding ENSO diversity, Bull. Amer. Met. Soc., in press.

Carranza, L., 1891: Contra-corriente marítima, observada en Paita y Pacasmayo, Bol. Soc. Geogr. Lima, 1 (9), 344-345.

Carrillo, C. N., 1892: Hidrografía oceánica, Bol. Soc. Geogr. Lima, 2, 72-110.

Chiodi, A. M. and D. E. Harrison, 2015: Equatorial Pacific Easterly Wind Surges and the Onset of La Niña Events, Journal of Climate, doi: 10.1175/JCLI-D-14-00227.1

Choi, J., S.-I. An, J.-S. Kug, and S.-W. Yeh, 2011: The role of mean state on changes in El Niño's flavor, Clim. Dyn., 37, 1205–1215, doi:10.1007/s00382-010-0912-1.

Choi, J., S.-I. An, and S.-W. Yeh, 2012: Decadal amplitude modulation of two types of ENSO and its relation ship with the mean state. Climate Dynamics, 38, 2631-2644.

Clarke, A. J., 2010: Analytical theory for the quasi-steady and low frequency equatorial ocean response to wind forcing: The ''tilt'' and ''warm water volume'' modes Journal of Physical Oceanography, 40, 121–137, doi:10.1175/2009JPO4263.1.

Clarke, A. J., 2008: An Introduction to the Dynamics of El Niño and the Southern Oscillation. Academic Press, 308 pp.

Clarke, A. J., and C. Shi, 1991: Critical frequencies at ocean boundaries, J. Geophys. Res., 96, 10,731–10,738, doi:10.1029/91JC00933.

Cravatte, S., J. Picaut, and G. Eldin, 2003: Second and first baroclinic Kelvin modes in the equatorial Pacific at intraseasonal timescales, Journal of Geophysical Research-Oceans, 108(C8).

Cushman, G., 2004: Enclave Vision: Foreign Networks in Peru and the Internationalization of El Niño Research during the 1920s, History of Meteorology, 1, 1, 65-74.

Dewitte B., J. Vazquez-Cuervo, K. Goubanova, S. Illig, K. Takahashi, G. Cambon, S. Purca, D. Correa, D. Gutierrez, A. Sifeddine and L. Ortlieb, 2012: Change in El Niño flavours over 1958-2008: Implications for the long-term trend of the upwelling off Peru, Deep Sea Research II, doi:10.1016/j.dsr2.2012.04.011.

Dewitte B., D. Gushchina, Y. duPenhoat and S. Lakeev, 2002: On the importance of subsurface variability for ENSO simulation and prediction with intermediate coupled models of the Tropical Pacific: A case study for the 1997-1998 El Niño. Geoph. Res. Lett., vol. 29, no. 14, 1666, 10.1029/2001GL014452.

Dewitte B., S. Illig, L. Parent, Y. duPenhoat, L. Gourdeau and J. Verron, 2003: Tropical Pacific baroclinic mode contribution and associated long waves for the 1994-1999 period from an assimilation experiment with altimetric data, J. Geophys. Res., 108 (C4), 3121-3138.

Dewitte B., G. Reverdin and C. Maes, 1999: Vertical structure of an OGCM simulation of the equatorial Pacific Ocean in 1985-1994, J. Phys. Oceanogr., 29, 1542-1570.

Dewitte B., S. Purca, S. Illig, L. Renault and B. Giese, 2008: Low frequency modulation of the intraseasonal equatorial Kelvin wave activity in the Pacific ocean from SODA: 1958-2001, J. Clim., 21, 6060-6069.

Dewitte, B., K. Takahashi y K. Mosquera, 2014: Teorías simples de El Niño-Oscilación Sur: Más allá del Oscilador Carga-Descarga, Boletín Técnico "Generación de modelos climáticos para el pronóstico de la ocurrencia del Fenómeno El Niño", Instituto Geofísico del Perú, August, 1, 8.

Fedorov, A. V., 2010: Ocean response to wind variations, warm wáter volume, and simple models of ENSO in the low frequency approximation, Journal of Climate, 23, 3855–3873, doi:10.1175/2010JCLI3044.1.

Giese, B. S., and D. E. Harrison, 1990: Aspects of the Kelvin wave response to episodic wind forcing. J. Geophys. Res., 95, 7289 – 7312, doi: 10.1029/JC095iC05p07289.

Giese, B. S., 1989: Equatorial oceanic response to forcing on time scales from days to months. NOAA Tech. Memo. ERL PMEL- 87, 104 pp.

Gushchina D. and B. Dewitte, 2012: Intraseasonal tropical atmospheric variability associated to the two flavors of El Niño. Month. Wea. Rev., Vol. 140, N° 11. 3669-3681.

Harrison, D. E., and G. A. Vecchi, 1997: Westerly wind events in the tropical Pacific, 1986–1995, J. Clim., 10, 3131–3156.

Hendon, H. H., M. C. Wheeler, and C. Zhang (2007), Seasonal Dependence of the MJO–ENSO Relationship. J. Climate, 20, 531–543. doi: http://dx.doi.org/10.1175/JCLI4003.1

Hendon, H. H., B. Liebmann, and J. D. Glick, 1998: Oceanic Kelvin waves and the Madden–Julian oscillation. J. Atmos. Sci., 55, 88–101.

Hu, Z.-Z., A. Kumar, B. Jha, W. Wang, B. Huang, and B. Huang, 2012: An analysis of warm pool and cold tongue El Ni~nos: Air-sea coupling processes, global influences, and recent trends, Clim. Dyn., 38(9–10), 2017–2035, doi:10.1007/s00382-011-1224-9.

Illig, S., B. Dewitte, K. Goubanova, G. Cambon, J. Boucharel, F. Monetti, C. Romero, S. Purca, and R. Flores, 2014: Forcing mechanisms of intraseasonal SST variability off Central Peru in 2000–2008, J. Geophys. Res. Oceans, 119, 3548–3573, doi:10.1002/2013JC009779.

Jin, F.-F., 1997: An equatorial ocean recharge paradigm for ENSO. Part I: conceptual model, J Atmos. Sci., 54:811–829.

Kessler, W.S. and R. Kleeman, 2000: Rectification of the Madden-Julian Oscillation into the ENSO cycle, J. Clim., 13:3560-357.

Kim, W., S.-W. Yeh, J.-H. Kim, J.-S. Kug, and M. Kwon, 2011: The unique 2009–2010 El Niño event: A fast phase transition of warm pool El Niño to La Niña, Geophys. Res. Lett., 38, L15809, doi:10.1029/2011GL048521.

Kug, J.-S., F.-F. Jin, and S.-I. An, 2009: Two types of El Niño events: cold tongue El Niño and warm pool El Niño, J. Clim., 22, 1499–1515.

Kug, J.-S., J. Choi, S.-I. An, F.-F. Jin, and A. T. Wittenberg, 2010: Warm Pool and Cold Tongue El Niño events as simulated by the GFDL 2.1 coupled GCM, J. Climate., 23, 1226-1239.

Latif, M., J. Biercamp, and H. von Storch, 1988: The response of a coupled Ocean-Atmosphere General Circulation Model to Wind Bursts, J. Atmos. Sci., 45, 964–976.

Large, W., McWilliams, J., and Doney, S., 1994: Oceanic vertical mising: A review and a model with a nonlocal boundary layer parameterization, Rev. Geophys., 32, 363–403.

Lee T. and M. J. McPhaden, 2010: Increasing intensity of El Niño in the central-equatorial Pacific, Geophys Res Lett 37:L14603. doi:10.1029/2010GL044007.

Legeckis, R., 1977: Long waves in the eastern equatorial Pacific Ocean: A review from a geostationary satellite, Science, 197, 1179–1181, doi:10.1126/science.197.4309.1179.

Lengaigne, M., J.-P. Boulanger, C. Menkes, S. Masson, G. Madec, and P. Delecluse, 2002: Ocean Response to the March 1997 Westerly Wind Event, J. Geophys. Res., 107, 8015, doi:10.1029/2001JC000841.

Lengaigne, M., E. Guilyardi, J. P. Boulanger, C. Menkes, P. Delecluse, P. Inness, J. Cole and J. Slingo, 2004: Triggering of El Niño by westerly wind events in a coupled general circulation model, Clim. Dyn. 23, 601–620.

Luther, D. S., and D. E. Harrison, 1984: Observing Long-Period Fluctuations of Surface Winds in the Tropical Pacific: Initial results from Island Data. Mon. Weather Rev., 112, 285–302.

Luther, D. S., and E. S. Johnson, 1990: Eddy energetics in the upper equatorial Pacific during Hawaii-to-Tahiti ShuttleExperiment. J. Phys. Oceanogr., 20, 913-944.

Madden, R., and P. Julian, 1972: Description of global-scale circulation cells in the tropics with a 40–50 day period, J. Atmos.Sci., 29, 1109–1123.

McCreary, J.P., 1976: Eastern tropical ocean response to changing wind systems: with application to El Niño, Journal of Physical Oceanography, 6, 632–645.

McPhaden, M.J. , A.J. Busalacchi, R. Cheney, J.R. Donguy, K.S. Gage, D. Halpern, M. Ji, P. Julian, G. Meyers, G.T. Mitchum, P.P. Niiler, J. Picaut, R.W. Reynolds, N. Smith, K. Takeuchi, 1998: "The Tropical Ocean-Global Atmosphere (TOGA) observing system: A decade of progress", J. Geophys. Res., 103, 14,169–14,240.

McPhaden, M. J., 2012: A 21st Century Shift in the Relationship between ENSO SST and Warm Water Volume Anomalies, Geophysical Research Letters, 39, L09706, doi: 10.1029/2012GL051826.

McPhaden, M. J., T. Lee, and D. McClurg, 2011: El Niño and its relationship to changing background conditions in the tropical Pacific. Geophys. Res. Lett. 38, L15709, doi:10.1029/2011GL048275.

McPhaden, M. J., X. Zhang, H. H. Hendon, and M. C. Wheeler, 2006: Large scale dynamics and MJO forcing of ENSO variability, Geophys. Res. Lett., 33, L16702, doi:10.1029/2006GL026786.

McPhaden, M. J., 2004: Evolution of the 2002/03 El Niño, Bull. Am. Meteorol. Soc., 85, 677–695.

Meinen, C. S. and M. J. McPhaden, 2000: Observations of Warm Water Volume Changes in the Equatorial Pacific and Their Relationship to El Niño and La Niña. J. Climate, 13, 3551–3559.

Menkes, C., J.-P. Boulanger, and Busalacchi, A. J., 1995a: Evaluation of TOPEX/POSEIDON and TOGA- TAO sea level topographies and their derived geostrophic currents. J. Geophys. Res., Vol. 100, C12, 25087–25099 doi: 10.1029/95JC03026.

Menkes C. and A. J. Busalacchi: 1995b: Contrasting the evolution of the 1986-1989 and 1992-1993 ENSO events. In : Proceedings of the International Scientific Conference on the Tropical Ocean Global Atmosphere (TOGA) Programme : 2-7 April 1995, Melbourne, Australia. Genève : OMM, 1995, (91; 717), p. 48-52. (WCRP (CHE); WMO/TD ; 91; 717). International Scientific Conference on Tropical Ocean Global Atmosphere (TOGA) Programme, Melbourne, 1995/04/02-07.

Menkes C. E., M. Lengaigne, J. Vialard, M. Puy, P. Marchesiello, S. Cravatte, G. Cambon, 2014: About the role of Westerly Wind Events in the possible development of an El Niño in 2014. Geophysical Research Letters, doi: 10.1002/2014GL061186.

Moore, D. W., 1968: Planetary-gravity waves in an equatorial ocean, Ph.D. thesis, Harvard Univ., Cambridge, Mass.

Moore, D. W., and S. G. H. Philander,1977: Modeling of the Tropical Ocean Circulation. In “The Sea,” Vol. 6, pp. 319–361 (Goldberg et al., ed.). Wiley, New York.

Mosquera, K., 2014: Ondas Kelvin oceánicas y un modelo oceánico simple para su diagnóstico y pronóstico, Boletín Técnico "Generación de modelos climáticos para el pronóstico de la ocurrencia del Fenómeno El Niño", Instituto Geofísico del Perú, January, 1, 1, 4-7.

Mosquera, K., 2009: Variabilidad intra-estacional de la Onda de Kelvin Ecuatorial en el Pacífico (2000–2007): Simulación numérica y datos observados, MS thesis, 76 pp., Univ. Nacl. Mayor de San Marcos, Lima, Perú.

Mosquera, K., B. Dewitte y P. Lagos, 2011: Variabilidad Intra-estacional de la onda de Kelvin ecuatorial en el Pacífico (2000-2007): simulación numérica y datos observados. Magistri et Doctores, Revista de la Escuela de Posgrado de la Universidad Nacional Mayor de San Marcos, Lima, Año 5, No9, julio-diciembre de 2010, p. 55.

Mosquera-Vásquez, K., B. Dewitte, S. Illig, K. Takahashi, and G. Garric, 2013: The 2002/03 El Niño: Equatorial wave sequence and their impact on sea surface temperature, J. Geophys. Res., 118, doi:10.1029/2012JC008551.

Mosquera-Vásquez, K., B. Dewitte and S. Illig, 2014: The Central Pacific El Niño Intraseasonal Kelvin wave, Journal of Geophysical Research, doi:10.1002/2014JC010044.

Murphy, R. C., 1926: Oceanic and climatic phenomena along the west coast of South America during 1925, Geographical Review, 16 (1), 26-54.

Périgaud C. and B. Dewitte, 1996: El Niño-La Niña events simulated with the Cane and Zebiak's model and observed with satellite or in situ data. Part I: Model data comparison. J. Climate, 9, 66-84.

Perigaud, C. M., and C. Cassou, 2000: Importance of oceanic decadal trends and westerly wind bursts for forcasting El Niño, Geophys. Res. Lett., 27, 389–392.

Puy, M., J. Vialard, M. Lengaigne, E. Guilyardi, 2015: Modulation of equatorial Pacific Westerly/Easterly Wind Events by the Madden-Julian Oscillation and convectively-coupled Rossby waves. Clim. Dyn., in revisión.

Ramos M., B. Dewitte, O. Pizarro and G. Garric, 2008: Vertical propagation of the extra-tropical Rossby wave during the 1997/98 El Niño off the west coast of South-America in a medium-resolution OGCM simulation. J. Geophys. Res., vol. 113, C08041, doi:10.1029/2007JC004681.

Reynolds, R.W., N.A. Rayner, T.M. Smith, D.C. Stokes, and W. Wang, 2002: An Improved In Situ and Satellite SST Analysis for Climate. J. Climate, 15, 1609-1625

Rodríguez, H., 2001: El diluvio de 1891, "El Niño en América Latin" J Tarazona y otros. CONCYTEC, Lima.

Roundy, P. E., and J. R. Kravitz, 2009: The association of the evolution of intraseasonal oscillations to ENSO phase. J. Climate, 22, 381-395.

Smith, T.M., R.W. Reynolds, T.C. Peterson, and J. Lawrimore, 2008: Improvements NOAAs Historical Merged Land–Ocean Temp Analysis (1880–2006). Journal of Climate, 21, 2283–2296.

Suarez, M. J., and P. S. Schopf, 1988: A delayed action oscillator for ENSO, Journal of Atmospheric Sciences, 45, 3283-3287.

Takahashi, K., A. Montecinos, K. Goubanova, and B. Dewitte, 2011: ENSO regimes: Reinterpreting the canonical and Modoki El Niño, Geophys. Res. Lett., 38, L10704, doi:10.1029/2011GL047364.

Takahashi, K., 2004: The atmospheric circulation associated with extreme rainfall events in Piura, Peru, during the 1997-98 and 2002 El Niño events. Annales Geophysicae 22, 3917-26.

Takahashi, K., R. Martínez, A. Montecinos, B. Dewitte, D. Gutierrez, and E. Rodriguez-Rubio; 2014: TPOS White Paper #8a – Regional applications of observations in the eastern Pacific: Western South America. In Proceedings of the

Tropical Pacific Observing System 2020 Workshop, A Future Sustained Tropical Pacific Ocean Observing System for Research and Forecasting, WMO and Intergovernmental Oceanographic Commission, La Jolla, Calif., 27–30 January. [Available at http://www.wmo.int/pages/prog/gcos/Publications/gcos-184_II.pdf.]

Takahashi, K. and B. Dewitte, 2015: Strong and moderate nonlinear El Niño regimes, Climate Dynamics, doi:10.1007/s00382-015-2665-3

Thual S., B. Dewitte, N. Ayoub and O. Thual, 2013: An Asymptotic Expansion for the Recharge–Discharge Model of ENSO. Journal of Physical Oceanography, 43, 1407–1416.

Wang, C., and J. Picaut, 2004: Understanding ENSO physics - A review. In: Earth's Climate: The Ocean-Atmosphere Interaction. C. Wang, S.-P. Xie, and J. A. Carton, Eds., AGU Geophysical Monograph Series, 147:21-48

Wang, W., M. Chen, A. Kumar, and Y. Xue, 2011: How important is intraseasonal surface wind variability to real-time ENSO prediction?, Geophys. Res. Lett., 38, L13705, doi:10.1029/2011GL047684.

Wyrtki K., 1975: El Niño - The dynamic response of the equatorial Pacific Ocean to atmospheric forcing, Journal of Physical Oceanography, 5, 572- 584

Xiang, B., B. Wang, and T. Li, 2013: A new paradigm for the predominance of standing Central Pacific Warming after the late 1990s. Clim. Dyn., 41 (2), 327-340, doi:10.1007/s00382-012-1427-8.

Xue, Y., M. Chen, A. Kumar, Z.-Z. Hu, and W. Wang, 2013: Prediction skill and bias of tropical Pacific sea surface temperatures in the NCEP climate forecast system version 2, J. Clim., 26, 5358–5378

Yeh, S.-W., B. Dewitte, J.-G. Jhun and I.-S. Kang, 2001: The characteristic oscillation induced by coupled processes between oceanic vertical modes and atmospheric modes in the tropical Pacific. Geoph. Res. Lett., Vol.28, N°14, 2847-2850

Yeh S-W, S-J Kug, B. Dewitte, M-H Kwon, B. P. Kirtman, F-F Jin, 2009: El Niño in a changing climate, Nature 461:511–514.

Yu, J.-Y., H.-Y. Kao, T. Lee, and S.T. Kim, 2011: Subsurface ocean temperature indices for Central-Pacific and Eastern-Pacific types of El Niño and La Niña events, Theoretical Appl. Climatol., 103:337–344.

Yu, J.-Y.,and S. T. Kim, 2010: Three evolution patterns of Central Pacific El Niño, Geophys. Res. Lett., 37, L08706, doi:10.1029/2010GL042810.

Zhang, C., 2005: Madden-Julian Oscillation, Rev. Geophys., 43, RG2003, doi: 10.1029/2004RG000158.